PEER Preliminary Notes and Observations on the August 24, 2014, South Napa Earthquake

Pacific Earthquake Engineering Research Center

Report No. 2014/13

Grace S. Kang
Stephen A. Mahin
Editors

Headquarters, University of California, Berkeley

September 17, 2014

ACKNOWLEDGMENTS

The information contained in this report is the result of extensive preliminary field reconnaissance and initial analysis of ground motion records obtained in the days following the South Napa earthquake. A large number of faculty, staff, and students affiliated with the Pacific Earthquake Engineering Research Center and other research and educational groups at affiliated campuses have been involved in these studies.

It is not possible to list all of the researchers who have been deployed to the field. The investigators contributing to this report are: Norman Abrahamson (Pacific Gas & Electric Company), Clement Barthes (PEER), Yousef Bozorgnia (UC Berkeley), Jonathan Bray (UC Berkeley), Brian Chiou (CalTrans), Robert Darragh (Pacific Engineering & Analysis), Douglas S. Dreger (UC Berkeley), Amir Gilani (Miyamoto International), Bob Glasgow (Miyamoto International), Selim Gunay (PEER), Carlos Gutierrez (CGS), Justin Hollenback (PEER), Tara Hutchinson (UC San Diego), Tadahiro Kishida (PEER), Falko Kuester (UC San Diego), Jiun-Wei Lai (UC Berkeley), Eric Lo (UC San Diego), Yuan Lu (UC Berkeley), Steve Mahin (UC Berkeley), Christopher Markam (UC Berkeley), Silvia Mazzoni (PEER), Dominique Meyer (UC San Diego), Khalid Mosalam (UC Berkeley), Mohamed Moustafa (UC Berkeley), Sifat Muin (UC Berkeley), Marios Panagiotou (UC Berkeley), Nicolas Peralta (UC Berkeley), Charles Scawthorn (PEER), Andreas Schellenberg (PEER), Matthew J. Schoettler (PEER), Barbara Simpson (UC Berkeley), Jonathan Stewart (UCLA), Shakhzod Takirov (PEER), Shanshan Wang (UC Berkeley), Christine Wittich (UC San Diego), and Jenna Wong (UC Berkeley).

Strong-motion records quoted were provided by the Center for Engineering Strong Motion Data (CESMD), a cooperative center established by the U.S. Geological Survey (USGS) and the California Geological Survey (CGS). The CESMD integrates earthquake strong-motion data from the CGS California Strong Motion Instrumentation Program, the USGS National Strong Motion Project, the Advanced National Seismic System (ANSS), and others.

Access in field reconnaissance was aided greatly by the California Department of Transportation (CalTrans) and the California Highway Patrol. Information was also generously provided by CalTrans, the Strong Motion Instrumentation Program (SMIP) of the California Department of Conservation, the USGS, the California Seismic Safety Commission, and various building officials and professional engineers.

Additionally, the efforts of Grace Kang, Stephen Labounty, and Claire Johnson in compiling and preparing the report for publication are greatly appreciated.

This report has been prepared and distributed by PEER, with the financial support from the Transportation Systems Research Program, Business and Industrial Partners program, and core funds.

INTRODUCTION

At 3:20 AM, on the morning of August 24, 2014, the San Francisco Bay area was shaken by the South Napa, California, earthquake. According to the USGS, the earthquake had a magnitude (M_w) of 6, making it the largest earthquake to strike the San Francisco Bay Area since 1989, when the region was shaken by the magnitude 6.9 Loma Prieta earthquake. The epicenter was located about 8 km (5 miles) SSW of Napa, a city of about 77,000 people. Other nearby cities include American Canyon, Vallejo, and Sonoma. Located on the northern shores of San Francisco Bay, this region is a popular tourist destination and internationally known for its burgeoning wine industry.

While relatively modest in intensity, the South Napa earthquake caused significant ground shaking and damage in the epicentral region. For instance, in the city of Napa alone, around 500 buildings have been yellow-tagged, and an additional 120 damaged buildings have been red-tagged (Figure 1). These numbers are expected to grow as detailed inspections continue.

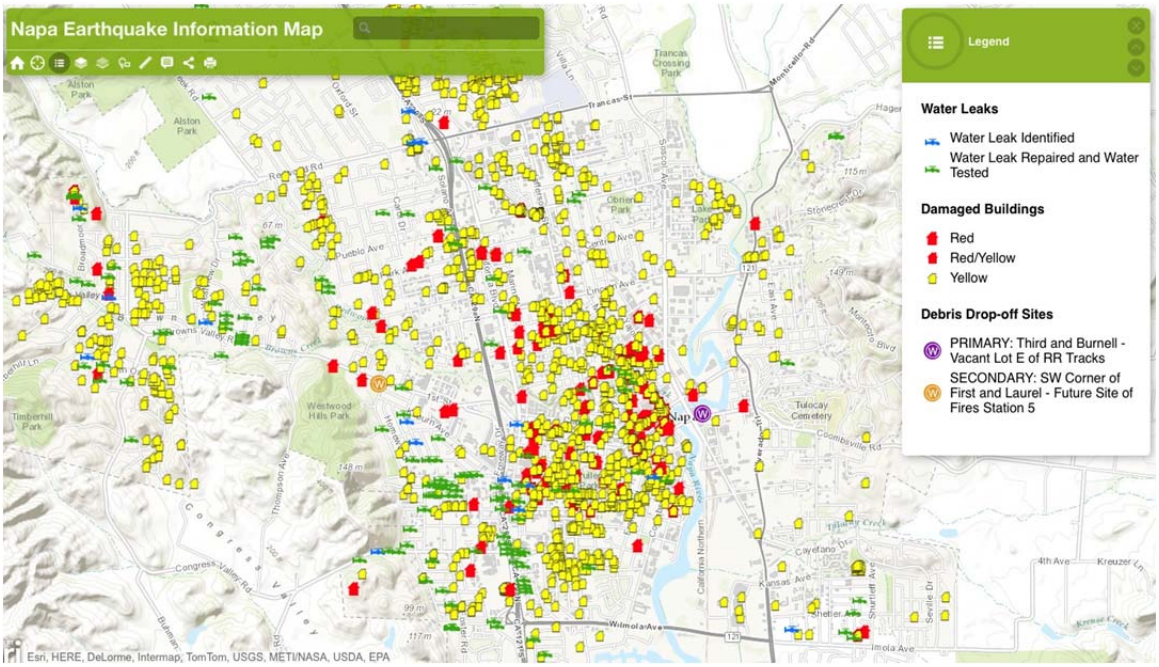

Figure 1 Map of Tagged Buildings in Napa, California, damaged in the August 24, 2014, South Napa Earthquake (*http://bit.ly/1lsdLpf*, accessed September 15, 2014).

Preliminary reports from the USGS Prompt Assessment of Global Earthquakes for Response (PAGER) system estimated that economic losses directly attributable to the earthquake damage would likely be in the range of 500,000 to over 1 billion dollars U.S.. Business interruption and other indirect losses are expected to contribute significantly to the total losses. The actual loss will require some time to determine, but losses to date are sufficient for a Presidential Major Disaster Declaration to be issued on September 11, making damaged facilities owned by certain government and not-for-profit organizations eligible for federal assistance. Although there were no immediate fatalities attributed to the earthquake, one person died about two weeks later due to injuries inflicted as a result of falling debris. Many have postulated that injuries and potential

casualties would have been far greater in number if the earthquake had occurred during normal business hours.

Numerous researchers affiliated with the Pacific Earthquake Engineering Research Center (PEER) were quickly deployed to the Napa Valley area immediately following the earthquake. Working in conjunction with investigators from the Earthquake Engineering Research Institute (EERI), Geotechnical Extreme Events Reconnaissance (GEER), the California Department of Transportation, and others, these PEER-affiliated researchers gathered perishable data for use in subsequent investigations to better understand the causes and implications of seismic damage, and to identify effective methods to mitigate future losses due to such damage.

To date, investigative teams have included faculty, research staff, and students from campuses of the University of California at Berkeley, Davis, and San Diego, Oregon State University, and Stanford University. In the field, geotechnical engineering teams focused on the characteristics and consequences of fault rupture, the behavior of soil, levees, and structures supported on vulnerable soils, and dams. In addition, structural engineering investigators focused on damage to various types of buildings, including non-structural elements and contents, transportation facilities, and lifelines systems. Efforts remain underway to identify the consequences of the earthquake on businesses and the local economy. In addition, teams of experts in geophysics, geology, seismology, and engineering examined the characteristics of the strong-motion records and how they relate to current engineering estimates of earthquake hazard.

This report has been compiled from preliminary observations made by some of the PEER-affiliated investigative teams. The sections in this report reflect observations and a sampling of data collected over a short period of time following the South Napa earthquake. The data presented in this report ranges from cursory to a more studied level. It should be recognized that the situation in the field continues to change each day as field investigations continue, and with the consequences of ongoing occurrence of aftershocks, cleanup and recovery efforts, and cordoning and access restrictions. Thus, the material and observations presented in this report are preliminary, and represent the findings of the individual authors alone. As such, the report may contain inconsistencies from section to section, which reflect the restrictions inherent with limited time in the field.

The material in this report includes discussion of:

1. Characteristics of strong motion records
2. Overview of damage in downtown Napa
3. Behavior of nonstructural elements in buildings
4. Detailed examination of some unreinforced masonry buildings (URM)
5. Examination of some buildings in Downtown Napa
6. Drone-enabled aerial and ground-based LIDAR surveys of damage to bridges and buildings
7. Fire following earthquakes

These preliminary observations provide a basis for the individual authors' own research, but they also provide useful information in pursuing multidisciplinary research in the earth sciences, engineering, and social sciences. These reports will support PEER's further development of

performance-based earthquake engineering, in particular PEER's research efforts on Building Systems, Bridges, and Transportation systems, Lifelines, and Seismic Hazards research. They are also being used to identify and assess newer technologies for future reconnaissance efforts.

Additional information can be found in companion documents prepared by GEER, "August 24, 2014 South Napa, California Earthquake," GEER Association Report No. GEER-037, *http://www.geerassociation.org/GEER_Post%20EQ%20Reports/SouthNapa_2014/index.html*, and EERI's Earthquake Clearinghouse, *http://www.eqclearinghouse.org/2014-08-24-south-napa/preliminary-reports*/. In the future, more comprehensive and verified information, and results of additional detailed investigations and analyses will become available through traditional mechanisms.

Stephen Mahin, Ph.D.
Director, Pacific Earthquake Engineering Research Center
Byron and Elvira Nishkian Professor of Structural Engineering
University of California, Berkeley

Grace Kang, SE
Director of Communications, Pacific Earthquake Engineering Research Center
University of California, Berkeley

Contents

1 Strong-Motion Records[+]

Tadahiro Kishida[1], Shanshan Wang[1], Silvia Mazzoni[1], Christopher Markam[2], Yuan Lu[2], Yousef Bozorgnia[1], Stephen Mahin[1], Jonathan Bray[2], Marios Panagiotou[2], Jonathan Stewart[3], Robert Darragh[5], Norman Abrahamson[4], Justin Hollenback[1], Carlos Gutierrez[6], Brian Chiou[7], Sifat Muin[2], and Douglas S. Dreger[8]

This report summarizes a preliminary study on the characteristics of the strong-motion recordings from the **M** 6.0 South Napa, California, earthquake of August 24, 2014. The effort includes strong-motion data collection, data processing, metadata computation such as source-to-site distances, and estimates of site parameters such as V_{s30}. Strong motion recordings (PGA $\geq$0.30*g*) are reviewed at near-fault stations. Pseudo-spectral acceleration (PSA) values (5% damped) are compared to those estimated with the latest ground motion prediction equations (GMPEs) and current design spectra.

1.1 INTENSITY DISTRIBUTIONS

The South Napa Earthquake occurred in August 24, 2014, at 10:20:44 (UTC) near the West Napa fault zone. Figure 1 shows the ShakeMap from the USGS website for this event (*http://earthquake.usgs.gov/earthquakes/eventpage/nc72282711#shakemap*, last accessed 09/10/2014). The hypocenter is located at the south end of Napa Valley at a depth of 10 km. Instrumental intensity measurements from ShakeMap were distributed along the Napa Valley with a maximum of IX at Napa Fire Station No. 3. The figure also shows the stations for which strong-motion data were processed for inclusion of the PEER strong-motion database.

1.2 STRONG-MOTION RECORDINGS

1.2.1 ACCELERATION TIME SERIES OBSERVATIONS

Strong ground motions were downloaded from the Center for Engineering Strong Motion Data (CESMD) at the web site (http://strongmotioncenter.org/, last accessed 09/13/2014). A total of 214 three-component uncorrected digital accelerograms were downloaded. These records were processed following the PEER standard procedure [Ancheta et al. 2014], which includes inspection of record quality, selection of time windows, such as P-waves, -waves, and coda waves, and component specific filter corner frequencies to optimize the usable frequency range.

[+] Any observations, opinions, findings, and conclusions or recommendations expressed in this material are preliminary and are those of the authors, and do not necessarily reflect those of the Pacific Earthquake Engineering Research Center. The information, data and images contained in this report may not be published or presented without permission from the authors.

[1] Pacific Earthquake Engineering Research Center, Berkeley
[2] Department of Civil and Environmental Engineering, University of California, Berkeley
[3] Department of Civil and Environmental Engineering, University of California, Los Angeles
[4] Pacific Gas & Electric, Co.
[5] Pacific Engineering and Analysis
[6] California Geological Survey
[7] California Department of Transportation
[8] Department of Earth and Planetary Science, University of California, Berkeley

Table 1 shows seven stations that recorded a median horizontal peak ground acceleration (PGA) (RotD50; Boore, 2010) greater than 0.3*g*. Three stations in Table 1 are in the City of Napa, for which the arithmetic average of PGA was 0.40*g*. The average PGA decreased to 0.07*g* in the cities of Petaluma and Pinole, and less than 0.03*g* in Berkeley and San Francisco.

Figure 2 shows the acceleration time series recorded at the stations listed in Table 1. Figure 2a, 2b, and 2c show the time series for Up-Down (UD), North-South (NS), and East-West (EW) components, respectively. The records from the Carquinez Bridge Geotechnical Array #1 shows high-frequency spikes and recorded the largest PGA of nearly 1.0*g* in NS direction (Figure 2b). Napa, Fire station No. 3 shows a long-period pulse in EW direction (Figure 2c), and recorded the largest instrumental intensity of IX (Figure 1). Figure 2 also shows that all the records have a significant duration of less than 10 sec.

Table 1 Stations that recorded median PGA (RotD50) greater than 0.3*g*.

Station Name	Network[a]	Station ID	Latitude (deg)	Longitude (deg)	R_{rup}[b] (km)	V_{s30}[c] (m/sec)	PGA (*g*)
Napa; Fire Station No. 3	USGS	1765	38.330	-122.318	2.6	332	0.42
Huichica Creek	NCSN	NHC	38.217	-122.358	3.9	217	0.31
Main St, Napa	NCSN	N016	38.299	-122.285	3.9	285	0.45
Napa – Napa College	CGS	68150	38.270	-122.277	4.1	339	0.34
Lovall Valley Loop Rd	NCSN	N019B	38.301	-122.402	6.1	710	0.35
Crockett–Carquinez Bridge Geotechnical Array #2	CGS	68259	38.055	-122.226	19.9	342	0.34
Crockett–Carquinez Bridge Geotechnical Array #1	CGS	68206	38.054	-122.225	20.0	342	0.70

[a] CGS = California Geological Survey \ California Strong Motion Instrumentation Program, NCSN = USGS Northern California Seismic Network.

[b] Source-to-site distance based on Boatwright [2014] preliminary finite fault plane model.

[c] Estimated V_{s30}.

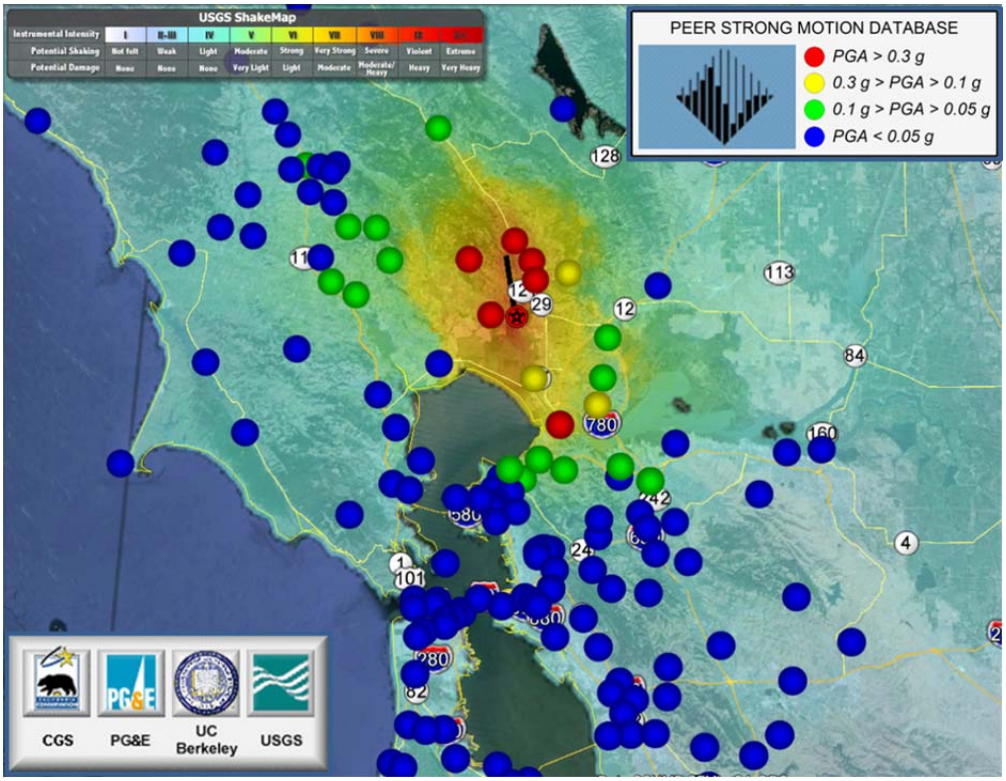

Figure 1 ShakeMap for South Napa earthquake from the USGS overlaid with strong-motion stations processed by PEER.

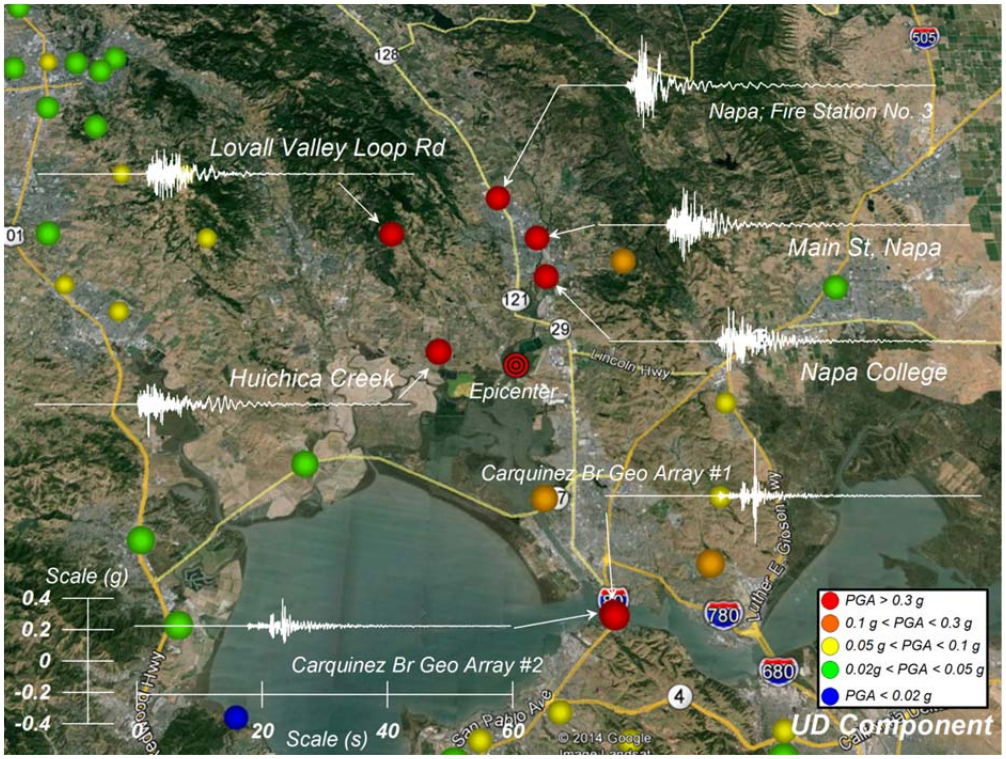

Figure 2a Acceleration time series, UD component.

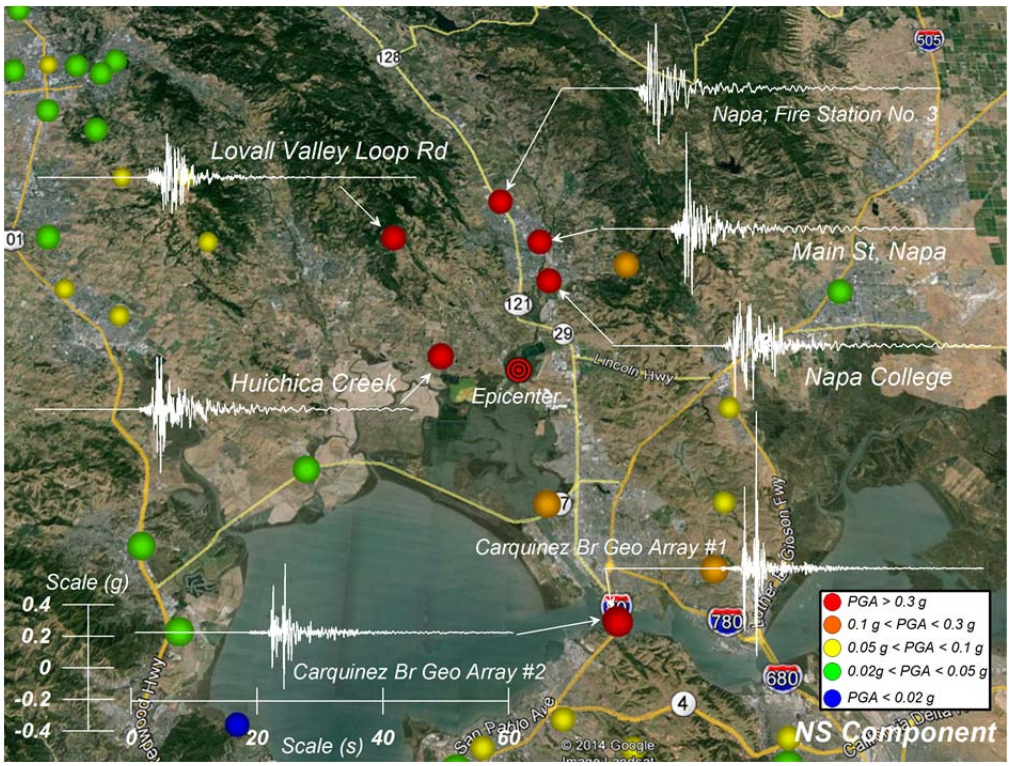

Figure 2b Acceleration time Series, NS Component

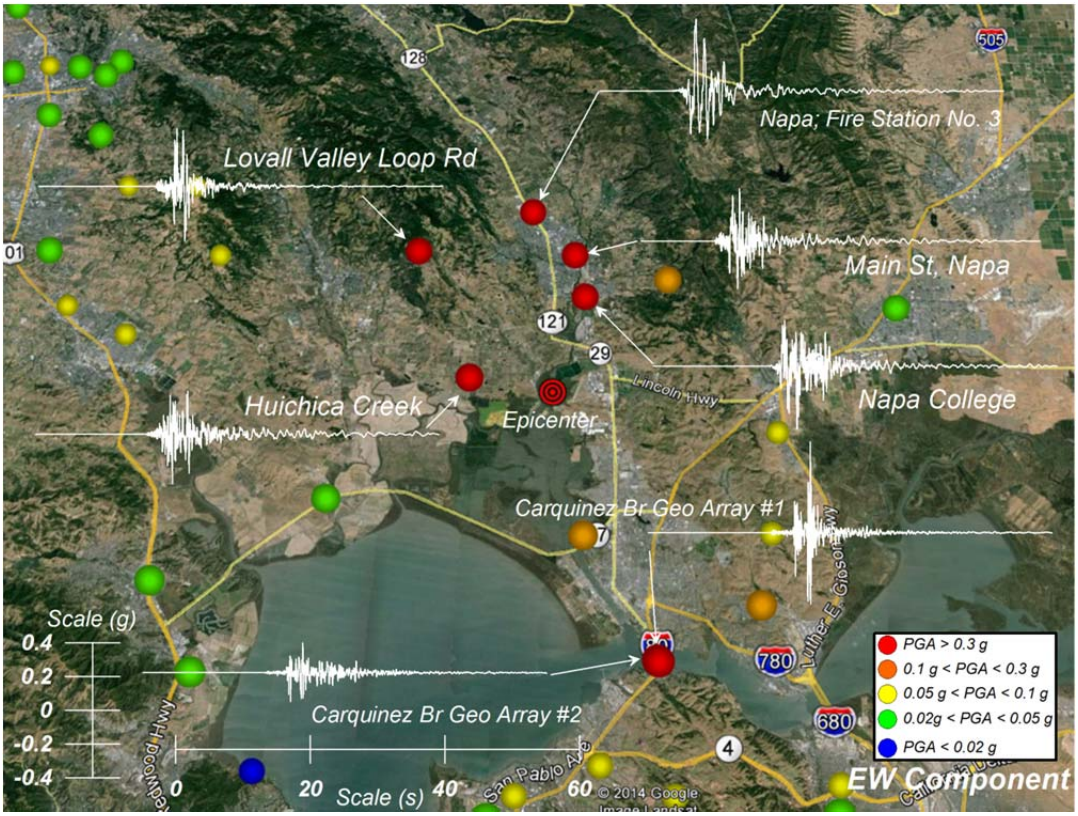

Figure 2c Acceleration time series, EW component.

1.2.2 NEAR-FAULT PULSE OBSERVATIONS

Pulse-like waveforms were observed in several of the velocity time series at the near-fault stations shown in Figure 2. On the basis of this observation, the horizontal components of near-fault velocity time series were rotated into fault-normal (FN) and fault-parallel (FP) orientations where the fault strike was taken as 155° (Figure 3). Maximum peak ground velocity (PGV) was recorded as 84 cm/sec in FP direction at Napa Fire Station No. 3. Based on visual inspection of Figure 3, Napa Fire Station No. 3 (FN, FP components), Lovall Valley Loop Rood (FN, FP components), Main St. (FN component), Huichica Creek (FP component), and Napa College (FN, FP components) show pulse-like waveforms in the velocity time series.

Appendix A Table 1 shows the recorded PGV (RotD50), expected PGVs and the periods by Bray et al. [2009] for these five stations. The Bray et al. [2009] relationship estimates a median PGV of about 50 to 60 cm/sec for the fault-normal component of the five near-fault strong motion stations with a 16% to 84% range of about 35 to 85 cm/sec. This captures the recorded near FN component PGVs fairly well. The period of the near-fault FN velocity pulse was estimated to be within the range of 0.7 sec to 2.0 sec (16% to 84% values, respectively). The recorded velocity time series of the five near-fault records for the M6 South Napa earthquake contained shorter period velocity pulses within this estimated range, but they also contained longer period pulses significantly higher than this range. It is not clear if the longer period pulses were due to fault mechanism or site effects (e.g., deep basin response).

The following sections describe the characteristics of the velocity pulse near the fault evaluated by several different approaches.

1.2.2.1 Examination of Velocity Pulse by Hayden[2014] and Shahi [2013] Approaches

The presence of pulse-like motions in the near-fault region was studied through the examination of velocity records at five recording stations. Two methods were used to classify motions as pulse-like or non-pulse-like. The first scheme was proposed by Hayden et al. [2014], while the second classification scheme was proposed in Shahi [2013]. Table 2 lists the recording stations examined and summarizes the results of the classification process. Plots of the resulting velocity records for the components with the highest “pulse-like tendencies” for each recording station for both the Hayden et al. [2014] and Shahi [2013] methods are provided in Appendix A.

For three of the five stations examined (Fire Station No. 3, Lovall Valley Loop Rd., and Huichica Creek) the two methods agree with regards to pulse classification. For the two remaining stations (Napa College and Main St. Napa), the two methods disagree with regards to the identification of a pulse-like motion. For the Napa College station, the Shahi [2013] scheme identifies a pulse, while the Hayden et al. [2014[method yields a pulse score of 25%, which is below the proposed pulse score threshold of 60%. The discrepancy between the two classifications for this station could be due to the presence of two significant cycles in the velocity time history, which downgrades the significant cycle sub-score that contributes to the overall pulse score in the Hayden et al. [2014] procedure. The discrepancy between the classification results for the Main St. Napa station is not as easily explained through the salient features of the velocity time series.

Importantly, the Huichica Creek station was in a backward directivity location, and its maximum velocity and pulse component was roughly in the fault-parallel orientation. Three of the four remaining sites were in forward directivity locations and their maximum velocity and pulse components were within 30° of the fault normal orientation.

Table 2 Results of pulse classification methods.

Station name (RSN)	Hayden et al. [2014]				Shahi [2013]		
	Pulse score (%)	PPV (cm/sec)	Pulse period (sec)	Azimuth of max PPV(°)	Pulse identified	Azimuth of max pulse (°)	Pulse period (sec)
Fire Station No. 3	100	111	3.8	62	Yes	61.5	4.4
Huichica Creek	100	58.5	5.5	351	Yes	283.6	2.8
Lovall Valley Loop Rd.	100	64.3	3.9	61	Yes	20.7	3.6
Main St. Napa	92	62.3	3.4	56	No	29.7	3.9
Napa College	25	104	1.6	340	Yes	296.0	2.0

[a] PPV = Peak-to-peak velocity (see Hayden et al. [2014]).

1.2.2.2 Characterization of Near-Fault Ground Motion Records by Lu and Panagiotou [2014]

This section presents a wavelet analysis of the ground motions recorded at two stations during the **M** 6 South Napa earthquake: Napa Fire Station No. 3 and Main St. recording stations. The originally recorded ground motion records were rotated (by Lu and Panagiotou) to the FN and FP directions. The rotated ground acceleration and ground velocity histories, as well as the acceleration and displacement response spectra, for both components are shown in Appendix D Figure 1 and 2 for the Napa Fire Station #3 and in Appendix D Figures 3 and 4 for the Main St. records. Both stations were expected to have been significantly affected by forward directivity.

The wavelet analysis was conducted using the cumulative pulse extraction (CPE) method described in Lu and Panagiotou [2014]. The analysis was conducted in the velocity time domain and the order of the extracted pulses was determined based on the energy of the pulses ($CPE_{V,EN}$ method). For each motion, three pulses were extracted. The sum of the pulses in the time domain result in a representation of the ground motion. Appendix D Figures 1 to 4 show the extracted pulses in both the acceleration and the velocity time domains.

The Napa Fire Station No. 3 recordings include multiple strong pulses of significantly different predominant period T_P. The FP component (Appendix D Figure 1) exhibits the largest PGV, which is the result of two pulses, one with $T_{P,1}$ = 1.1 sec and another with $T_{P,2}$ = 3.9 sec. The peaks of these two pulses are well correlated in the time domain. The FN component (Appendix D Figure 2) of the ground motion at Napa Fire Station No. 3 includes a strong pulse of $T_{P,1}$ = 1.9 sec, which determines the PGV of this motion. After that pulse a pulse with $T_{P,3}$ = 1.1 sec follows in the time domain. The spectral demands for T larger than 3 sec are dominated from the combination of the two pulses with $T_{P,1}$ =1.9 sec and $T_{P,3}$ = 3.3 sec. The FP component of the Main St. record (Appendix D Figure 3) exhibits a larger PGA than that of the FN component while the latter exhibits a larger PGV. The ground velocity waveform of the FN component is

quite complex with the three pulses (T_{P1} = 3.1 sec, $T_{P,2}$ = 1.2 sec, and $T_{P,3}$ = 0.6 sec) to be highly correlated in the time domain.

1.2.3 CARQUINEZ BRIDGE GEOTECHNICAL ARRAY RECORDINGS

This section discusses the time series recorded at the two Crockett–Carquinez Bridge Geotechnical Arrays by comparing the records along the source-to-site path and those from the three downhole arrays. The Geotechnical Arrays are a cooperative project of California Department of Transportation (Caltrans) and CSMIP.

The Crockett–Carquinez Bridge Geotechnical Array #1 recorded the largest PGA during the **M** 6 South Napa earthquake where the NS component reached approximately 1.0*g* as shown in Figure 2a. Figure 4 shows the acceleration time series along strike direction from the epicenter to the Carquinez Bridge. The recording at Carquinez Bridge Geotechnical Array #1 shows two high-frequency spikes (approximately 10 Hz) after the *S*-wave arrival that have peak amplitudes of approximately 1.0*g* in the North direction. Similar spikes were observed in the recordings at Carquinez Bridge Geotechnical Array #2, the Vallejo–Hwy 37/Napa River East Geotechnical Array, and at Napa College in Figure 4, although these amplitudes are smaller than those measured at the Carquinez Bridge Geotechnical Array #1. The record at Pinole Ridge did not show these spikes in the records. This observation may indicate that these spikes were amplified from the source to the Carquinez Bridge Geotechnical Array #1 site by path effects.

Figure 5 shows the downhole records for acceleration time series, 5%-damped PSA and Fourier Amplitude Spectra (FAS) at Carquinez Bridge Geotechnical Array #1, #2, and Vallejo–Hwy. 37/Napa River East Geotechnical Array. Figures 5a and 5c show that the frequency content near 10 Hz were amplified through subsurface soil deposits of less than 20 m where Figure 5b shows that the frequency content near 3 Hz were amplified through subsurface soil deposit of less than 60 m. At all three arrays most of the amplification occurs between the middle sensor and the surface with less amplification between the deepest recording and the middle recording. The two high-frequency spikes are observed after the direct *S*-wave arrival at all downhole arrays; these arrivals may be from *S*-waves radiated from other portions of the fault rupture to the north (e.g., *http://earthquake.usgs.gov/earthquakes/eventpage/nc72282711#scientific_finite-fault*).This observation may indicate that the large PGA observed at Carquinez Bridge could be a site effect caused by the soft soil deposits. These observations do not exclude the possibility of soil-structure interaction effects on the measured recordings, because these time series were recorded near bridge abutments and structures. Additional study is needed to understand the effects of source, path, site, and nearby structures on these recordings.

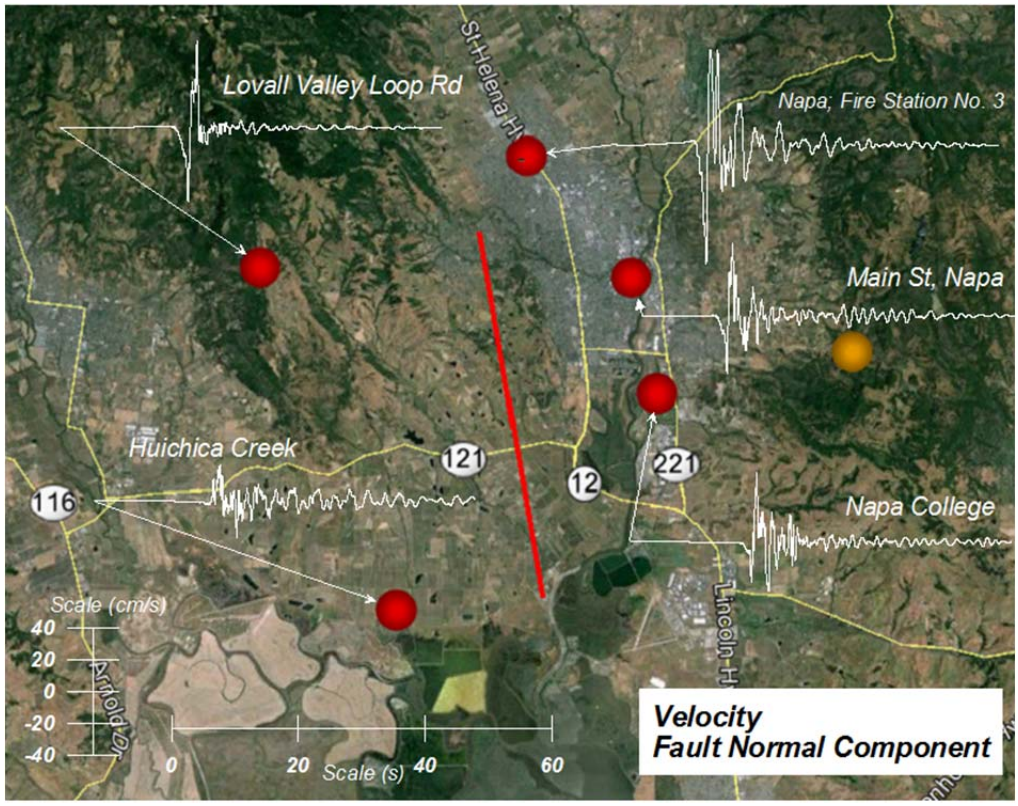

Figure 3a. Fault-normal velocity time series.

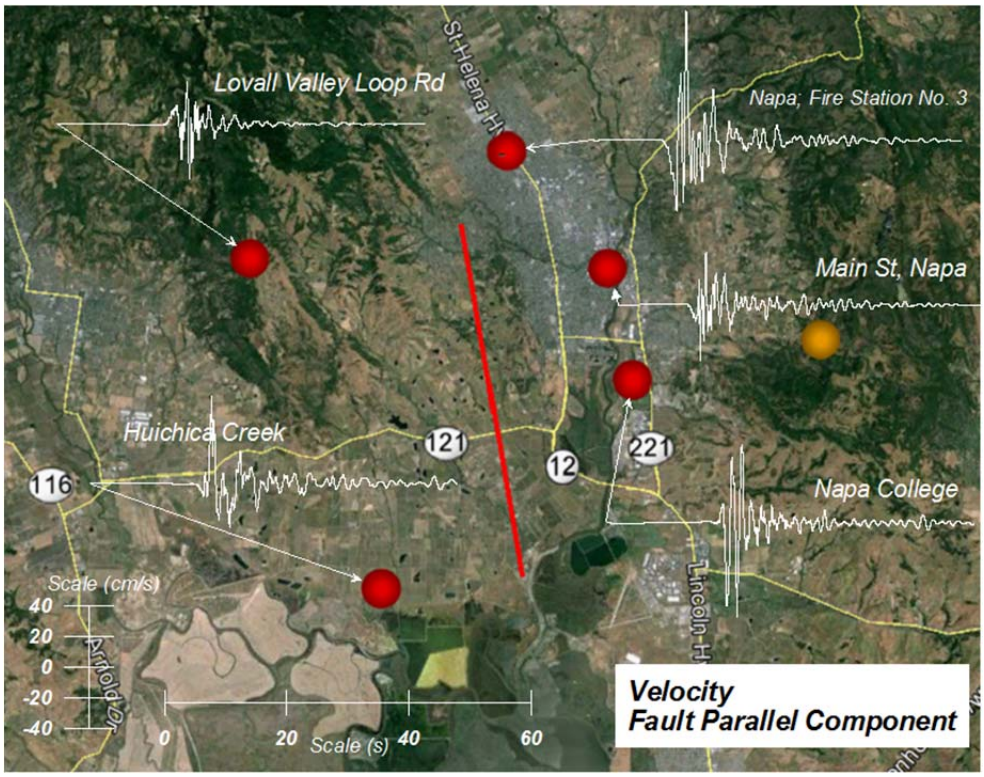

Figure 3b Fault parallel velocity time series.

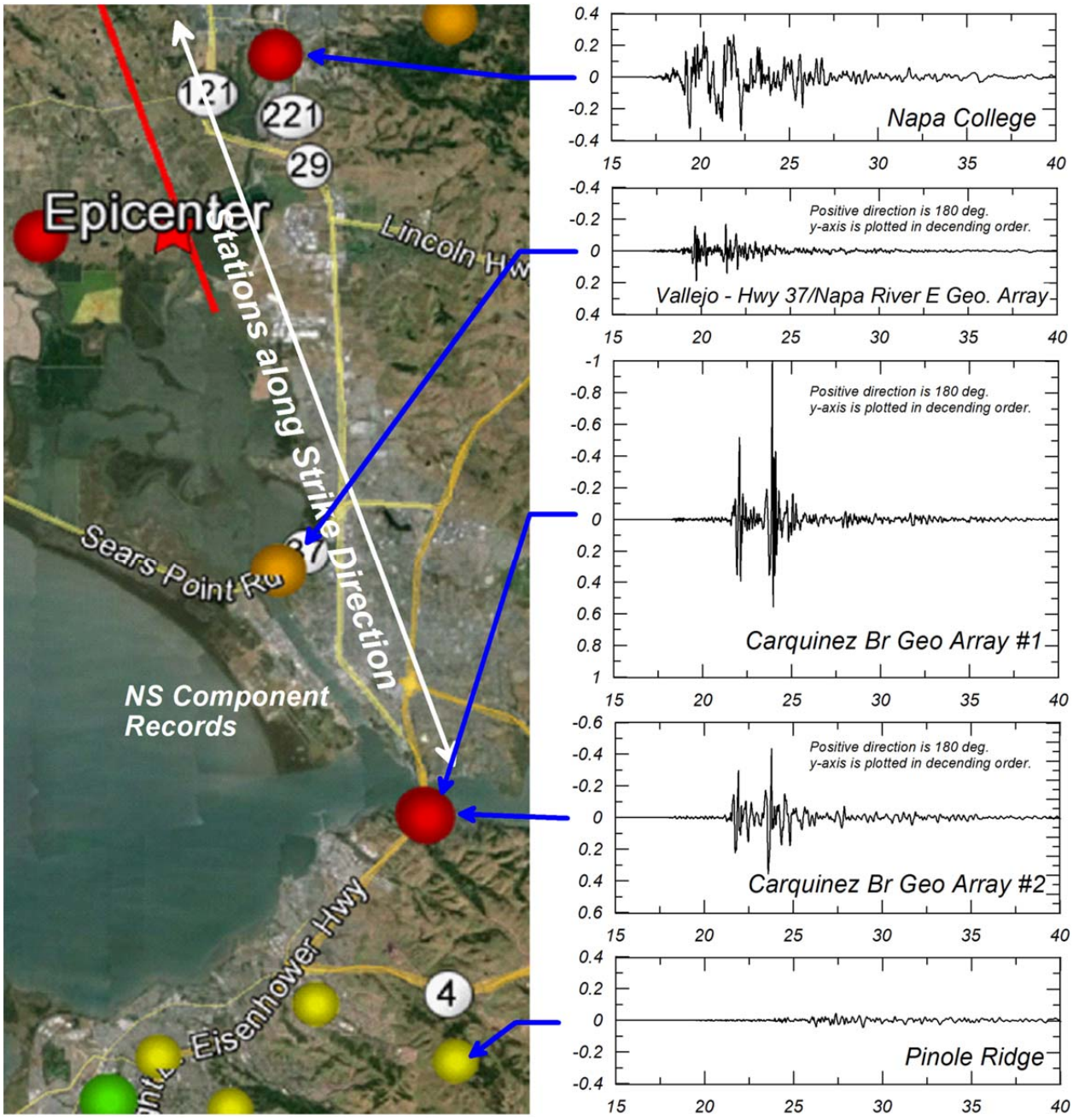

Figure 4 Acceleration time series along strike direction from source to Carquinez Bridge.

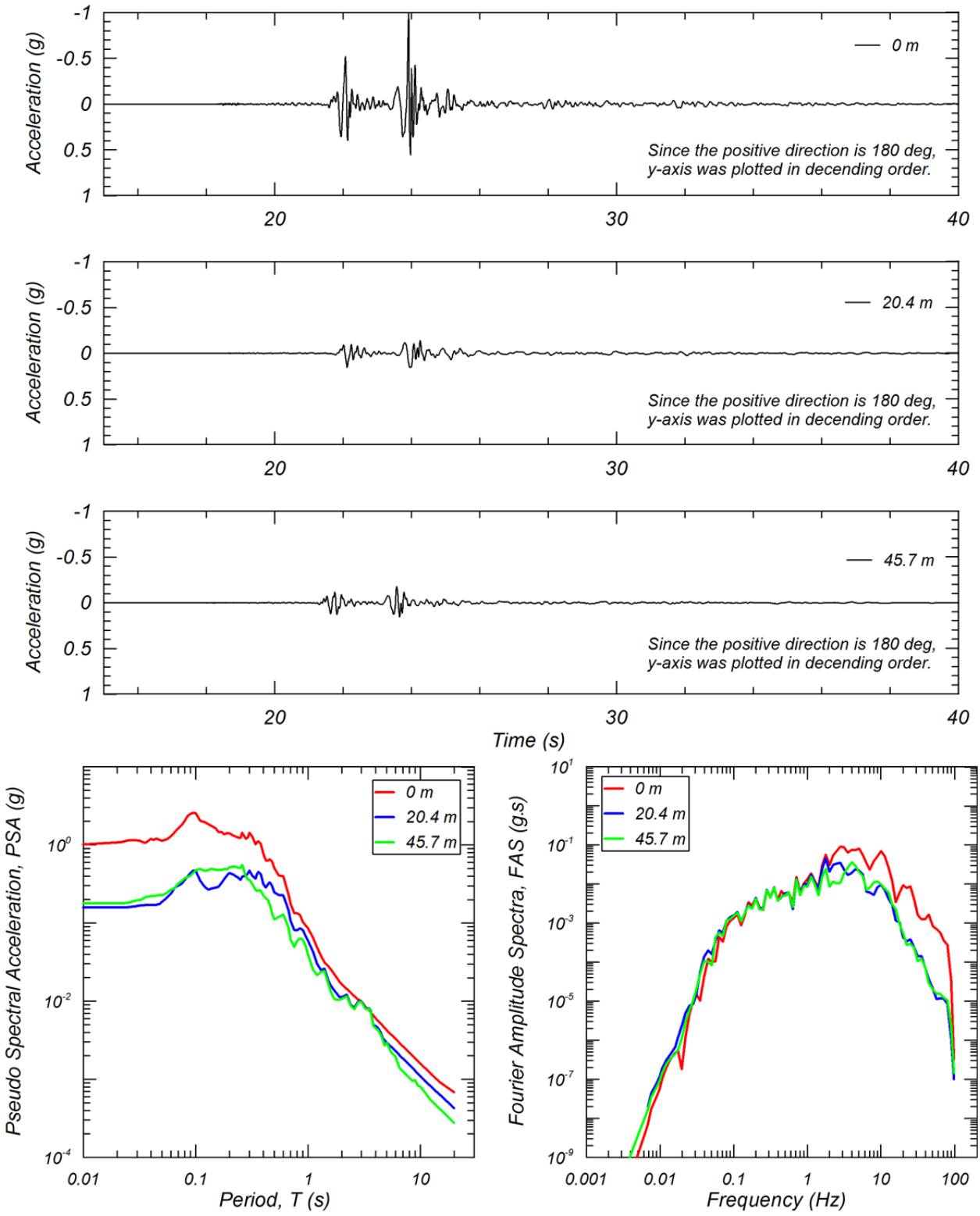

Figure 5a Acceleration time series, 5%-damped PSA, and FAS for Carquinez Bridge Geotechnical Array #1, NS component.

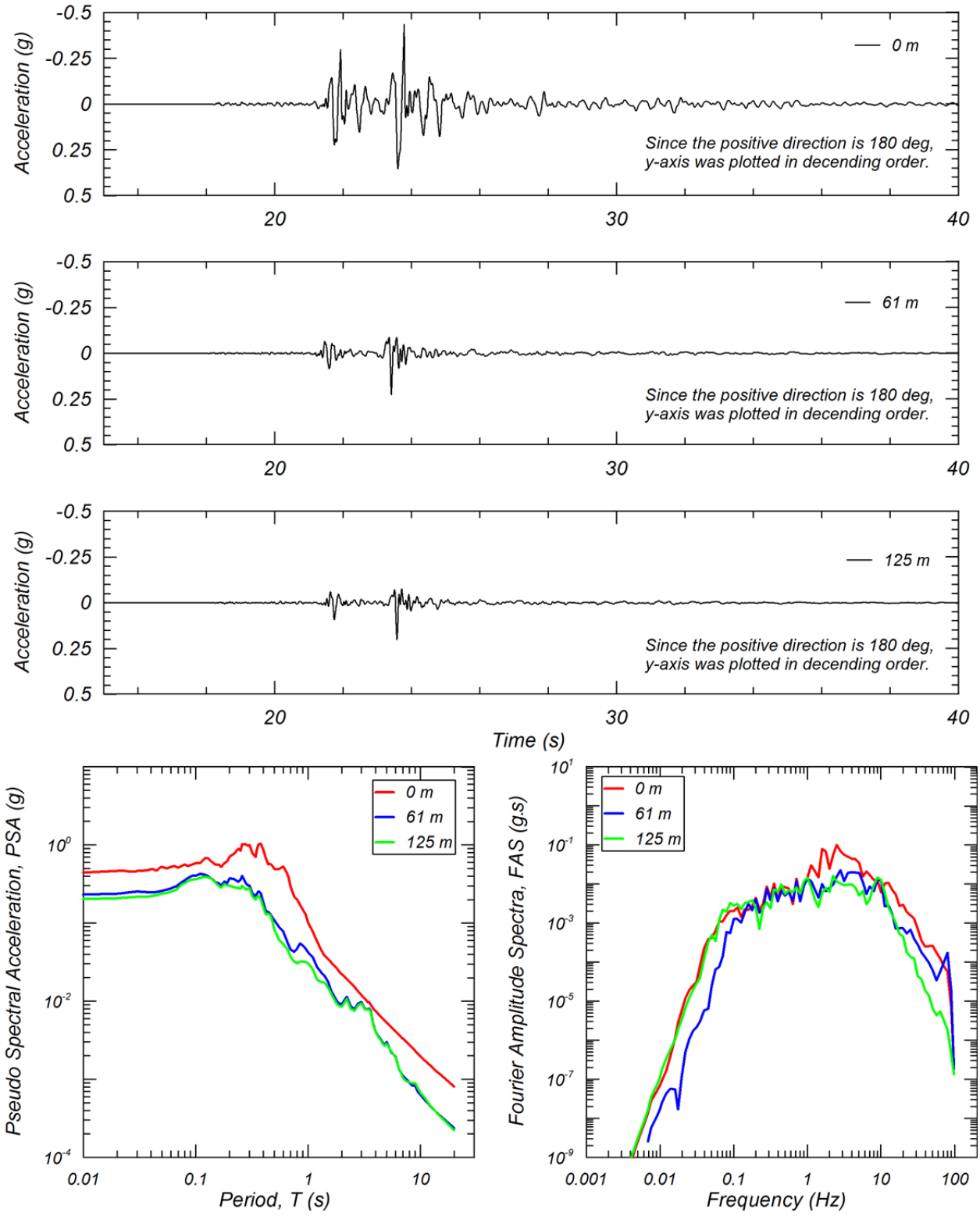

Figure 5b Acceleration time series, 5%-damped PSA, and FAS for Carquinez Bridge Geotechnical Array #2, NS component.

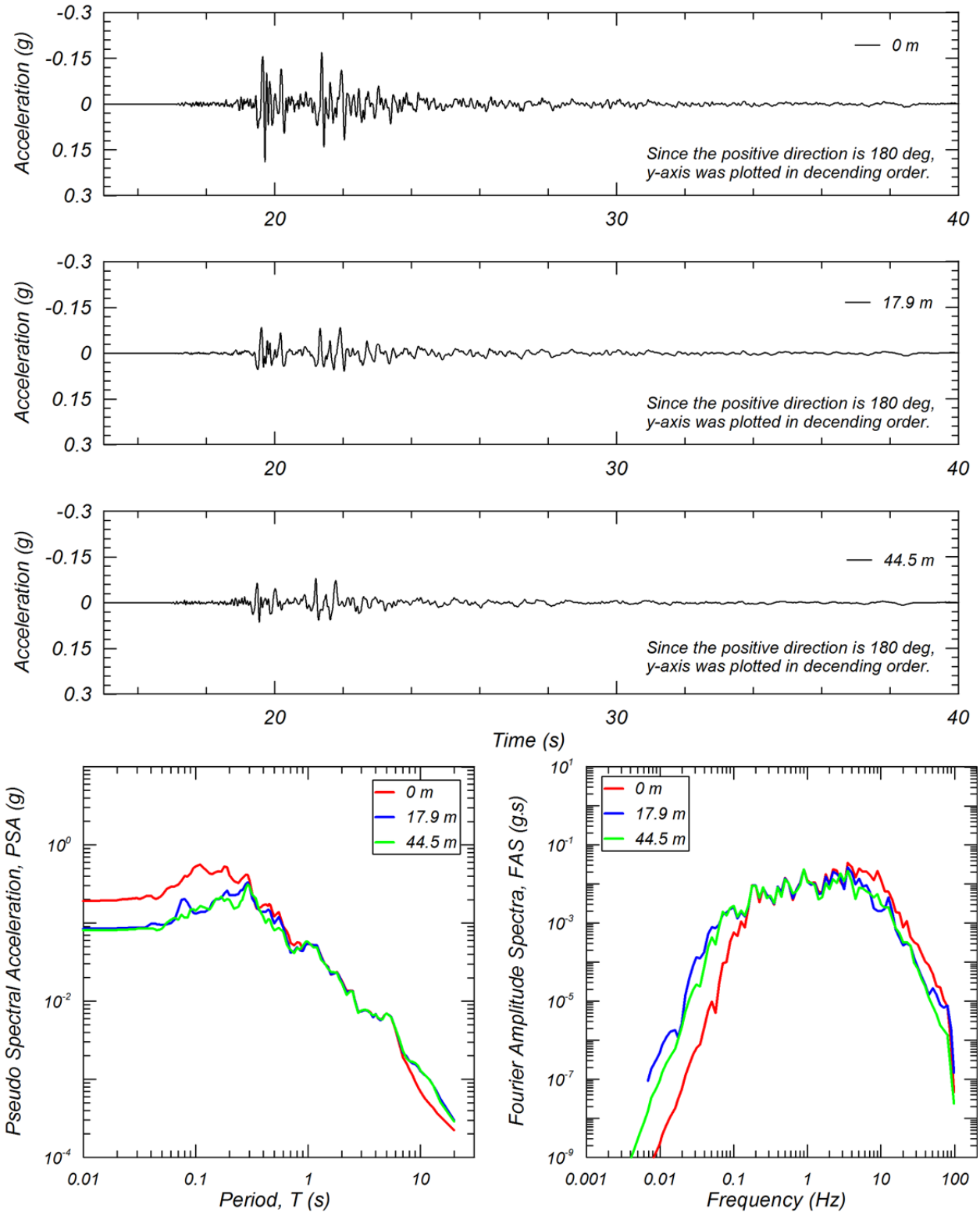

Figure 5c Acceleration time series,5%-damped PSA, and FAS for Vallejo–Hwy 37/Napa River East Geotechnical Array, NS component.

1.3 ACCELERATION, VELOCITY, AND DISPLACEMENT TIME SERIES

The acceleration, velocity, and displacement time series are plotted in Figure 6 for the NS component of Napa College Station. The figure also shows the Arias Intensity (AI), 5%-damped PSA and FAS.

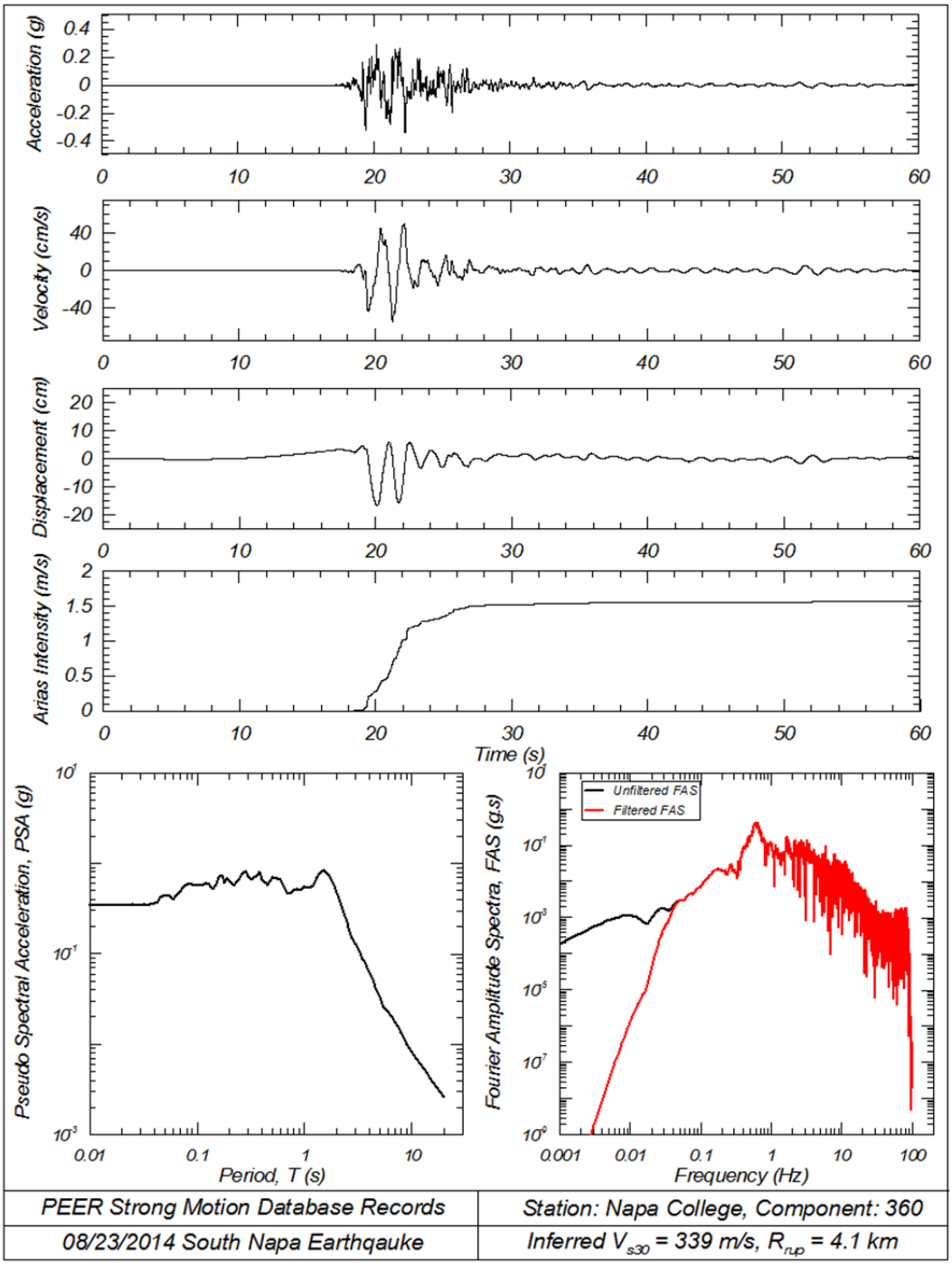

Figure 6 Summary of time series and spectra at Napa College Station (NS component).

The PGA, PGV and AI recorded at this station were 0.339*g*, 54.8 cm/sec, and 1.56 m/sec, respectively. The figure also shows the velocity pulse in the *S*-wave that was discussed in the previous section. The period of this waveform is approximately 1.5 sec, which is also seen in the PSA in the figure. Similarly, the FAS has a peak amplitude near 0.7 Hz. Similar plots are presented in Appendix B for the other stations listed in Table 1.

1.4 COMPARISON TO GROUND-MOTION PREDICTION EQUATIONS

1.4.1 FAULT LOCATION AND RECORDING SITE CONDITIONS

We reviewed the available surface slip and fault slip inversions and selected a preliminary preferred fault model for distance calculations. Fault mechanism and hypocenter location were obtained from the Northern California Earthquake Data Center (NCEDC) (*http://www.ncedc.org/, last accessed 09/07/2014*) (Table 3). The table shows that the earthquake fault mechanism is strike-slip based on the rake angle. Two preliminary finite fault models were available at the USGS website (*http://earthquake.usgs.gov/earthquakes/eventpage/nc72282711#scientific_finite-fault*, last accessed at 09/07/2014). One model inverts regional seismic waveforms for slip amplitude on the fault [Dreger 2014]. The second inverts regional GPS and InSAR data obtained by the USGS NEIC [Barnhart 2014]. Field observation of surface rupture are also available from the University of California, Davis (*http://blogs.agu.org/tremblingearth/2014/08/30/earthquake-rupture-u-s-suburb/*), last accessed at 09/07/2014) [Elliot 2014]. The model using regional GPS and InSAR agree closely to the inversion model using regional seismic data regarding the depth and amount of peak slip. On the basis of these observations, we selected the finite fault model based on the inversion model using regional seismic data in Table 4 where rupture was extended to the ground surface based on the study by Boatwright [2014]: *http://earthquake.usgs.gov/product/shakemap/nc72282711/nc/1409779655706/download/boat_fault.txt*, last accessed at 09/10/2014), which was based on observation of surface rupture. By using this preliminary fault model, the distance measures (R_{epi}, R_{hyp}, R_{rup}, R_{jb}, R_{sei}, and R_x) were computed for all 214 records. The strike and dip of the selected finite fault model in Table 4 are 170 and 90, respectively. These values are different from those by NCEDC in Table 3. However, we preferred the preliminary fault model in Table 4, because it will potentially provide distances with smaller errors taking into account the uncertainties in dip direction and the number of rectangular fault segments.

Table 4 Fault mechanism and hypocenter location [NCEDC 2014].

Magnitude (M)	6.02
Fault strike (deg)	155
Fault dip (deg)	82
Fault rake (deg)	172
Hypocenter latitude (deg)	38.20837
Hypocenter longitude (deg)	-122.29894
Hypocenter depth (km)	10.117

Table 5 Rectangular finite fault models used in this study [Boatwright 2014].

Corner	Latitude (deg)	Longitude (deg)	Depth (km)
1	38.2200	-122.3130	0.0000
2	38.3100	-122.3331	0.0000
3	38.3100	-122.3330	11.0000
4	38.2200	-122.3131	11.0000

For site conditions, the site database developed by PEER during NGA-West2 study [Seyhan et al. 2014] was used. From the NGA-West2 site database, site parameters such as V_{s30}, $Z_{1.0}$, and $Z_{2.5}$ were obtained for 98 out of the 214 stations. For the 116 stations for which we did not have V_{s30} values, the estimated values were computed [Gutierrez 2014, personal communication] according to the methodology described by Seyhan et al. [2014]. V_{s30} for the selected stations were also estimated from Geomatrix 3rd letter and the method by Wald and Allen [2007]. $Z_{1.0}$ and $Z_{2.5}$ are estimated from V_{s30} as described in Chiou and Young [2014] and Campbell and Bozorgnia [2014], respectively. Based on this approach, these site-condition metadata were estimated for all 214 stations. As a result, the number of stations belonging to site class A, B, C, D, and E [ASCE 2010] are 0, 8, 126, 75, and 5, respectively. The median V_{s30} of all sites is 490 m/sec, which will be used in the following section as reference V_{s30} to compare the recorded PSA to GMPE predictions.

1.4.2 COMPARISON OF PSEUDO-SPECTRAL ACCELERATION (PSA) TO GROUND-MOTION PREDICTION EQUATIONS (GMPES)

The 5%-damped PSA for the motions recorded at the stations listed in Table 1 were compared to the 2014 NGA-West2 GMPEs (Abrahamson et al. 2014 [ASK14], Boore et al. 2014 [BSSA14], Campbell and Bozorgnia 2014 [CB14], and Chiou and Youngs 2014 [CY14]) by using the appropriate distance metrics and site conditions described in the previous sections. Figure 7 shows the horizontal PSA based on RotD50 compared with the weighted geometric mean of the GMPEs (ASK14, BSSA14, CB14, and CY14 with equal weight). The results show that the PGA predicted by the GMPEs match well with the recorded values except Carquinez Bridge Geotechnical Array #1 and #2 shown in Figure 7(c) and (d). This observation indicates that the amplification of high-frequency content described in the previous section is larger than the site effects expected from GMPEs by V_{s30}. It is also observed that the GMPEs tend to underestimate the PSA at periods greater than 0.5 sec at Lovall Valley Loop Rd. and Napa Fire Station No. 3 in Figure 7(e) and (f). These stations are located at northern edge of the fault model as shown in Figure 3. It is also observed that GMPEs do not capture the pulse observed at a period of 1.5 sec for the Napa College records in Figure 7(a).

Figure 8 shows the vertical PSA compared with the GMPE by Bozorgnia and Campbell [2014**]**. The comparisons show a general satisfactory agreement between recorded and estimated values, especially at the short vertical periods that are important for the vertical component, with the following exceptions. Figure 8 shows that PGA are underestimated for Carquinez Bridge Geotechnical Array #1 and #2 in Figure 8(c) and (d). Similarly, PSA greater than 1 sec are

underestimated at Lovall Valley Loop Rd. and Napa Fire Station No. 3 in Figure 8(e) and (f). These trends observed in vertical PSA are similar to those observed in horizontal PSA.

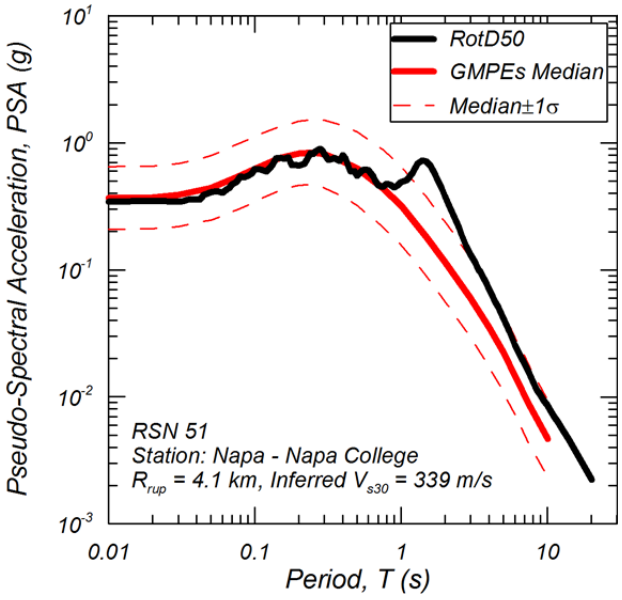

(a) Napa College

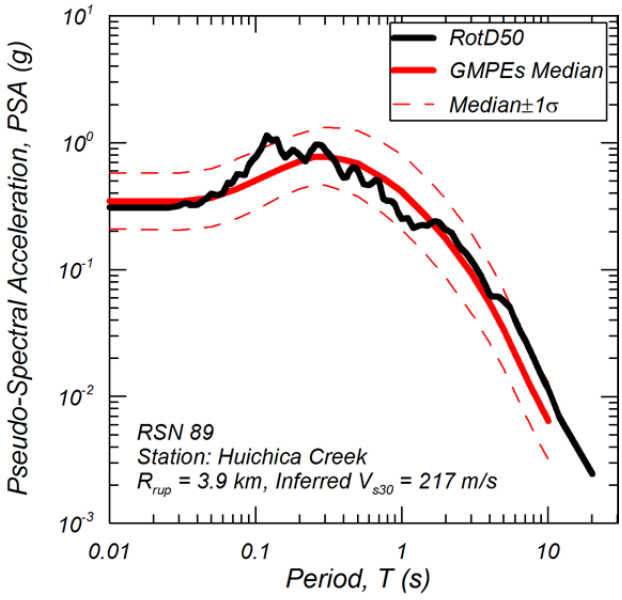

(b) Huichica Creek

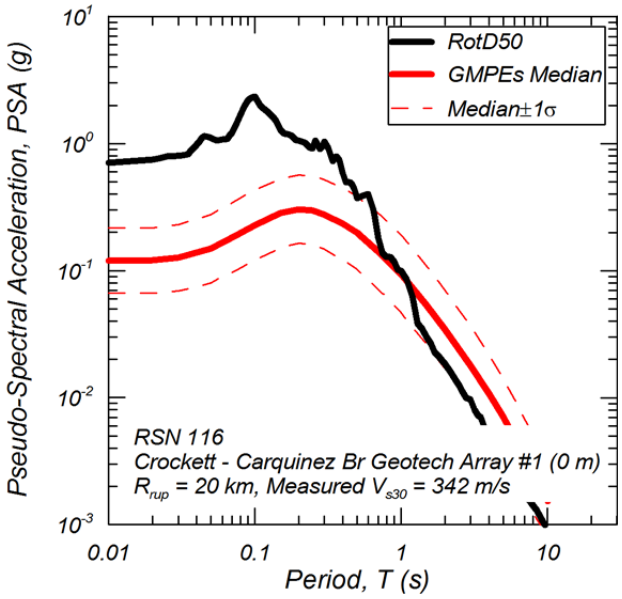

(c) Carquinez Br Geotech Array #1

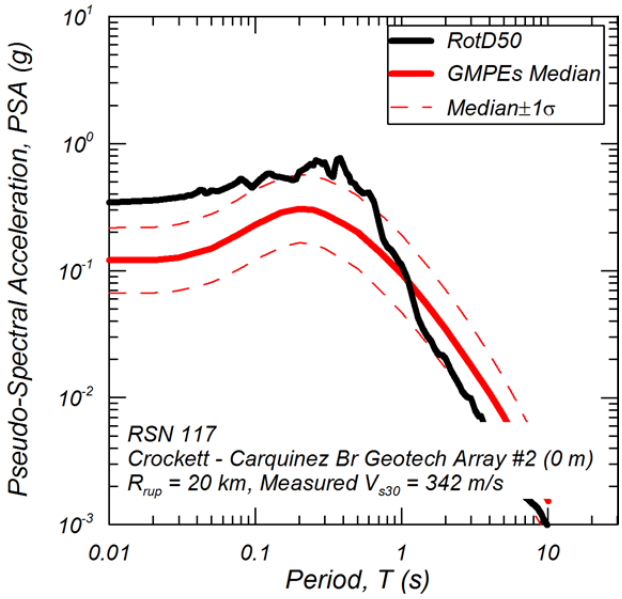

(d) Carquinez Br Geotech Array #2

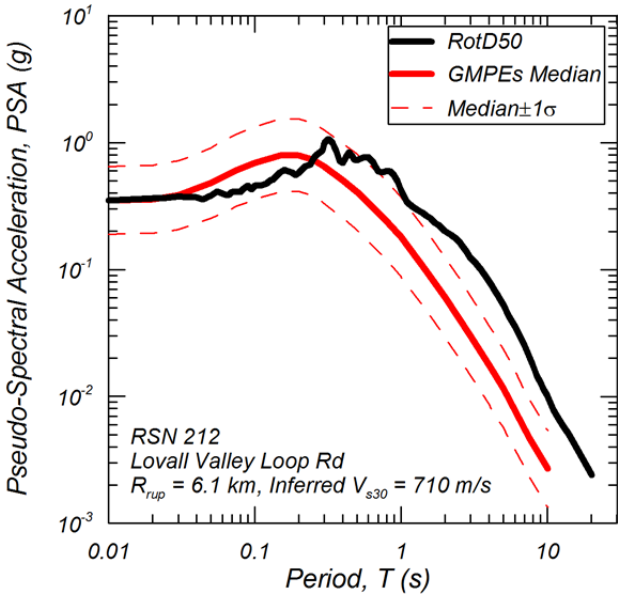

(e) Lovall Valley Loop Rd.

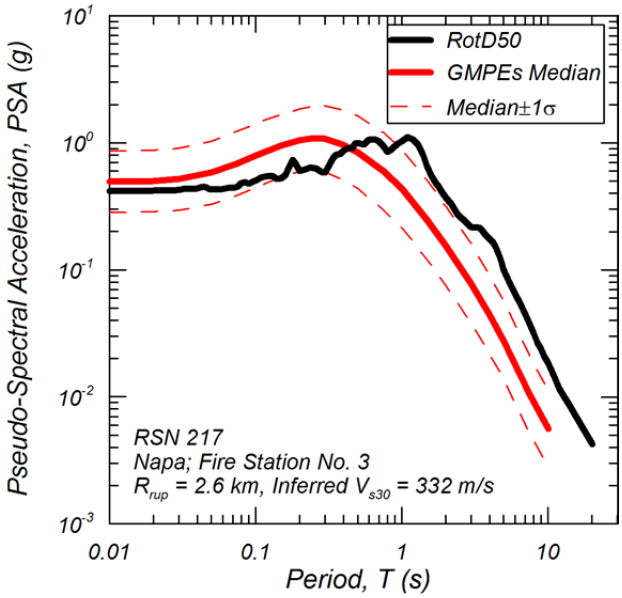

(f) Napa Fire Station No. 3

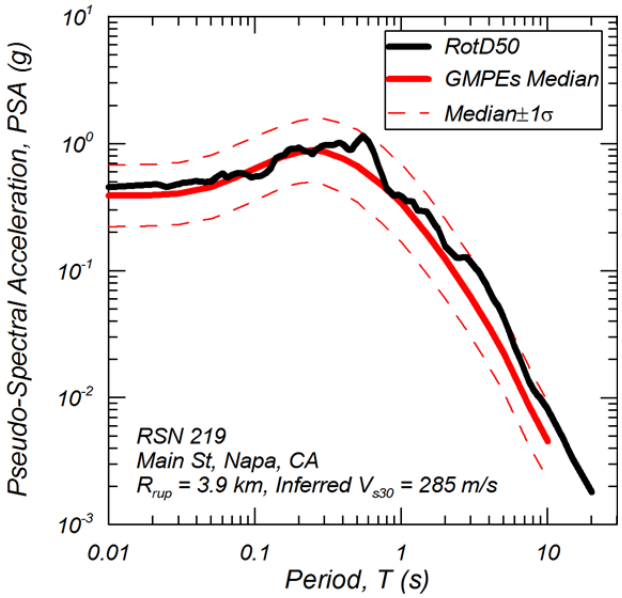

(g) Main St. Napa

Figure 7 Horizontal PSA (RotD50) compared to mean NGA-West2 GMPEs (2014).

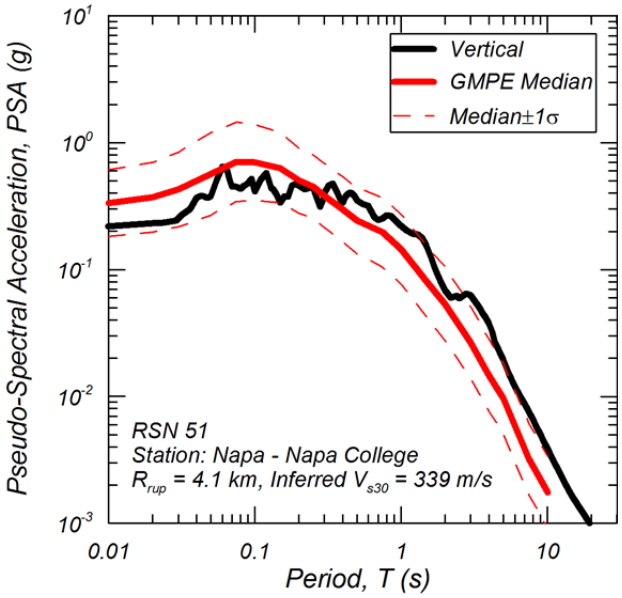

(a) Napa College

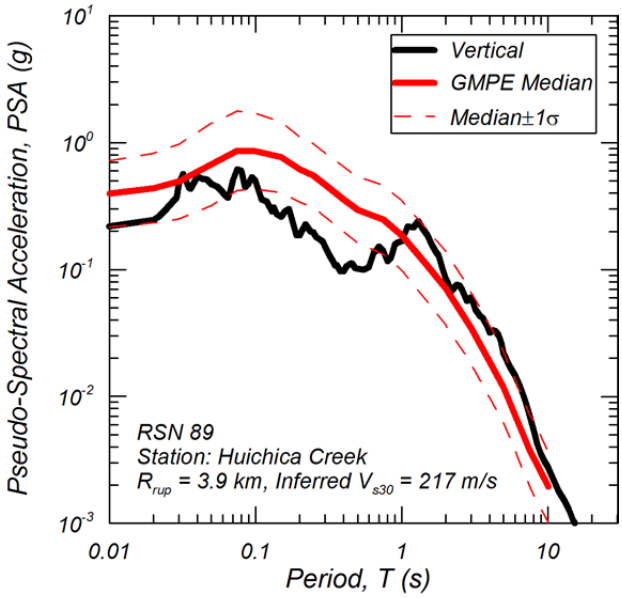

(b) Huichica Creek

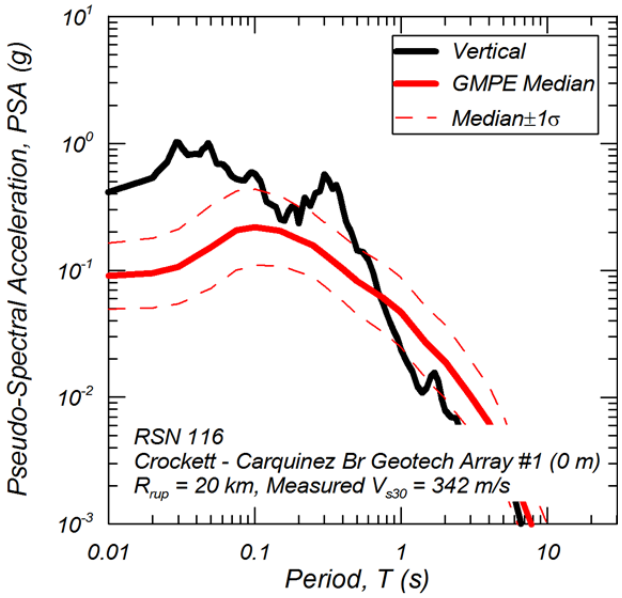

(c) Carquinez Br Geotech Array #1

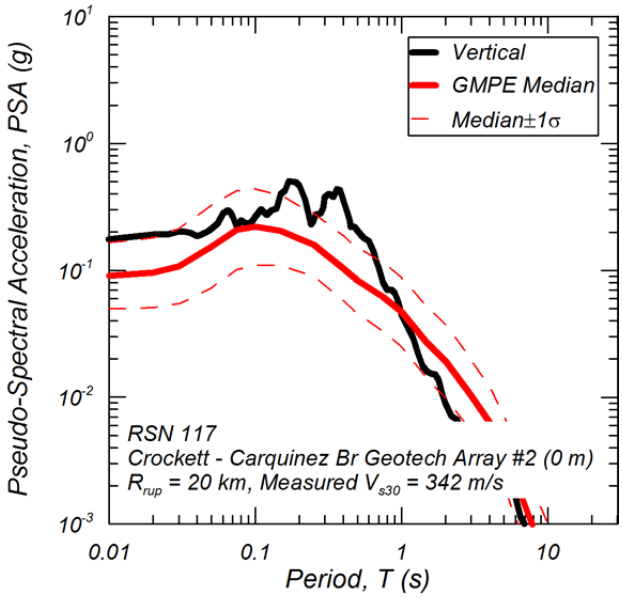

(d) Carquinez Br Geotech Array #2

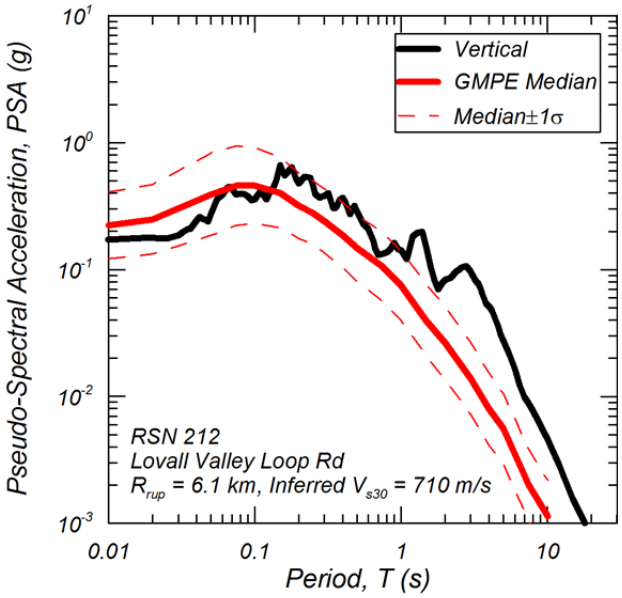

(e) Lovall Valley Loop Rd

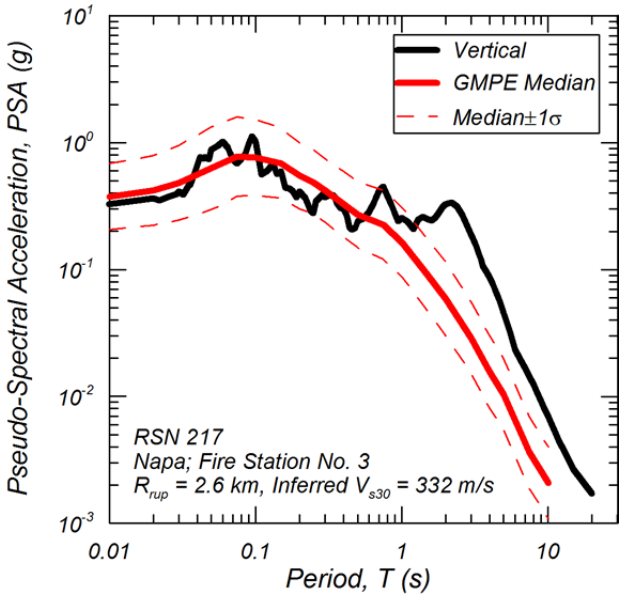

(f) Napa Fire Station No. 3

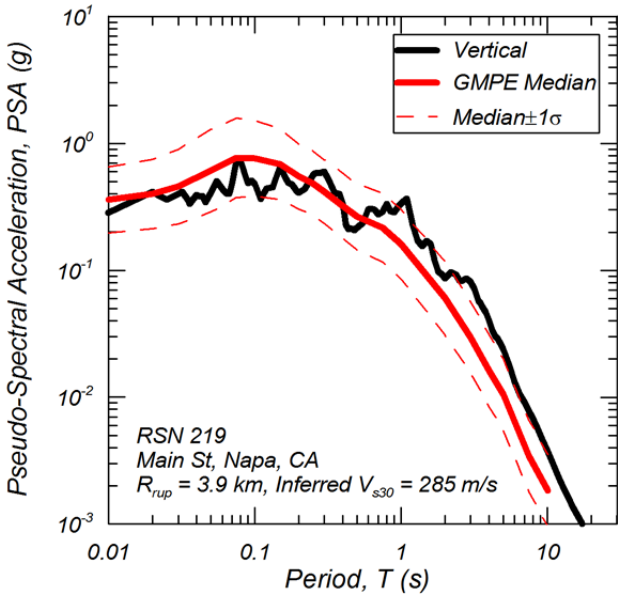

(g) Main St. Napa

Figure 8 Vertical acceleration resposne spectra compared to Bozorgnia and Campbell [2014].

Horizontal PSA for all the stations were compared to the predicted median values obtained by taking the geometric mean of ASK14, BSSA14, CB14, and CY14. Figure 9 shows the comparison of PGA, PSA at T=0.2 sec [PSA(0.2)], PSA at T=1.0 sec [PSA(1.0)], and PSA at T=3.0 sec [PSA(3.0)] against R_{rup} where V_{s30} of 490 m/sec is used in GMPEs. The PSA of the records were adjusted to a reference V_{s30} of 490 m/sec by V_{s30} scaling to these records. The figures show that PGA and PSA(0.2) are reasonably predicted within R_{rup} of 10 km, whereas PSA(1.0) is underpredicted for this range. At distances greater than about 10 km, the median GMPE tends to overpredict PGA and spectral values at 0.2 and 1.0 sec.

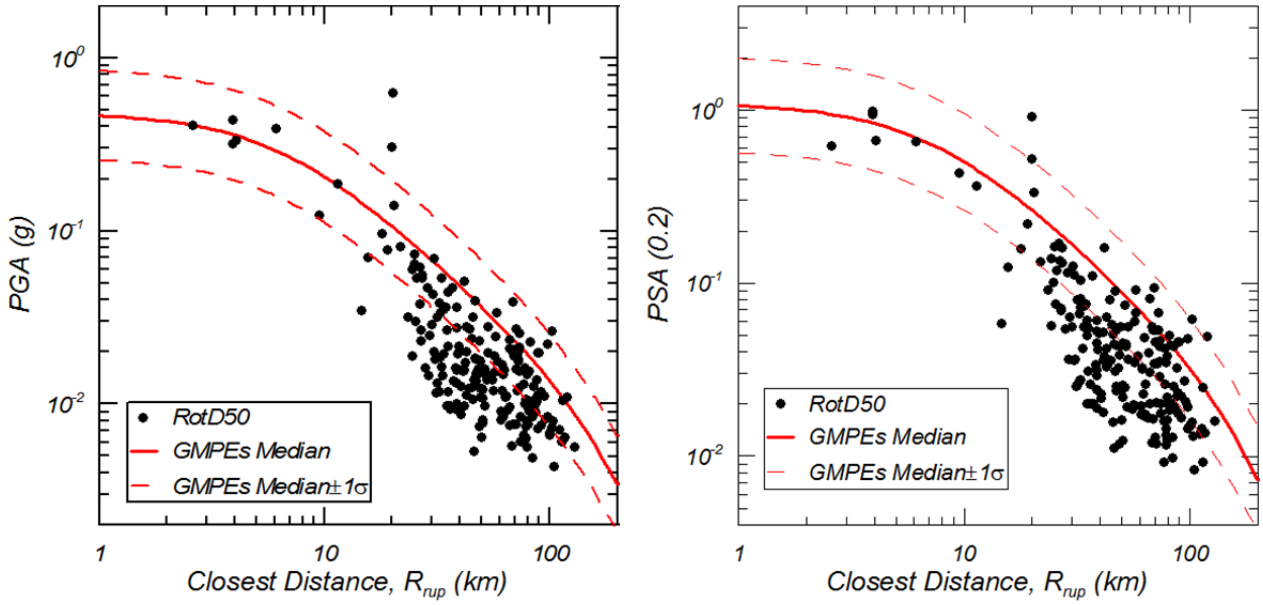

(a) PGA

(b) PSA (0.2)

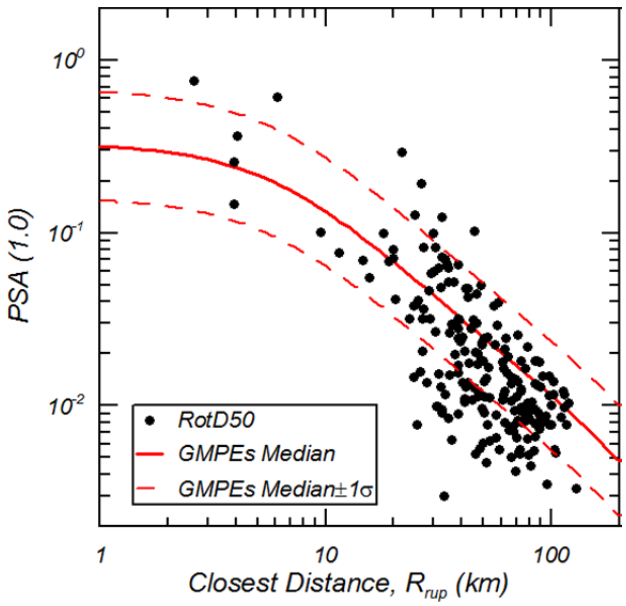

(c) PSA(1.0)

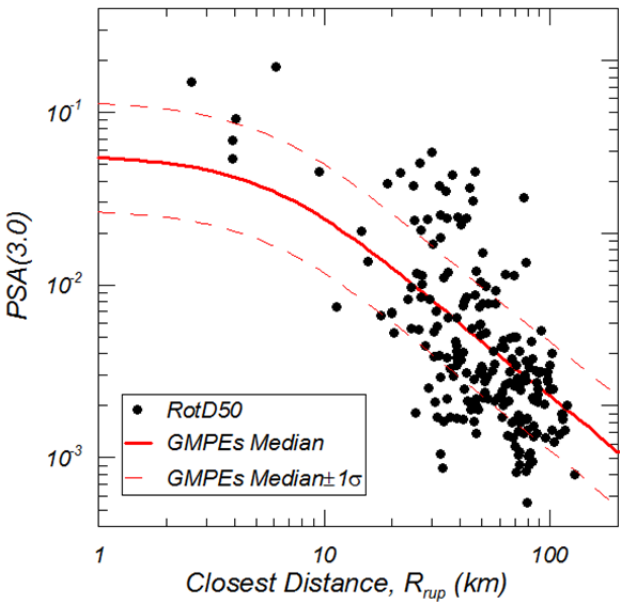

(d) PSA (3.0)

Figure 9 Comparison of horizontal PSA (RotD50) with GMPEs against R_{rup}.

Figure 10 shows the within-event residuals of PGA, PSA(0.2), PSA(1.0), and PSA(3.0) against R_{rup} after subtracting the event terms from the residuals. Event terms were computed for R_{rup} less than 50 km. The figures show that the event terms are negative for all parameters, indicating that the ground shaking was lower than the median predicted by the GMPEs.

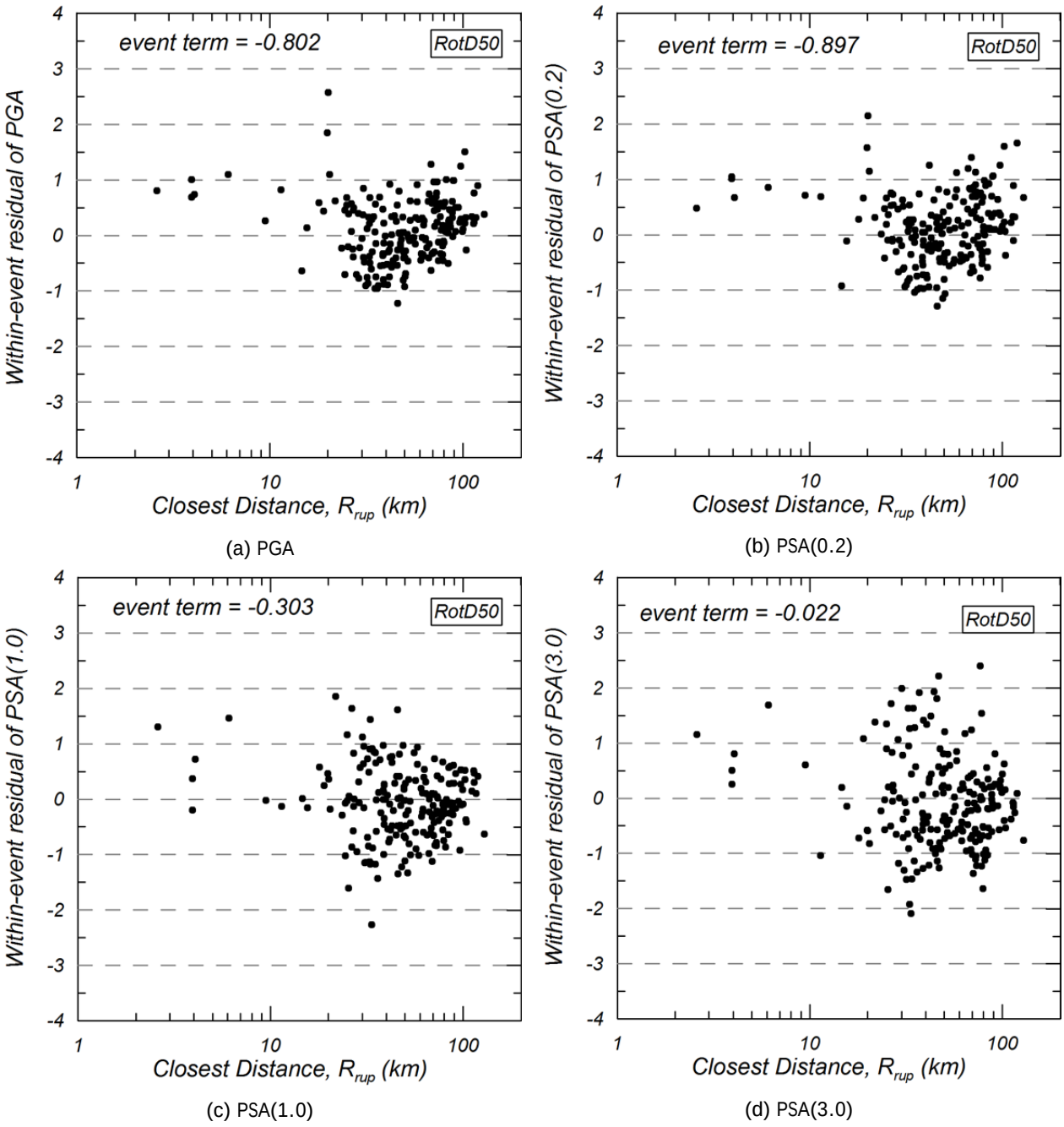

Figure 10 Within-event residuals of horizontal PSA (RotD50) with GMPEs against R_{rup} (event term was computed for stations within R_{rup} of 50 km.).

Vertical PSA were compared to the predicted values obtained by Bozorgnia and Campbell [2014]. Figure 11 shows the comparison of PGA, PSA(0.2), PSA(1.0), and PSA(3.0) against R_{rup} where V_{s30} of 490 m/sec is used in the GMPE. The PSA of the records were also adjusted to a V_{s30} of 490 m/sec, as was done for the horizontal records. The comparison shows that PSA are reasonably estimated within R_{rup} of 10 km, even though it shows a slight underprediction for PSA(1.0) and PSA(3.0).

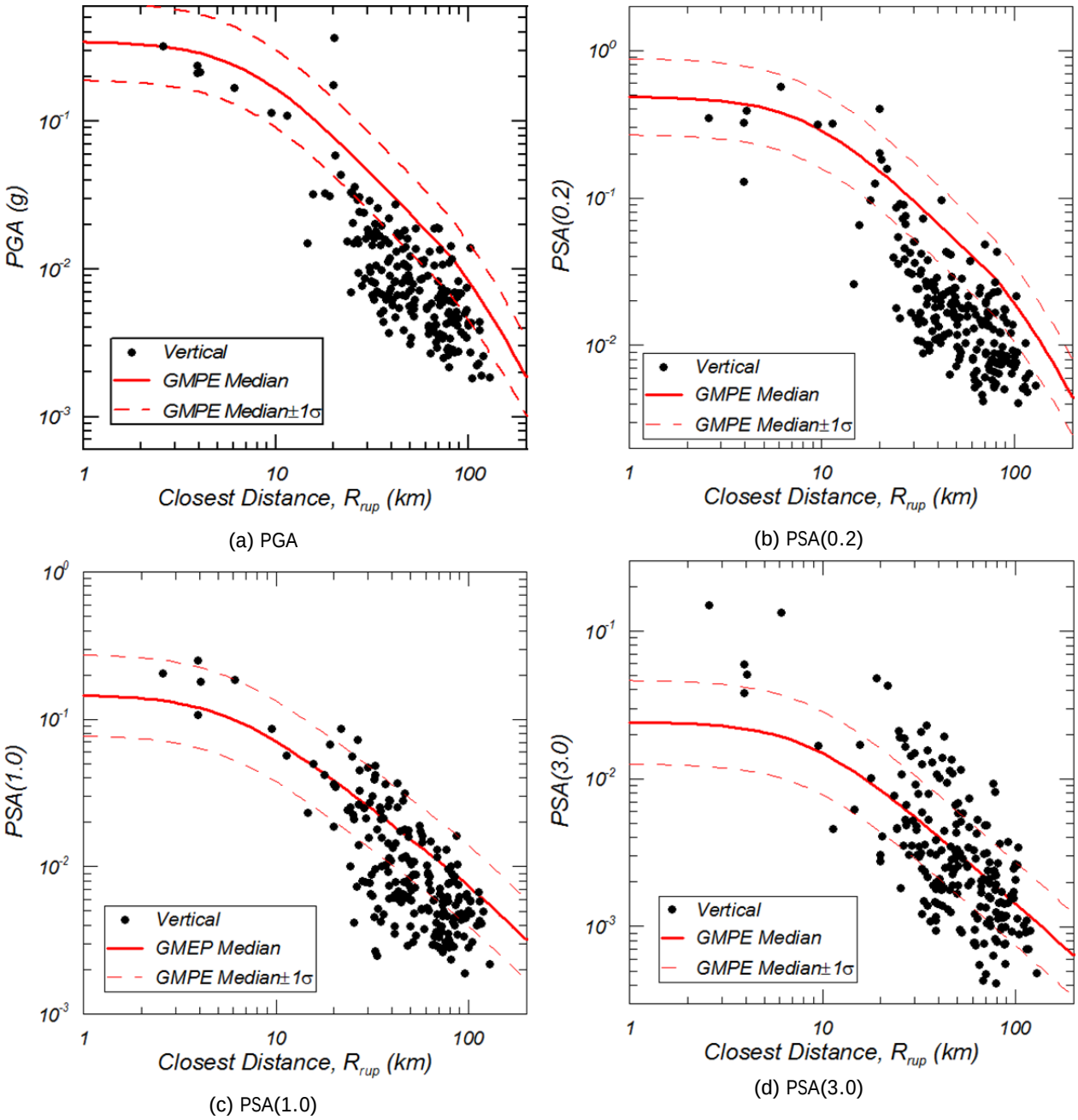

(a) PGA

(b) PSA(0.2)

(c) PSA(1.0)

(d) PSA(3.0)

Figure 11 Comparison of vertical PSA with GMPE against R_{rup}.

Figure 12 shows the within-event residuals of PGA, PSA(0.2), PSA(1.0) and PSA(3.0) against R_{rup} after subtracting the event term from the residuals. Event terms were computed for R_{rup} less than 50 km. The figures show that the event terms are negative for all PSA, indicating that the ground shaking was lower than the median values predicted by the GMPE.

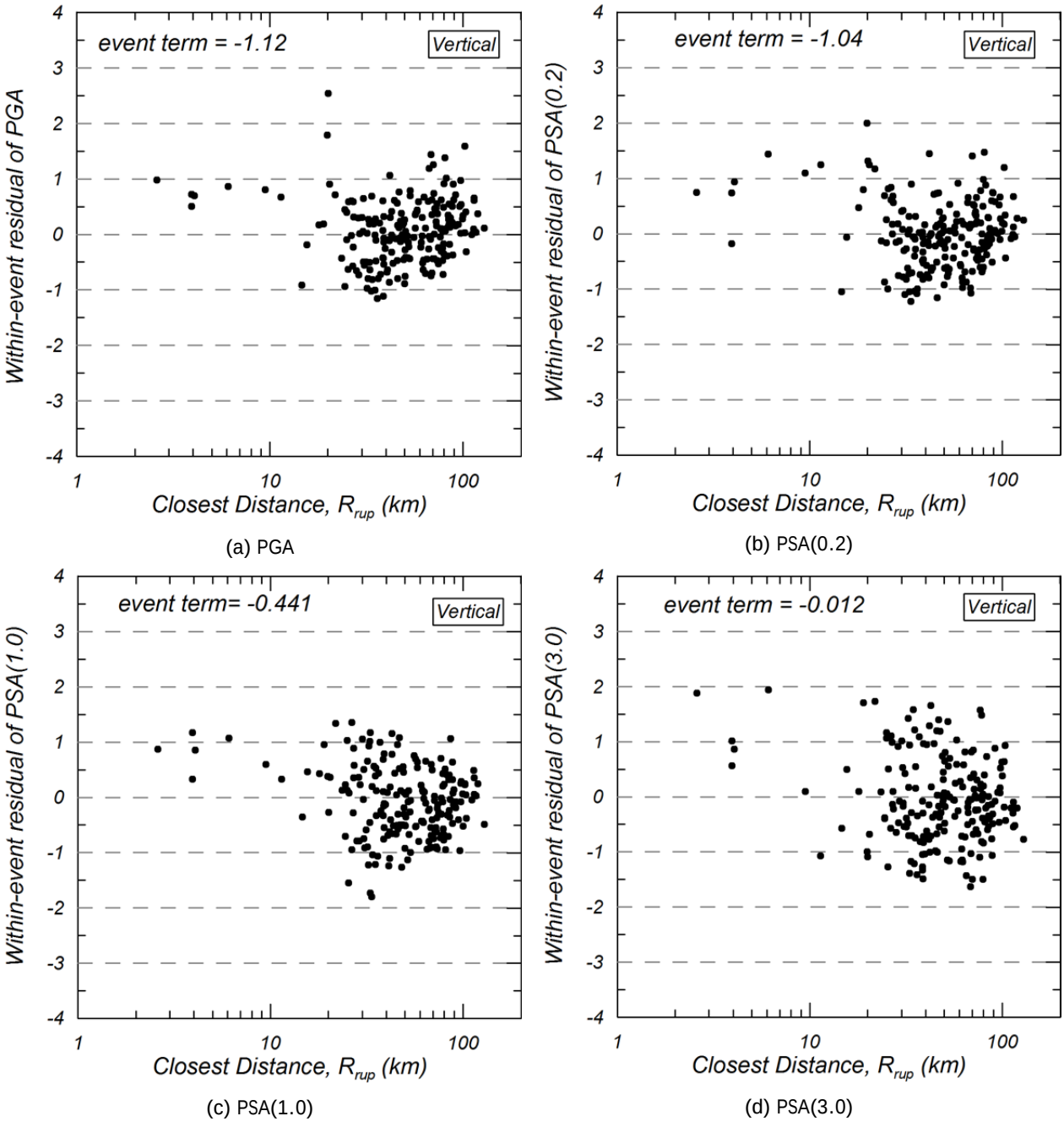

(a) PGA (b) PSA(0.2)

(c) PSA(1.0) (d) PSA(3.0)

Figure 12 Within-event residuals of vertical PSA with GMPE against R_{rup} (event term was computed within R_{rup} of 50 km).

1.5 COMPARISON OF RECORD RESPONSE SPECTRA AND CODE-BASED DESIGN SPECTRA

In this section, the 5% damped acceleration response spectra of the recorded ground motions are compared to the various code-based design spectra. Two sets of plots are presented. The first set directly compares the three recorded components with the code spectra. The second set compares the processed spectra with the code-based spectra; this comparison is for design purposes with respect to certain ground motion selection requirements documented in ASCE 7-10. In addition, the pseudo-spectral acceleration, Uniform Hazard Response Spectra (UHRS), and displacement spectra for different return periods are presented for Napa College, Napa Main St., Napa Fire Station No. 3, and the surface recording from the Vallejo–Hwy 37 Geotechnical Array. Similar plots for the other stations listed in Table 1 are presented in Appendix C. All the spectra presented in this section correspond to a 5% damping ratio.

1.5.1 DESIGN SPECTRA

The design spectra for buildings were constructed based on ASCE 7-10, Chapter 11, while the Caltrans Seismic Design Criteria, Appendix B (version 1.7, 2013), was used to construct the design spectra for bridges, such as the Highway 37/Napa Valley Bridge.

1.5.1.1 ASCE 7-10 Design Spectra for Buildings

The site class for each station is determined based on the V_{s30} value, as discussed in Section 1.4.1. The risk-targeted mapped acceleration parameters, such as S_{d1}, S_{ds}, S_{m1}, and S_{ms}, were obtained using the USGS Seismic Design Maps online tool: *http://earthquake.usgs.gov/designmaps/us/application.php*. With those values, the design spectra for Design Based Earthquake (DBE) and Maximum Considered Earthquake (MCE) were constructed for different period ranges. The period range is 0–3.0 sec for all spectra plotted in this chapter since this range covers almost all fundamental periods for structures in built-up areas in Napa.

1.5.1.2 Caltrans Design Spectra for Bridges

The Caltrans design spectrum was based on the envelope of a deterministic and probabilistic spectrum for each location. The deterministic spectrum was calculated as the arithmetic average of the median response spectra calculated using CB08, CY08, and the probabilistic spectrum was obtained from the USGS Seismic Hazard Map [Petersen et al. 2008] for the 5% in 50-year probability of exceedance (975-year return period), taking into account of the spectrum adjustment factors such as near-fault effects, basin effects, etc. Site specific analyses are also required if the soil profile includes soft clay deposits

1.5.2 RESULTANT SPECTRA

The Square Root Sum of Squares (SRSS) of the two horizontal components was calculated for each recording station. Additional resultants, such as the RotD50 (median rotated component) and rotD100 (maximum rotated direction component), were also calculated [Boore 2010].

1.5.3 UNIFORM HAZARD RESPONSE SPECTRA

Another set of plots comparing the median-rotated component and UHRS for different hazard levels are also included. The UHRS for selected station were constructed from the USGS online tool: *http://geohazards.usgs.gov/hazardtool/application.php*.

Station Name: Napa College
V_{s30}(m/sec): 339
Soil Type: D
PGA: 0.344*g*

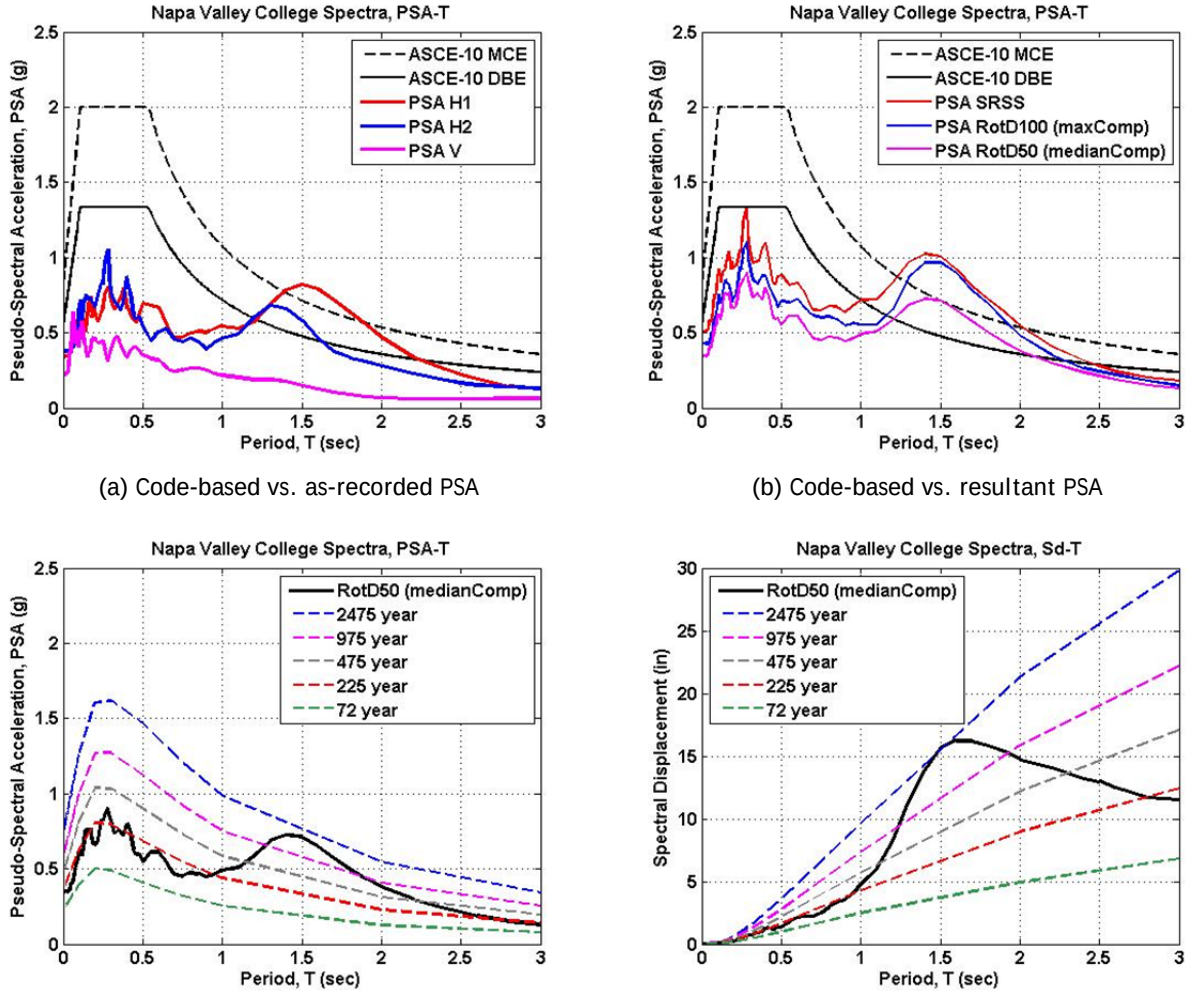

(a) Code-based vs. as-recorded PSA

(b) Code-based vs. resultant PSA

(c) UHRS vs. median component PSA

(d) UHRS vs. median component Sd

Figure 13 Spectra comparison for Napa Valley College.

Station Name: Napa Main St.
V_{s30} (m/sec): 285
Soil Type: D
PGA: 0.445*g*

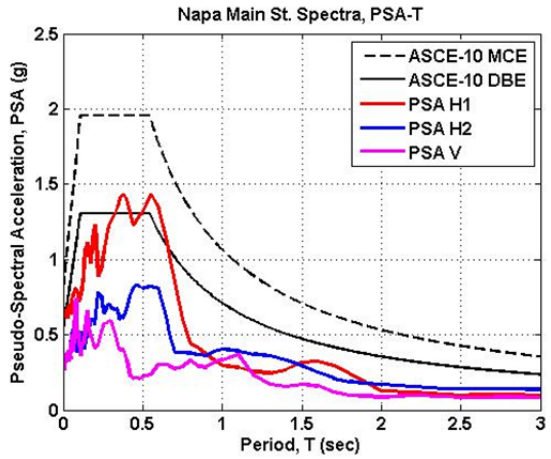

(a) Code-based vs. as-recorded PSA

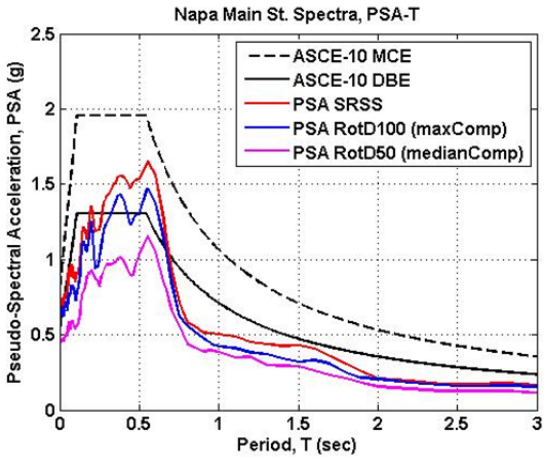

(b) Code-based vs. resultant PSA

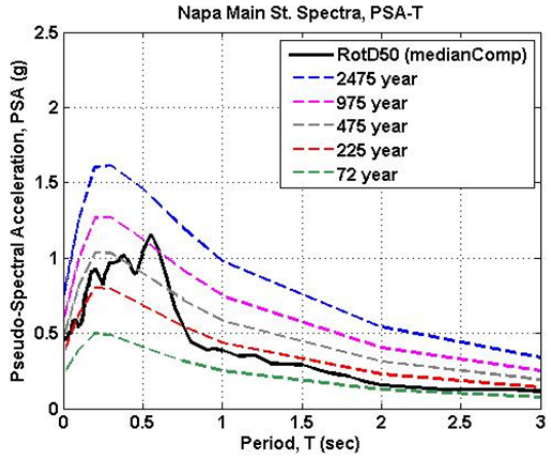

(c) UHRS vs. median component PSA

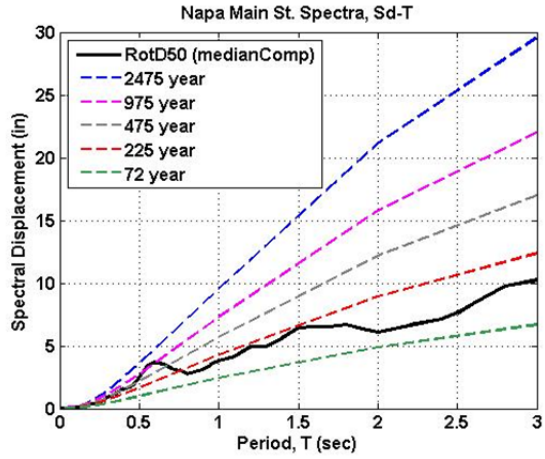

(d) UHRS vs. median component Sd

Figure 14 Spectra comparison for Napa Main St.

Station Name: Napa Fire Station No. 3.
V_{s30} (m/sec): 332
Soil Type: D
PGA: 0.346*g*

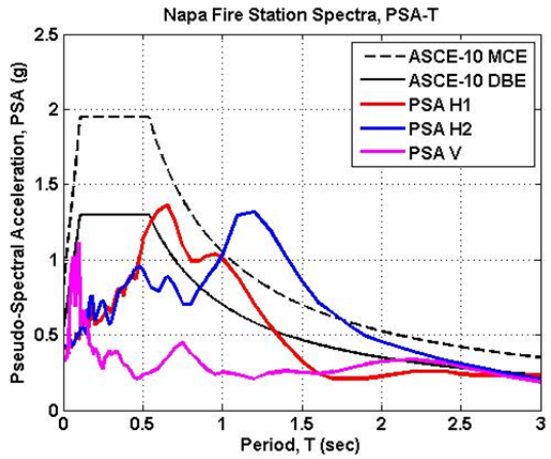

(a) Code-based vs. as-recorded PSA

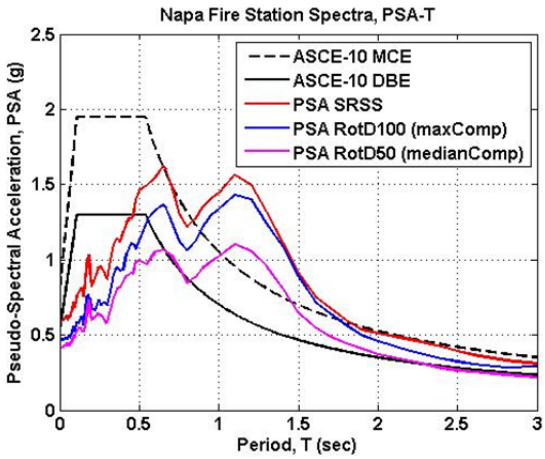

(b) Code-based vs. resultant PSA

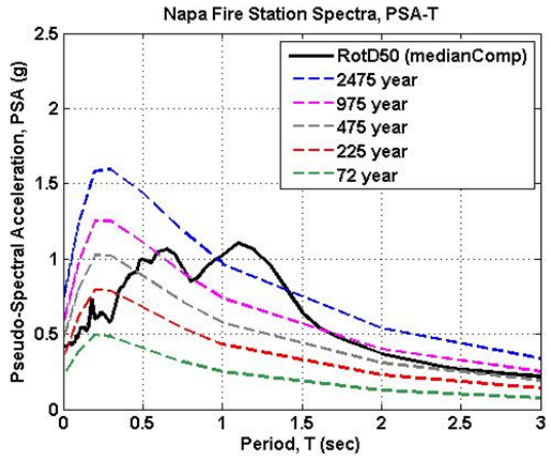

(c) UHRS vs. median component PSA

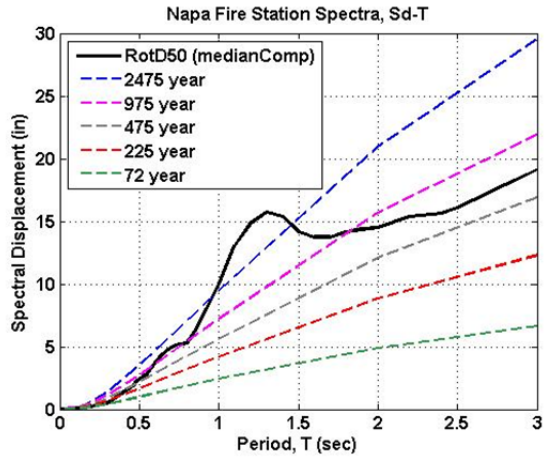

(d) UHRS vs. median component Sd

Figure 15 Spectra comparison for Napa Fire Station No. 3.

Station Name: Vallejo - Hwy 37/Napa River E Geotech Array (0m)
Vs30 (m/sec): 509
Soil Type: C
PGA: 0.198*g*

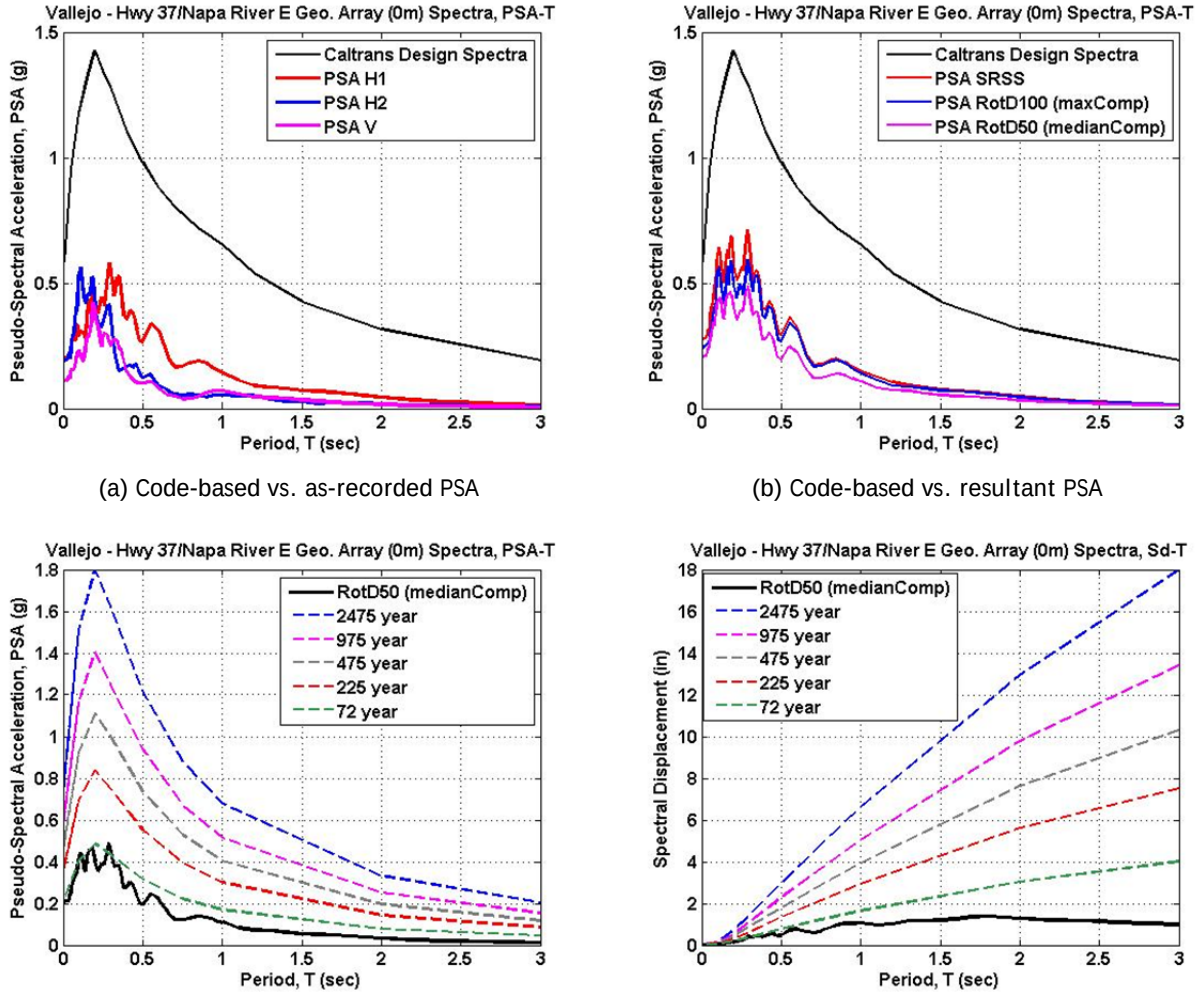

(a) Code-based vs. as-recorded PSA

(b) Code-based vs. resultant PSA

(c) UHRS vs. median component PSA

(d) UHRS vs. median component Sd

Figure 16 Spectra comparison for Vallejo-Hwy 37/Napa River E Geotech Array (0m).

1.6 SUMMARY OF GROUND MOTION OBSERVATION

This report summarizes a preliminary study on the characteristics of the strong-motion recordings from the South Napa earthquake of August 24th, 2014. The strong-motion data were downloaded from CESMD website and processed following the PEER standard data-processing methodology. Associated metadata such as source-to-site distances and estimated site parameters such as V_{s30} were estimated following the approached developed in the PEER NGA-West2 study. Strong ground motions were observed within Napa Valley where PGA values greater than 0.3*g* were recorded.

Velocity pulses were observed near the fault for which five time series were examined by using the approaches by Hayden et al. [2014] and Shahi [2013]. The results show that these records were classified as pulse-type motions in the near-fault region even though a discrepancy between these approaches exists for the Main St. Napa and Napa College stations.

Four near-fault ground motions were similarly characterized using the proposed method by Lu and Panagiotou [2014] (Napa Fire Station No. 3, Napa Main St., fault-normal and fault-parallel directions). Analyses showed that each of the records includes more than one strong long-period pulse with the predominant period (TP) of the multiple pulses to differ significantly. The TP of the long-period pulses ranged between 0.8 and 3.9 sec. All four ground motions, included two strong long-period pulses of significantly different TP that were well correlated in the time domain. All motions also included strong short-period pulses (TP < 0.6 sec).

High-frequency spikes were observed in the records at Carquinez Bridge Geotechnical Array #1, which reached approximately 1.0*g* for the NS component. These spikes were investigated by comparing the acceleration time series at several stations along the path from the epicenter to the sites and the downhole array records. These spikes were observed in the *S*-wave portion of the records based on visual inspection. Acceleration time series along the source to site travel path shows the similar spikes at the recordings at Napa College, Vallejo–Hwy 37/Napa River East Geotechnical Array, and Carquinez Bridge Geotechnical Arrays #1 and #2. This suggests that the spikes could be a result of path effects. The spikes increase in amplitude from Vallejo–Hwy 37/Napa River East Geotechnical Array to Carquinez Bridge Geotechnical Array #1. Downhole records show that two high-frequency spikes are observed in the *S*-wave portion of the waveform from a depth below 100 m to the surface. This observation may indicate that the large PGA observed at Carquinez Bridge Geotechnical Array #1 could also be the result of site amplification through the soft soil deposits. However, these observations do not exclude the possibility of soil-structure interaction effects on the measured recordings. Further investigation is recommended to study the observed high-frequency content near the Carquinez Bridge.

The pseudo-spectral accelerations (5% damped) from the recorded ground motions were compared to the recent NGA-West2 GMPEs for PGA, 0.2, 1.0 and 3.0 sec. The comparison shows generally a good agreement for both of horizontal and vertical components near the fault with the exception of the large high-frequency motions observed near the Carquinez Bridge.

Recorded ground motions were also compared to the code-based design spectra. The comparison shows that the pseudo-spectral accelerations recorded at Napa College and Napa Fire Station No. 3 exceeded the MCE design spectra at a period around 1.5 sec near the fault. This observation is

related to the near-fault velocity pulses discussed in the report. The comparison also shows that the pseudo-spectral acceleration recorded at Carquinez Bridge exceeded the Caltrans design spectra for short periods. This observation is related to the amplification of high-frequency spikes discussed in the report. Further investigation is recommended to study the damage observations related to the recorded ground motions and design spectra. There needs to be more research into which pulse features may have damaging effects on elastic and inelastic systems.

1.7 REFERENCES

Abrahamson N.A., Silva W.J., Kamai R. (2014). Summary of the Abrahamson, Silva, and Kamai NGA-West2 ground-motion relations for active crustal regions, *Earthq. Spectra*, EERI, Pre-Print.

Abrahamson N.A., Atkinson G., Boore D.M., Bozorgnia Y., Campbell K.W., Chiou B.S.-J., Idriss I.M., Silva W.J., Youngs R.R. (2008). Comparisons of NGA ground-motion relations, *Earthq. Spectra*, 24(1): 45–66.

Ancheta T.D., Darragh R.B., Stewart J.P., Seyhan E., Silva W.J., Chiou B.S.-J., Wooddell K.E., Graves R.W., Kottke A.R., Boore D.M., Kishida T., Donohue J.L. (2014). PEER NGA-West2 Database, *Earthq. Spectra*, EERI, Pre-Print.

Boore D. M (2010). Orientation-independent, nongeometric-mean measures of seismic intensity from two horizontal components of motion, *Bull. Seismol. Soc. Am*., 100: 1830–1835.

Boore D.M., Stewart J.P., Seyhan E., Atkinson G.A. (2014). NGA-West2 equations for predicting response spectral accelerations for shallow crustal earthquakes, *Earthq. Spectra*, EERI, Pre-Print.

Bozorgnia Y., Campbell K.W. (2014). Vertical ground motion model using NGA-West2 database, *Earthq. Spectra*, submitted for publication.

Bray J.D., Rodriguez-Marek A., Gillie J. L. (2009). Design ground motions near active faults, *Bull. NZ. Soc. Earthq. Eng.*, 42(1), 8 pgs.

Campbell K.W., Bozorgnia Y. (2008). NGA ground motion model for the geometric mean horizontal component of PGA, PGV, PGD and 5% damped linear elastic response spectra for periods ranging from 0.01 to 10s, *Earthq. Spectra*, 24(1): 139–171.

Campbell K.W., Bozorgnia Y. (2014). Campbell-Bozorgnia NGA-West2 ground motion model for the average horizontal components of PGA, PGV, and 5%-damped linear response spectra, *Earthq. Spectra*, EERI, Pre-Print.

Chiou B. S.-J., Youngs R. R. (2008). An NGA model for the average horizontal component of peak ground motion and response spectra, *Earthq. Spectra*, 24(1): 173–215.

Chiou B.S.-J., Youngs R. R. (2014). Update of the Chiou and Youngs NGA ground motion model for average horizontal component of peak ground motion and response spectra, *Earthq. Spectra*, EERI, Pre-Print.

Hayden C.P., Bray J.D., Abrahamson N.A. (2014). Selection of near-fault pulse motions, *J. Geotech. Geoenviron. Eng*., 140(7): 04014030.

Lu Y., Panagiotou M. (2014). Characterization and representation of near-fault ground motions using cumulative pulse extraction with wavelet analysis, *Bull. Seismol. Soc. Am*., 104: 410–426.

Petersen M.D., Frankel A. D., Harmsen S. C., Mueller C. S., Haller K. M., Wheeler R. L., Wesson R.L.,, Zeng Y., Boyd O. S., Perkins D. M., Luco N., Field E. H., Wills C. J., Rukstales K. S. (2008). Documentation for the 2008 update of the United States National Seismic Hazard Maps, United States Geological Survey, *USGS Open-File Report 2008–1128*, Washington, D.C.

Shahi S. (2013). *A Probabilistic Framework to Include the Effects of Near-Fault Directivity in Seismic Hazard Assessment*, Ph.D. Thesis, Department of Civil and Environmental Engineering, Stanford University, Stanford, CA.

APPENDIX A VELOCITY RECORDS CORRESPONDING TO THE COMPONENT OF MAXIMUM PEAK-TO-PEAK VELOCITY PULSE CLASSIFICATION SCHEMES

A.1 FROM HAYDEN ET AL. [2014] *

Table 1 Estimation of PGV and T_v using Bray et al. [2009] empirical relationship.

Station Name	R_{rup}[1] (km)	PGV RotD50 (cm/sec)	PGV[2] Median (cm/sec)	PGV $-\sigma_{total}$ (cm/sec)	PGV $+\sigma_{total}$ (cm/sec)	T_v[3] Median (sec)	T_v $-\sigma_{total}$ (sec)	T_v $+\sigma_{total}$ (sec)
Fire Station No. 3	1.8	80	62	40	96	1.2	0.7	2.0
Huichica Creek	4.2	43	53	34	82	1.2	0.7	2.0
Lovall Valley Loop Rd.	5.1	46	49	32	76	1.2	0.7	2.0
Main St. Napa	4.9	42	50	32	80	1.2	0.7	2.0
Napa College	4.5	56	51	33	80	1.2	0.7	2.0

[1] R_{rup} is closest distance between station and rupture plane

[2] PGV = Peak ground velocity

[3] Tv = Pulse period

* Note that all records have a low-pass, three-pole, causal Butterworth filter applied to the record (see Hayden et al. [2014]).

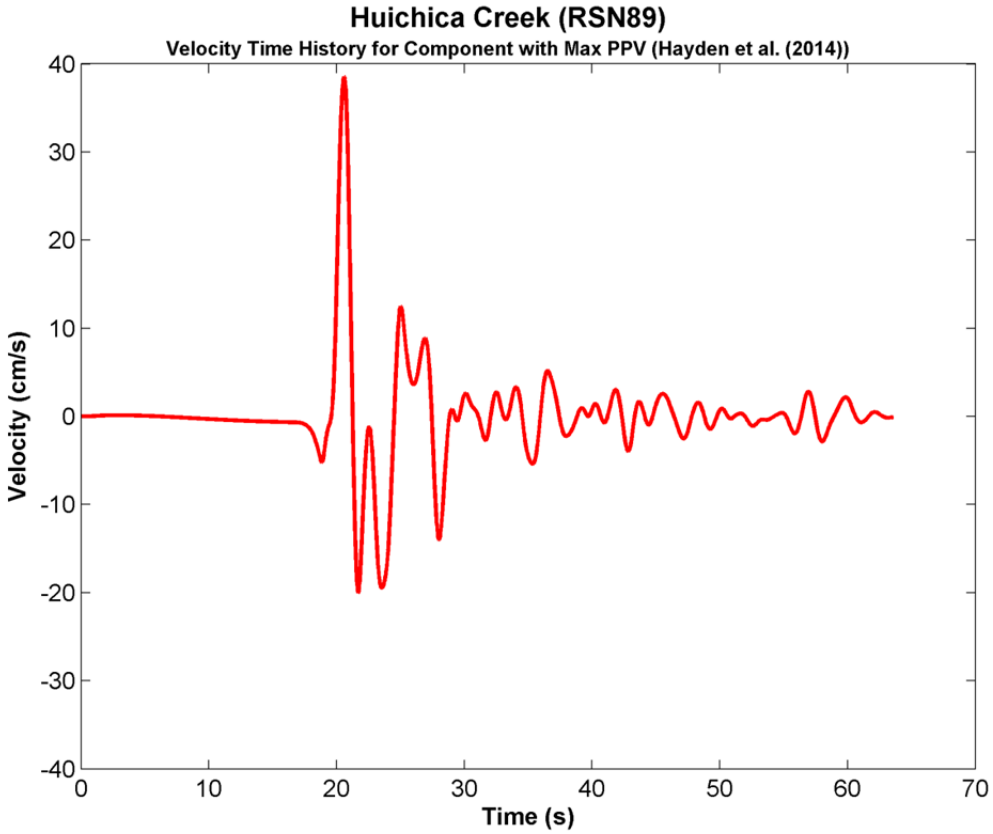
Huichica Creek (RSN89)
Velocity Time History for Component with Max PPV (Hayden et al. (2014))
Velocity (cm/s)
Time (s)
40
30
20
10
0
-10
-20
-30
-40
0
10
20
30
40
50
60
70

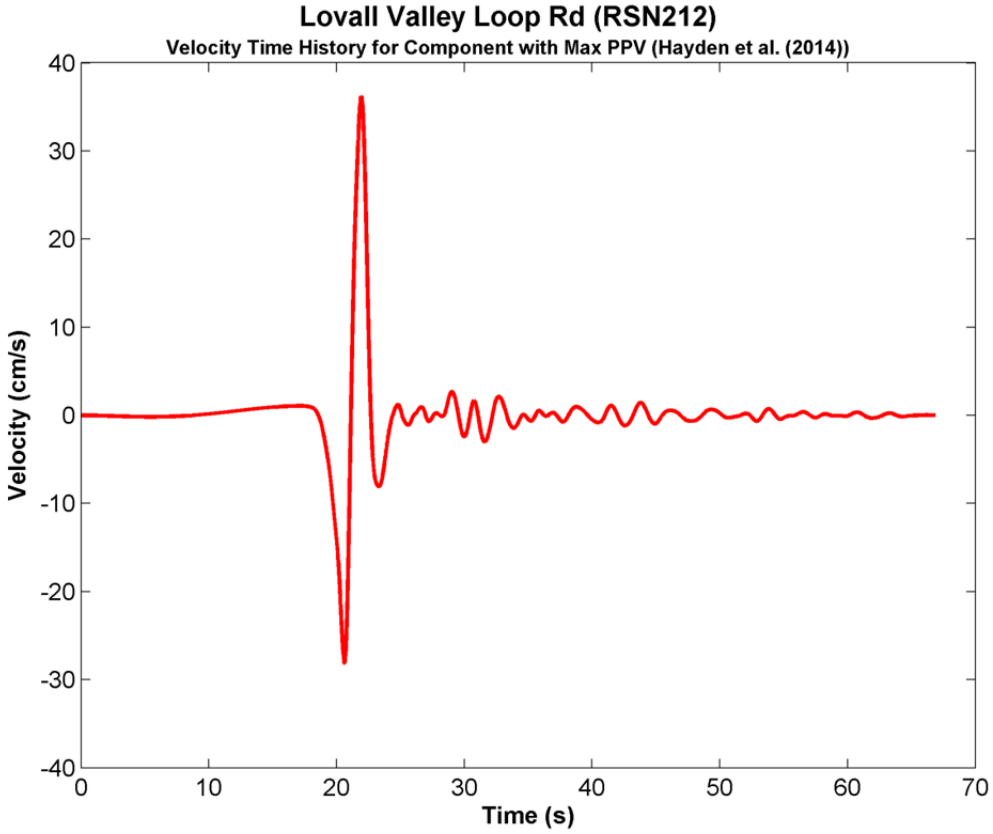
Lovall Valley Loop Rd (RSN212)
Velocity Time History for Component with Max PPV (Hayden et al. (2014))
Velocity (cm/s)
Time (s)
40
30
20
10
0
-10
-20
-30
-40
0
10
20
30
40
50
60
70

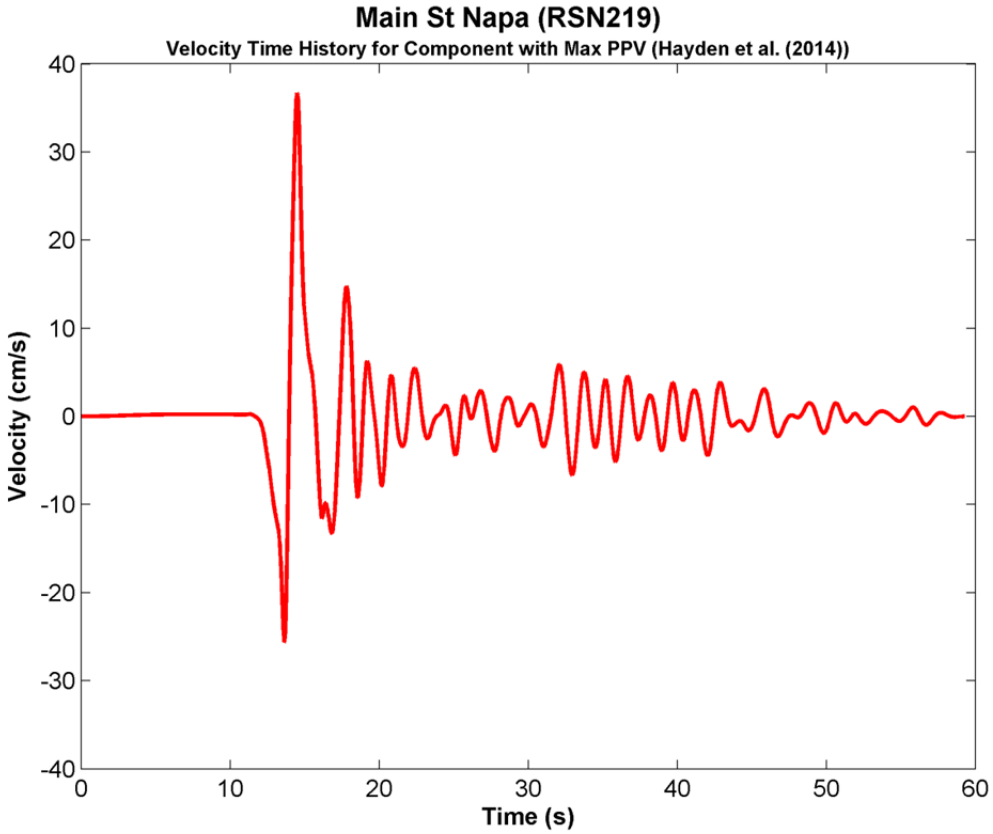
Main St Napa (RSN219)
Velocity Time History for Component with Max PPV (Hayden et al. (2014))
Velocity (cm/s)
Time (s)
40
30
20
10
0
-10
-20
-30
-40
0
10
20
30
40
50
60

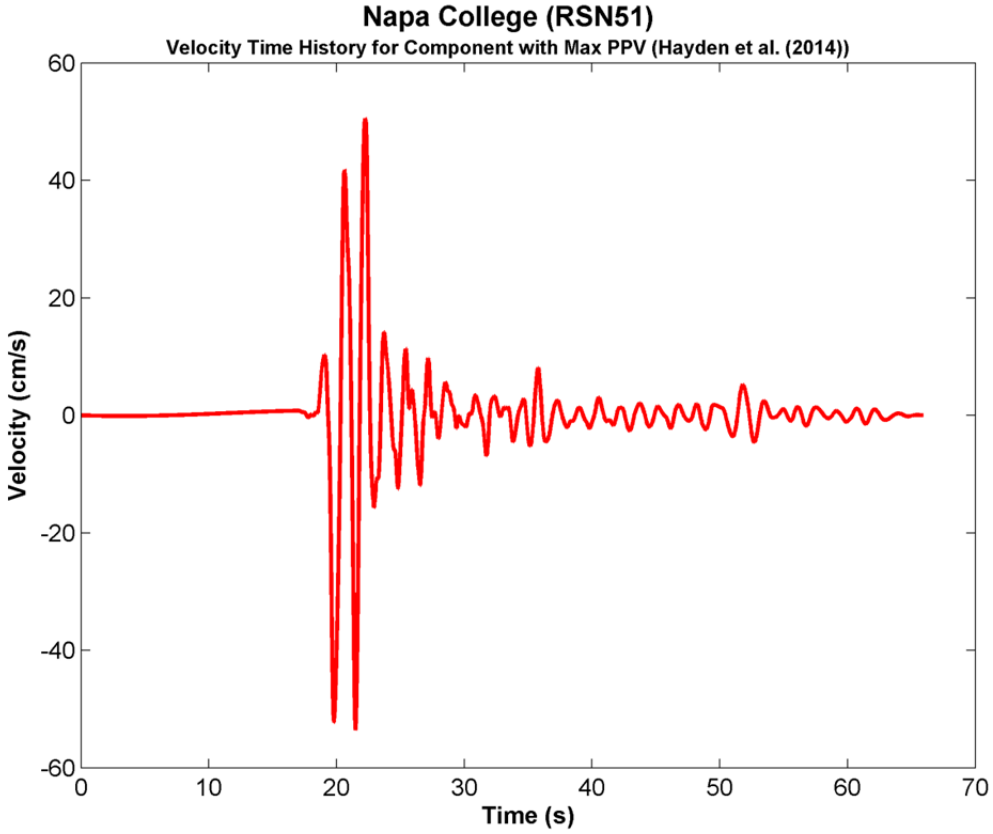
Napa College (RSN51)
Velocity Time History for Component with Max PPV (Hayden et al. (2014))
Velocity (cm/s)
Time (s)
60
40
20
0
-20
-40
-60
0
10
20
30
40
50
60
70

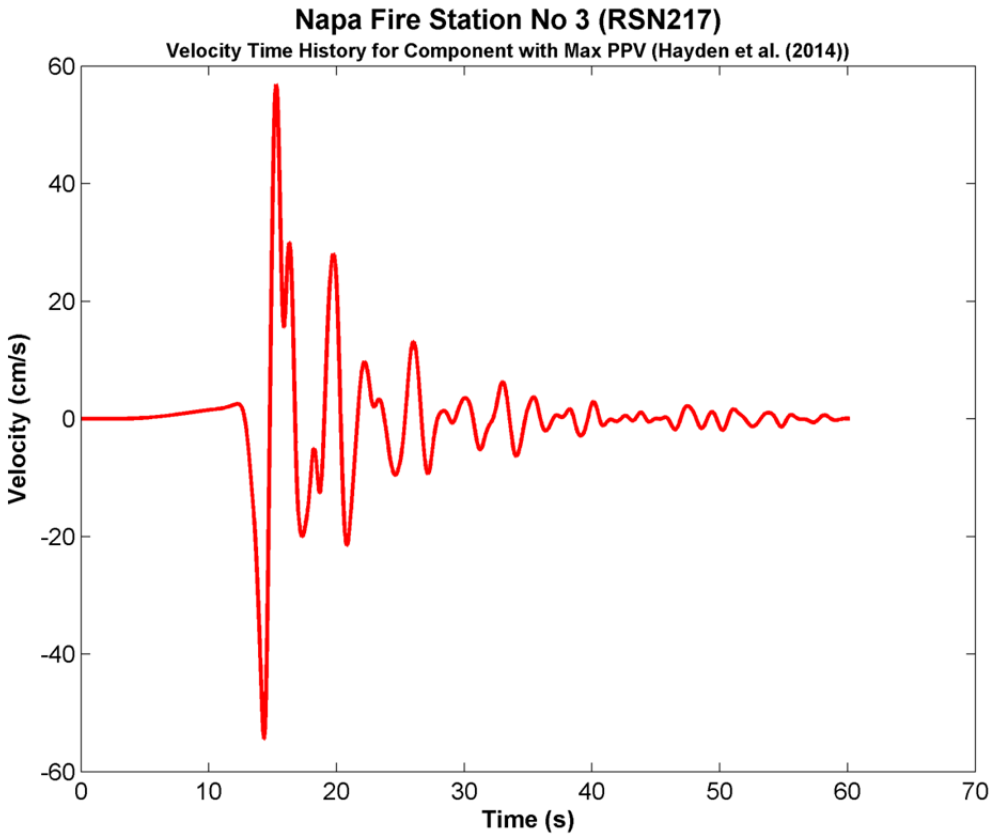
Napa Fire Station No 3 (RSN217)
Velocity Time History for Component with Max PPV (Hayden et al. (2014))
Velocity (cm/s)
Time (s)
60
40
20
0
-20
-40
-60
0
10
20
30
40
50
60
70

A.2 FROM SHAHI [2013]

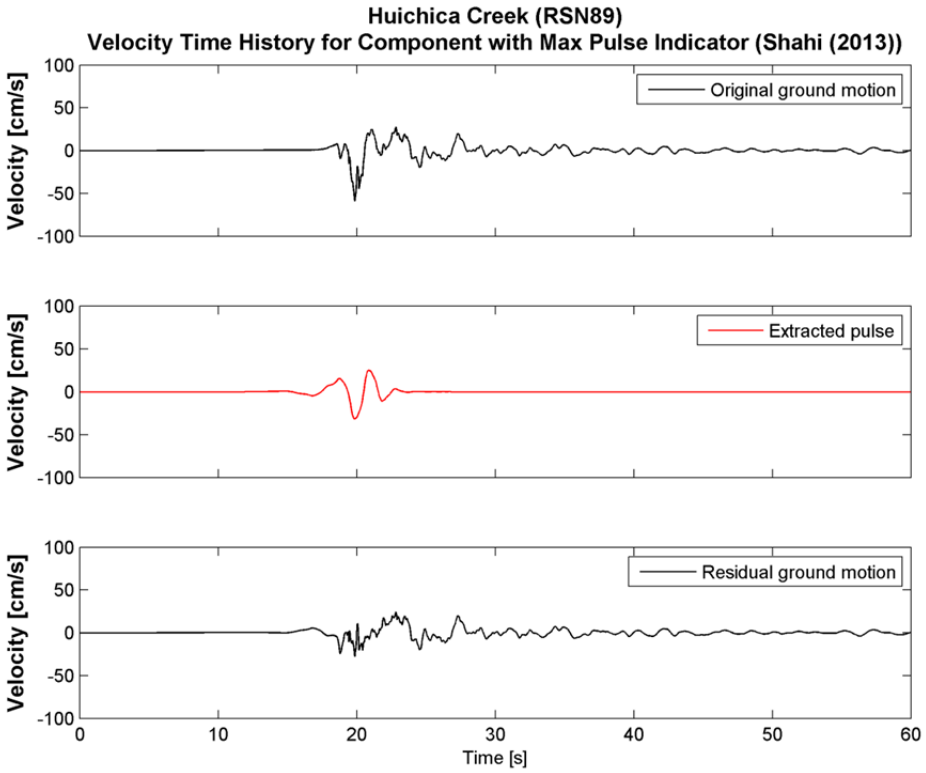

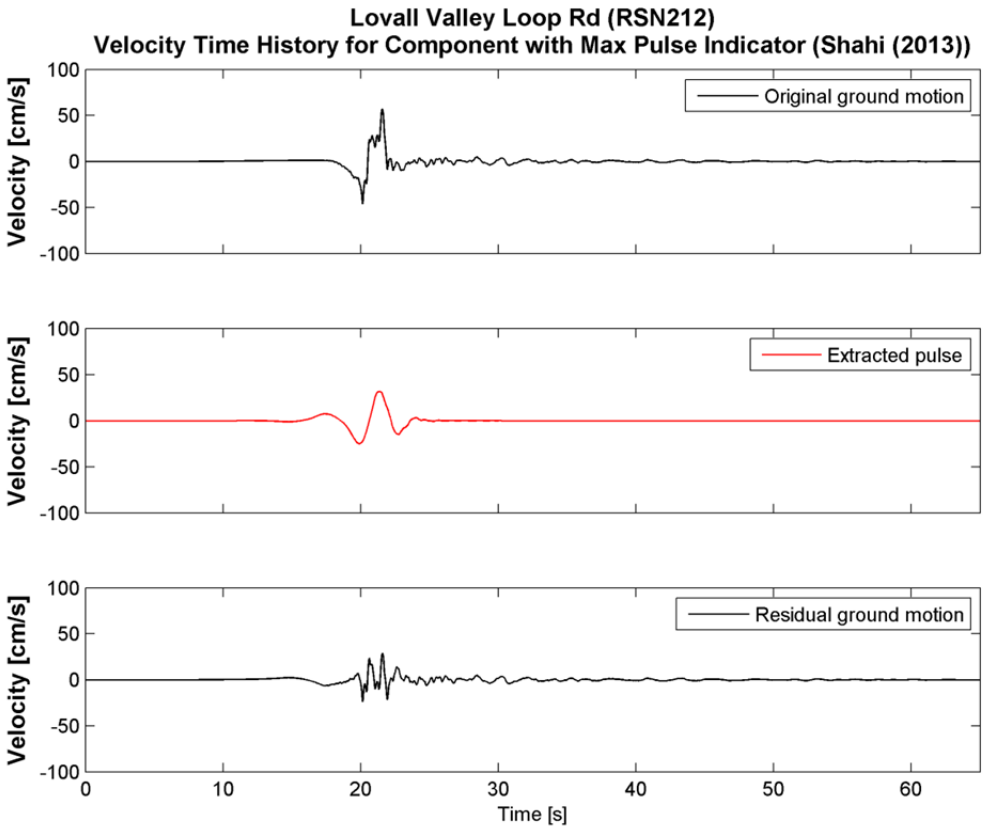

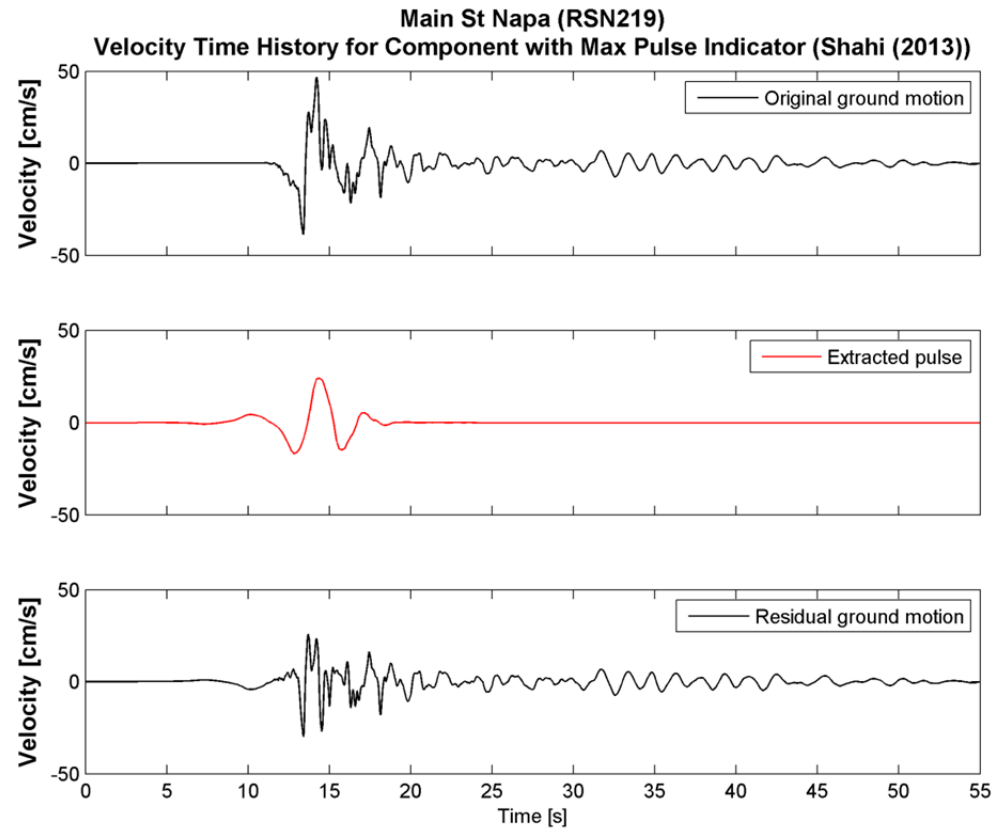
Main St Napa (RSN219)
Velocity Time History for Component with Max Pulse Indicator (Shahi (2013))
Original ground motion
Extracted pulse
Residual ground motion
Velocity [cm/s]
Time [s]

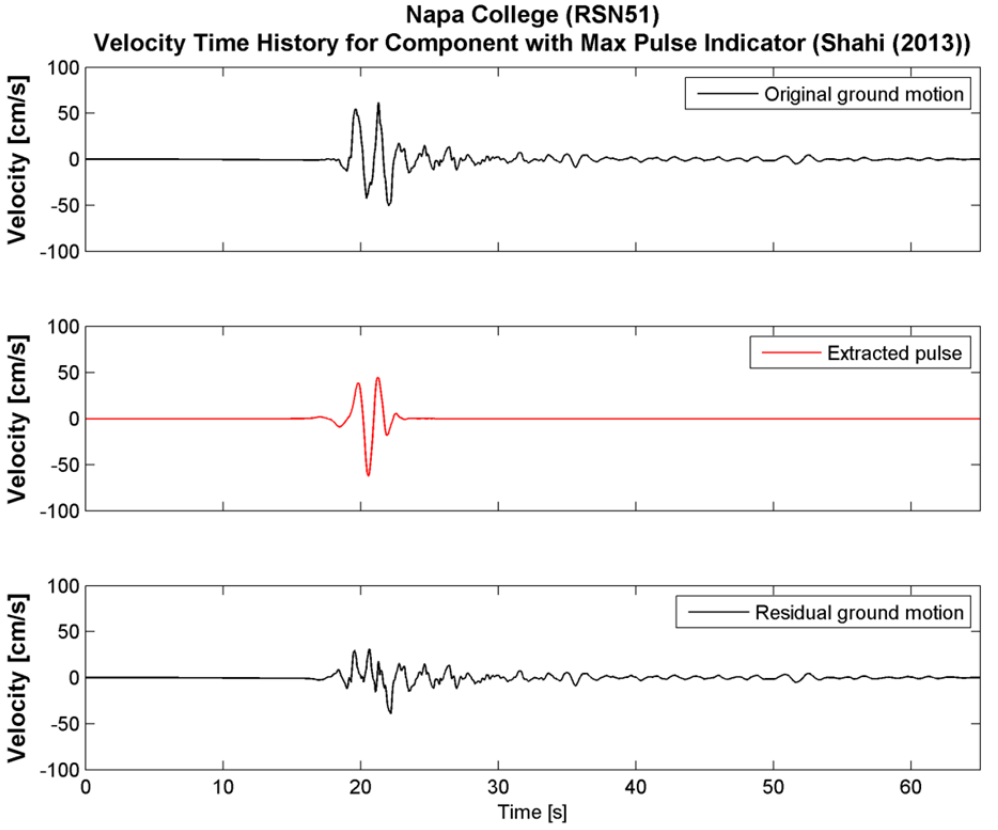
Napa College (RSN51)
Velocity Time History for Component with Max Pulse Indicator (Shahi (2013))
Original ground motion
Extracted pulse
Residual ground motion
Velocity [cm/s]
Time [s]

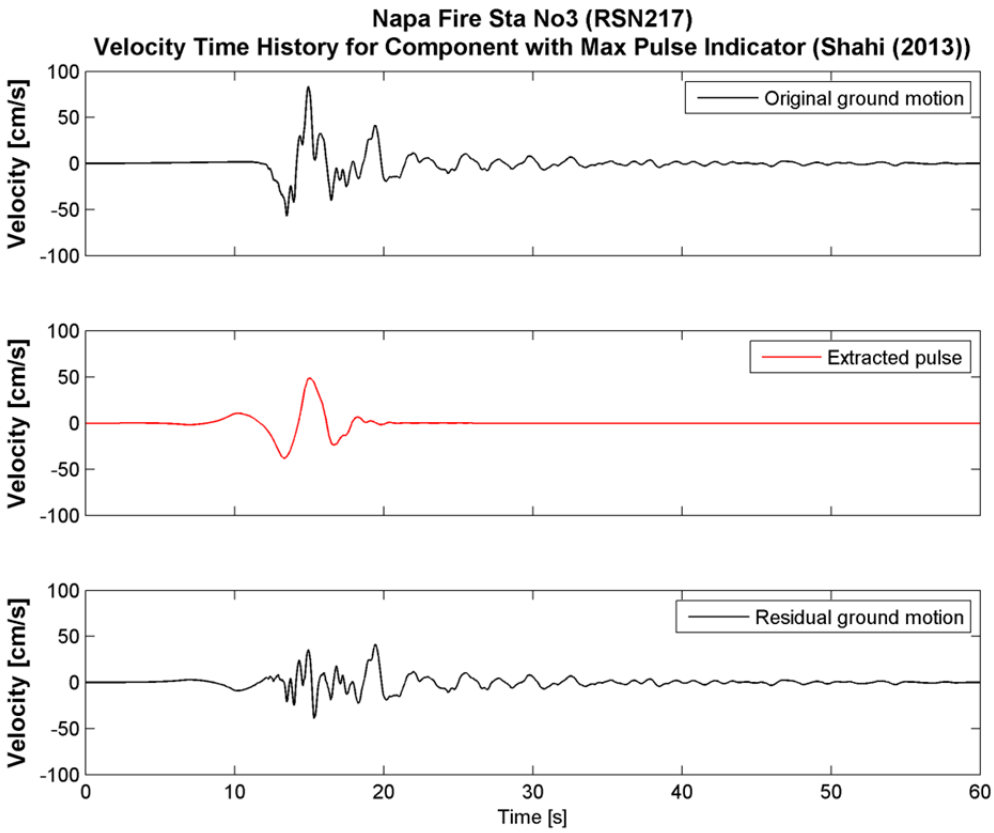
Napa Fire Sta No3 (RSN217)
Velocity Time History for Component with Max Pulse Indicator (Shahi (2013))
Original ground motion
Extracted pulse
Residual ground motion
Velocity [cm/s]
Time [s]
100
50
0
-50
-100
0
10
20
30
40
50
60

APPENDIX B ACCELERATION, VELOCITY, DISPLACEMENT TIME SERIES, PSEUDO-SPECTRAL ACCELERATION, AND FOURIER AMPLITUDE SPECTRA FOR SELECTED RECORDINGS

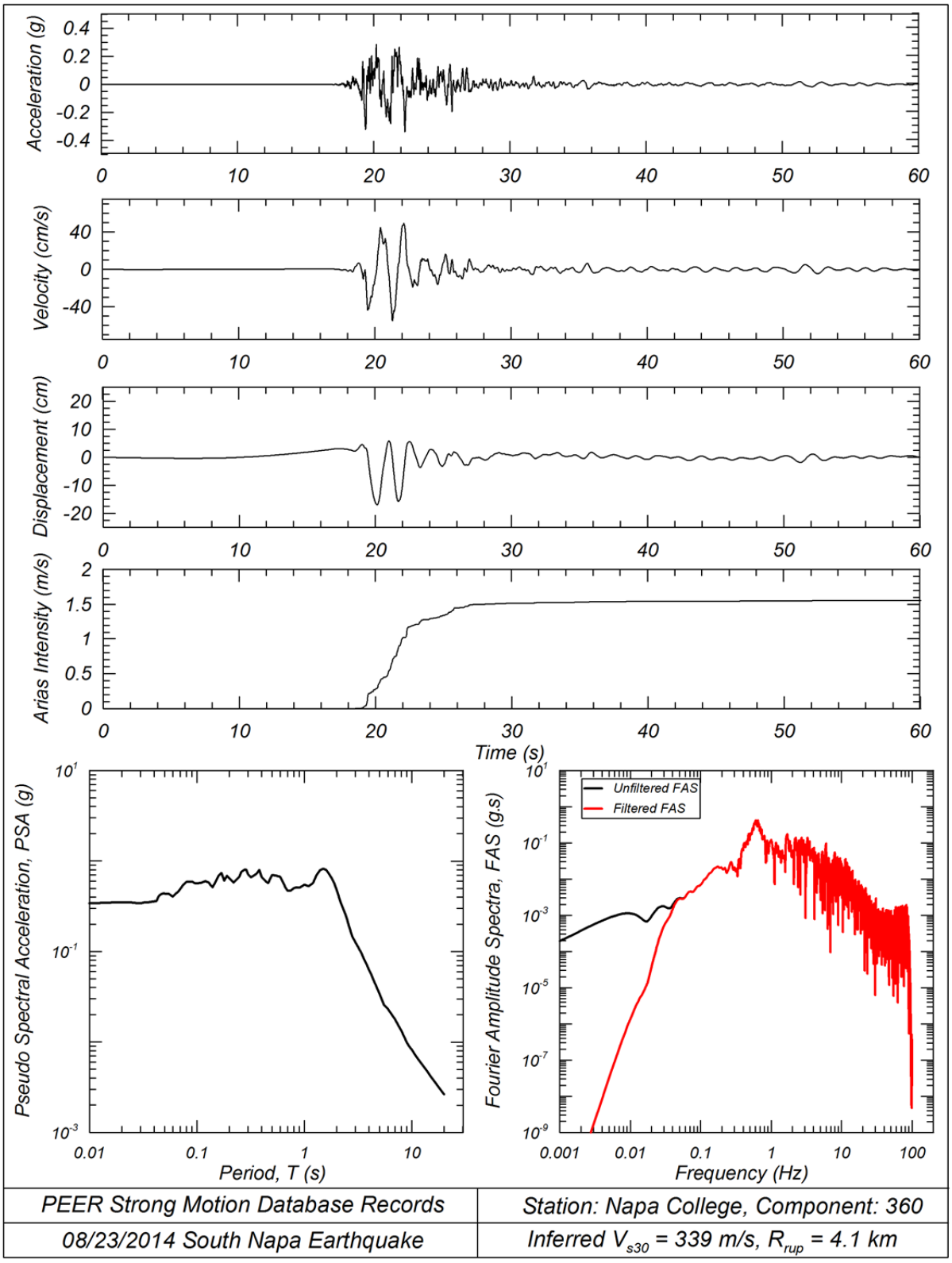
Acceleration (g)
Velocity (cm/s)
Displacement (cm)
Arias Intensity (m/s)
Time (s)
Pseudo Spectral Acceleration, PSA (g)
Period, T (s)
Fourier Amplitude Spectra, FAS (g.s)
Unfiltered FAS
Filtered FAS
Frequency (Hz)
PEER Strong Motion Database Records
Station: Napa College, Component: 360
08/23/2014 South Napa Earthquake
Inferred V_{s30} = 339 m/s, R_{rup} = 4.1 km

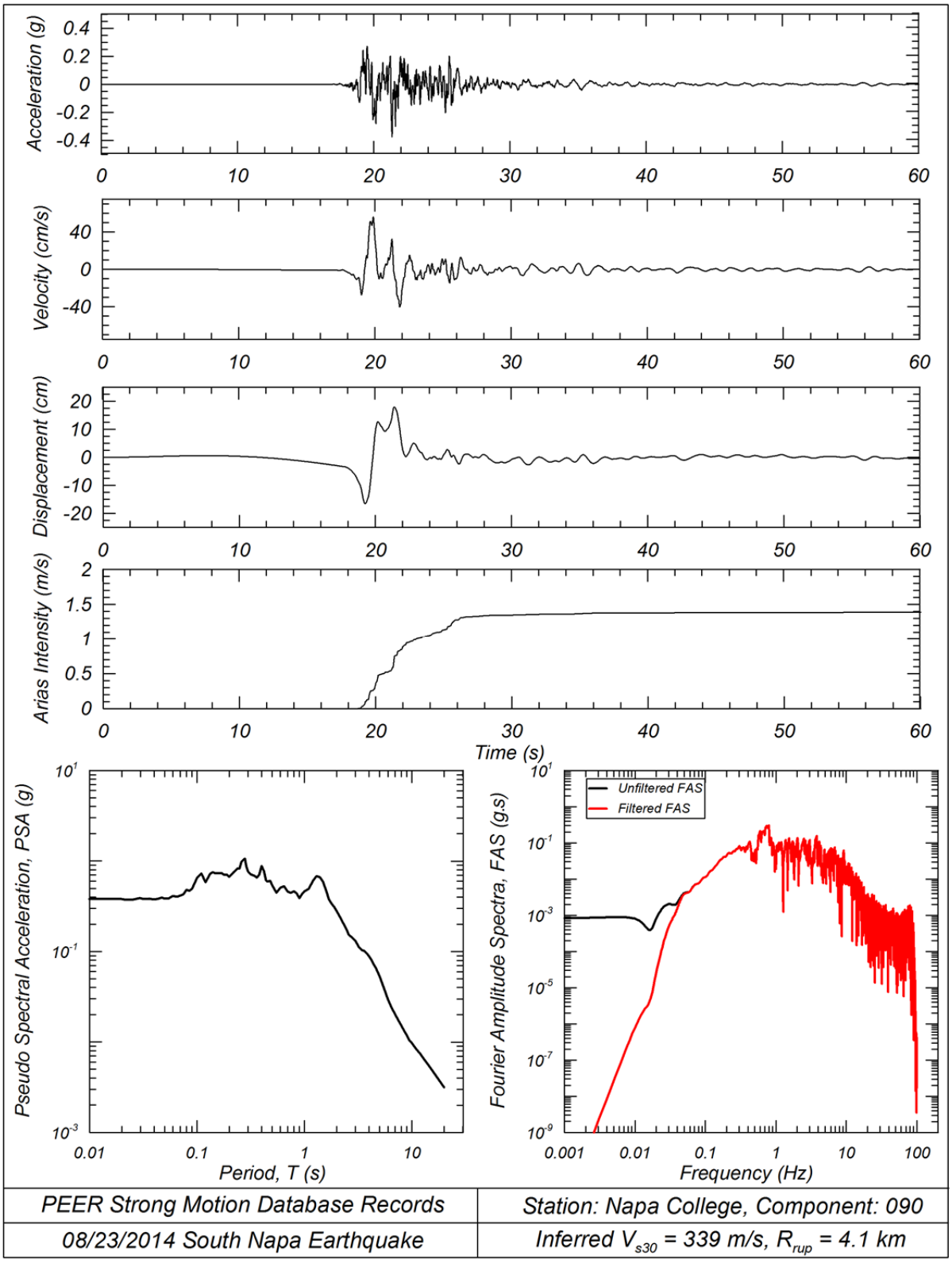
Acceleration (g)
Velocity (cm/s)
Displacement (cm)
Arias Intensity (m/s)
Time (s)
Pseudo Spectral Acceleration, PSA (g)
Period, T (s)
Fourier Amplitude Spectra, FAS (g.s)
Unfiltered FAS
Filtered FAS
Frequency (Hz)
PEER Strong Motion Database Records
Station: Napa College, Component: 090
08/23/2014 South Napa Earthquake
Inferred V_{s30} = 339 m/s, R_{rup} = 4.1 km

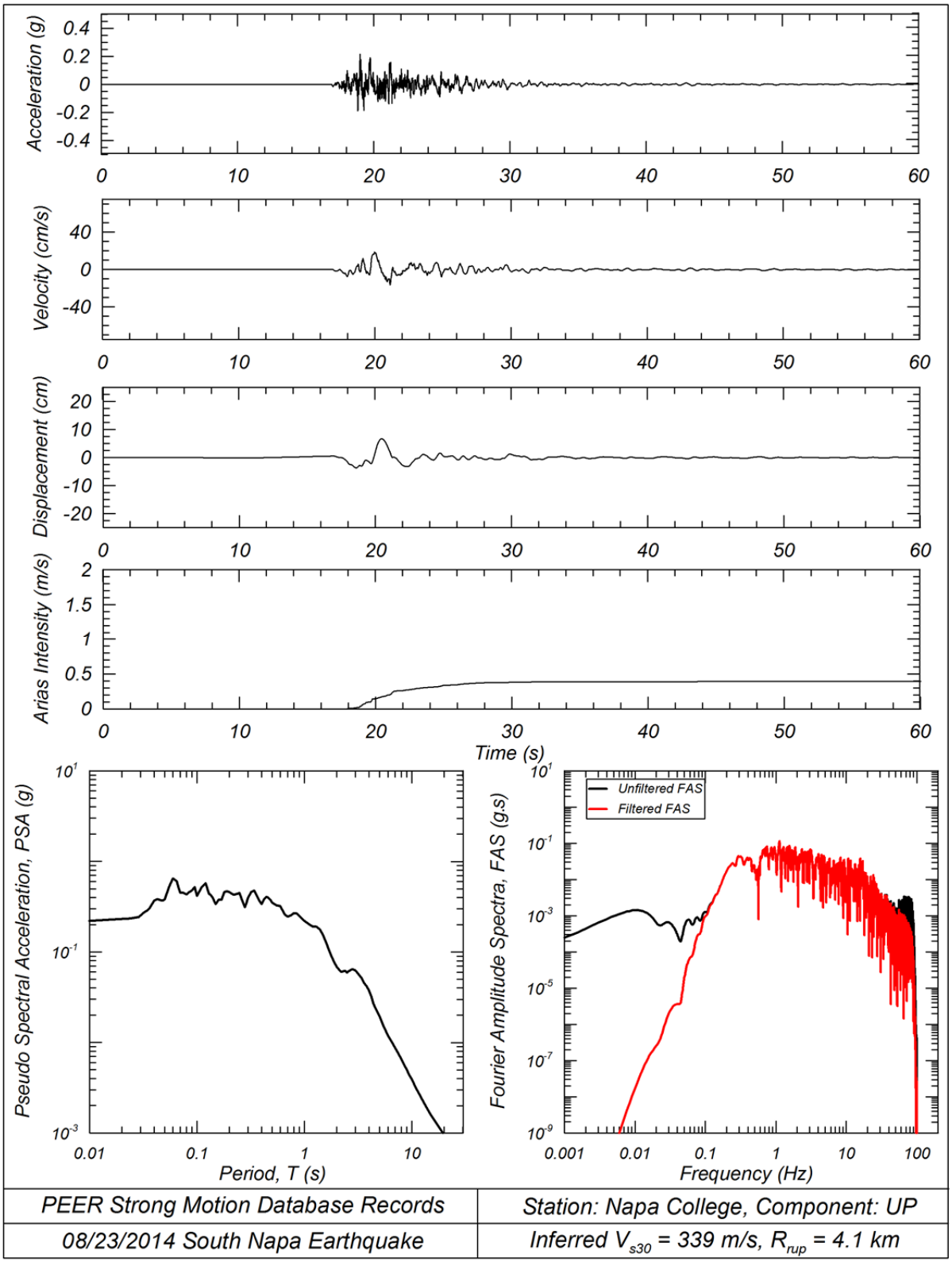
Acceleration (g)
Velocity (cm/s)
Displacement (cm)
Arias Intensity (m/s)
Time (s)
Pseudo Spectral Acceleration, PSA (g)
Period, T (s)
Fourier Amplitude Spectra, FAS (g.s)
Unfiltered FAS
Filtered FAS
Frequency (Hz)
PEER Strong Motion Database Records
08/23/2014 South Napa Earthquake
Station: Napa College, Component: UP
Inferred V_{s30} = 339 m/s, R_{rup} = 4.1 km

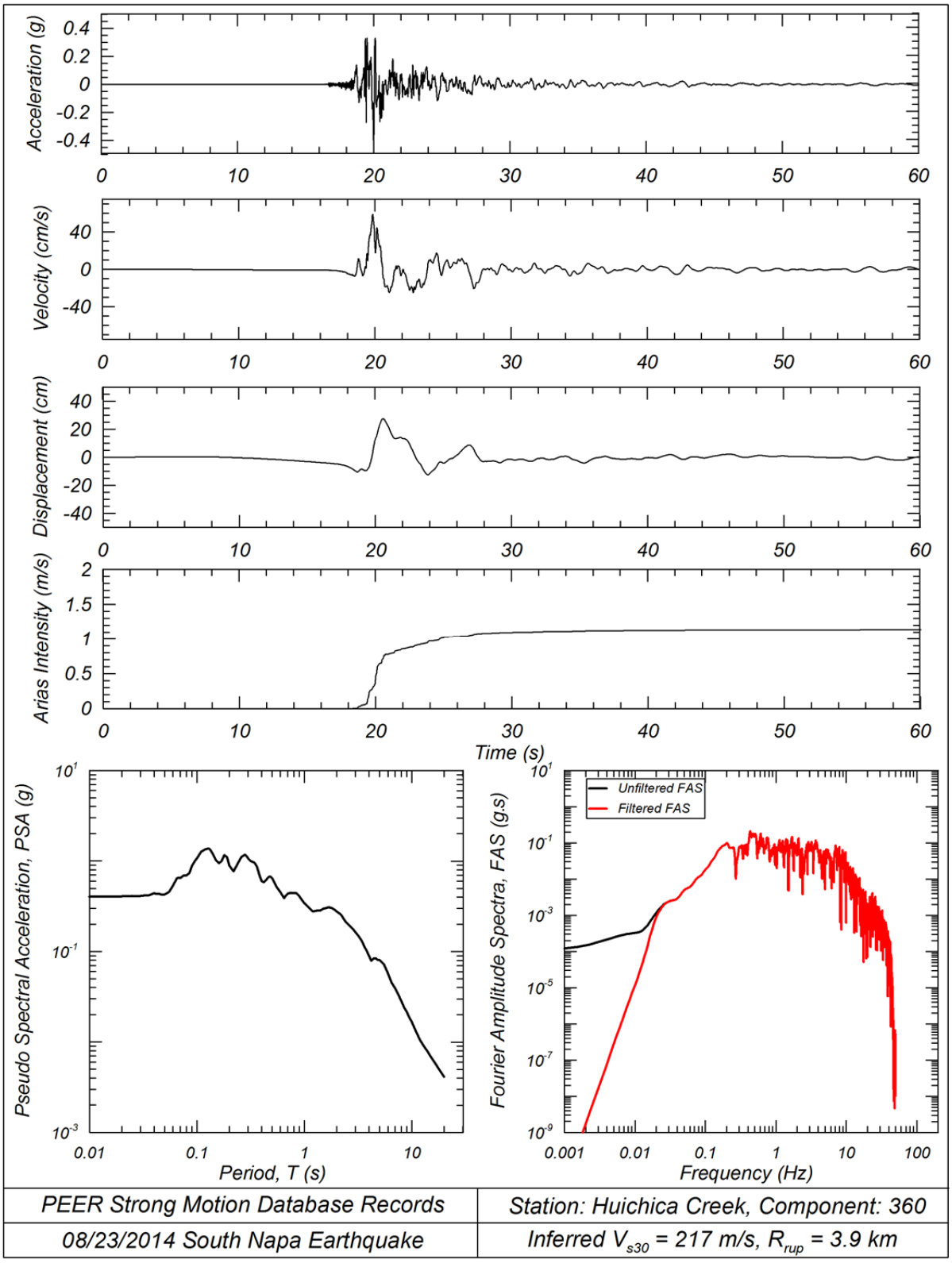
Acceleration (g)
Velocity (cm/s)
Displacement (cm)
Arias Intensity (m/s)
Time (s)
Pseudo Spectral Acceleration, PSA (g)
Period, T (s)
Fourier Amplitude Spectra, FAS (g.s)
Unfiltered FAS
Filtered FAS
Frequency (Hz)
PEER Strong Motion Database Records
08/23/2014 South Napa Earthquake
Station: Huichica Creek, Component: 360
Inferred V_{s30} = 217 m/s, R_{rup} = 3.9 km

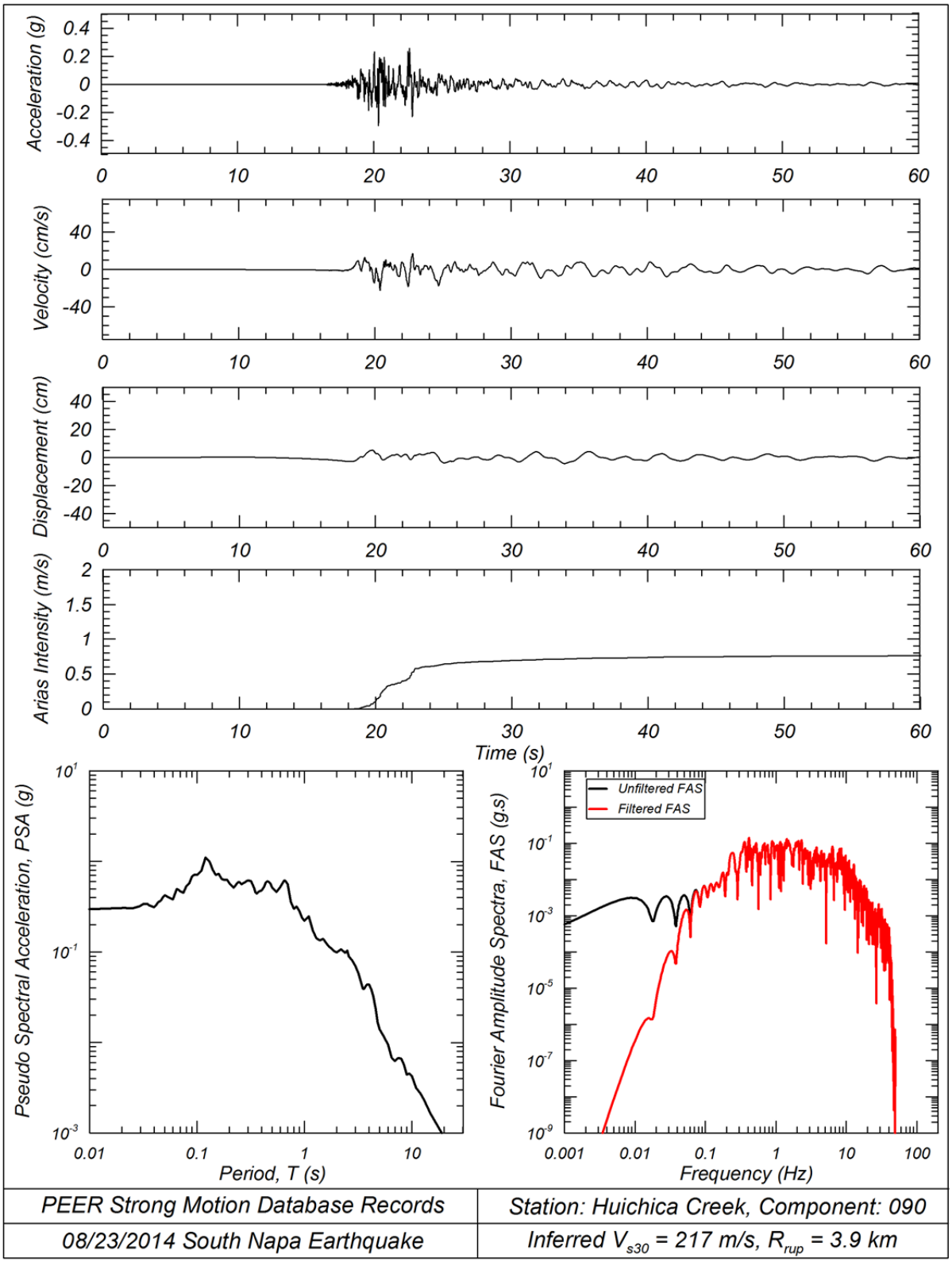
Acceleration (g)
Velocity (cm/s)
Displacement (cm)
Arias Intensity (m/s)
Time (s)
Pseudo Spectral Acceleration, PSA (g)
Period, T (s)
Fourier Amplitude Spectra, FAS (g.s)
Unfiltered FAS
Filtered FAS
Frequency (Hz)
PEER Strong Motion Database Records
08/23/2014 South Napa Earthquake
Station: Huichica Creek, Component: 090
Inferred V_{s30} = 217 m/s, R_{rup} = 3.9 km

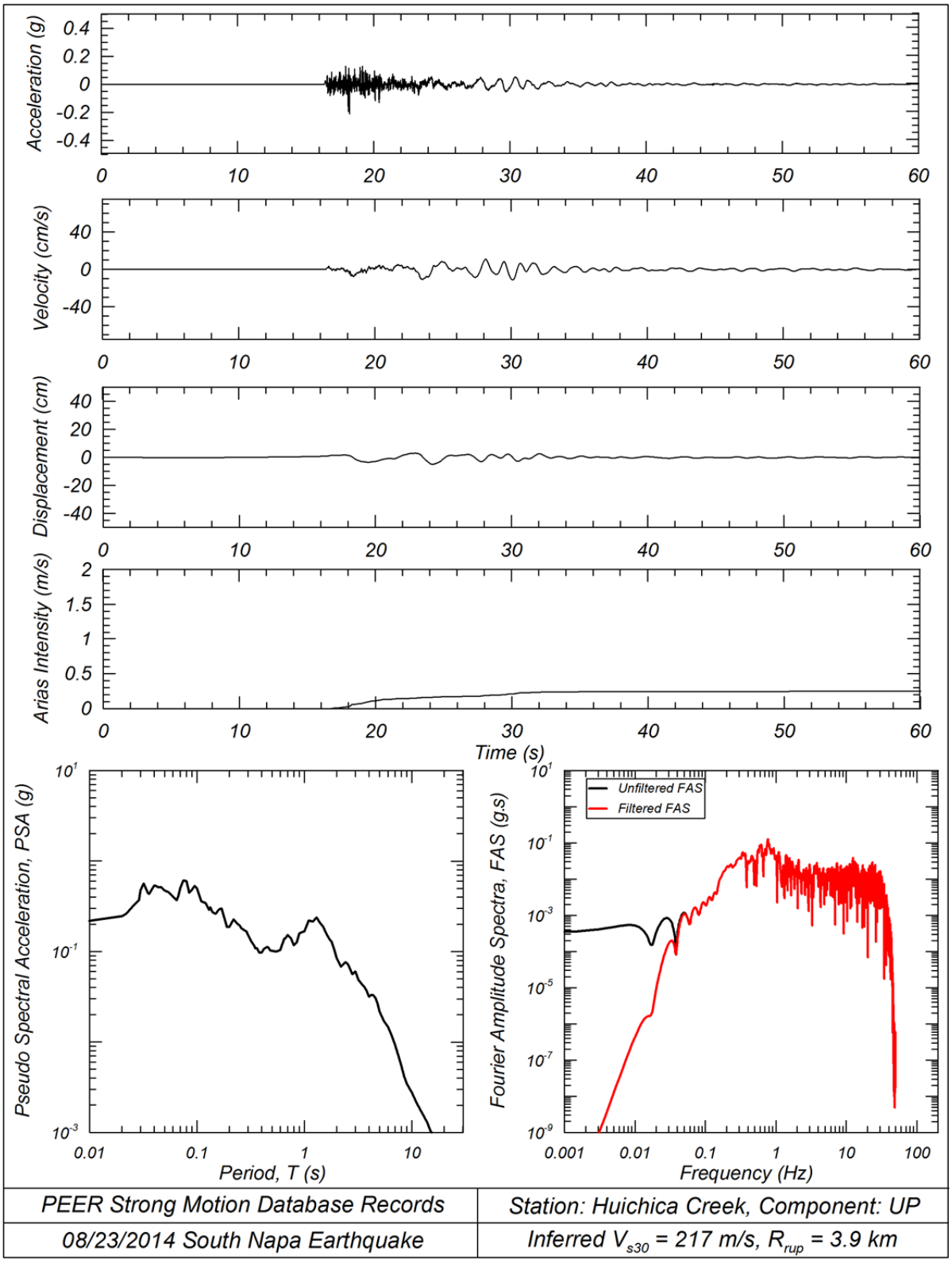
Acceleration (g)
Velocity (cm/s)
Displacement (cm)
Arias Intensity (m/s)
Time (s)
Pseudo Spectral Acceleration, PSA (g)
Period, T (s)
Fourier Amplitude Spectra, FAS (g.s)
Unfiltered FAS
Filtered FAS
Frequency (Hz)
PEER Strong Motion Database Records
08/23/2014 South Napa Earthquake
Station: Huichica Creek, Component: UP
Inferred V_{s30} = 217 m/s, R_{rup} = 3.9 km

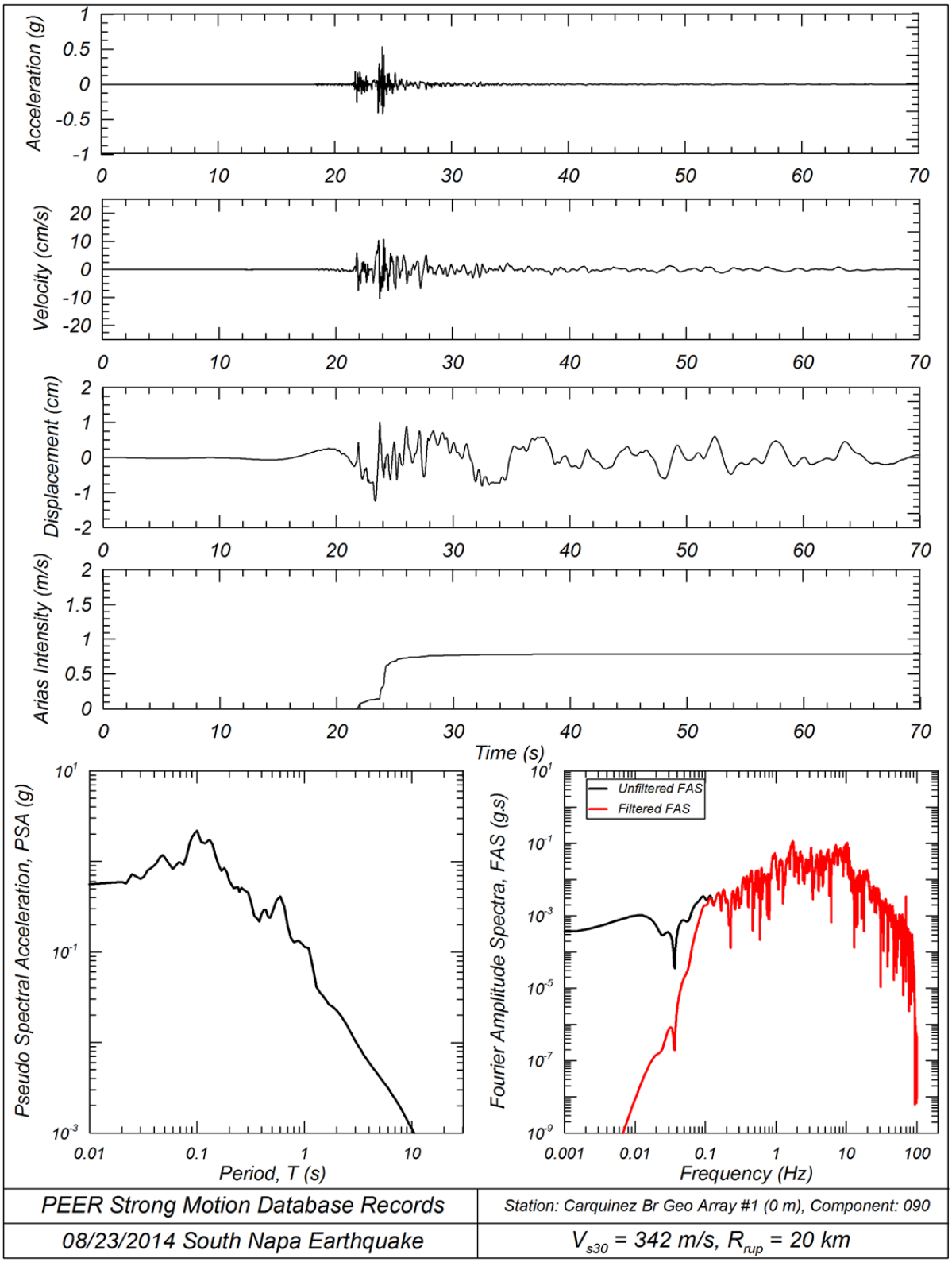
Acceleration (g)
Velocity (cm/s)
Displacement (cm)
Arias Intensity (m/s)
Time (s)
Pseudo Spectral Acceleration, PSA (g)
Period, T (s)
Fourier Amplitude Spectra, FAS (g.s)
Unfiltered FAS
Filtered FAS
Frequency (Hz)
PEER Strong Motion Database Records
Station: Carquinez Br Geo Array #1 (0 m), Component: 090
08/23/2014 South Napa Earthquake
V_{s30} = 342 m/s, R_{rup} = 20 km

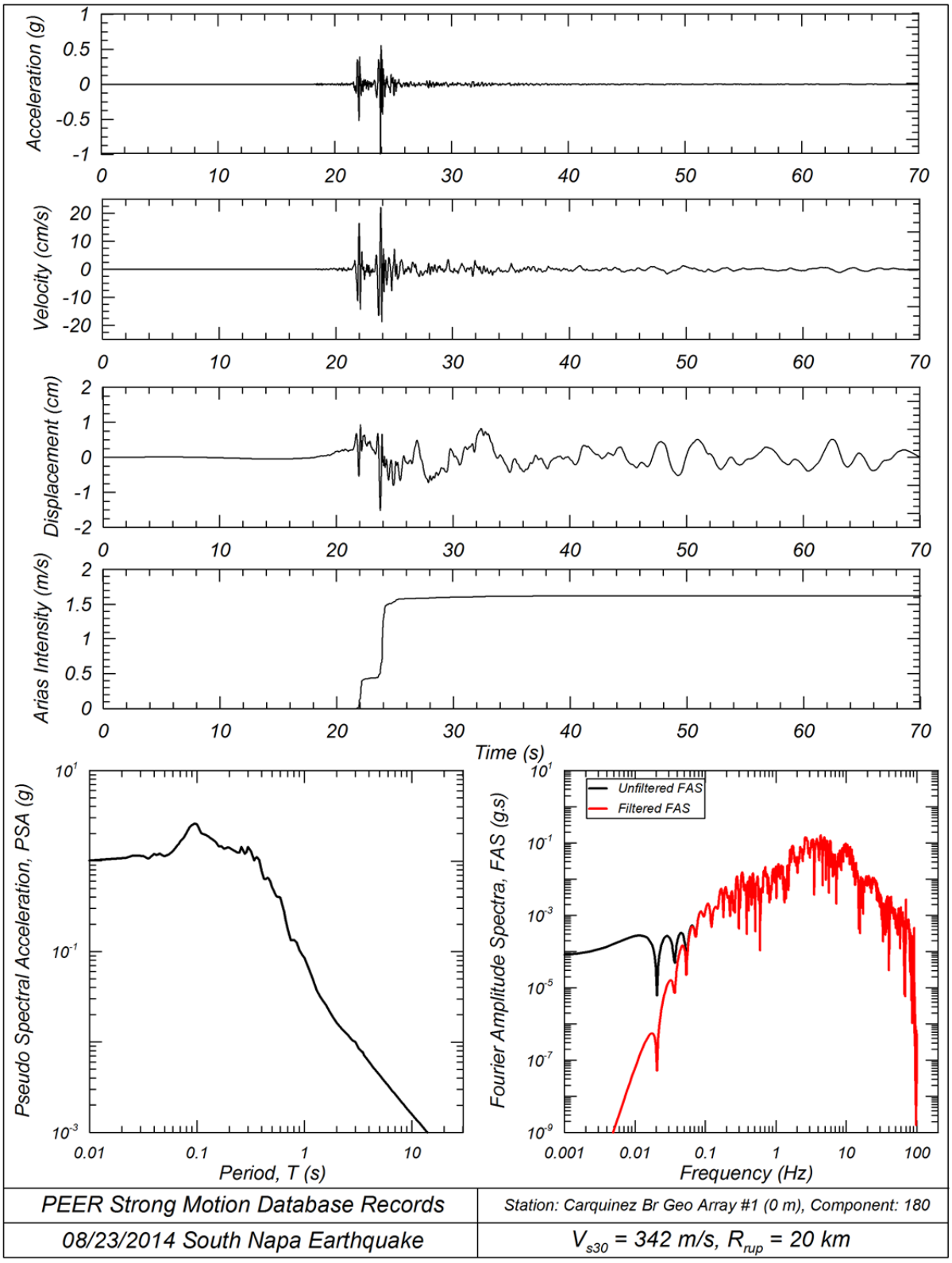
Acceleration (g)
Velocity (cm/s)
Displacement (cm)
Arias Intensity (m/s)
Time (s)
Pseudo Spectral Acceleration, PSA (g)
Period, T (s)
Fourier Amplitude Spectra, FAS (g.s)
Unfiltered FAS
Filtered FAS
Frequency (Hz)
PEER Strong Motion Database Records
Station: Carquinez Br Geo Array #1 (0 m), Component: 180
08/23/2014 South Napa Earthquake
V_{s30} = 342 m/s, R_{rup} = 20 km

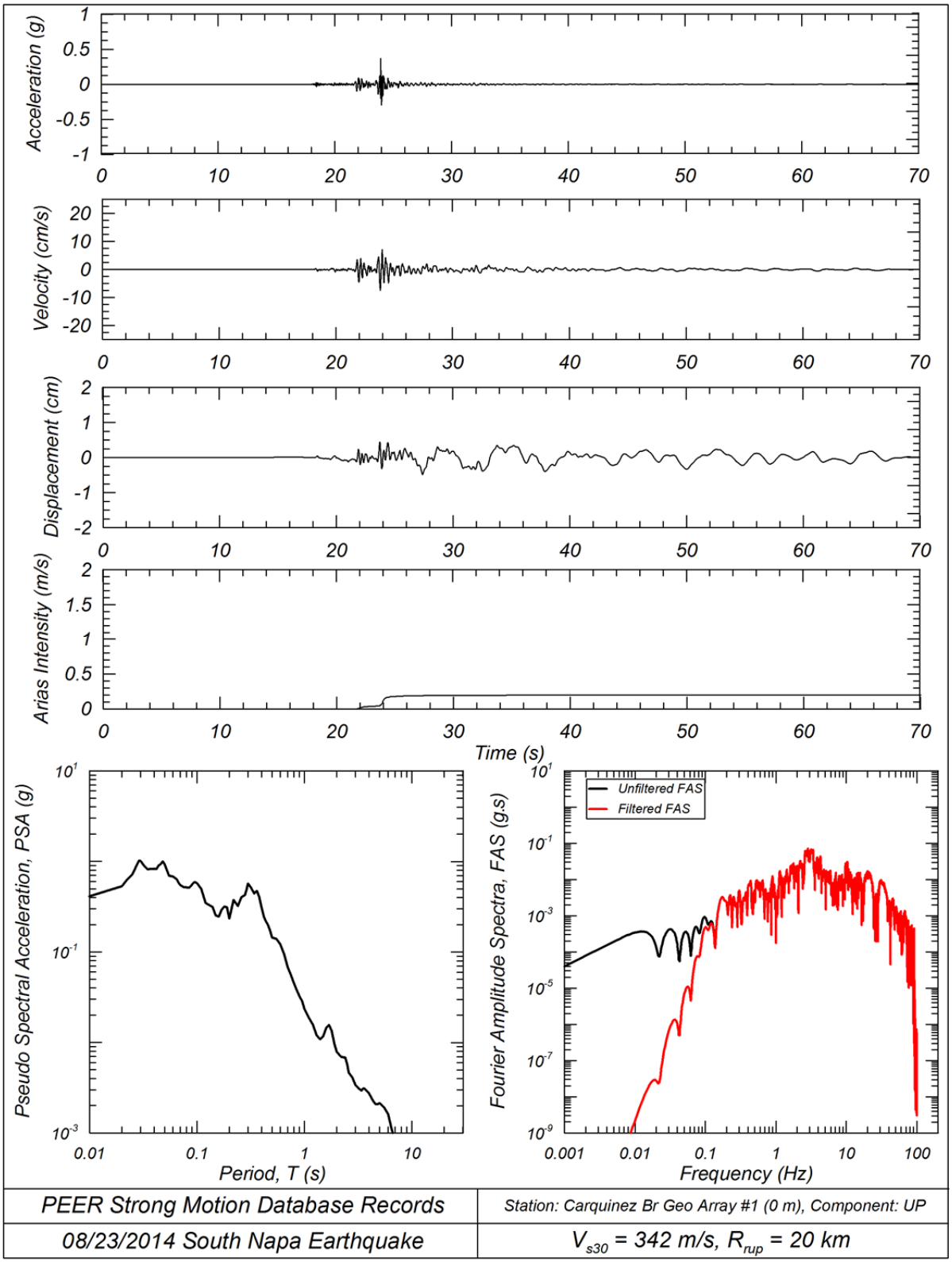
Acceleration (g)
Velocity (cm/s)
Displacement (cm)
Arias Intensity (m/s)
Time (s)
Pseudo Spectral Acceleration, PSA (g)
Period, T (s)
Fourier Amplitude Spectra, FAS (g.s)
Unfiltered FAS
Filtered FAS
Frequency (Hz)
PEER Strong Motion Database Records
Station: Carquinez Br Geo Array #1 (0 m), Component: UP
08/23/2014 South Napa Earthquake
V_{s30} = 342 m/s, R_{rup} = 20 km

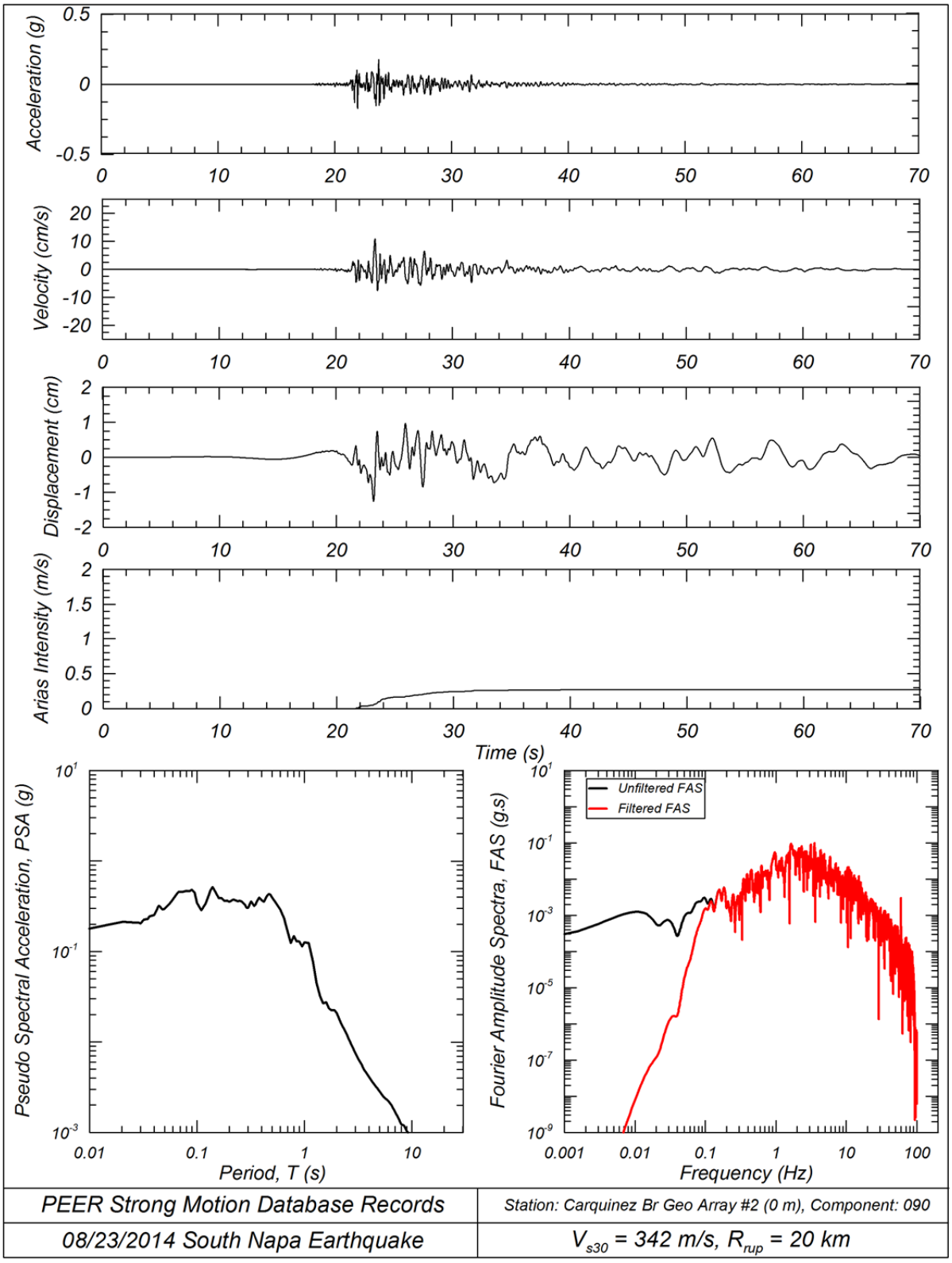
Acceleration (g)
Velocity (cm/s)
Displacement (cm)
Arias Intensity (m/s)
Time (s)
Pseudo Spectral Acceleration, PSA (g)
Period, T (s)
Fourier Amplitude Spectra, FAS (g.s)
Unfiltered FAS
Filtered FAS
Frequency (Hz)
PEER Strong Motion Database Records
Station: Carquinez Br Geo Array #2 (0 m), Component: 090
08/23/2014 South Napa Earthquake
V_{s30} = 342 m/s, R_{rup} = 20 km

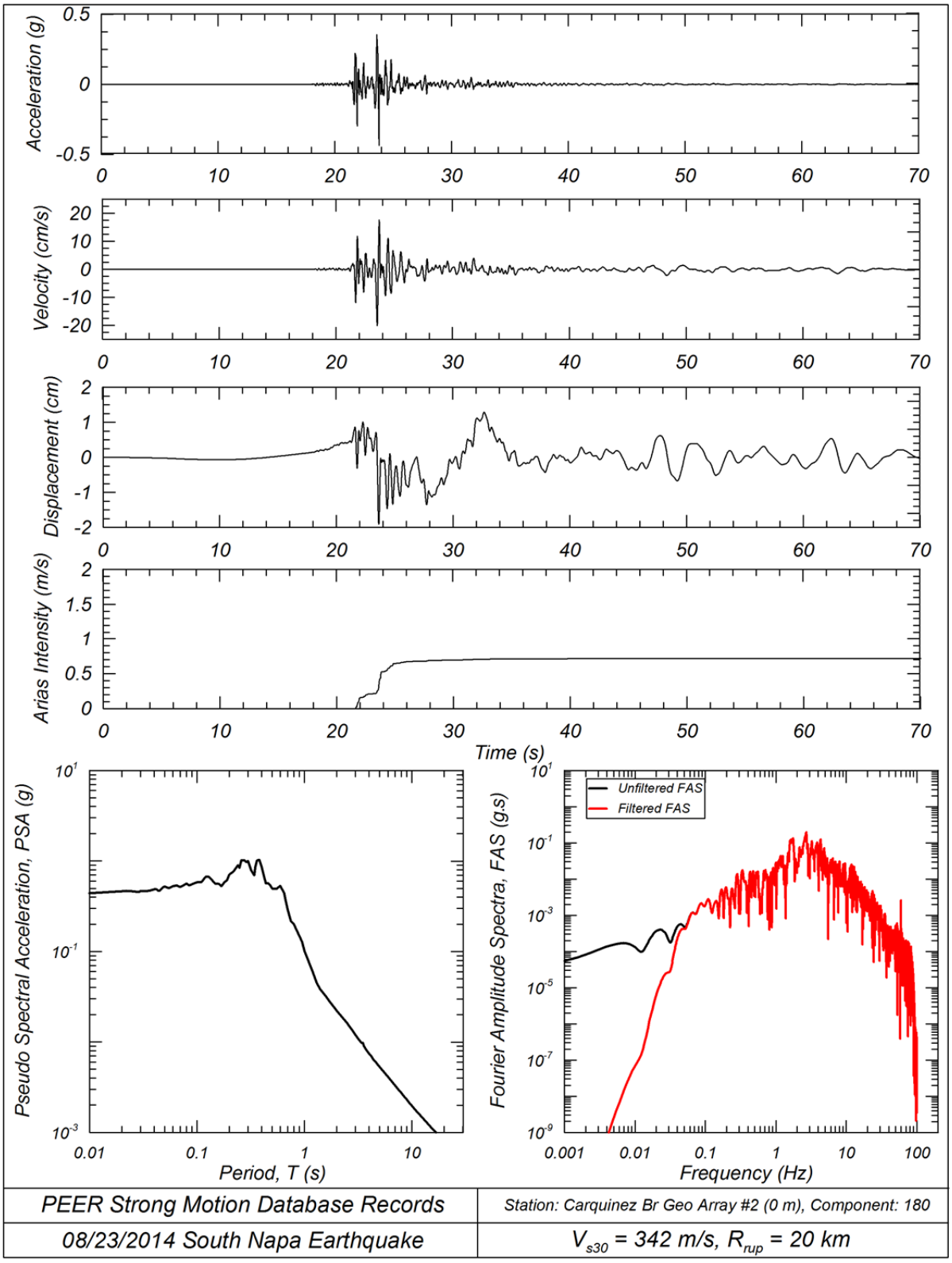
Acceleration (g)
Velocity (cm/s)
Displacement (cm)
Arias Intensity (m/s)
Time (s)
Pseudo Spectral Acceleration, PSA (g)
Period, T (s)
Fourier Amplitude Spectra, FAS (g.s)
Unfiltered FAS
Filtered FAS
Frequency (Hz)
PEER Strong Motion Database Records
Station: Carquinez Br Geo Array #2 (0 m), Component: 180
08/23/2014 South Napa Earthquake
V_{s30} = 342 m/s, R_{rup} = 20 km

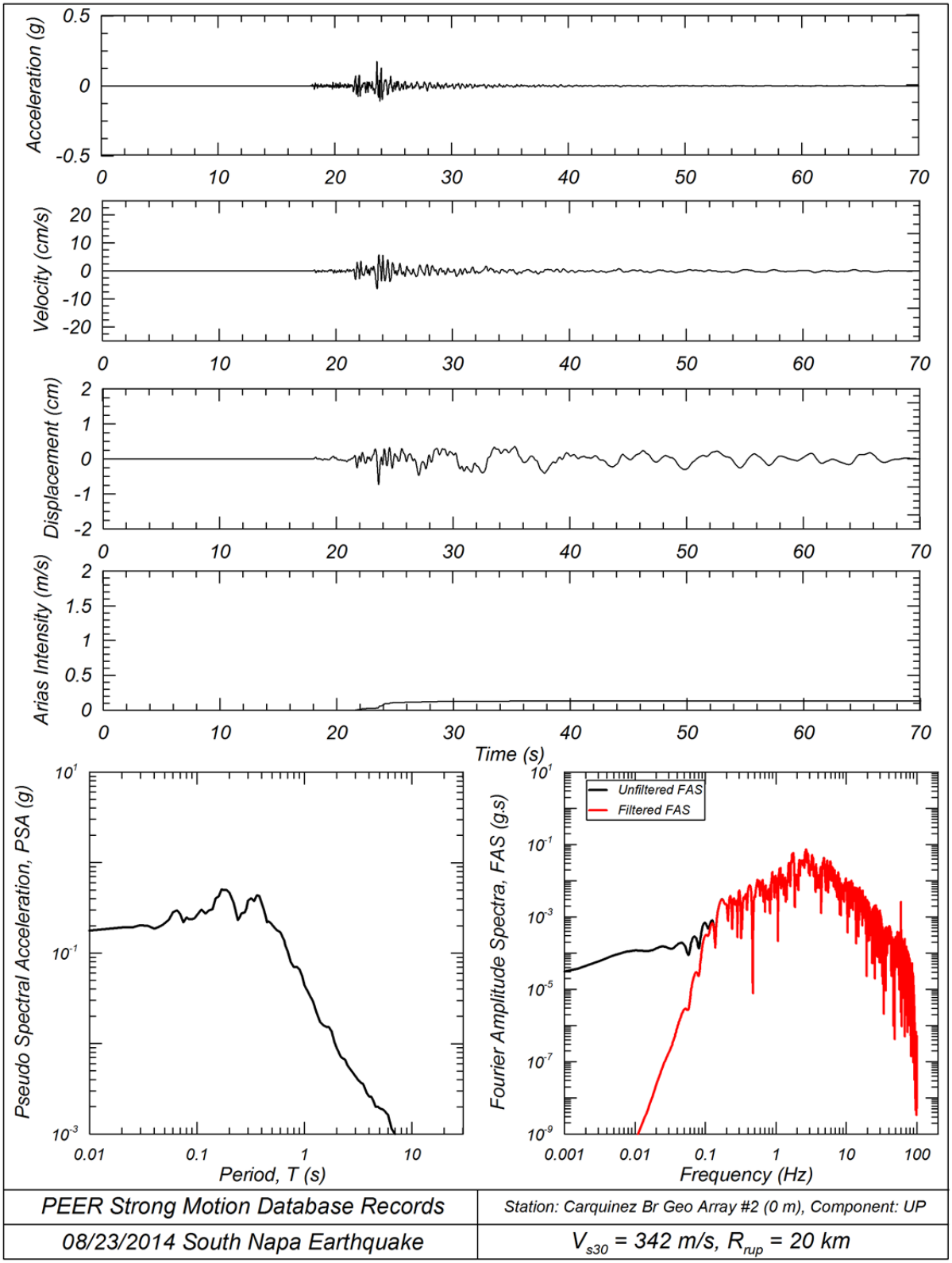
Acceleration (g)
Velocity (cm/s)
Displacement (cm)
Arias Intensity (m/s)
Time (s)
Pseudo Spectral Acceleration, PSA (g)
Period, T (s)
Fourier Amplitude Spectra, FAS (g.s)
Unfiltered FAS
Filtered FAS
Frequency (Hz)
PEER Strong Motion Database Records
Station: Carquinez Br Geo Array #2 (0 m), Component: UP
08/23/2014 South Napa Earthquake
V_{s30} = 342 m/s, R_{rup} = 20 km

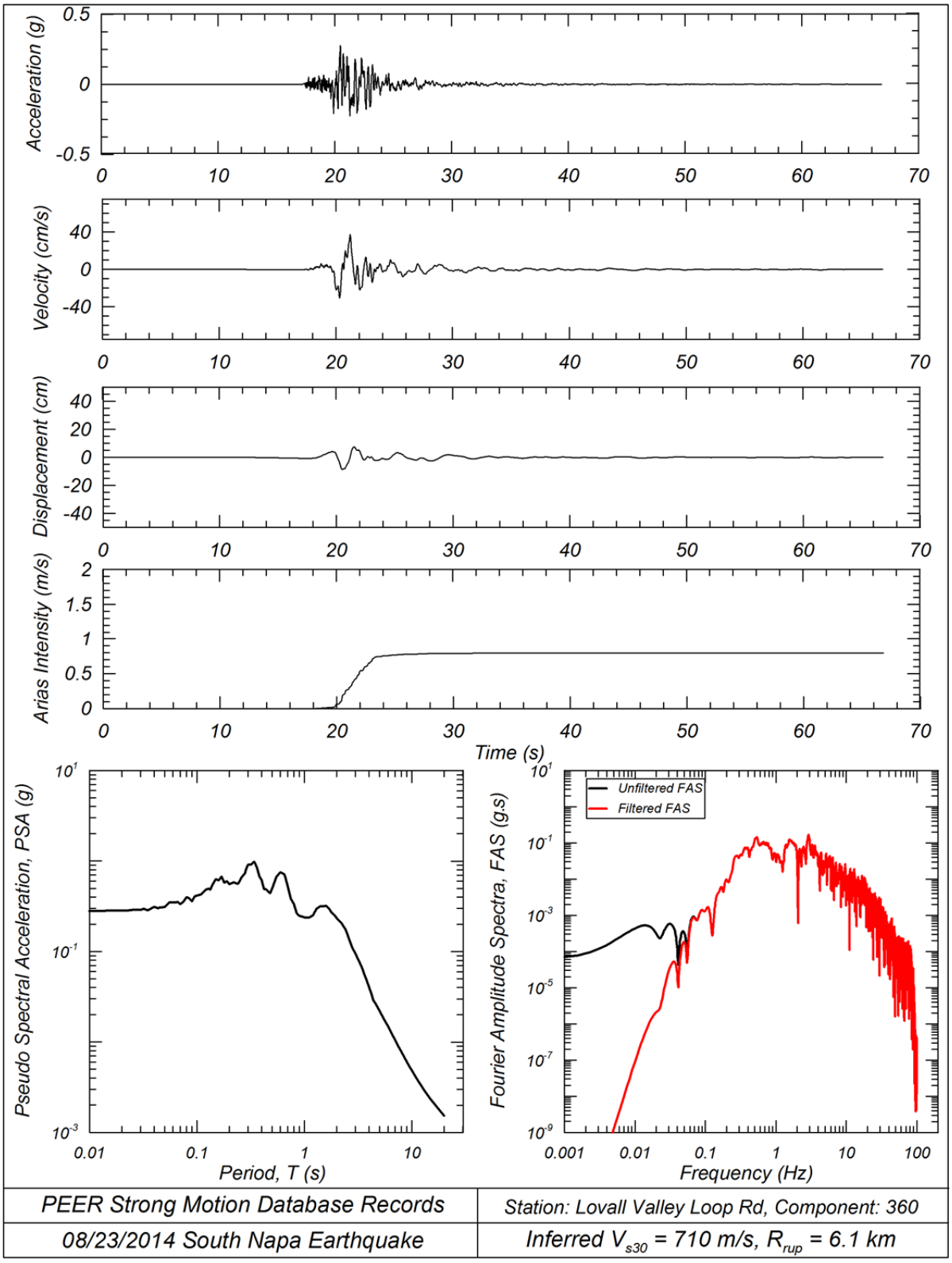
Acceleration (g)
Velocity (cm/s)
Displacement (cm)
Arias Intensity (m/s)
Time (s)
Pseudo Spectral Acceleration, PSA (g)
Period, T (s)
Fourier Amplitude Spectra, FAS (g.s)
Unfiltered FAS
Filtered FAS
Frequency (Hz)
PEER Strong Motion Database Records
08/23/2014 South Napa Earthquake
Station: Lovall Valley Loop Rd, Component: 360
Inferred V_{s30} = 710 m/s, R_{rup} = 6.1 km

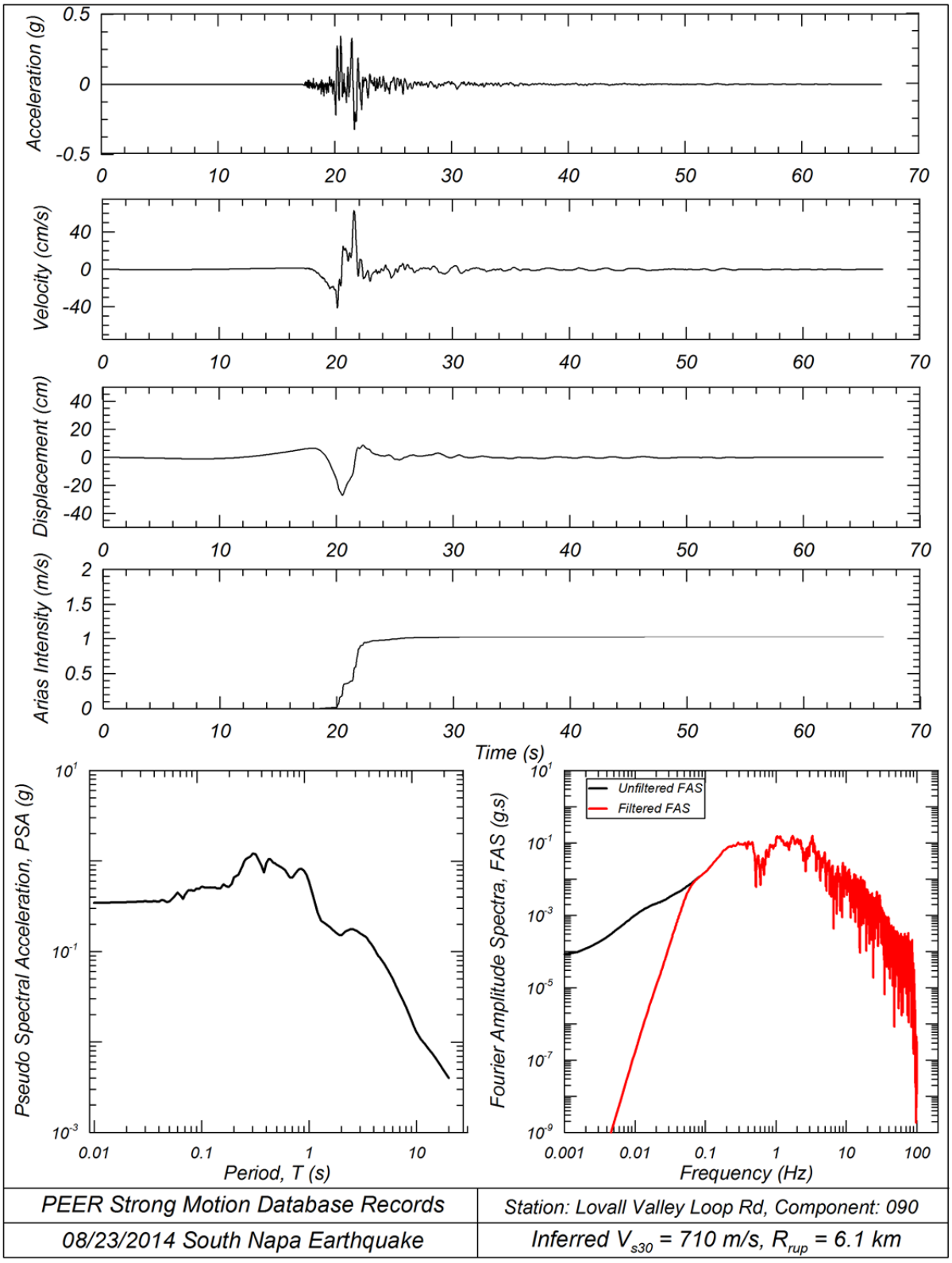
Acceleration (g)
Velocity (cm/s)
Displacement (cm)
Arias Intensity (m/s)
Time (s)
Pseudo Spectral Acceleration, PSA (g)
Period, T (s)
Fourier Amplitude Spectra, FAS (g.s)
Unfiltered FAS
Filtered FAS
Frequency (Hz)
PEER Strong Motion Database Records
08/23/2014 South Napa Earthquake
Station: Lovall Valley Loop Rd, Component: 090
Inferred V_{s30} = 710 m/s, R_{rup} = 6.1 km

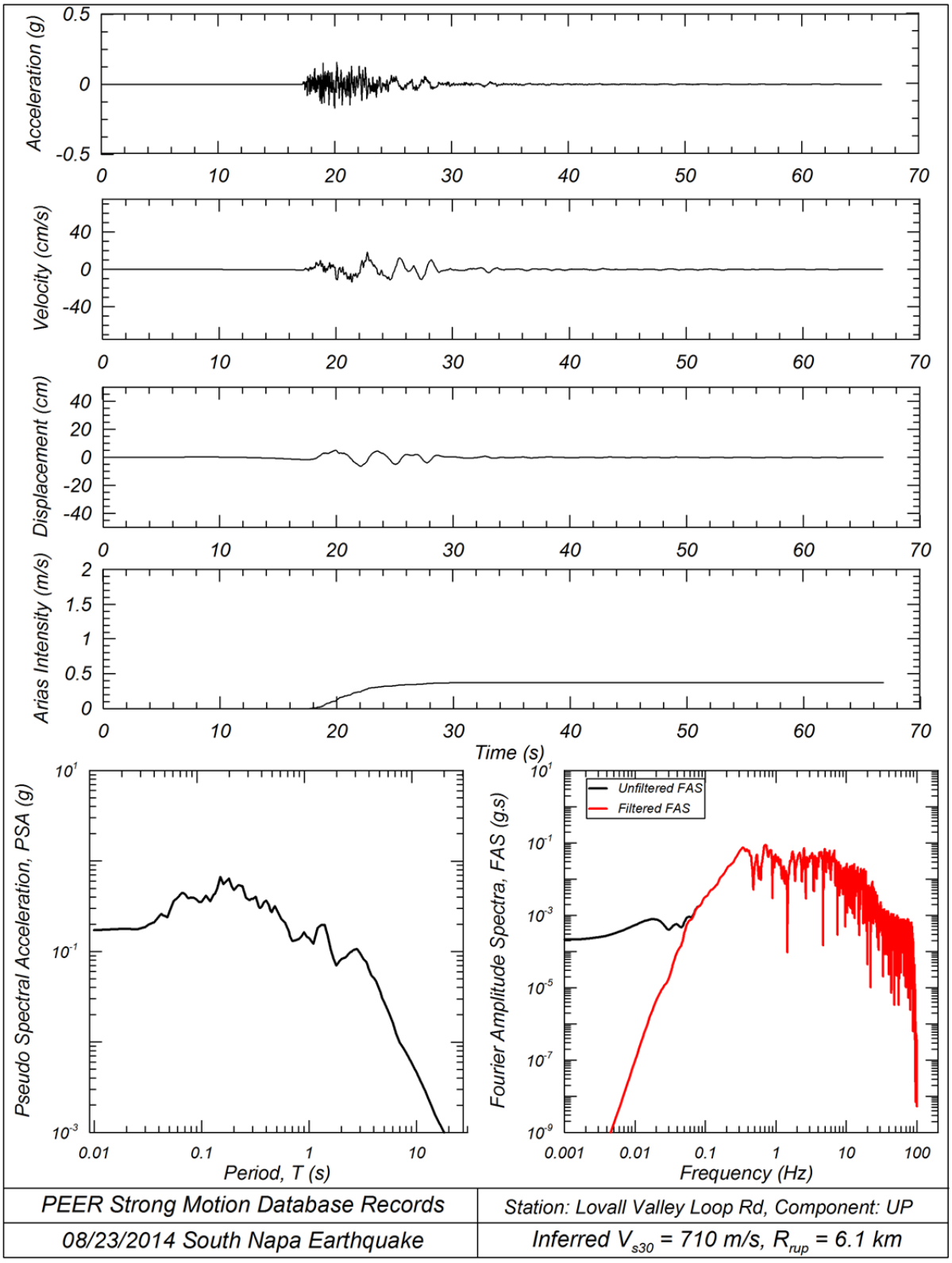
Acceleration (g)
Velocity (cm/s)
Displacement (cm)
Arias Intensity (m/s)
Time (s)
Pseudo Spectral Acceleration, PSA (g)
Period, T (s)
Fourier Amplitude Spectra, FAS (g.s)
Unfiltered FAS
Filtered FAS
Frequency (Hz)
PEER Strong Motion Database Records
08/23/2014 South Napa Earthquake
Station: Lovall Valley Loop Rd, Component: UP
Inferred V_{s30} = 710 m/s, R_{rup} = 6.1 km

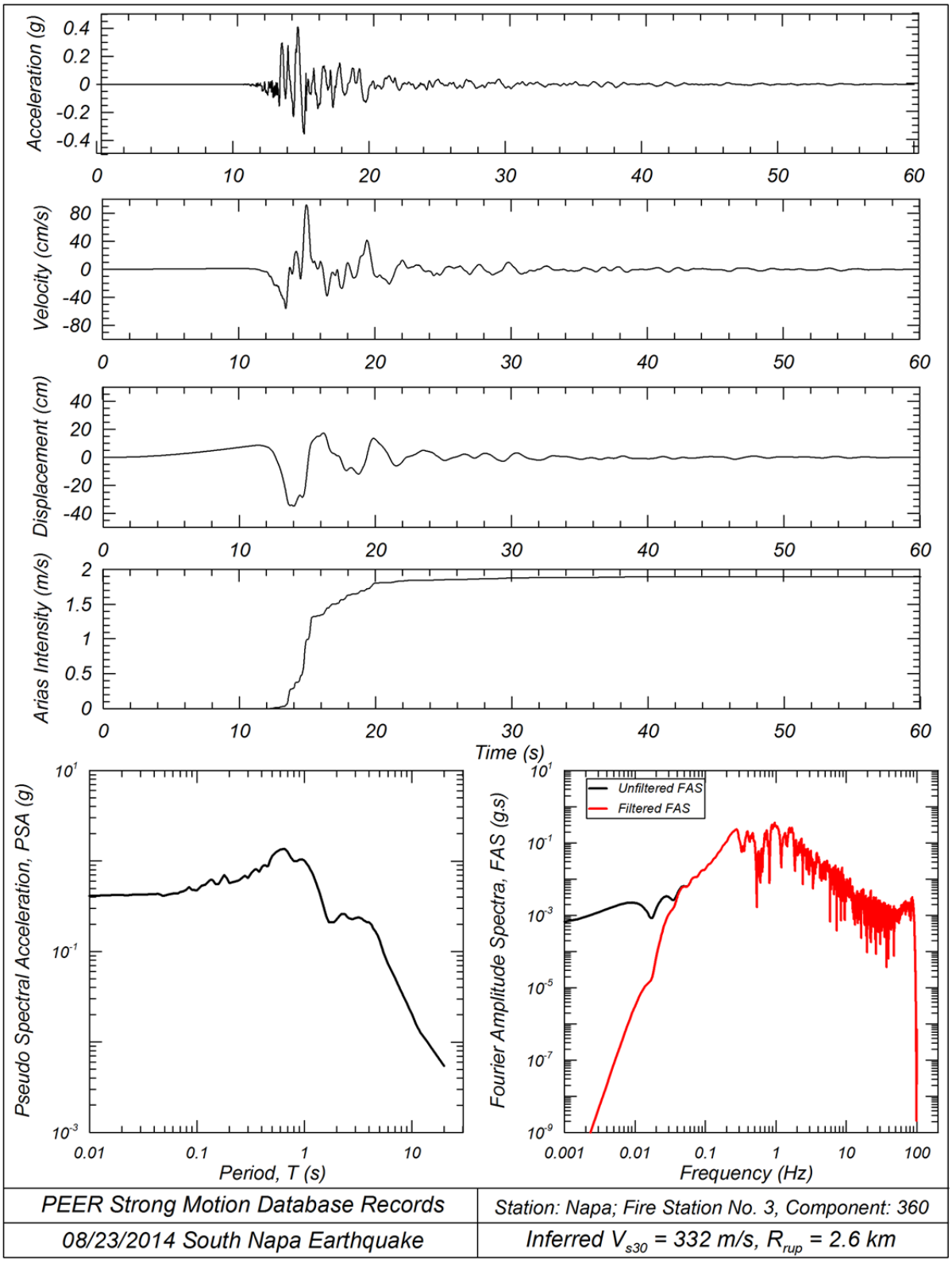
Acceleration (g)
Velocity (cm/s)
Displacement (cm)
Arias Intensity (m/s)
Time (s)
Pseudo Spectral Acceleration, PSA (g)
Period, T (s)
Fourier Amplitude Spectra, FAS (g.s)
Unfiltered FAS
Filtered FAS
Frequency (Hz)
PEER Strong Motion Database Records
08/23/2014 South Napa Earthquake
Station: Napa; Fire Station No. 3, Component: 360
Inferred V_{s30} = 332 m/s, R_{rup} = 2.6 km

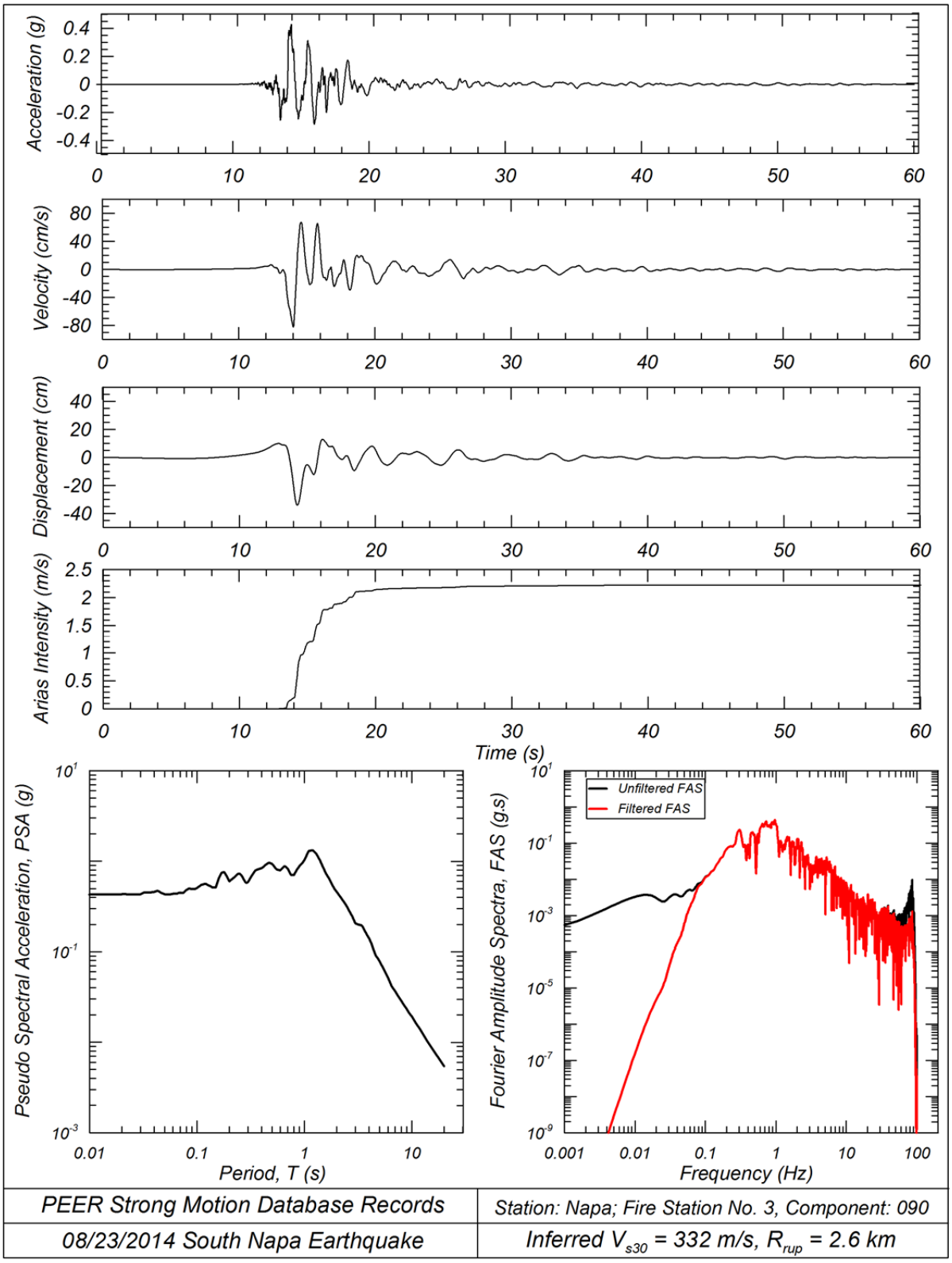
Acceleration (g)
Velocity (cm/s)
Displacement (cm)
Arias Intensity (m/s)
Time (s)
Pseudo Spectral Acceleration, PSA (g)
Period, T (s)
Fourier Amplitude Spectra, FAS (g.s)
Unfiltered FAS
Filtered FAS
Frequency (Hz)
PEER Strong Motion Database Records
08/23/2014 South Napa Earthquake
Station: Napa; Fire Station No. 3, Component: 090
Inferred V_{s30} = 332 m/s, R_{rup} = 2.6 km

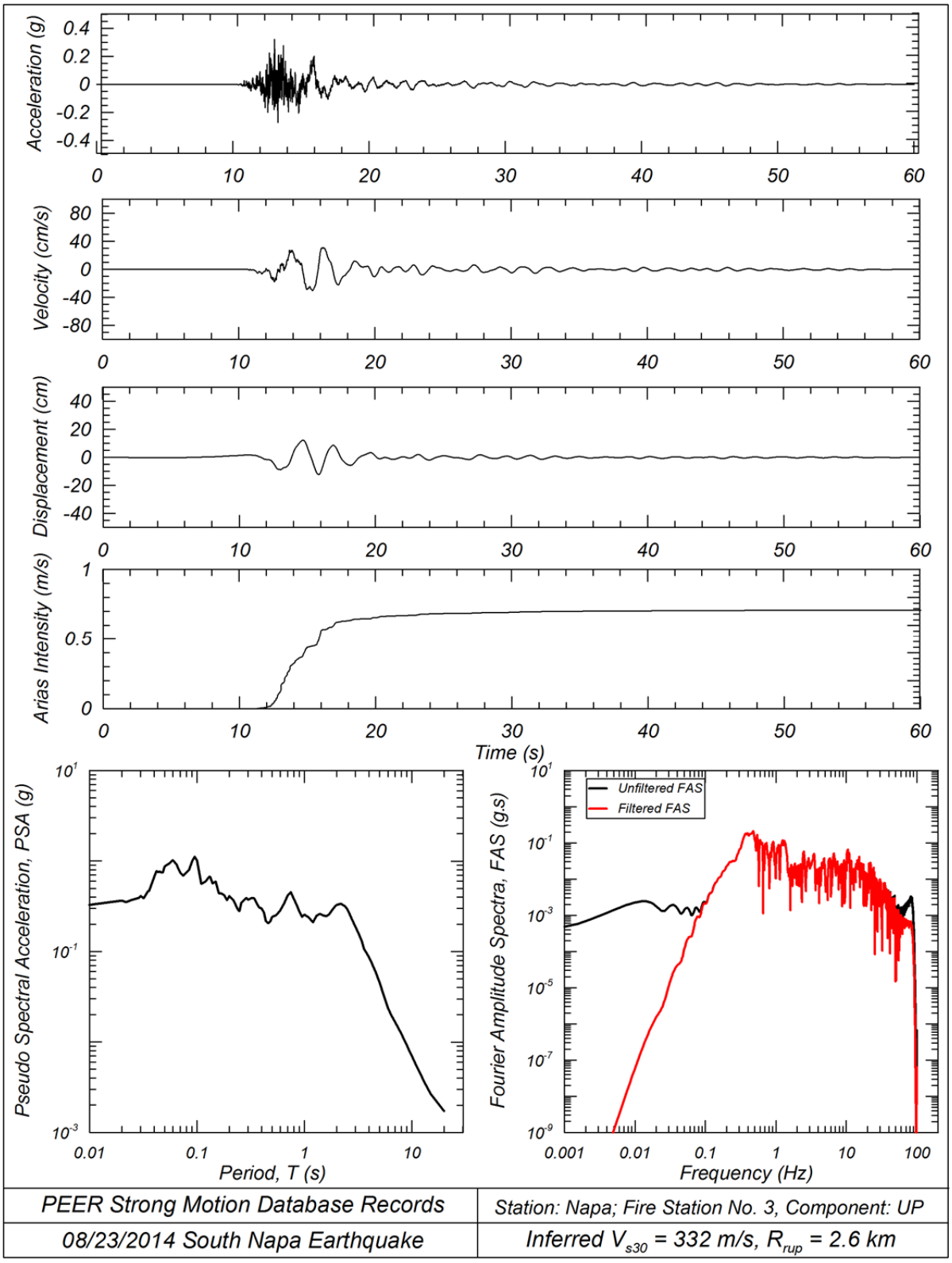
Acceleration (g)
Velocity (cm/s)
Displacement (cm)
Arias Intensity (m/s)
Time (s)
Pseudo Spectral Acceleration, PSA (g)
Period, T (s)
Fourier Amplitude Spectra, FAS (g.s)
Unfiltered FAS
Filtered FAS
Frequency (Hz)
PEER Strong Motion Database Records
08/23/2014 South Napa Earthquake
Station: Napa; Fire Station No. 3, Component: UP
Inferred V_{s30} = 332 m/s, R_{rup} = 2.6 km

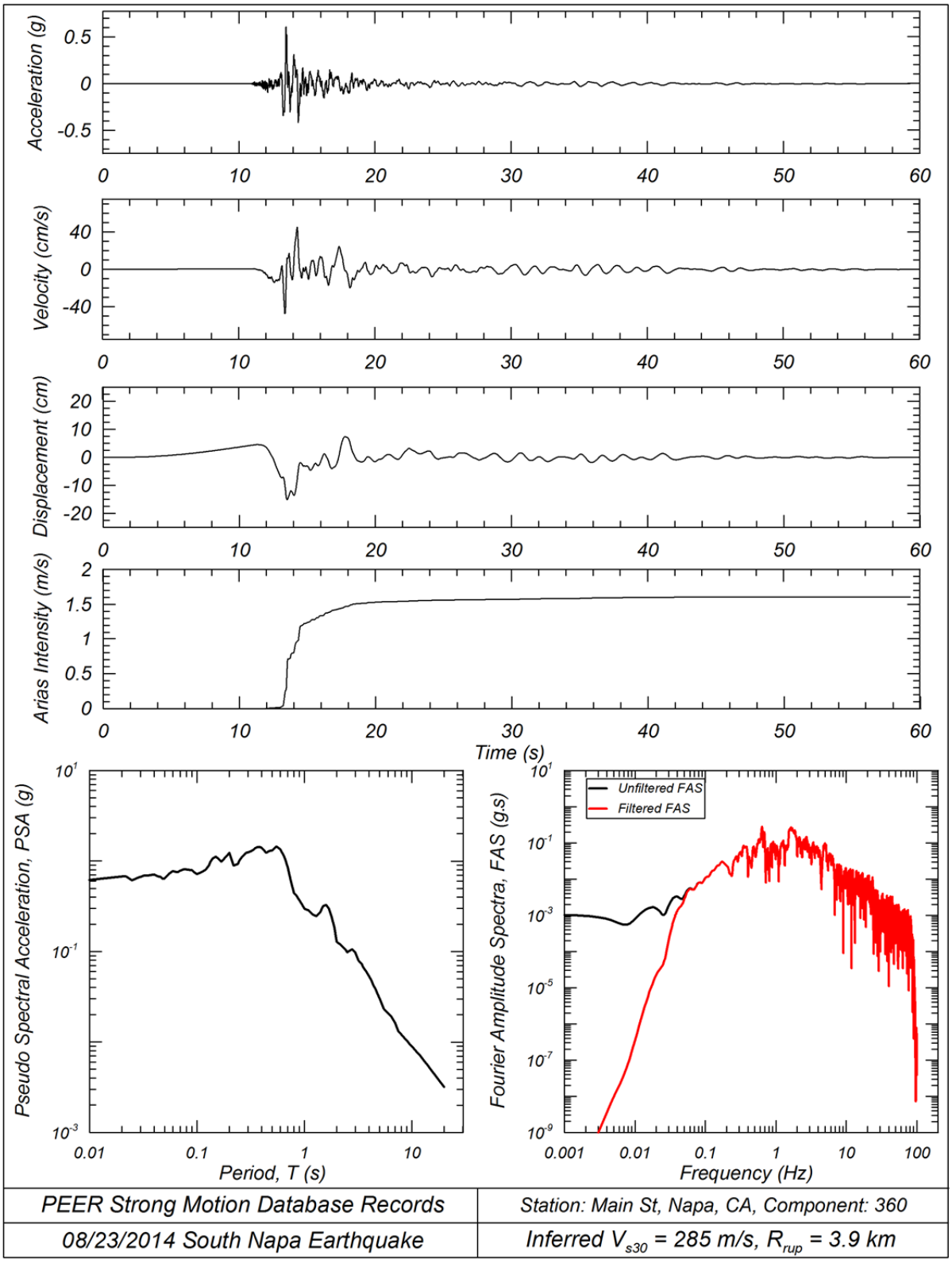
Acceleration (g)
Velocity (cm/s)
Displacement (cm)
Arias Intensity (m/s)
Time (s)
Pseudo Spectral Acceleration, PSA (g)
Period, T (s)
Fourier Amplitude Spectra, FAS (g.s)
Unfiltered FAS
Filtered FAS
Frequency (Hz)
PEER Strong Motion Database Records
Station: Main St, Napa, CA, Component: 360
08/23/2014 South Napa Earthquake
Inferred V_{s30} = 285 m/s, R_{rup} = 3.9 km

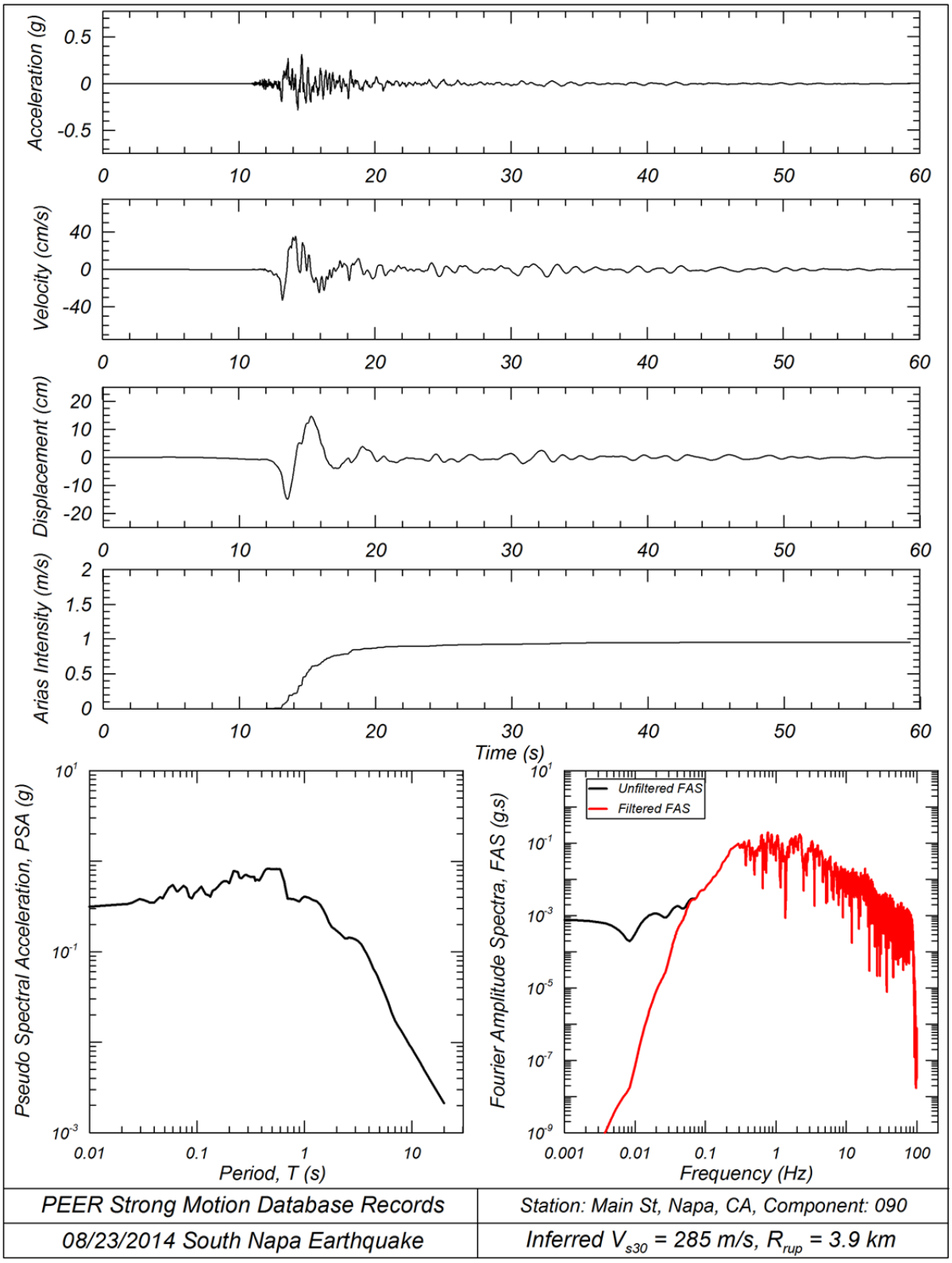
Acceleration (g)
Velocity (cm/s)
Displacement (cm)
Arias Intensity (m/s)
Time (s)
Pseudo Spectral Acceleration, PSA (g)
Period, T (s)
Fourier Amplitude Spectra, FAS (g.s)
Unfiltered FAS
Filtered FAS
Frequency (Hz)
PEER Strong Motion Database Records
Station: Main St, Napa, CA, Component: 090
08/23/2014 South Napa Earthquake
Inferred V_{s30} = 285 m/s, R_{rup} = 3.9 km

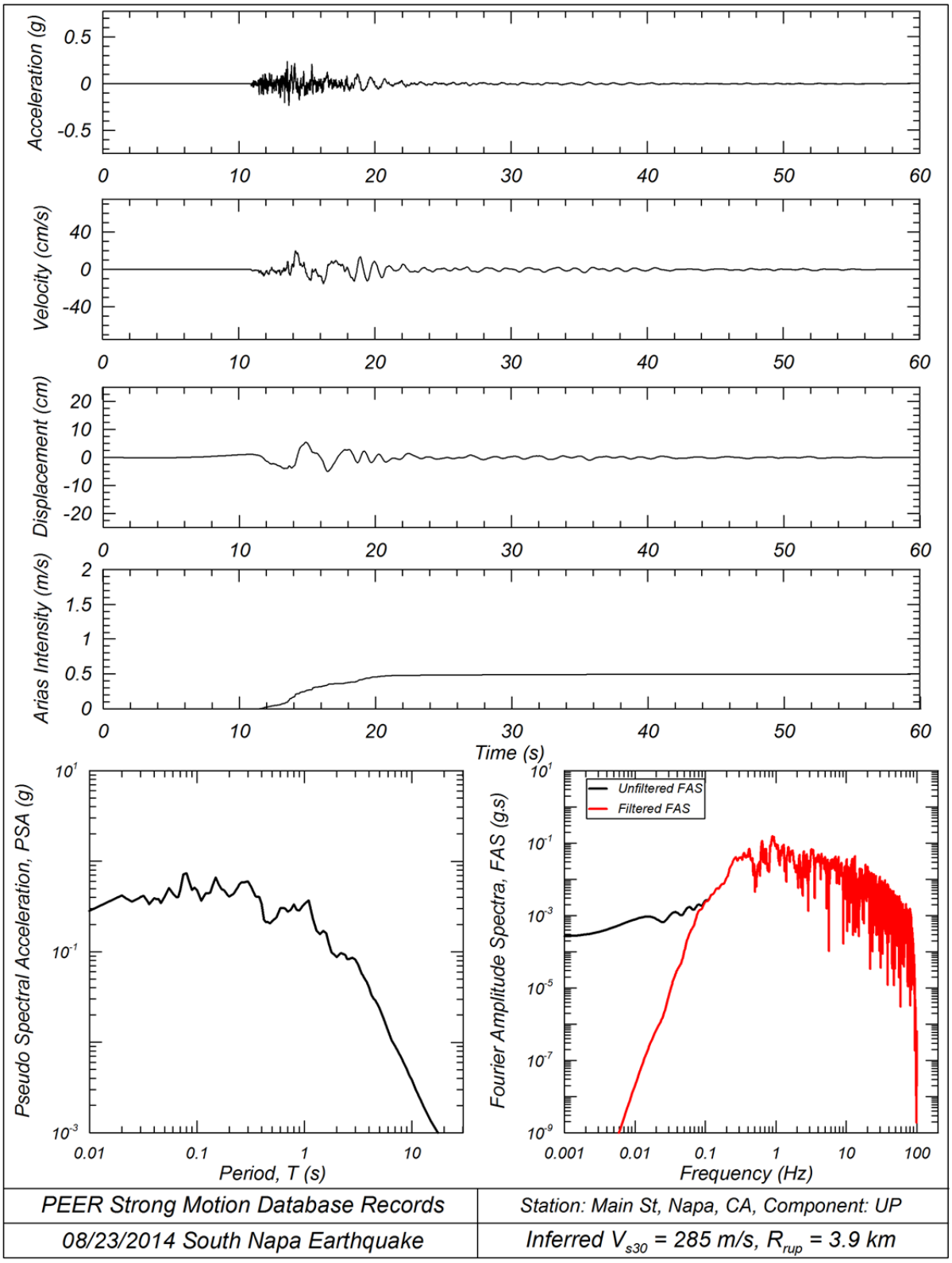
Acceleration (g)
Velocity (cm/s)
Displacement (cm)
Arias Intensity (m/s)
Time (s)
Pseudo Spectral Acceleration, PSA (g)
Period, T (s)
Fourier Amplitude Spectra, FAS (g.s)
Unfiltered FAS
Filtered FAS
Frequency (Hz)
PEER Strong Motion Database Records
08/23/2014 South Napa Earthquake
Station: Main St, Napa, CA, Component: UP
Inferred V_{s30} = 285 m/s, R_{rup} = 3.9 km

APPENDIX C COMPARISON OF RECORDED RESPONSE SPECTRA AND CODE-BASED DESIGN SPECTRA

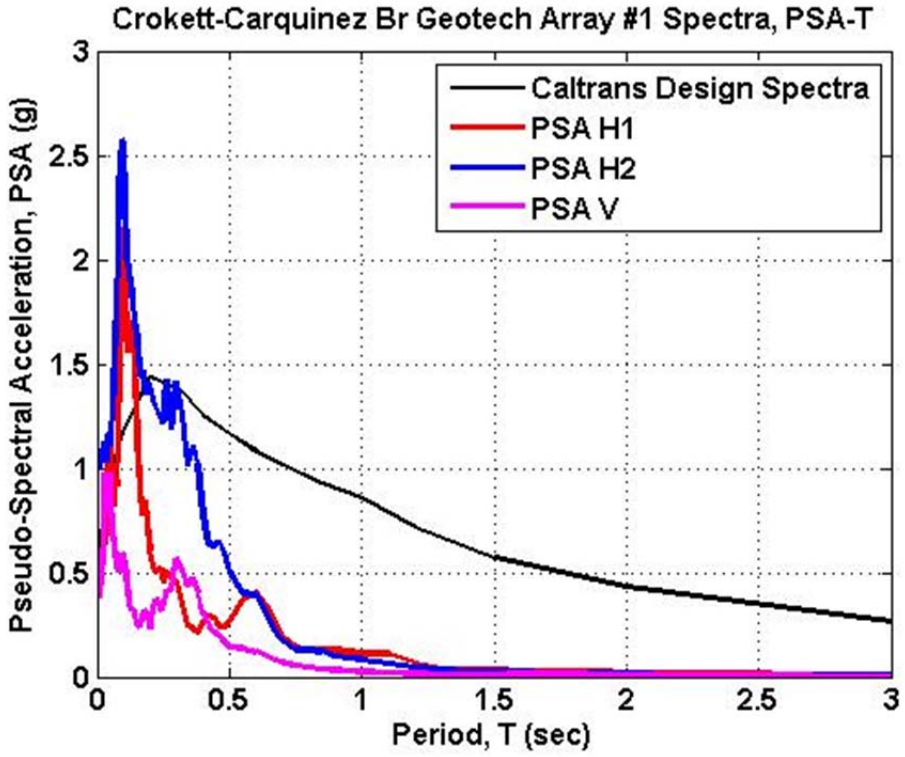

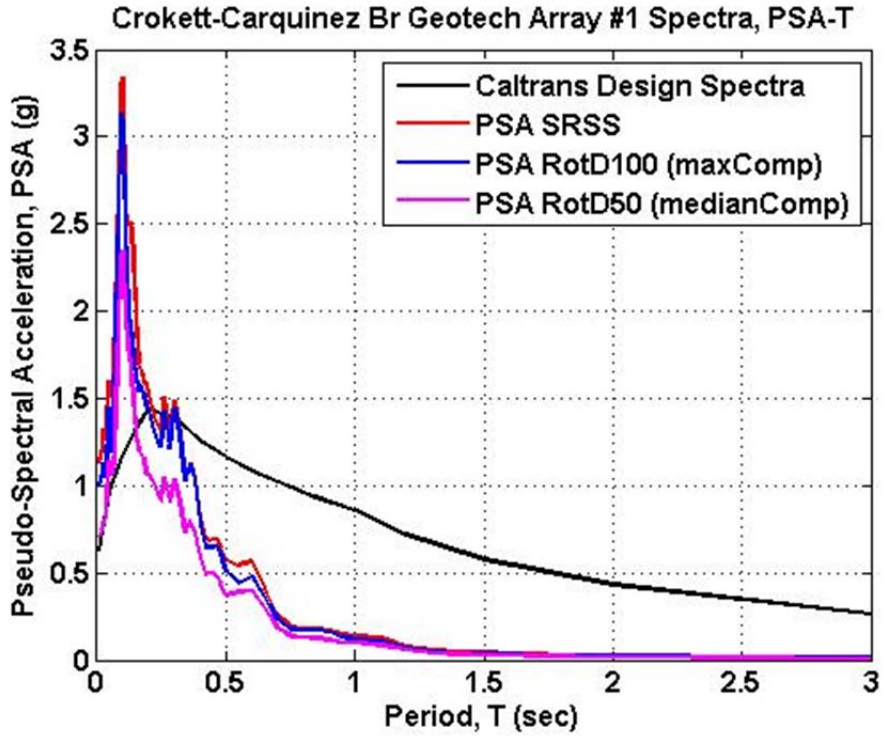

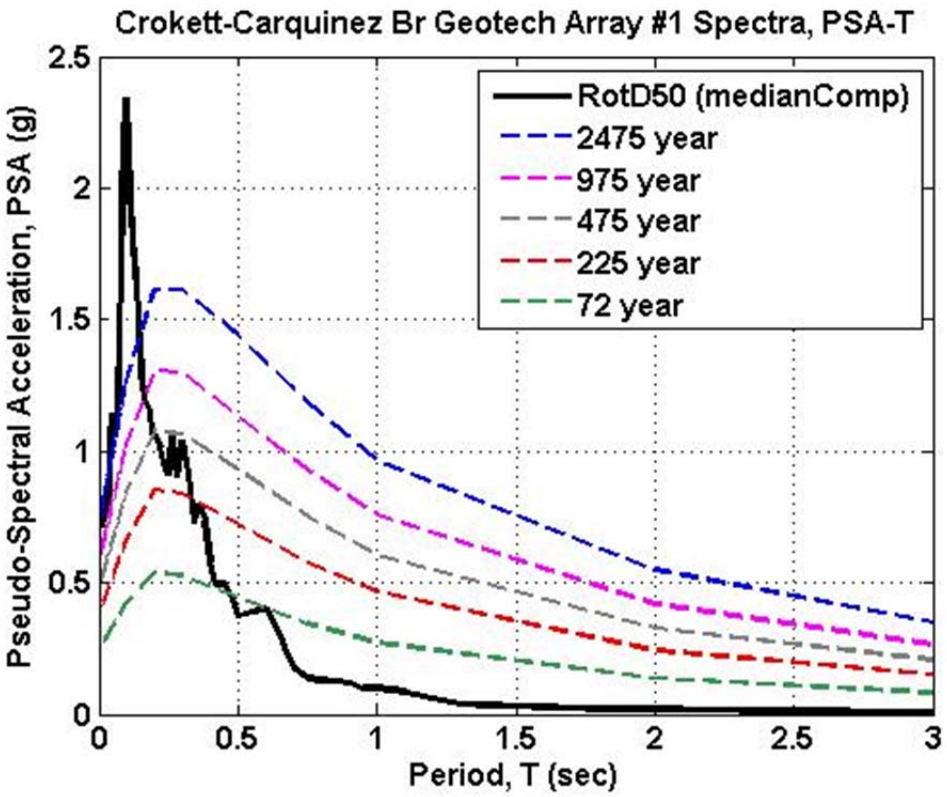
Crokett-Carquinez Br Geotech Array #1 Spectra, PSA-T
RotD50 (medianComp)
2475 year
975 year
475 year
225 year
72 year
Pseudo-Spectral Acceleration, PSA (g)
Period, T (sec)
0
0.5
1
1.5
2
2.5
3

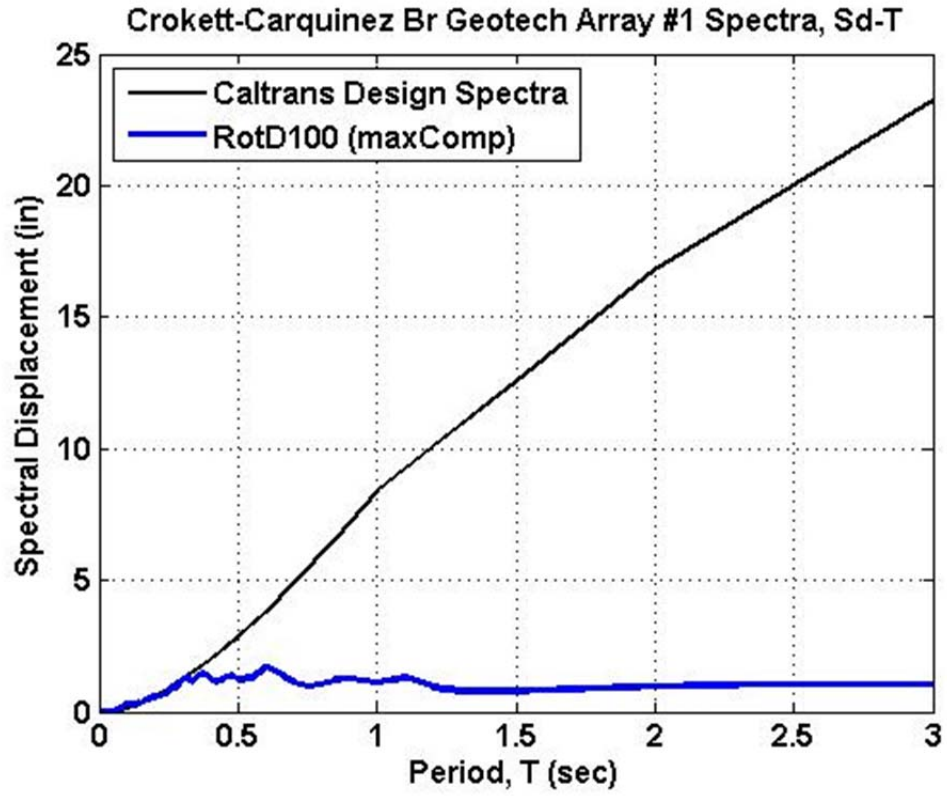
Crokett-Carquinez Br Geotech Array #1 Spectra, Sd-T
Caltrans Design Spectra
RotD100 (maxComp)
Spectral Displacement (in)
Period, T (sec)
0
5
10
15
20
25
0.5
1
1.5
2
2.5
3

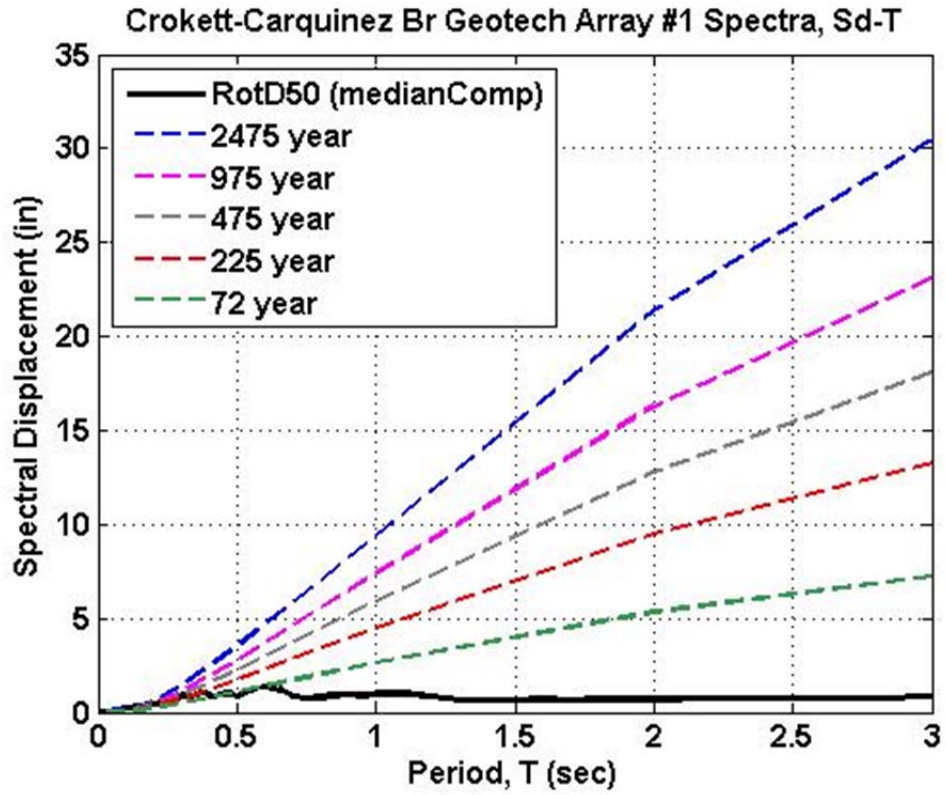
Crokett-Carquinez Br Geotech Array #1 Spectra, Sd-T
RotD50 (medianComp)
2475 year
975 year
475 year
225 year
72 year
Spectral Displacement (in)
Period, T (sec)
0
5
10
15
20
25
30
35
0
0.5
1
1.5
2
2.5
3

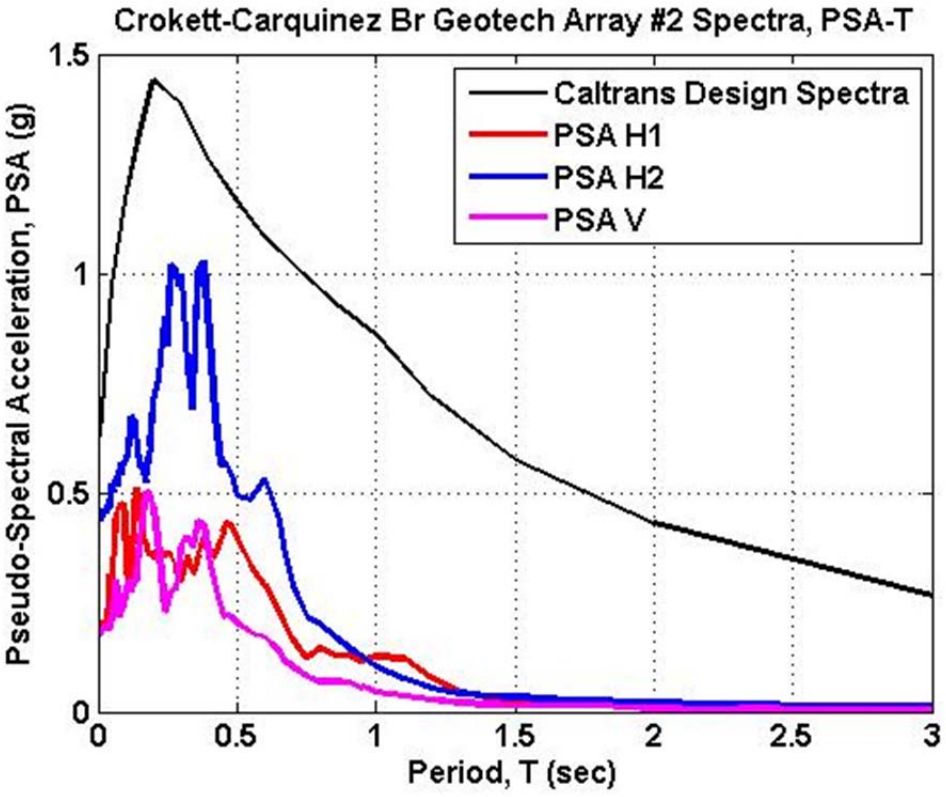
Crokett-Carquinez Br Geotech Array #2 Spectra, PSA-T
Caltrans Design Spectra
PSA H1
PSA H2
PSA V
Pseudo-Spectral Acceleration, PSA (g)
Period, T (sec)
0
0.5
1
1.5
0
0.5
1
1.5
2
2.5
3

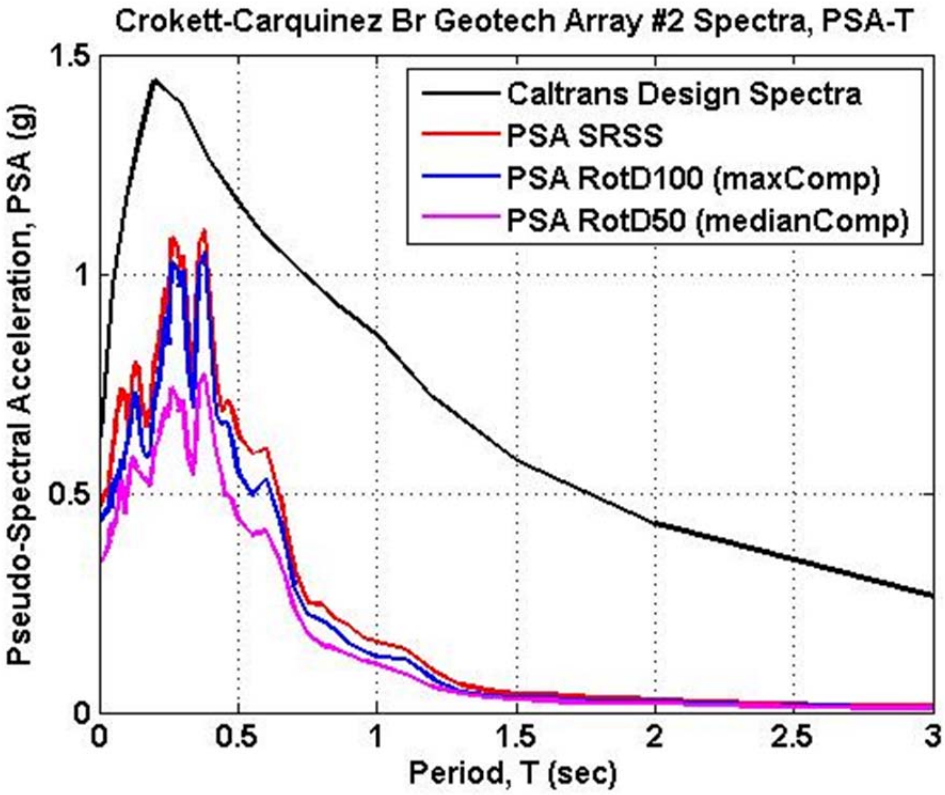
Crokett-Carquinez Br Geotech Array #2 Spectra, PSA-T
Caltrans Design Spectra
PSA SRSS
PSA RotD100 (maxComp)
PSA RotD50 (medianComp)
Pseudo-Spectral Acceleration, PSA (g)
Period, T (sec)
0
0.5
1
1.5
2
2.5
3

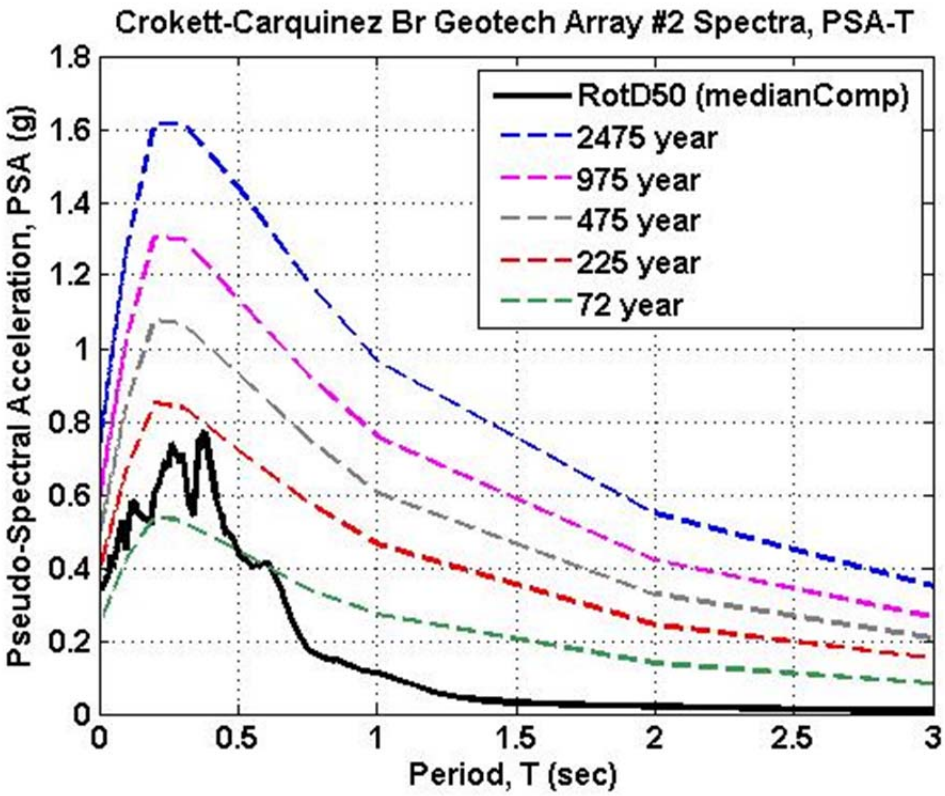
Crokett-Carquinez Br Geotech Array #2 Spectra, PSA-T
RotD50 (medianComp)
2475 year
975 year
475 year
225 year
72 year
Pseudo-Spectral Acceleration, PSA (g)
Period, T (sec)
0
0.2
0.4
0.6
0.8
1
1.2
1.4
1.6
1.8
0.5
1.5
2
2.5
3

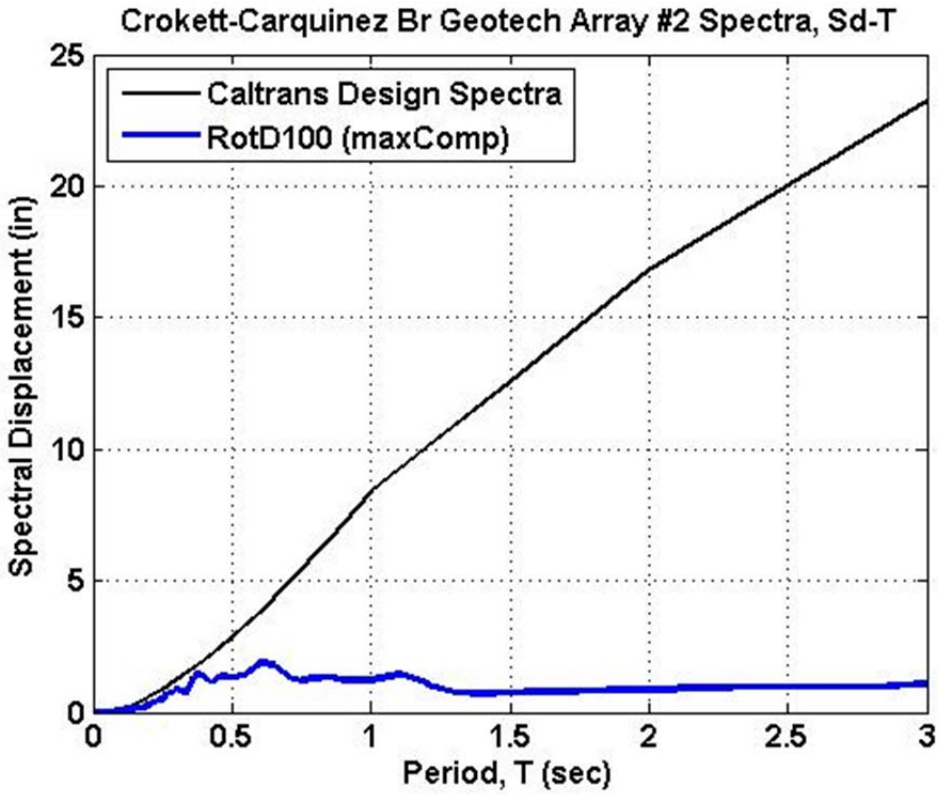
Crokett-Carquinez Br Geotech Array #2 Spectra, Sd-T
Caltrans Design Spectra
RotD100 (maxComp)
Spectral Displacement (in)
Period, T (sec)
0
5
10
15
20
25
0
0.5
1
1.5
2
2.5
3

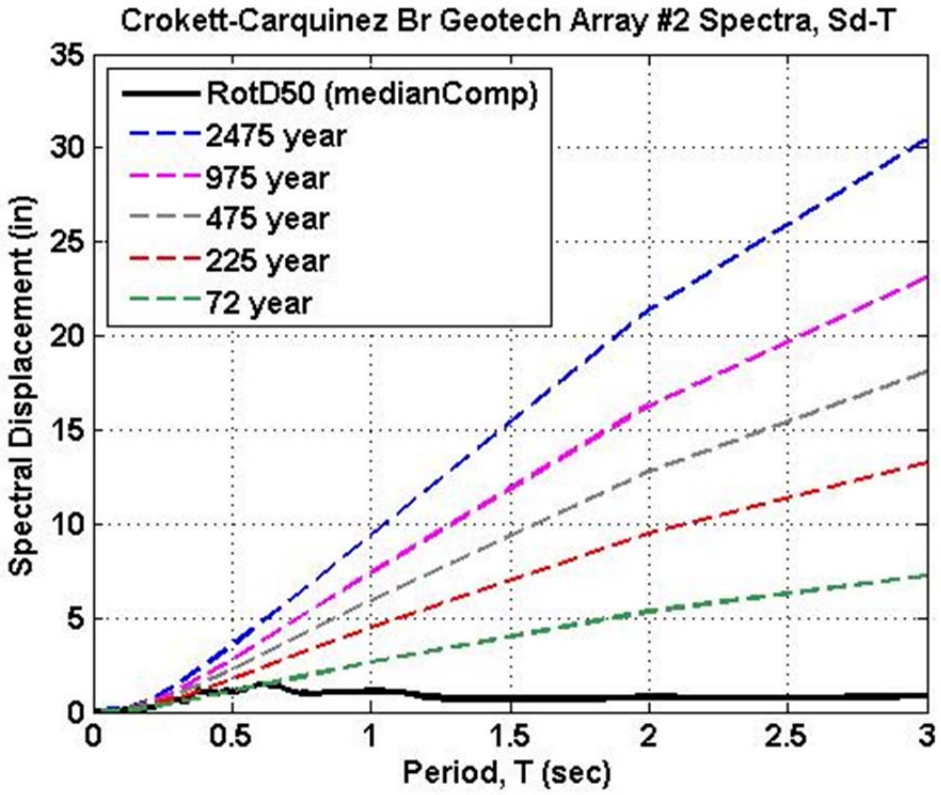
Crokett-Carquinez Br Geotech Array #2 Spectra, Sd-T
RotD50 (medianComp)
2475 year
975 year
475 year
225 year
72 year
Spectral Displacement (in)
Period, T (sec)
0
5
10
15
20
25
30
35
0
0.5
1
1.5
2
2.5
3

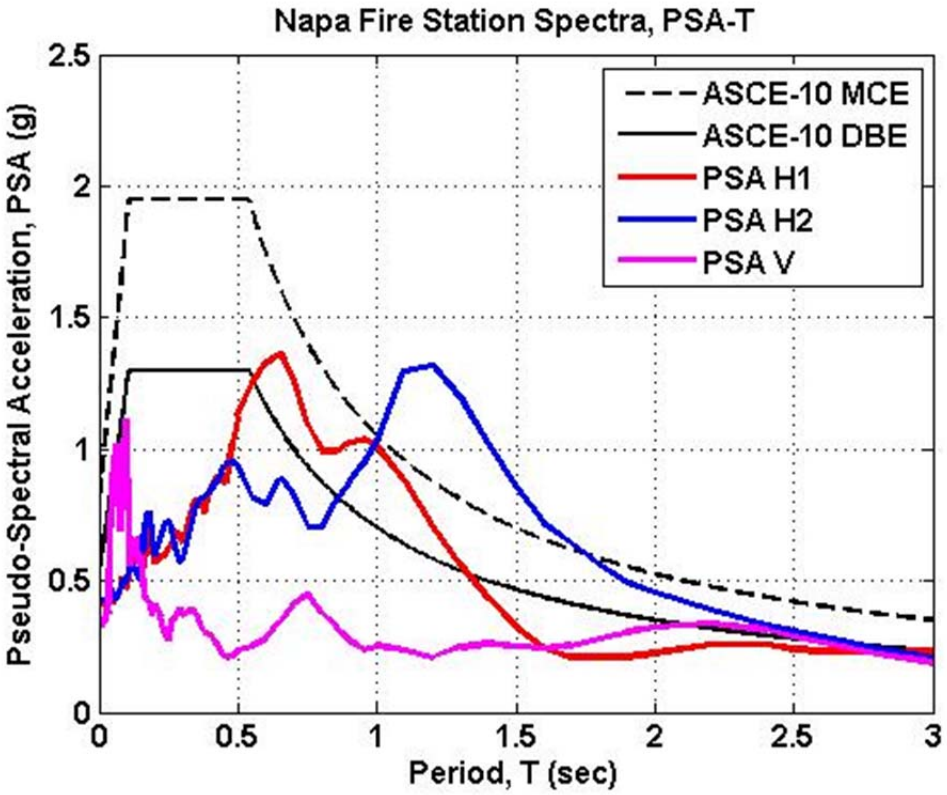
Napa Fire Station Spectra, PSA-T
ASCE-10 MCE
ASCE-10 DBE
PSA H1
PSA H2
PSA V
Pseudo-Spectral Acceleration, PSA (g)
Period, T (sec)
0
0.5
1
1.5
2
2.5
3

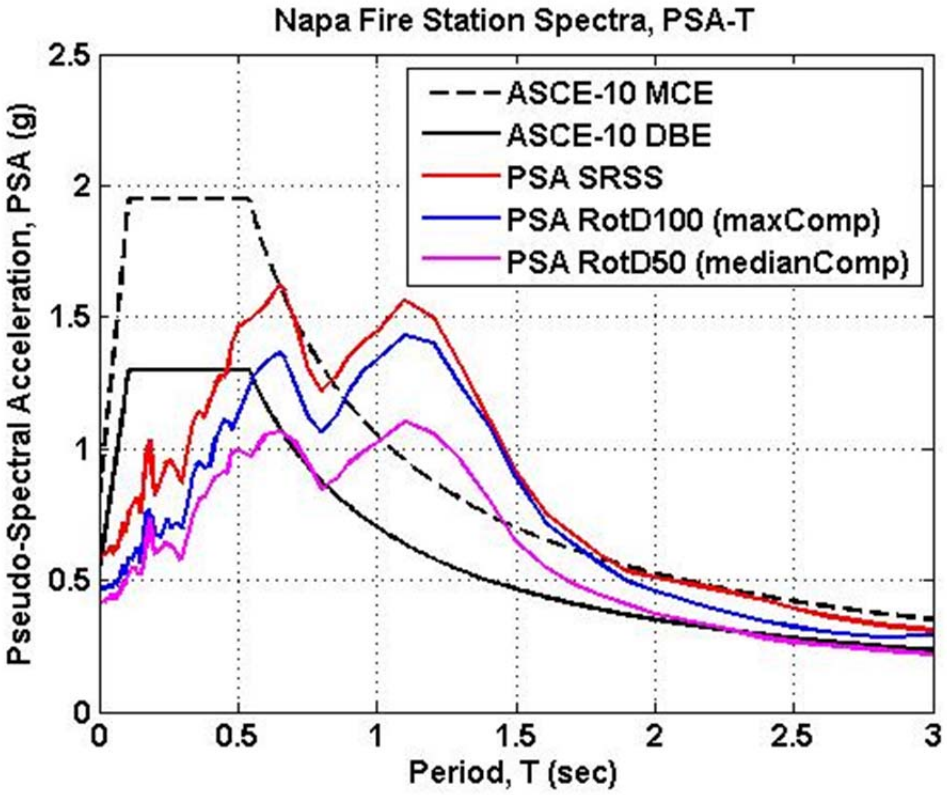
Napa Fire Station Spectra, PSA-T
ASCE-10 MCE
ASCE-10 DBE
PSA SRSS
PSA RotD100 (maxComp)
PSA RotD50 (medianComp)
Pseudo-Spectral Acceleration, PSA (g)
Period, T (sec)
0
0.5
1
1.5
2
2.5
3

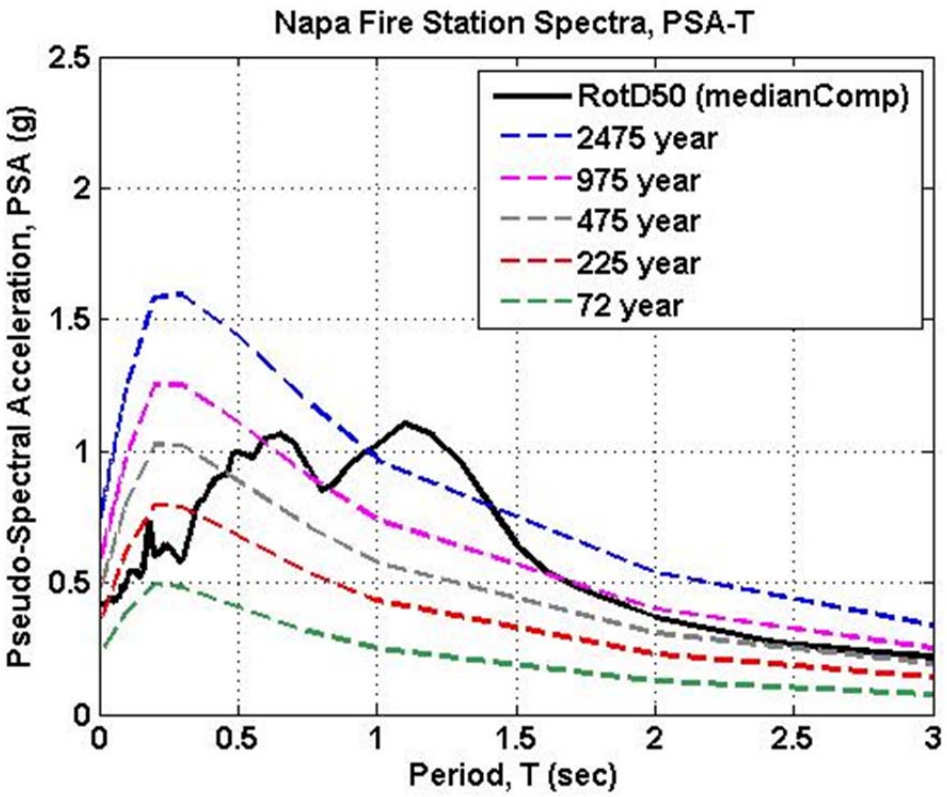
Napa Fire Station Spectra, PSA-T
RotD50 (medianComp)
2475 year
975 year
475 year
225 year
72 year
Pseudo-Spectral Acceleration, PSA (g)
Period, T (sec)
0
0.5
1
1.5
2
2.5
3

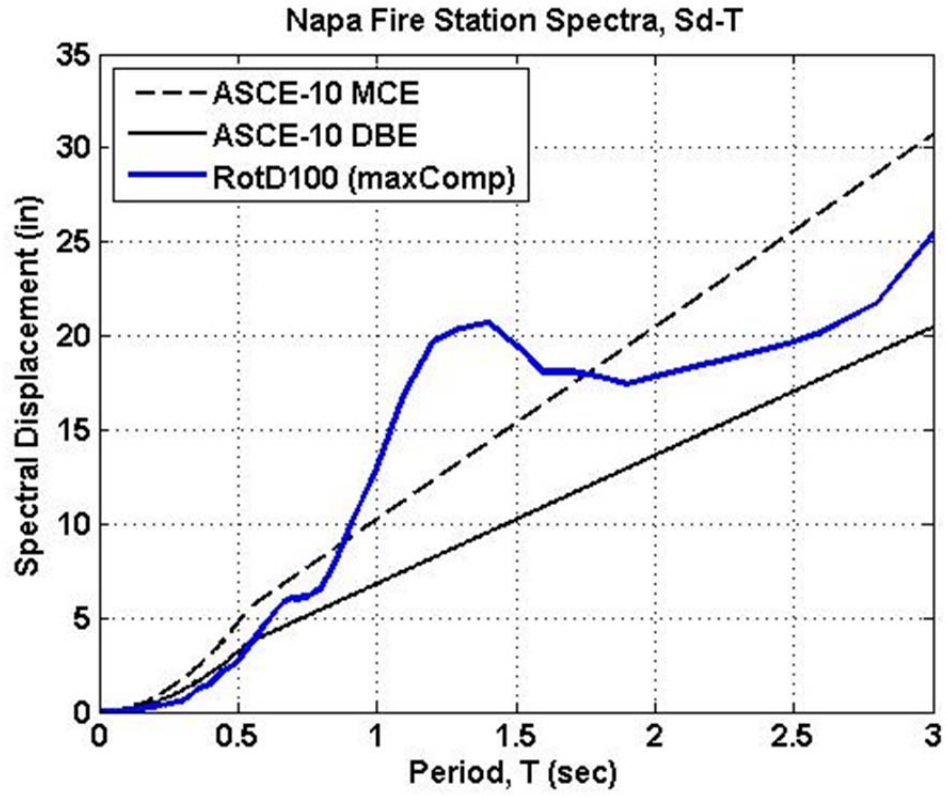
Napa Fire Station Spectra, Sd-T
ASCE-10 MCE
ASCE-10 DBE
RotD100 (maxComp)
Spectral Displacement (in)
Period, T (sec)
0
5
10
15
20
25
30
35
0.5
1
1.5
2
2.5
3

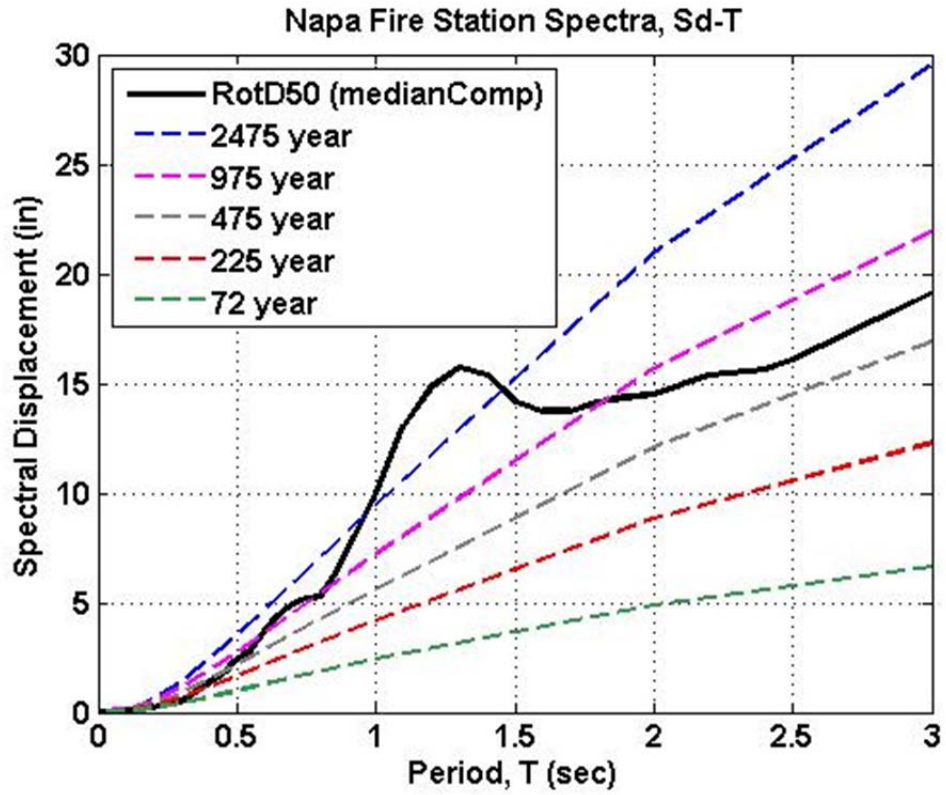
Napa Fire Station Spectra, Sd-T
RotD50 (medianComp)
2475 year
975 year
475 year
225 year
72 year
Spectral Displacement (in)
Period, T (sec)
0
5
10
15
20
25
30
0
0.5
1
1.5
2
2.5
3

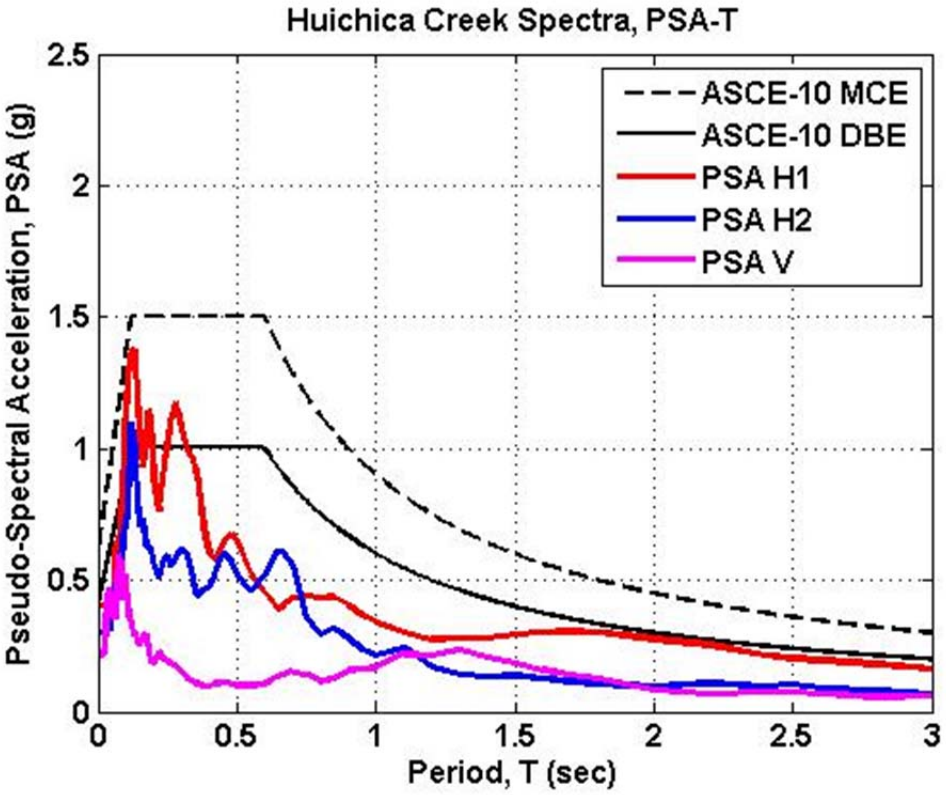
Huichica Creek Spectra, PSA-T
ASCE-10 MCE
ASCE-10 DBE
PSA H1
PSA H2
PSA V
Pseudo-Spectral Acceleration, PSA (g)
Period, T (sec)
0
0.5
1
1.5
2
2.5
0
0.5
1
1.5
2
2.5
3

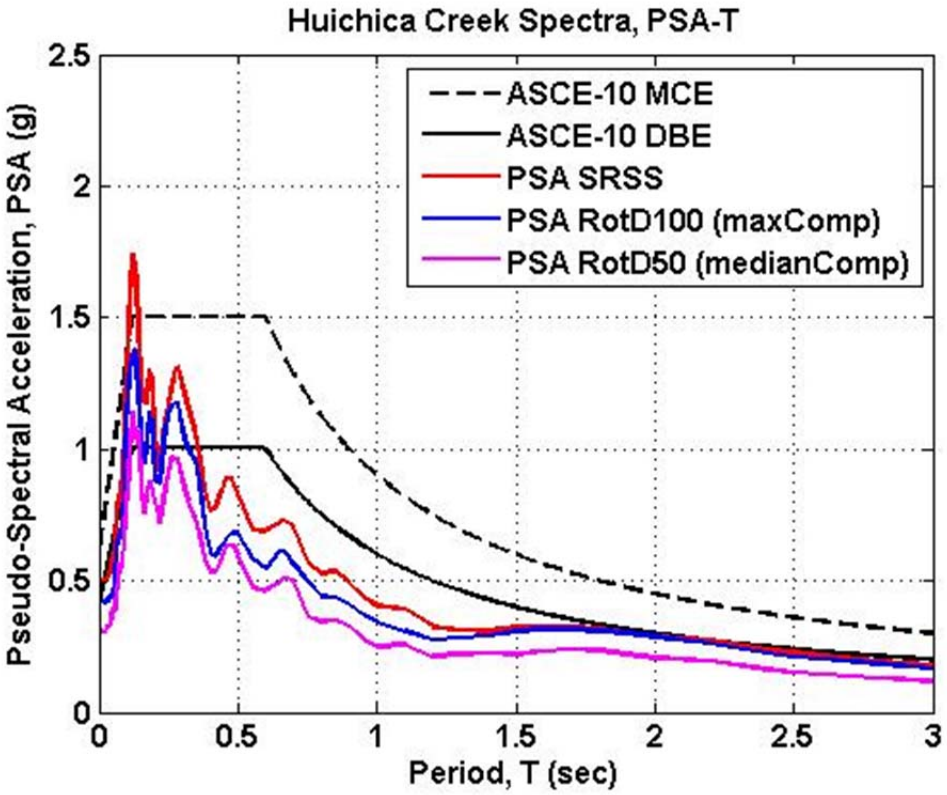
Huichica Creek Spectra, PSA-T
ASCE-10 MCE
ASCE-10 DBE
PSA SRSS
PSA RotD100 (maxComp)
PSA RotD50 (medianComp)
Pseudo-Spectral Acceleration, PSA (g)
Period, T (sec)
0
0.5
1
1.5
2
2.5
3

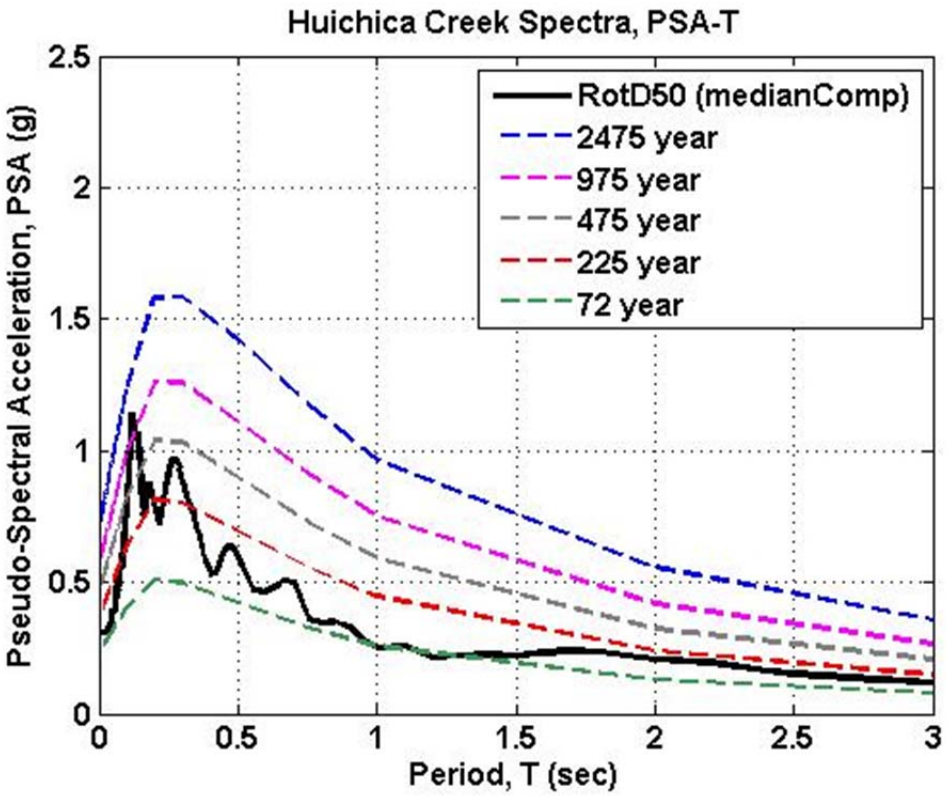
Huichica Creek Spectra, PSA-T
RotD50 (medianComp)
2475 year
975 year
475 year
225 year
72 year
Pseudo-Spectral Acceleration, PSA (g)
Period, T (sec)
0
0.5
1
1.5
2
2.5
3

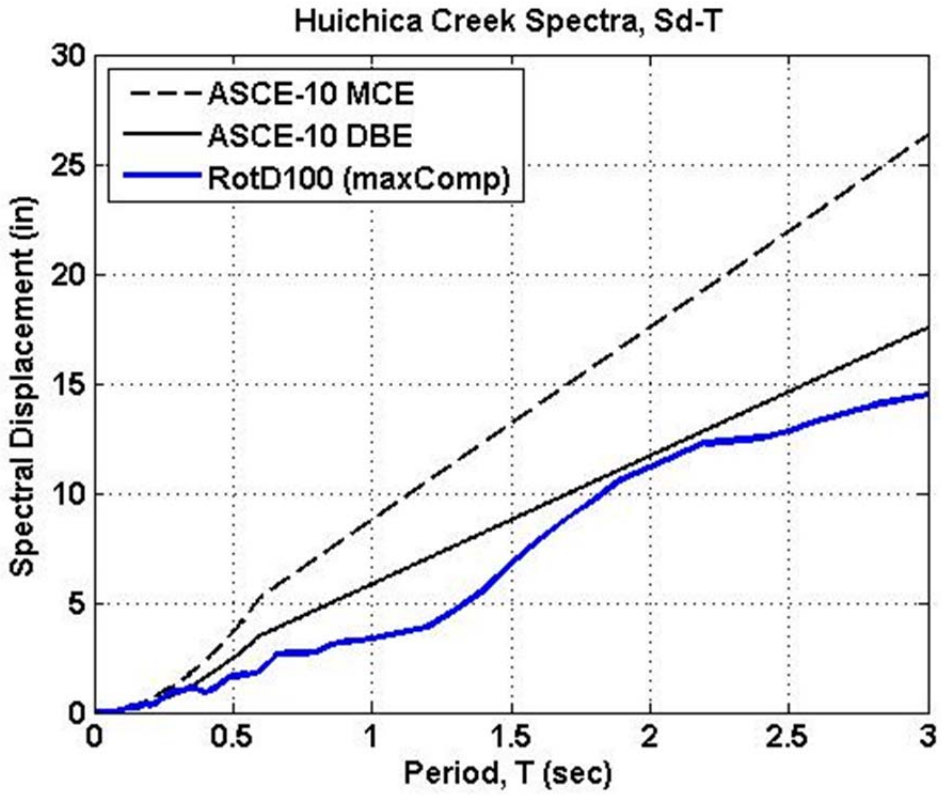
Huichica Creek Spectra, Sd-T
ASCE-10 MCE
ASCE-10 DBE
RotD100 (maxComp)
Spectral Displacement (in)
Period, T (sec)
0
5
10
15
20
25
30
0
0.5
1
1.5
2
2.5
3

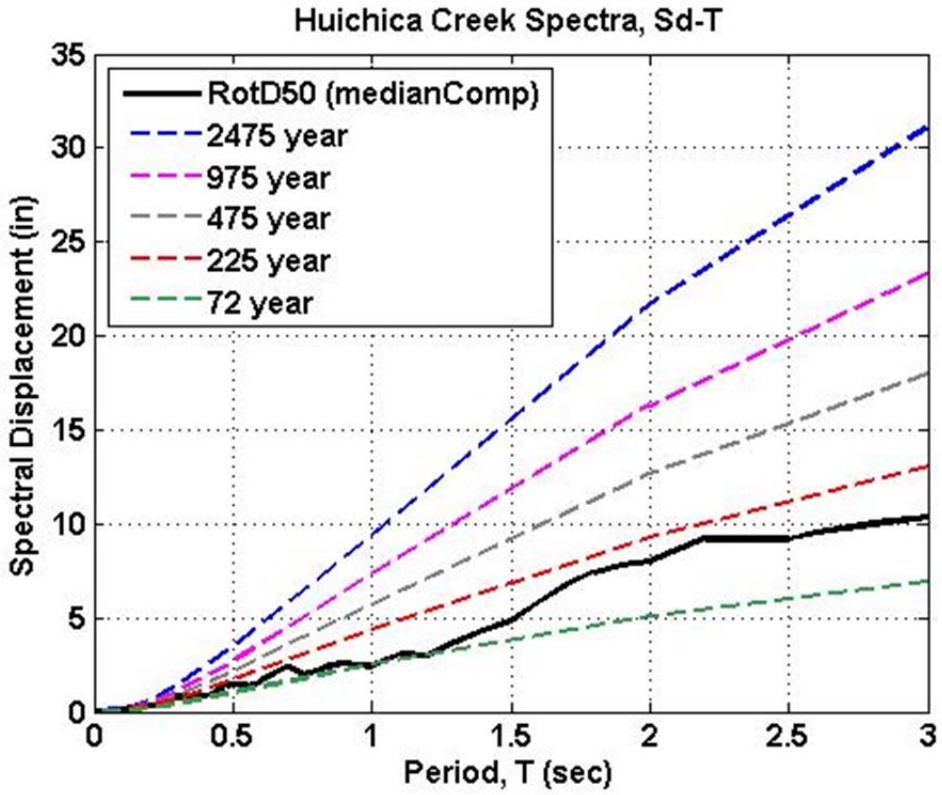
Huichica Creek Spectra, Sd-T
RotD50 (medianComp)
2475 year
975 year
475 year
225 year
72 year
Spectral Displacement (in)
Period, T (sec)
0
5
10
15
20
25
30
35
0
0.5
1
1.5
2
2.5
3

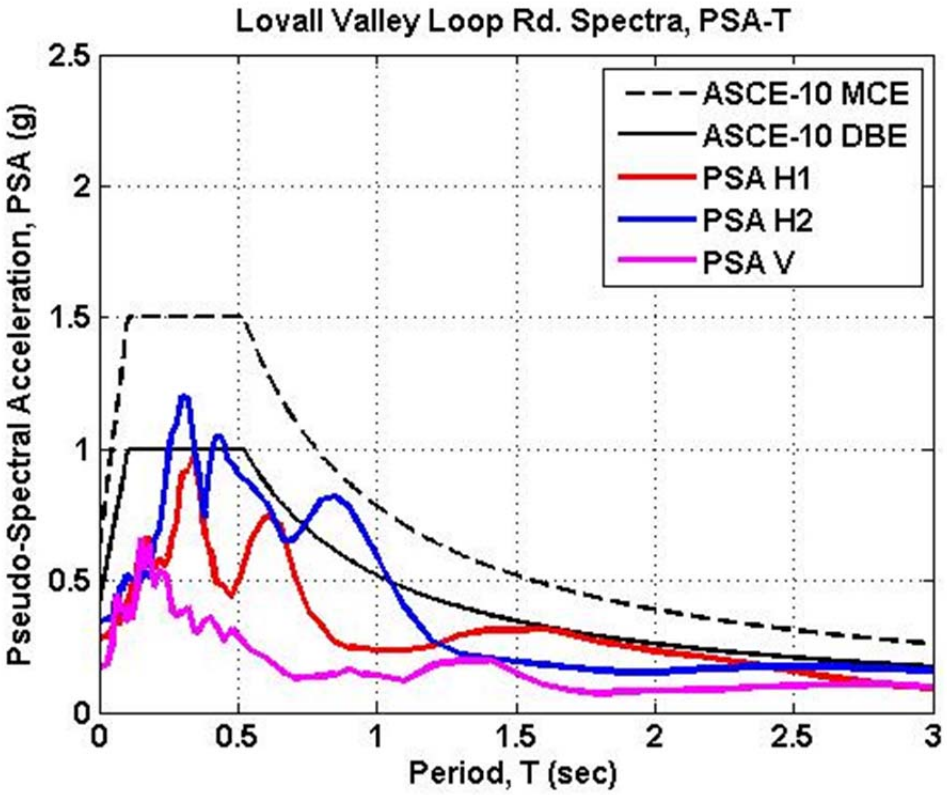
Lovall Valley Loop Rd. Spectra, PSA-T
ASCE-10 MCE
ASCE-10 DBE
PSA H1
PSA H2
PSA V
Pseudo-Spectral Acceleration, PSA (g)
Period, T (sec)
0
0.5
1
1.5
2
2.5
3

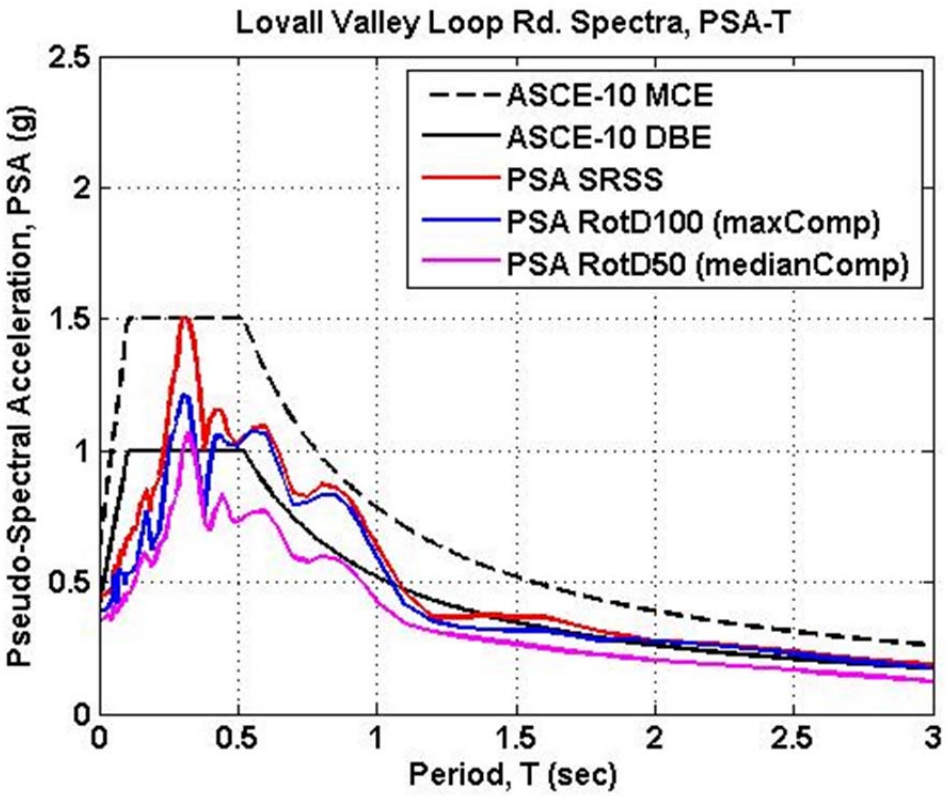
Lovall Valley Loop Rd. Spectra, PSA-T
ASCE-10 MCE
ASCE-10 DBE
PSA SRSS
PSA RotD100 (maxComp)
PSA RotD50 (medianComp)
Pseudo-Spectral Acceleration, PSA (g)
Period, T (sec)
0
0.5
1
1.5
2
2.5
3

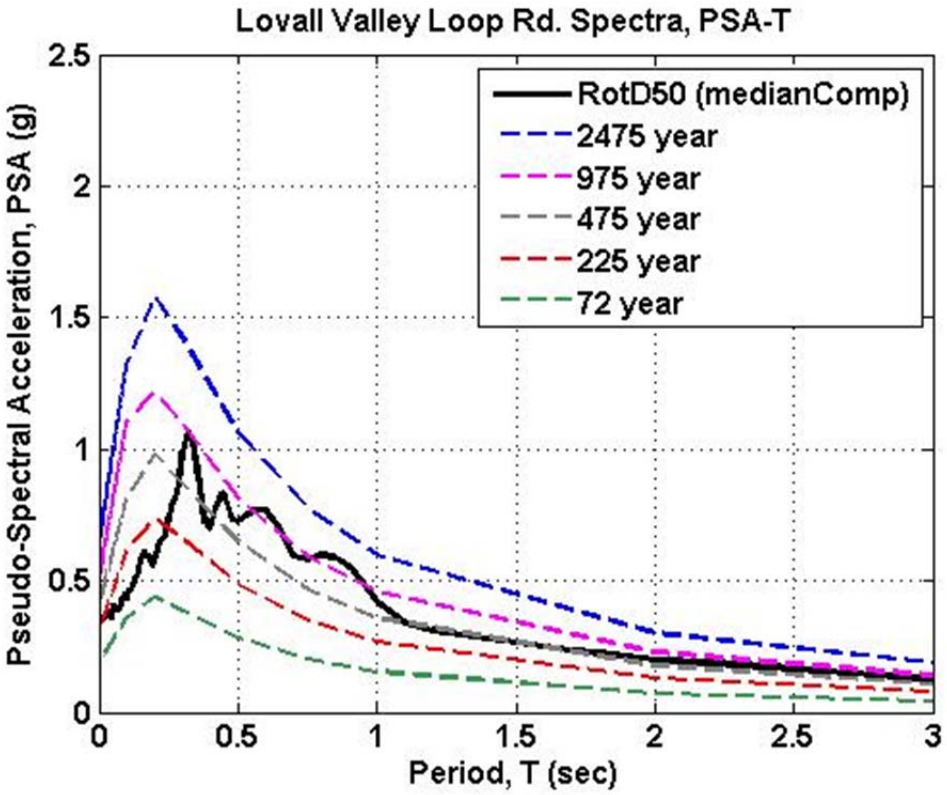
Lovall Valley Loop Rd. Spectra, PSA-T
Pseudo-Spectral Acceleration, PSA (g)
Period, T (sec)
RotD50 (medianComp)
2475 year
975 year
475 year
225 year
72 year
0
0.5
1
1.5
2
2.5
3

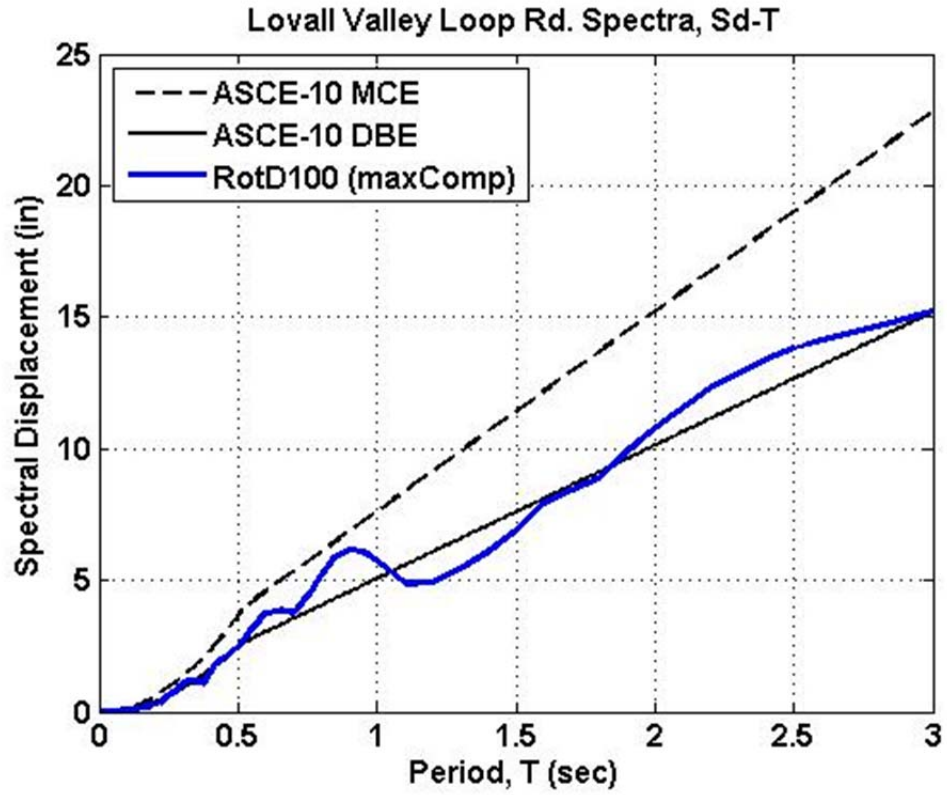
Lovall Valley Loop Rd. Spectra, Sd-T
Spectral Displacement (in)
Period, T (sec)
ASCE-10 MCE
ASCE-10 DBE
RotD100 (maxComp)
0
5
10
15
20
25
0.5
1
1.5
2
2.5
3

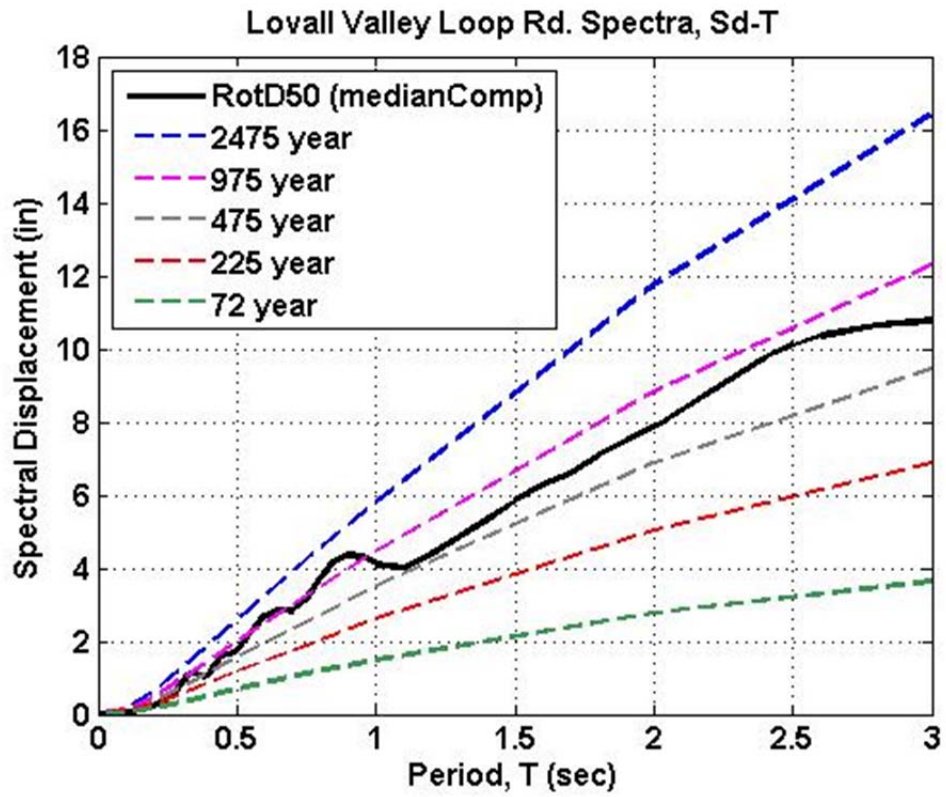
Lovall Valley Loop Rd. Spectra, Sd-T
RotD50 (medianComp)
2475 year
975 year
475 year
225 year
72 year
Spectral Displacement (in)
Period, T (sec)
0
2
4
6
8
10
12
14
16
18
0.5
1
1.5
2
2.5
3

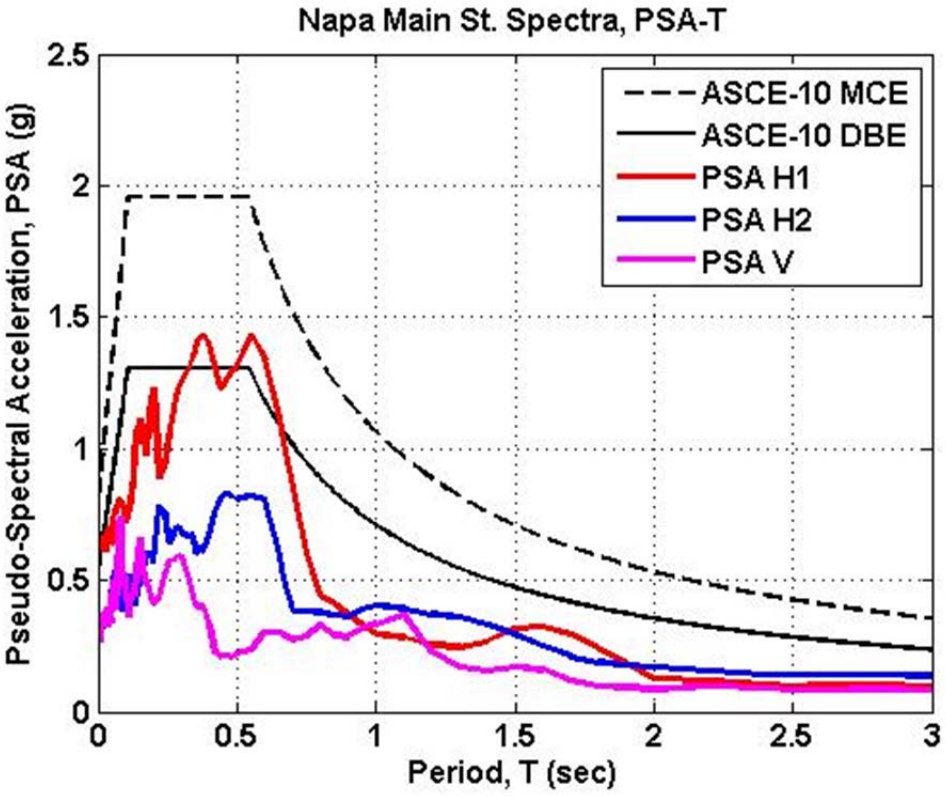
Napa Main St. Spectra, PSA-T
ASCE-10 MCE
ASCE-10 DBE
PSA H1
PSA H2
PSA V
Pseudo-Spectral Acceleration, PSA (g)
Period, T (sec)
0
0.5
1
1.5
2
2.5
3

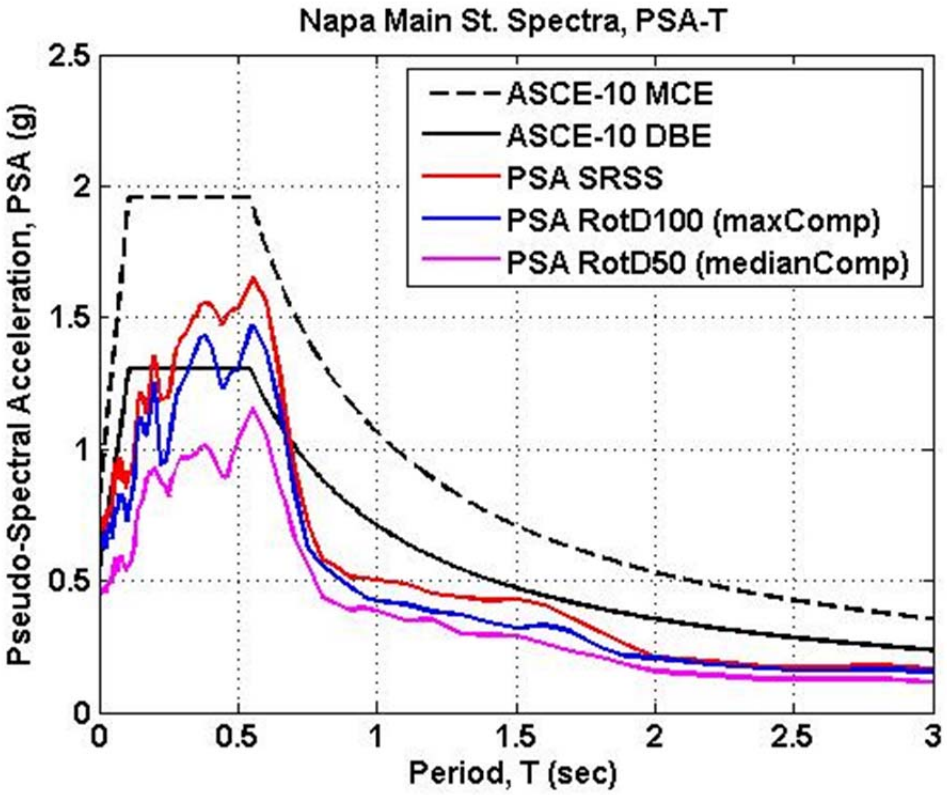
Napa Main St. Spectra, PSA-T
ASCE-10 MCE
ASCE-10 DBE
PSA SRSS
PSA RotD100 (maxComp)
PSA RotD50 (medianComp)
Pseudo-Spectral Acceleration, PSA (g)
Period, T (sec)
0
0.5
1
1.5
2
2.5
3

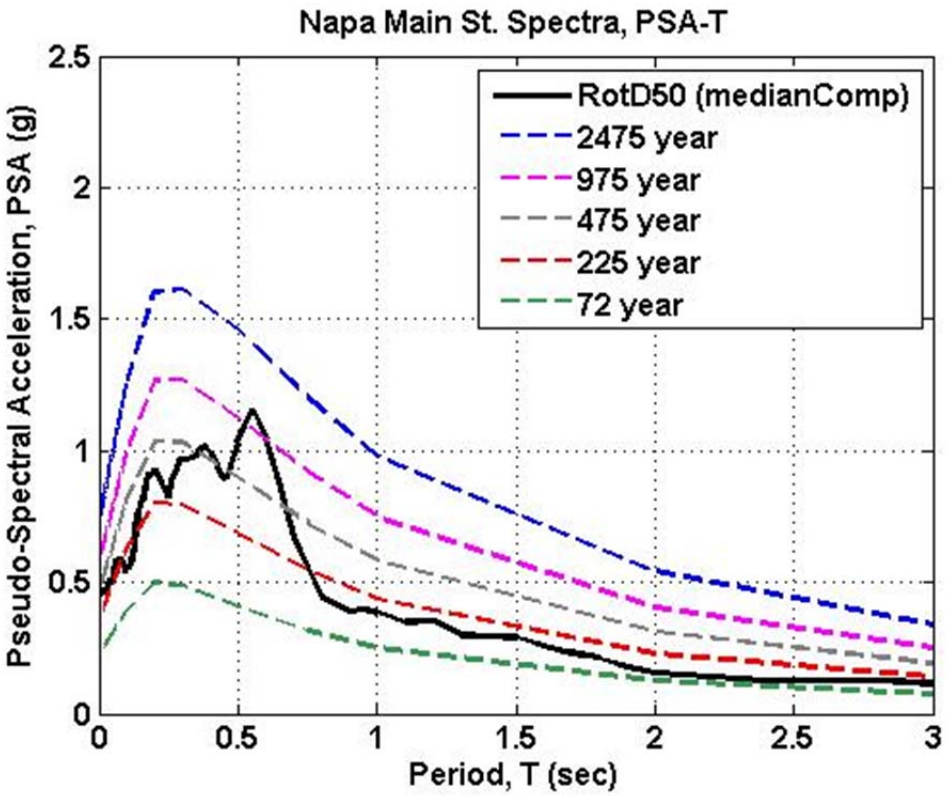
Napa Main St. Spectra, PSA-T
RotD50 (medianComp)
2475 year
975 year
475 year
225 year
72 year
Pseudo-Spectral Acceleration, PSA (g)
Period, T (sec)
0
0.5
1
1.5
2
2.5
3

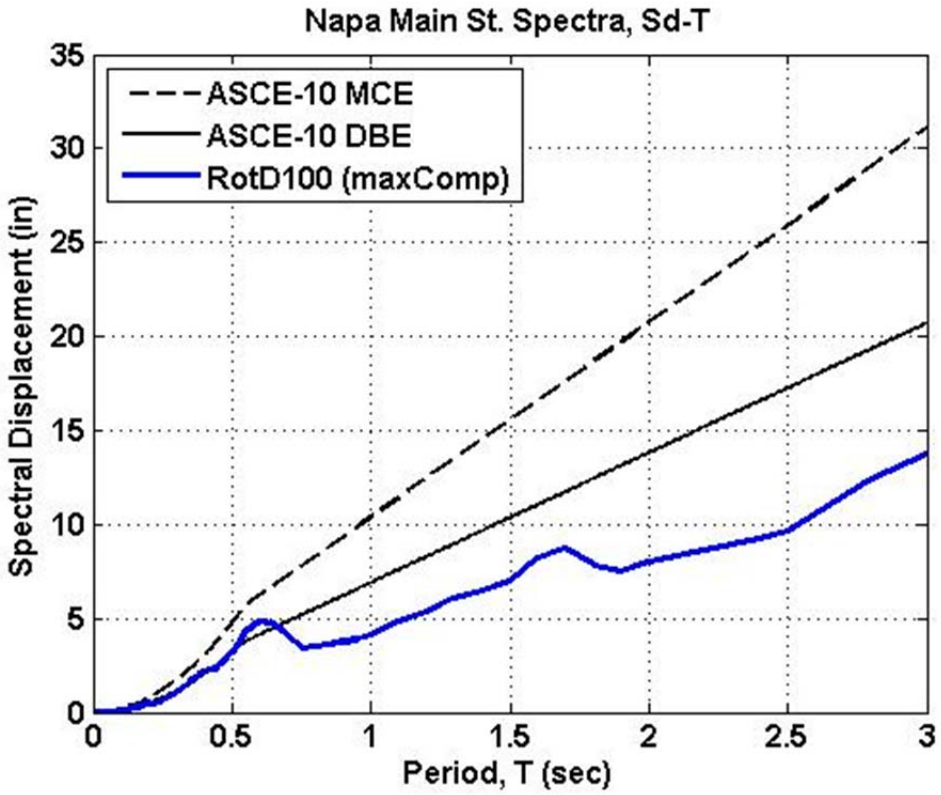
Napa Main St. Spectra, Sd-T
ASCE-10 MCE
ASCE-10 DBE
RotD100 (maxComp)
Spectral Displacement (in)
Period, T (sec)
0
5
10
15
20
25
30
35
0.5
1
1.5
2
2.5
3

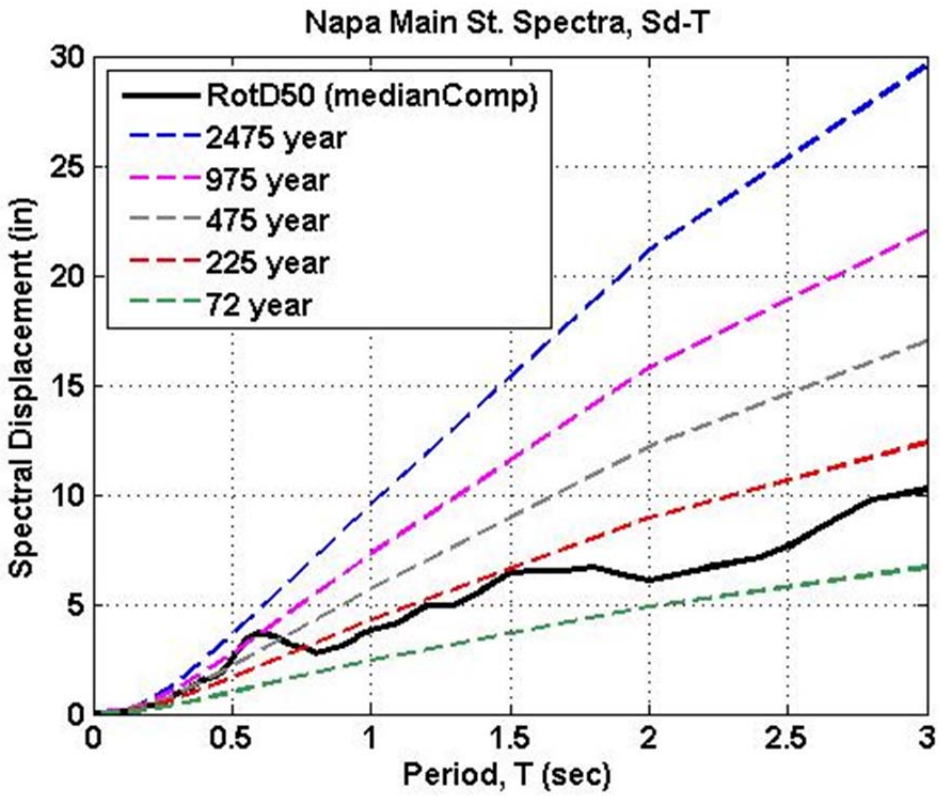
Napa Main St. Spectra, Sd-T
RotD50 (medianComp)
2475 year
975 year
475 year
225 year
72 year
Spectral Displacement (in)
Period, T (sec)
0
5
10
15
20
25
30
0.5
1
1.5
2
2.5
3

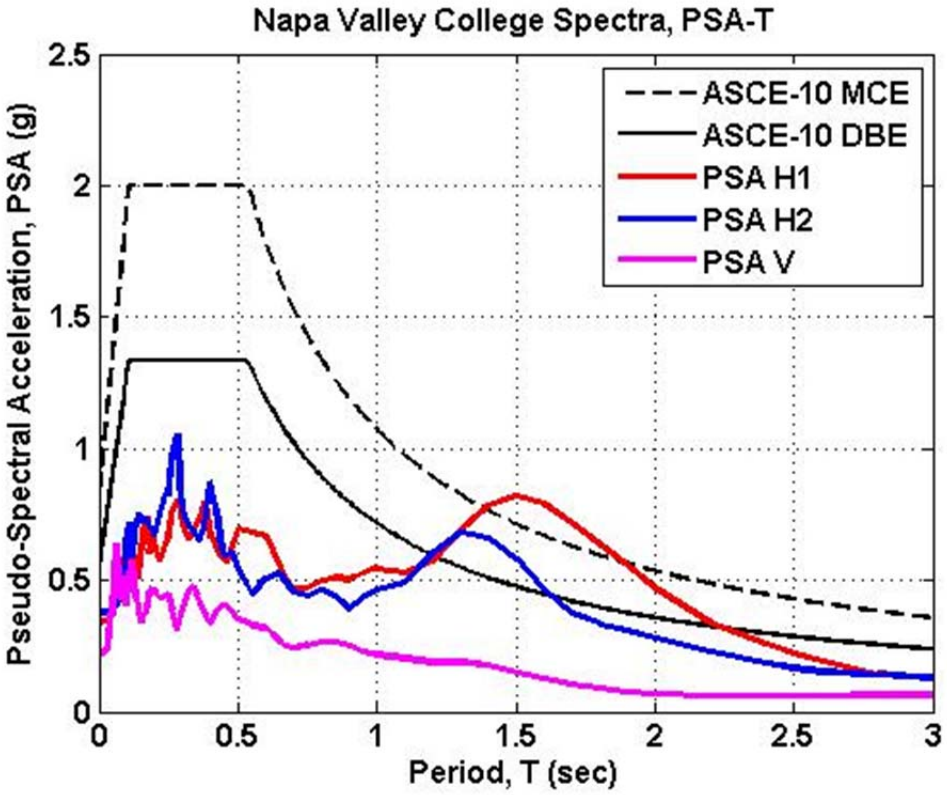
Napa Valley College Spectra, PSA-T
ASCE-10 MCE
ASCE-10 DBE
PSA H1
PSA H2
PSA V
Pseudo-Spectral Acceleration, PSA (g)
Period, T (sec)
0
0.5
1
1.5
2
2.5
3

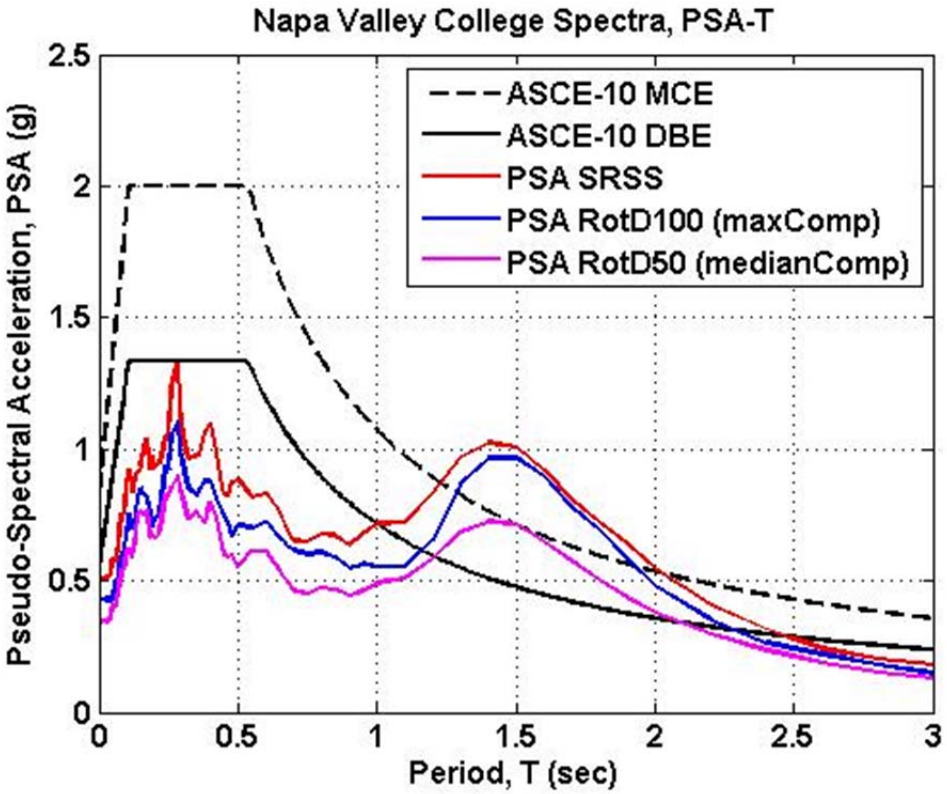
Napa Valley College Spectra, PSA-T
ASCE-10 MCE
ASCE-10 DBE
PSA SRSS
PSA RotD100 (maxComp)
PSA RotD50 (medianComp)
Pseudo-Spectral Acceleration, PSA (g)
Period, T (sec)
0
0.5
1
1.5
2
2.5
3

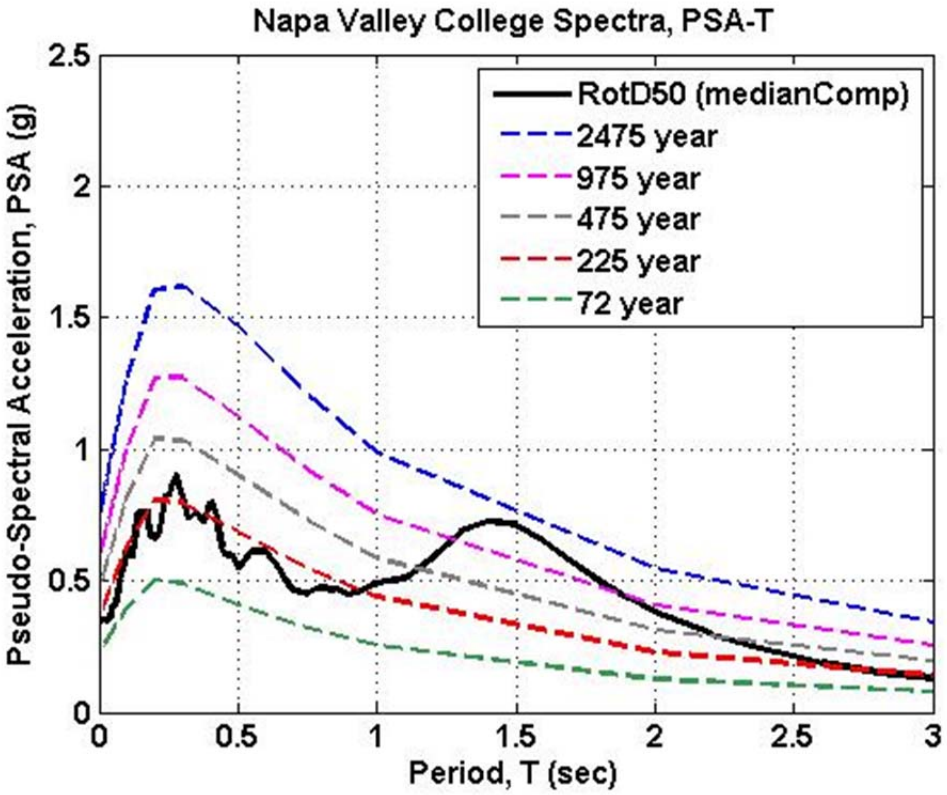
Napa Valley College Spectra, PSA-T
RotD50 (medianComp)
2475 year
975 year
475 year
225 year
72 year
Pseudo-Spectral Acceleration, PSA (g)
Period, T (sec)
0
0.5
1
1.5
2
2.5
3

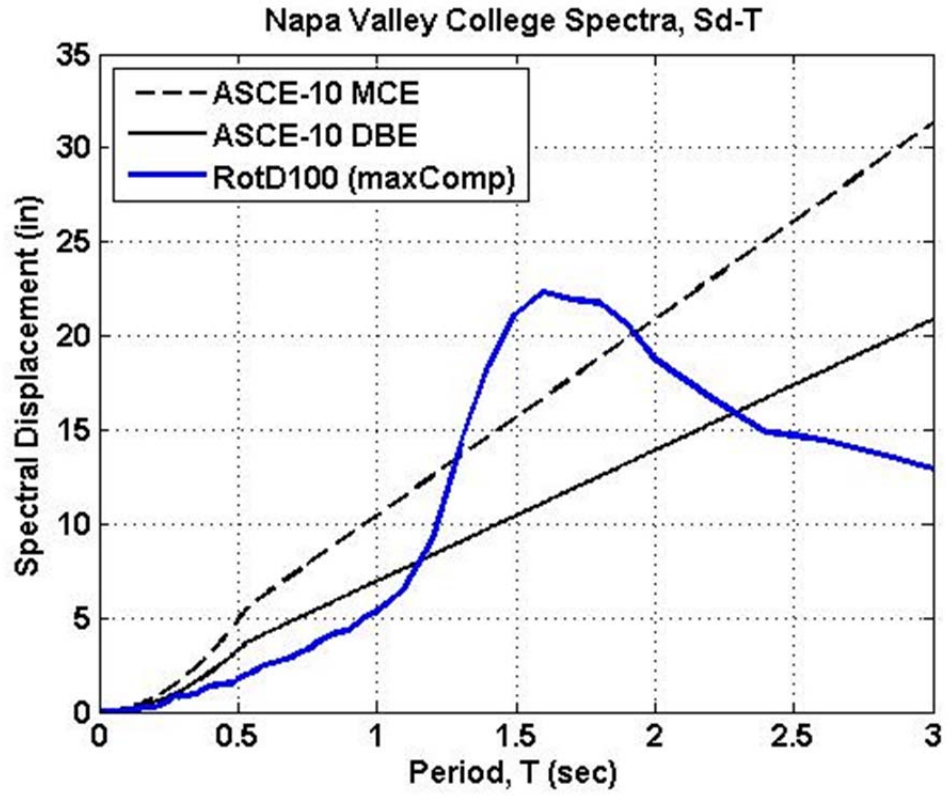
Napa Valley College Spectra, Sd-T
ASCE-10 MCE
ASCE-10 DBE
RotD100 (maxComp)
Spectral Displacement (in)
Period, T (sec)
0
5
10
15
20
25
30
35
0.5
1
1.5
2
2.5
3

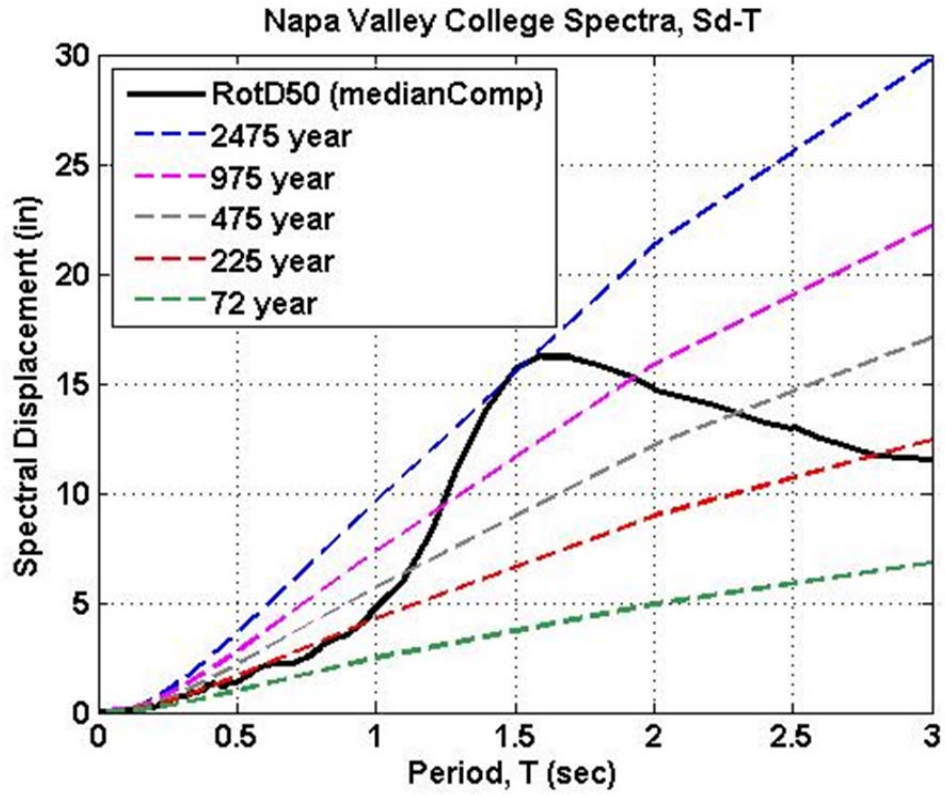
Napa Valley College Spectra, Sd-T
RotD50 (medianComp)
2475 year
975 year
475 year
225 year
72 year
Spectral Displacement (in)
Period, T (sec)
0
5
10
15
20
25
30
0
0.5
1
1.5
2
2.5
3

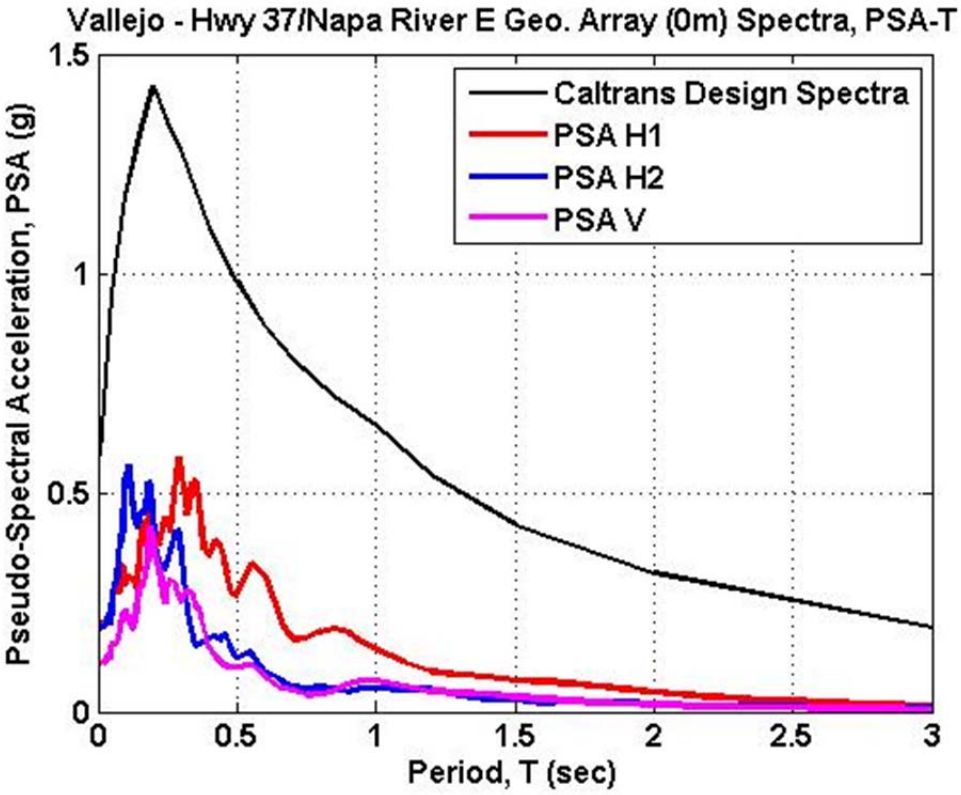
Vallejo - Hwy 37/Napa River E Geo. Array (0m) Spectra, PSA-T
Caltrans Design Spectra
PSA H1
PSA H2
PSA V
Pseudo-Spectral Acceleration, PSA (g)
Period, T (sec)
0
0.5
1
1.5
0
0.5
1
1.5
2
2.5
3

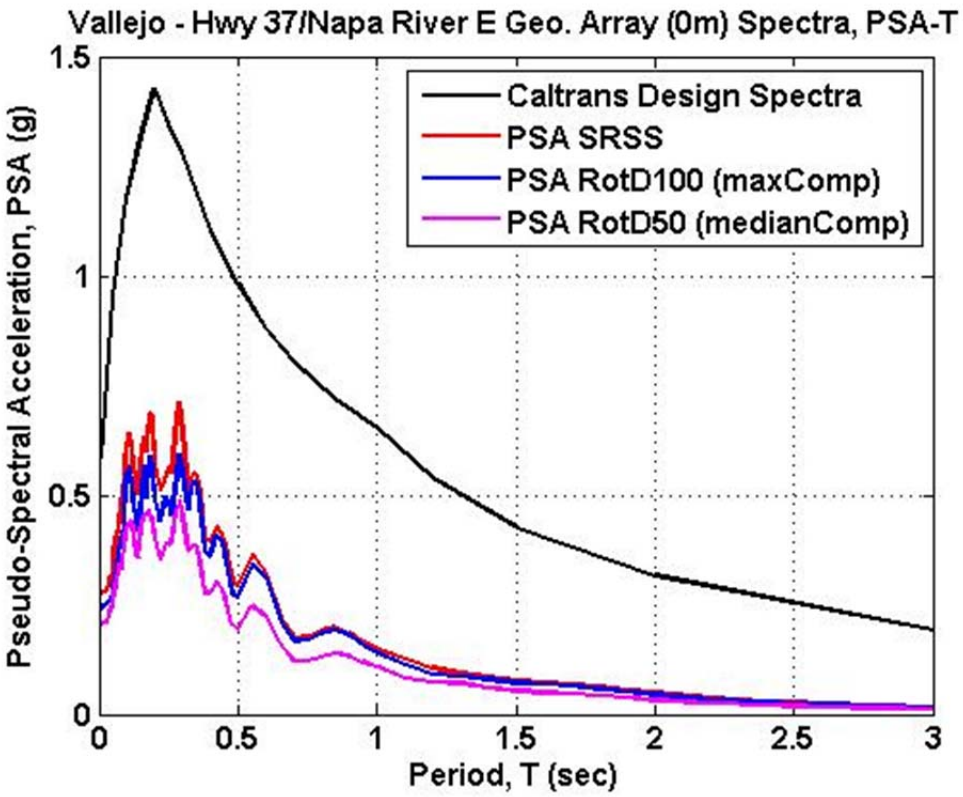
Vallejo - Hwy 37/Napa River E Geo. Array (0m) Spectra, PSA-T
Caltrans Design Spectra
PSA SRSS
PSA RotD100 (maxComp)
PSA RotD50 (medianComp)
Pseudo-Spectral Acceleration, PSA (g)
Period, T (sec)
0
0.5
1
1.5
2
2.5
3

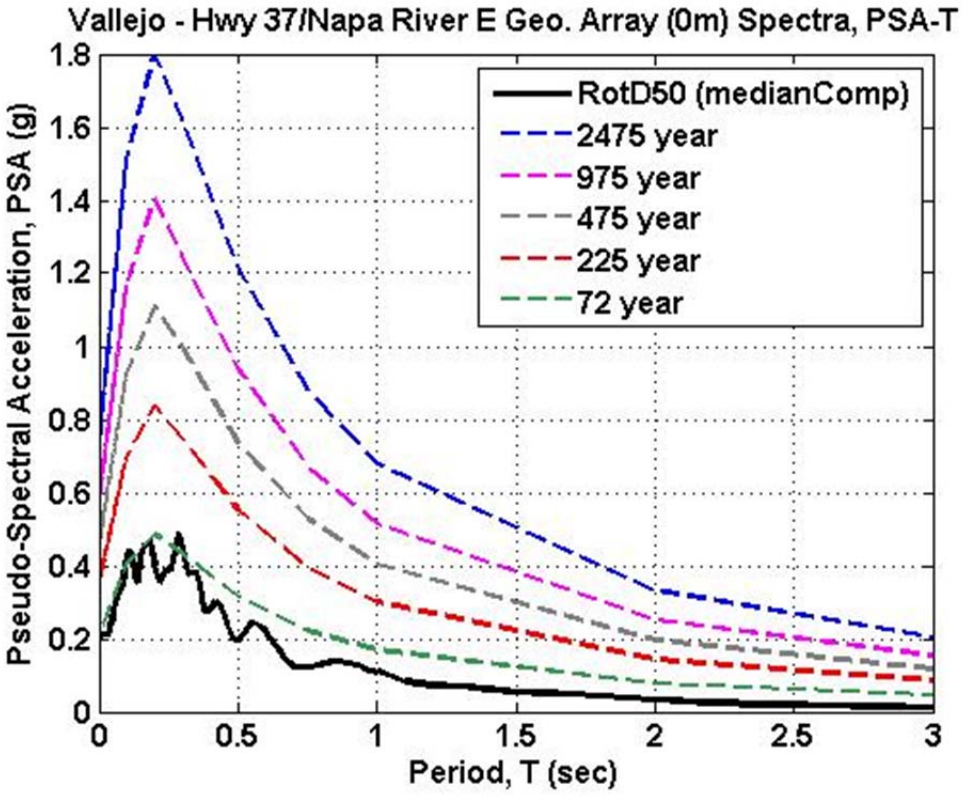
Vallejo - Hwy 37/Napa River E Geo. Array (0m) Spectra, PSA-T
RotD50 (medianComp)
2475 year
975 year
475 year
225 year
72 year
Pseudo-Spectral Acceleration, PSA (g)
Period, T (sec)
0
0.2
0.4
0.6
0.8
1
1.2
1.4
1.6
1.8
0.5
1.5
2
2.5
3

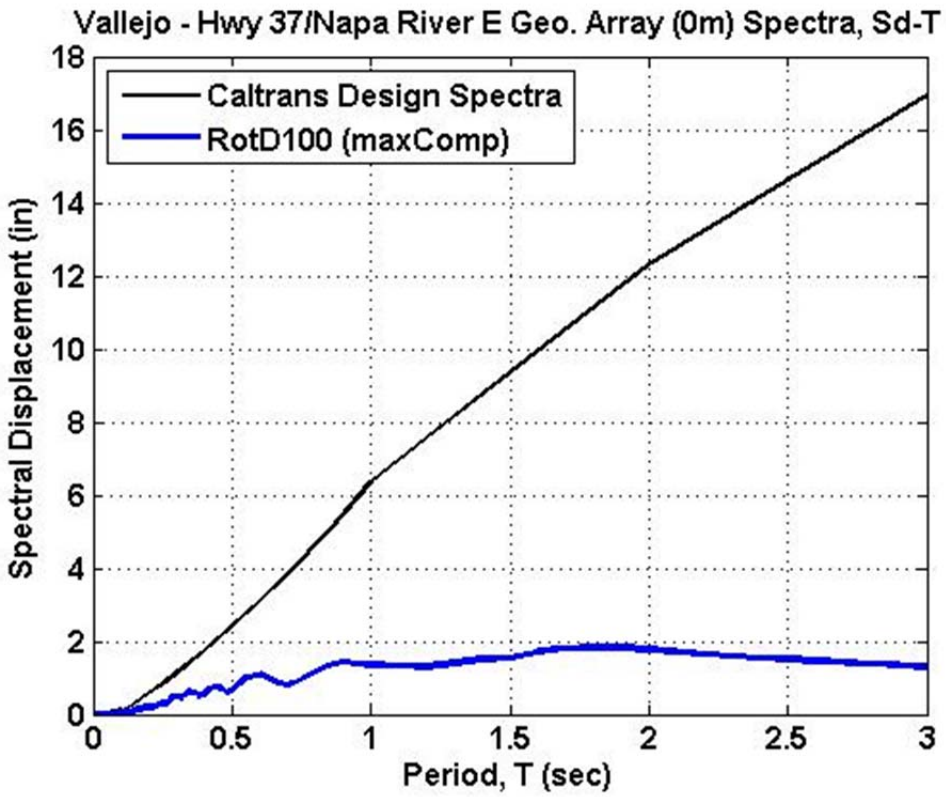
Vallejo - Hwy 37/Napa River E Geo. Array (0m) Spectra, Sd-T
Caltrans Design Spectra
RotD100 (maxComp)
Spectral Displacement (in)
Period, T (sec)
0
2
4
6
8
10
12
14
16
18
0
0.5
1
1.5
2
2.5
3

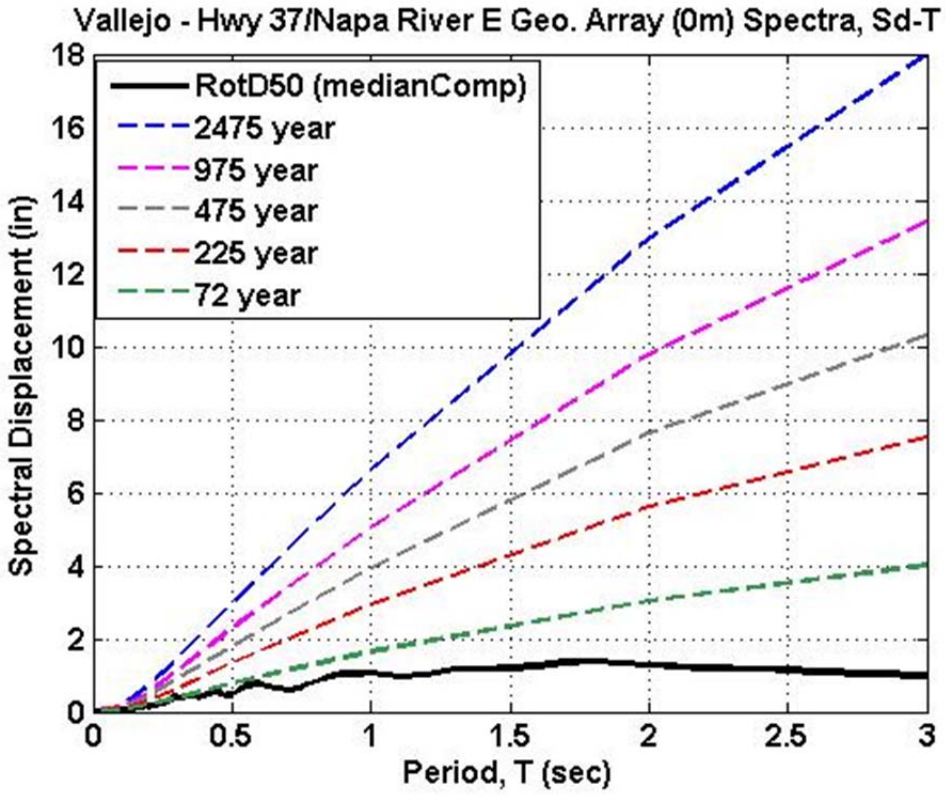
Vallejo - Hwy 37/Napa River E Geo. Array (0m) Spectra, Sd-T
RotD50 (medianComp)
2475 year
975 year
475 year
225 year
72 year
Spectral Displacement (in)
Period, T (sec)
0
2
4
6
8
10
12
14
16
18
0
0.5
1
1.5
2
2.5
3

APPENDIX D CHARACTERIZATION OF NEAR-FAULT GROUND MOTION RECORDS BY LU AND PANAGIOTOU [2014]

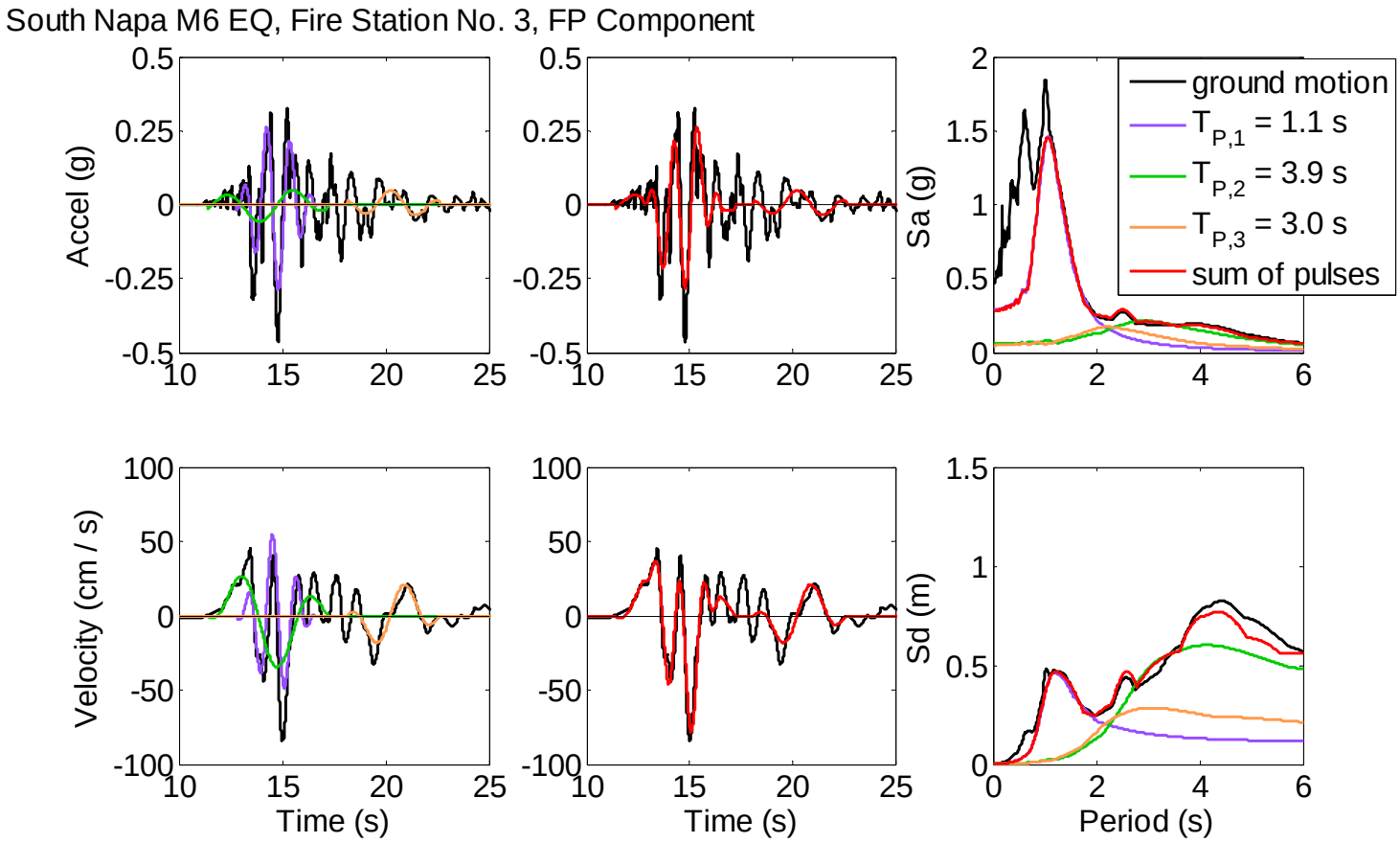

Figure 1 Fault-parallel component of ground acceleration and ground velocity histories recorded at the Fire Station No. 3; Extracted pulses using the $CPE_{V,EN}$ method; and Linear acceleration and displacement response spectra (2% damping) of the recorded histories, the extracted pulses, and the representation of the motion using the sum of the extracted pulses.

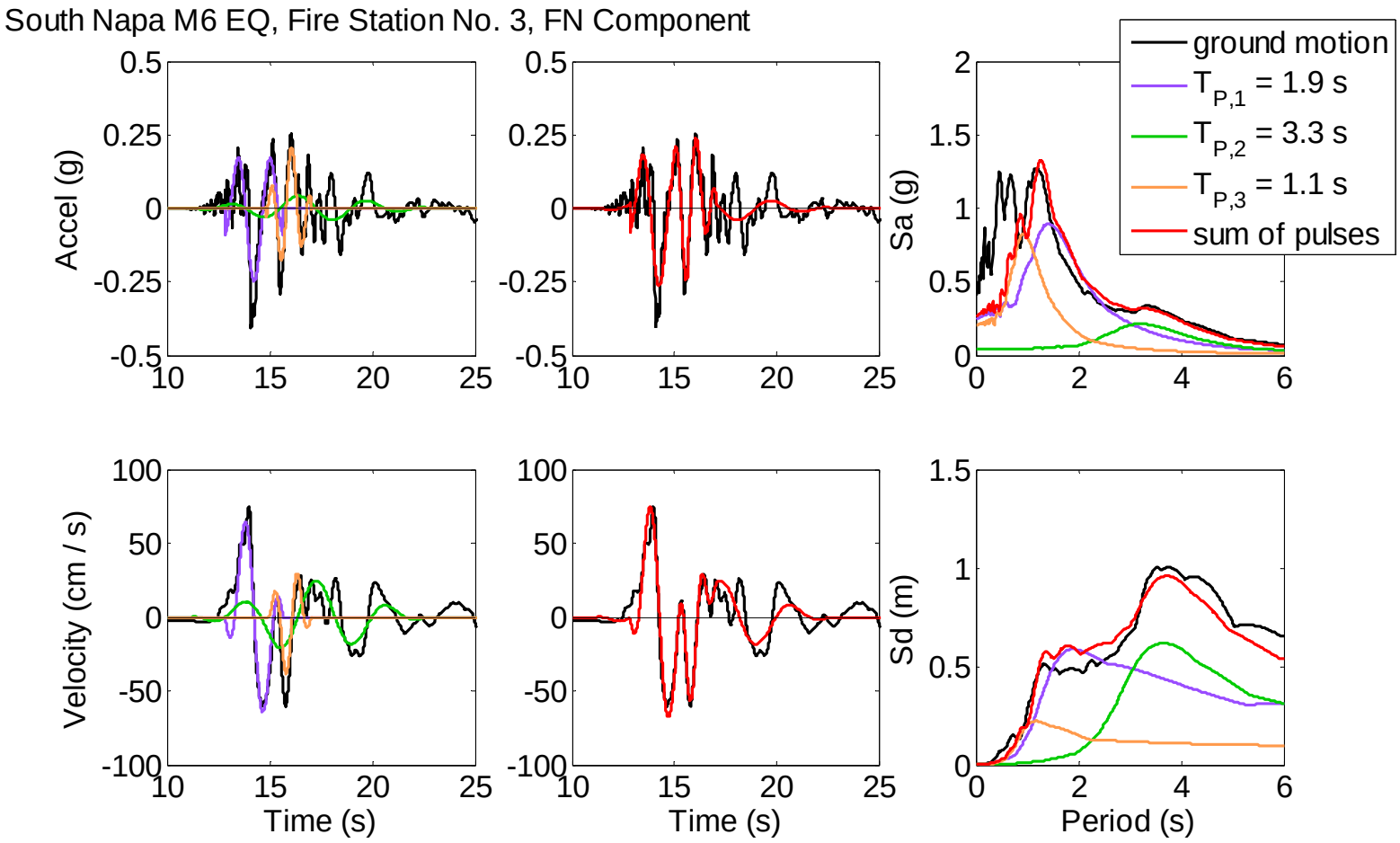

Figure 2 Fault-normal component of ground acceleration and ground velocity histories recorded at the Fire Station No. 3; Extracted pulses using the $CPE_{V,EN}$ method; and Linear acceleration and displacement response spectra (2% damping) of the recorded histories, the extracted pulses, and the representation of the motion using the sum of the extracted pulses.

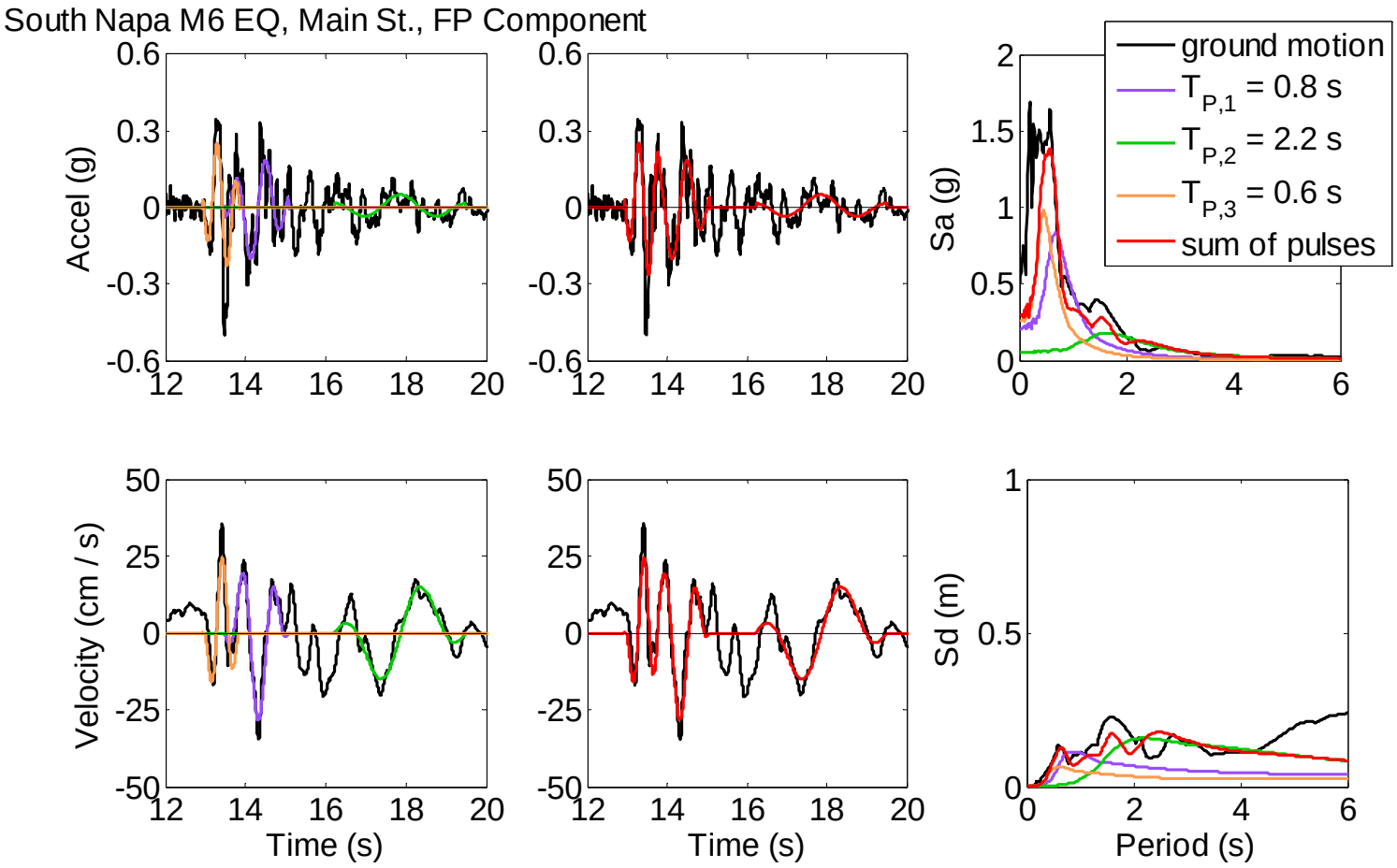

Figure 3 Fault-parallel component of ground acceleration and ground velocity histories recorded at Main St.; Extracted pulses using the $CPE_{V,EN}$ method; and Linear acceleration and displacement response spectra (2% damping) of the recorded histories, the extracted pulses, and the representation of the motion using the sum of the extracted pulses.

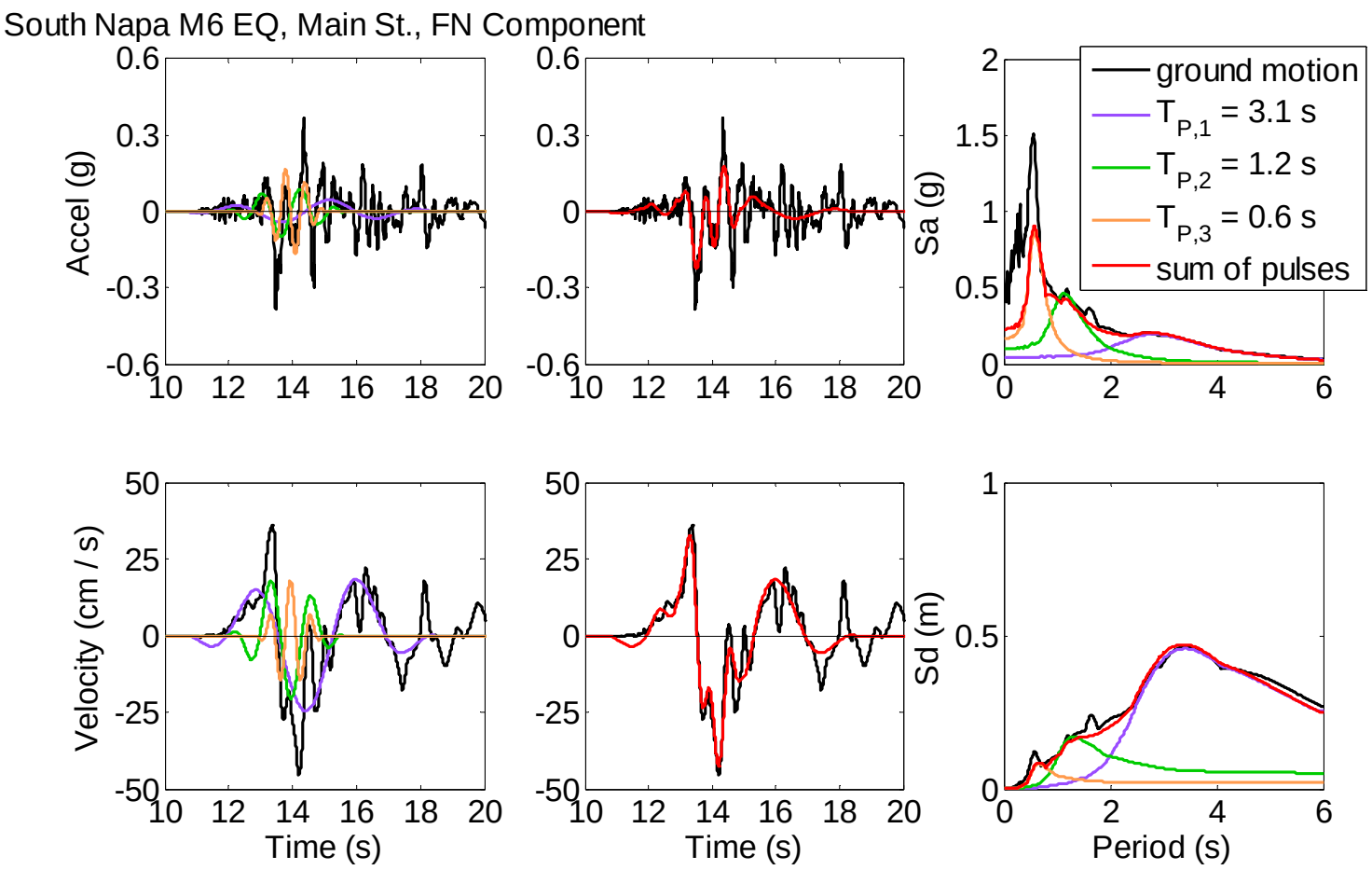

Figure 4 Fault-normal component of ground acceleration and ground velocity histories recorded at Main St.; Extracted pulses using the $CPE_{V,EN}$ method; and Linear acceleration and displacement response spectra (2% damping) of the recorded histories, the extracted pulses, and the representation of the motion using the sum of the extracted pulses.

2 Observations from South Napa Earthquake, 3:20 am. 8/24/2014: Field Investigation of the Napa Downtown Conducted on 8/24-25/2014[+]

Selim Günay[1], Khalid M. Mosalam[2], Mohamed Moustafa[3], Nicolas Peralta[4], and Shakhzod Takhirov[5]

2.1 INTRODUCTION

The earthquake occurred within a 70-km- wide (44 miles) set of major faults of the San Andreas Fault system that forms the boundary between the Pacific and North American tectonic plates; refer to the shake map in Figure 1. The persistent northwestward movement of the Pacific plate relative to North America primarily causes right-lateral slip across the major faults but also causes deformation between the major faults. The earthquake is located at the eastern shore of San Pablo Bay between two major active fault systems: the Hayward-Rodgers Creek Fault system on the west and the Concord-Green Valley Fault system on the east (see Figure 2). The earthquake occurred near the well-known West Napa Fault, and the less well-known Carneros-Franklin Faults, which juxtapose different suites of rocks [USGS 2014].

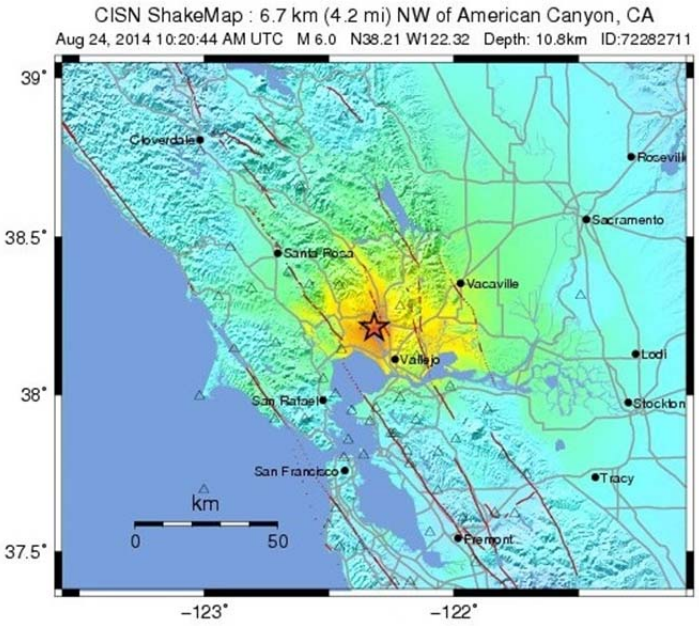

Figure 1 Shake map of South Napa earthquake on August 24, 2014.

[+] Any observations, opinions, findings, and conclusions or recommendations expressed in this material are preliminary and are those of the authors, and do not necessarily reflect those of the Pacific Earthquake Engineering Research Center. The information, data and images contained in this report may not be published or presented without permission from the authors.

[1] Project scientist, nees@berkeley site, UC-Berkeley
[2] Professor, Structural Engineering, Mechanics and Materials, UC-Berkeley
[3] PhD candidate, Structural Engineering, Mechanics and Materials, UC-Berkeley
[4] PhD candidate, Structural Engineering, Mechanics and Materials, UC-Berkeley
[5] Site operation manager, nees@berkeley site, UC-Berkeley

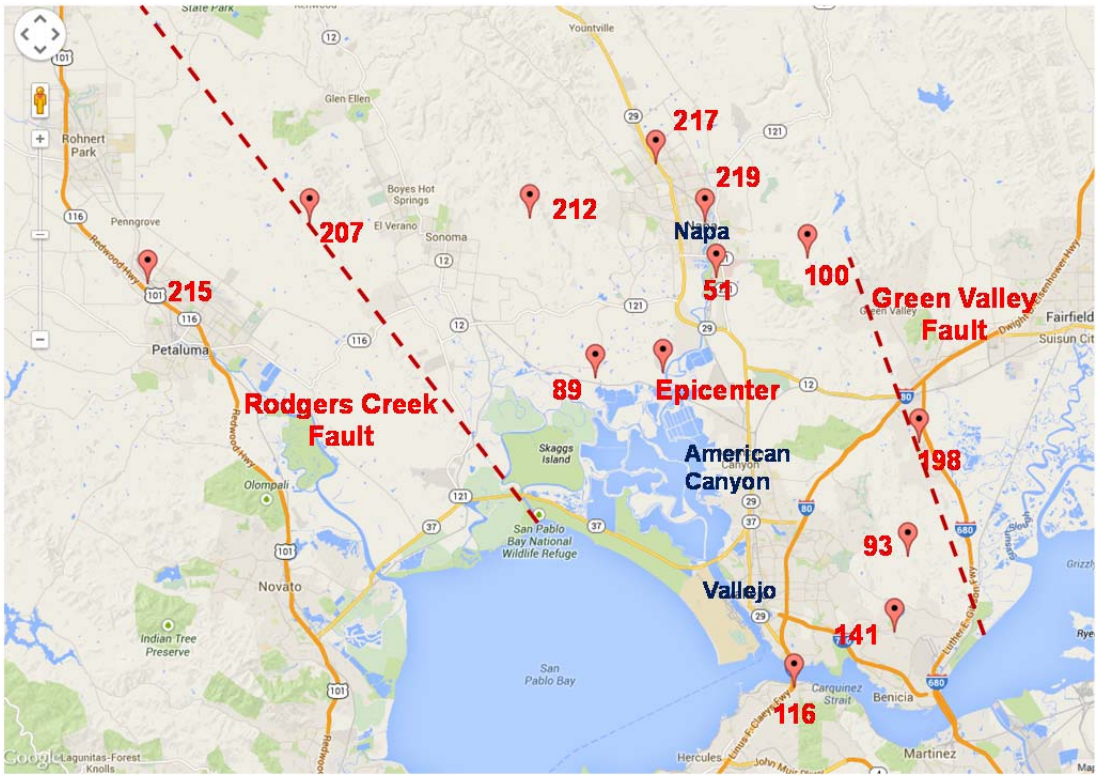

Figure 2 Locations of ground motion stations, the epicenter, and nearby faults.

The earthquake is located between two major, largely strike-slip fault systems: the Hayward-Rodgers Creek fault and the Concord Green Valley fault. The Hayward-Rodgers Creek fault system, which is approximately 7 km (4 miles) west of the site, generated damaging earthquakes in 1868 and probably in 1898. The Concord-Green Valley fault system, which is 12 km (7 miles) east of the site, produced a M5.5 earthquake in 1954; while it has not generated a large historical event, there is strong evidence for recent pre-historic activity. The 1999 Working Group on California Earthquake Probabilities [WG99 1999] concluded that the Hayward-Rodgers Creek fault system has a 32% probability of generation a large earthquake (M<6.7 to 7.4) by the year 2030, and the Concord Green Valley fault system has a 6% chance of generated a large earthquake ($M \geq 6.7$) in the same time period.

2.2 GROUND MOTION CHARACTERISTICS AND RELATION TO OBSERVED DAMAGE

Ground motions were recorded by a dense array of ground motions recording stations located in the area; see Figure 2. Peak values of the 13 strong ground motions are listed in Tables 1 and 2. Note that significantly large peak ground acceleration (PGA) 0.61*g*, and peak ground velocity (PGV), 92.4 cm/sec, values were recorded in some of the near-fault ground motions. Furthermore, a PGA value of 0.99*g* was recorded by the surface accelerometer of a geotechnical array (RSN 116 in Tables 1 and 2). However, considering the location of this station and the measurements in the nearby stations, this PGA value is not considered realistic. Ground-motion traces of four strong motions are plotted in Figures 3 and 4, where the presence of velocity pulses can be observed. Two-percent damped acceleration response spectra of the ground motions

recorded in these four stations are plotted in Figure 5. Significant spectral accelerations are observed for the low-to-medium period structures (0.6*g* to 1.8*g* for station 219, 0.4*g* to 1.7*g* for station 217, 0.4*g* to 1.6*g* to station 41, 0.3*g* and 1.8*g* for station 89), which comprise most of the building type structures located in the area. Despite the considerable level of shaking experienced, observed damage can be considered as low to moderate, which may be explained by three reasons.

- The low period structures are generally one- or two-story single-family wood structures, where the seismic mass is generally small. Accordingly, these structures have high base shear capacity ratios (base shear capacity divided by seismic mass), which can be as large as 1.0. Considering that the spectral accelerations in the low-period range are smaller than 0.8*g*, it is likely that these structures remained in the elastic range of response during the earthquake.
- The medium-period structures in the area are generally unreinforced masonry structure that have been retrofitted, which explains the low level of observed damage in these structures.
- The pulse period of near-fault ground motions, determined as the period corresponding to the peak of the velocity response spectrum (listed in Table 3) are high than the period range of the wood and unreinforced masonry structures, which reduces the effect of the pulse on these structures.

Table 1 Locations of ground motion stations.

Record Sequence Number (RSN)	Location
219	Main St., Napa
116	Crockett - Carquinez Br Geotech Array #1 (0 m)
217	Napa; Fire Station No. 3
89	Huichica Creek
51	Napa - Napa College
212	Lovall Valley Loop Rd.
216	St. Helena; Fire Station No. 17
141	McCall Drive, Benicia
198	Lynbrook Drive, Fairfield
93	Lake Herman
100	Green Valley Rd.
207	Mesquite Ct, Sonoma
215	Petaluma; Fire Station No. 2

Table 2 PGA, PGV, and PGD values of the recorded ground motions.

RSN	PGA (*g*)			PGV (cm/sec)			PGD (cm)			R_{RUP}* (km)	R_{JB}** (km)
	T	L	UP	T	L	UP	T	L	UP		
219	0.61	0.31	0.24	47.5	35.5	20.3	15.1	14.9	5.4	7.9	5.9
116	0.54	0.99	0.37	10.9	22.1	7.4	1.2	1.5	0.5	14.4	13.3
217	0.41	0.43	0.32	92.4	82.0	31.2	34.7	34.0	12.4	10.2	8.7
89	0.40	0.30	0.21	59.0	22.3	11.2	27.6	5.3	5.0	7.3	3.6
51	0.34	0.38	0.21	54.8	56.5	18.7	16.9	18.0	6.8	6.6	4.0
212	0.28	0.34	0.17	37.4	63.0	18.5	8.6	27.0	6.4	10.7	8.7
216	0.10	0.07	0.03	14.2	12.4	7.3	4.9	6.6	2.2	31.9	31.4
141	0.10	0.14	0.06	6.4	7.7	2.7	1.6	1.0	0.6	14.6	13.6
198	0.09	0.07	0.03	6.8	6.9	3.7	3.2	1.9	1.6	12.4	11.2
93	0.09	0.09	0.03	6.1	6.9	2.5	2.2	1.8	1.0	12.8	11.6
100	0.09	0.11	0.11	11.0	12.6	5.6	4.9	7.7	1.9	10.7	9.3
207	0.09	0.05	0.03	6.5	6.2	4.5	3.9	4.2	2.4	21.7	20.1
215	0.07	0.03	0.02	5.9	5.9	2.7	2.9	2.5	1.2	30.4	28.7

*The shortest distance between the recording site and the rupture plane of earthquakes
**The Joyner and Boore (1981) distance, a measure of how far the site is from being over the hanging wall

Table 3 Pulse periods of some of the near-fault ground motions.

RSN	Pulse Period (sec)	
	T	L
219	0.59	0.59
217	1.01	1.23
51	1.60	1.37
89	2.13	0.67

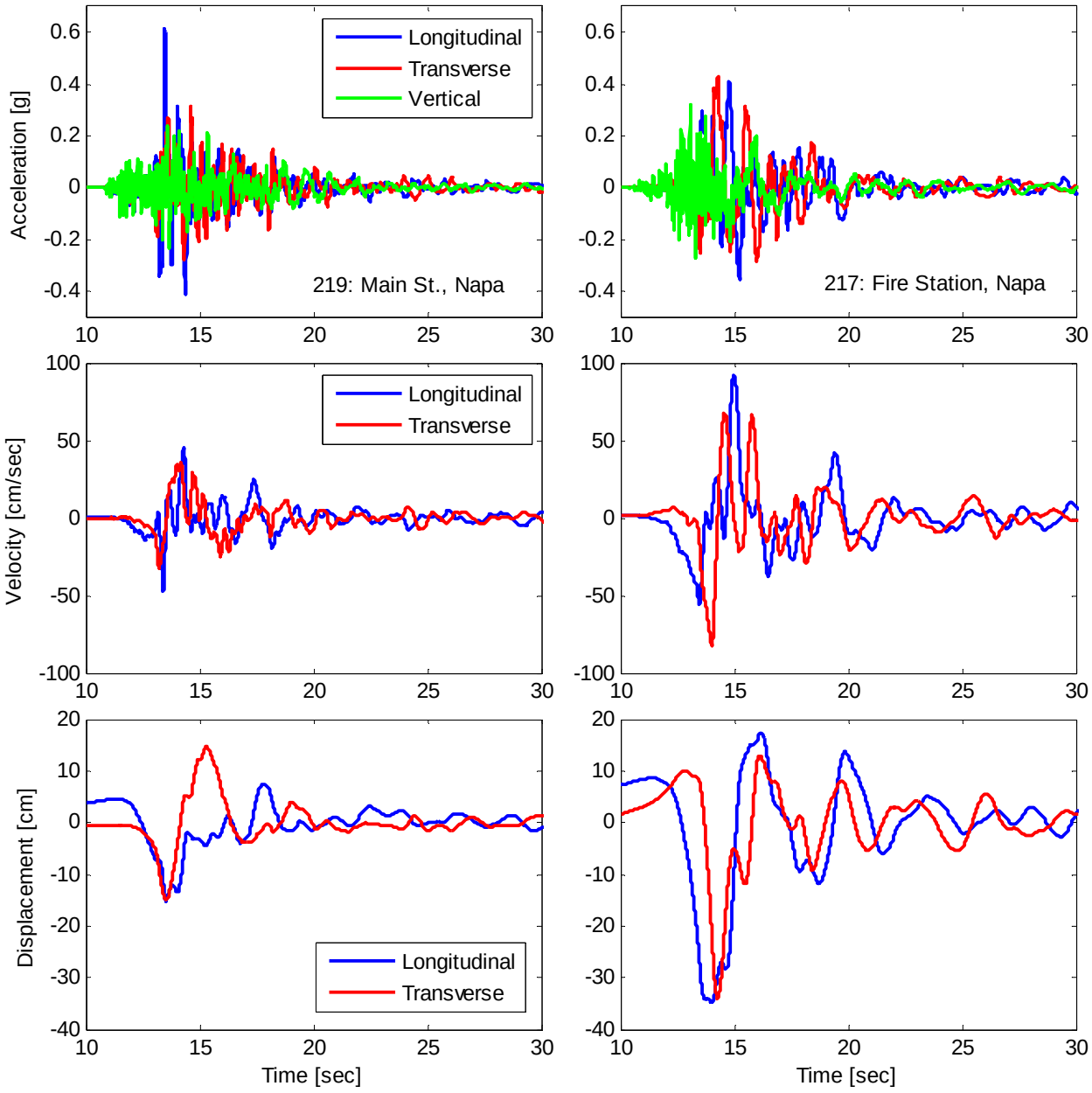

Figure 3 Ground motion traces at two near-fault stations located in Napa.

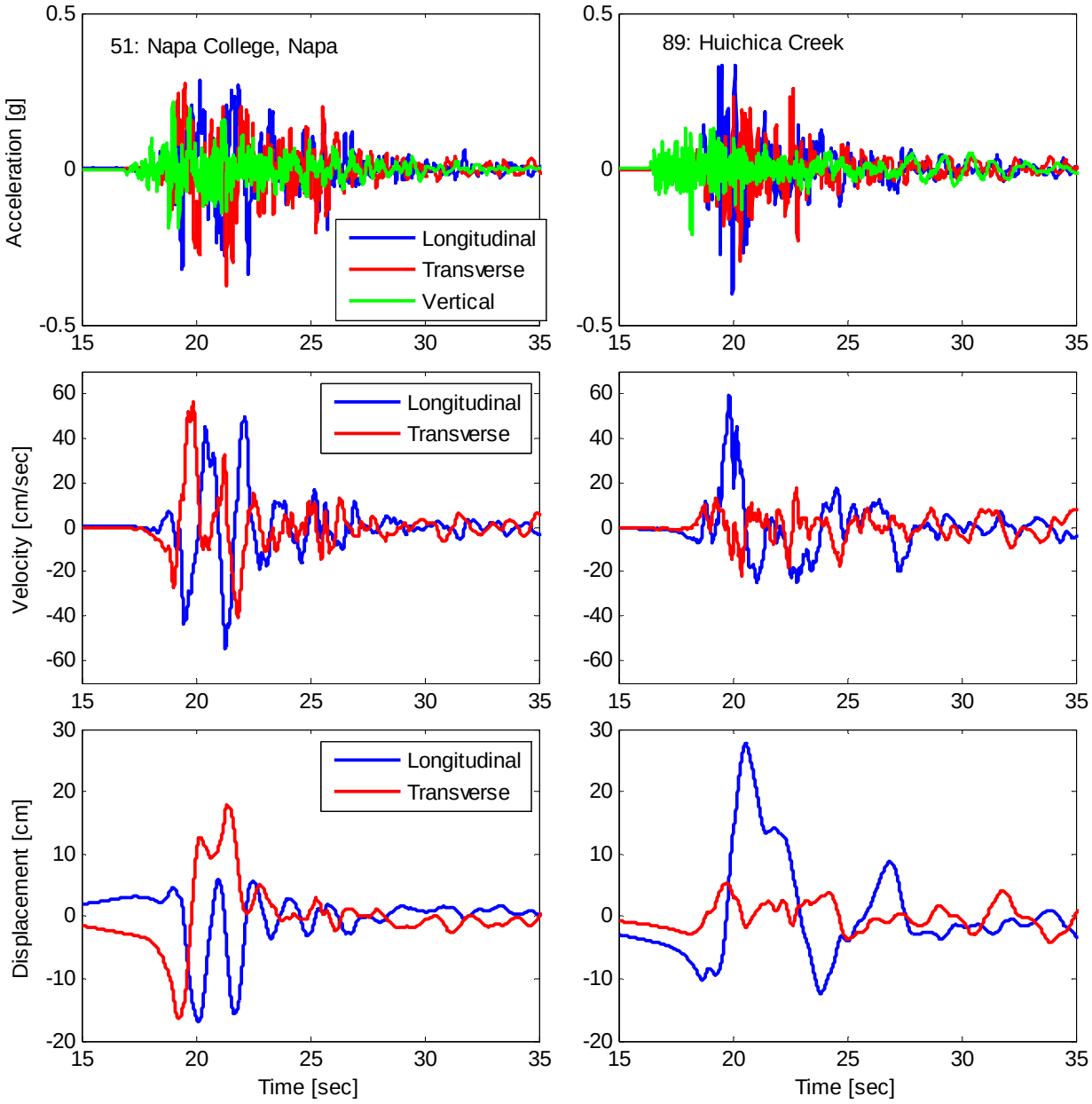

Figure 4 Ground motion traces at two other near-fault stations.

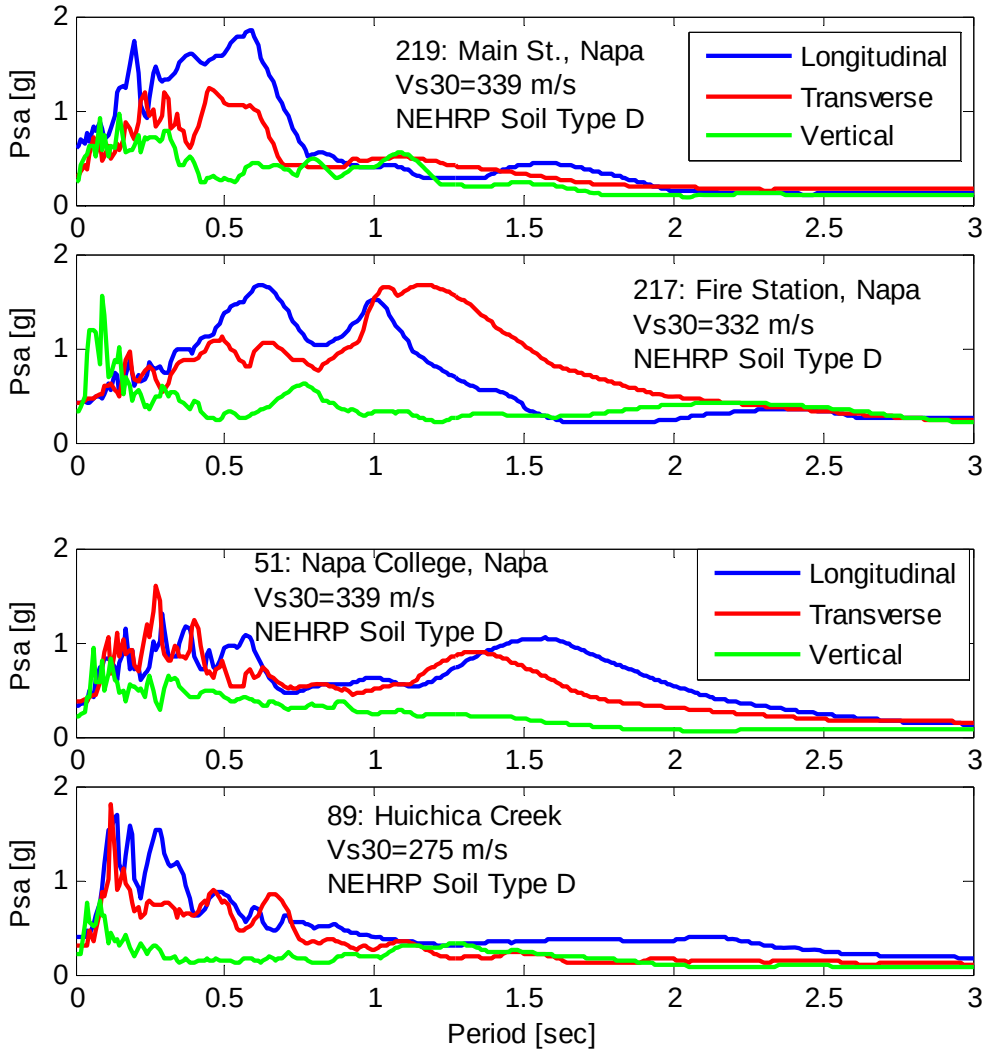

Figure 5 Response spectra of four near-fault ground motions.

2.3 BUILDINGS: DAMAGE INSPECTION

Several field trips were carried out the same day of the earthquake and the following week. Selected cases of structural and non-structural damages/failure observed in the Napa downtown area are presented in this section. A map of the Napa downtown area that identifies the buildings included in this discussion, designated as buildings A through K, is shown in Figure 6. The discussion is divided according to the broad categories of buildings structures: unreinforced masonry buildings (UMB), residential wood buildings, and reinforced concrete structures. In addition, an example of a recently retrofitted UMB that survived the earthquake without any damage is presented. The section concludes with few miscellaneous nonstructural damage observations.

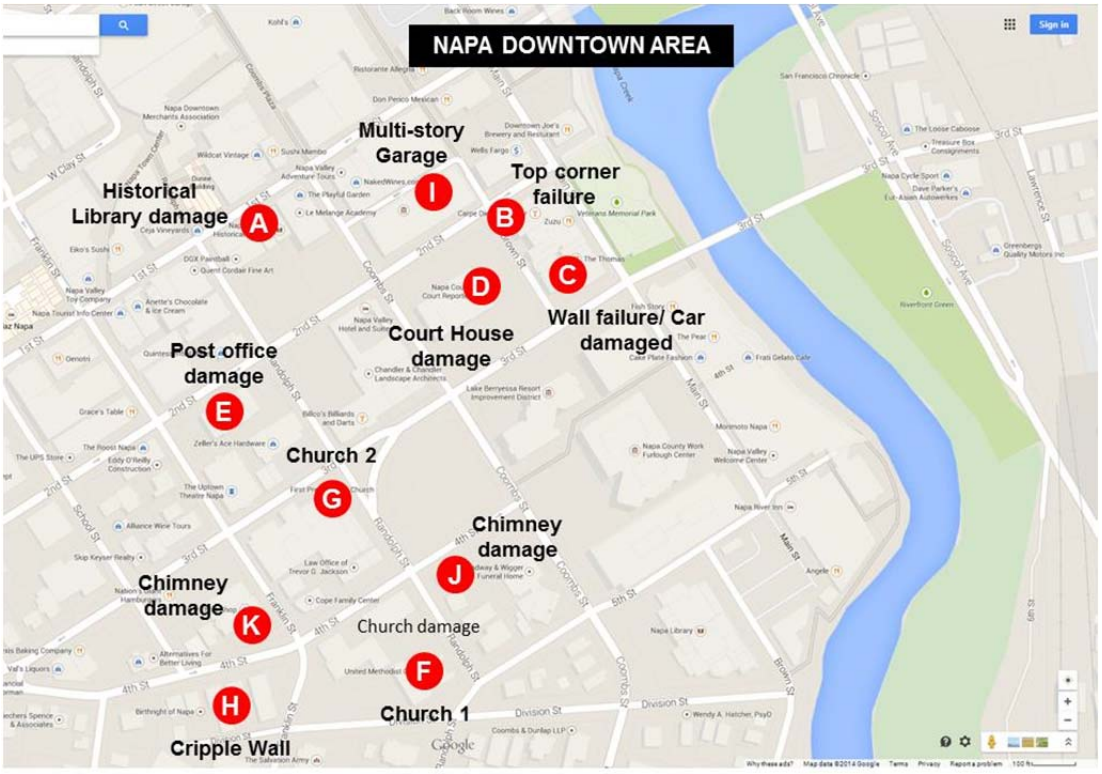

Figure 6 Map of Napa downtown area identifying the location of each of the buildings that experienced damage and presented in this report (designated as Buildings A through K).

2.3.1 UNREINFORCED MASONRY BUILDINGS (UMB)

Due to the historical nature of the Napa down area, most of the buildings are old UMB where most of the structural damage was observed after the earthquake. Selected examples of the most severely damaged historical, governmental, commercial, and church buildings are presented here.

Historical Buildings

Several historical buildings experienced either structural damage in load-bearing components—such as bearing walls—or non-structural damages in facades or windows or interior décor. One of the iconic historical buildings that had a structural damage in the walls is the Goodman Library (Building A in Figure 6 map). The 110-year-old library building was laid in 1901 and was built primarily from masonry blocks/bricks. An overview of the building after the earthquake is shown in Figure 7. The building was red-tagged immediately after the earthquake for structural damage (as shown in the same figure).

Figure 7 Overview of Goodman historical library building (Building A in the map in Figure 6) and red tag displayed at the building's entrance.

Commercial Buildings

Several multi-purpose buildings that are used for administrative and commercial purposes sustained damage. Two examples of the most severely damaged buildings are buildings B and C in the map shown in Figure 6. Building B had a structural failure of the post (column) supporting part of the roof at the building's top corner and the adjacent bearing walls. The post and walls collapse are shown in Figure 8. Building C had a partial wall collapse as shown in Figure 9. The collapsed wall bricks that dropped from the second floor damaged a car that was parked next to the building the night before the earthquake, as shown in Figure 9.

Figure 8 Overview of supporting column and walls at commercial building's top corner (Building B in the map in Figure 6).

Figure 9 Overview of side wall collapse of a commercial building leading to a the damage of a car parked next to the building (Building C in the map in Figure 6).

Governmental Buildings

The earthquake damage was extended to governmental buildings which led to downtime and temporarily suspended public services. Two examples of red-tagged governmental buildings are the court house and post-office building shown in Figures 10 and 11, respectively. The court house building (Building D in the map in Figure 6) experienced structural failure of the second

floor bearing wall, as shown in Figure 10. Several wide cracks were observed, as well at other regions of the building's bearing walls mainly in the second floor.

The U.S. Post Office (Building E in the map in Figure 6) experienced wide range of structural and non-structural damage. Partial damage in the masonry bearing walls at both of south and north lower corners of the building is shown in Figure 11 and 12. Most of the façade windows were damaged; see Figure 11.

Figure 10 Damage and wide cracks in the top floor bearing wall of Napa Court House (Building D in the map in Figure 6).

Figure 11 Damage in the north lower corner of Napa Post Office Building (Building E in the map in Figure 6) and smashed façade and glass windows.

Figure 12 Damage in the south lower corner of Napa Post Office Building (Building E in the map in Figure 6).

Churches

Another example of historical masonry buildings that were partially damaged after the earthquake is church buildings. The damage that took place in a 100-year-old church in downtown Napa (Building F in the map in Figure 6) is shown in Figures 13 and 14. A comparison of the before and after earthquake front side of the church is shown in Figure 13. The street view in Google Maps was utilized to generate the before earthquake picture. The wall on the east side of the church had a visible separation from the roof and it remained inclined toward the nearby street; see Figure 14. The separation can be approximately estimated to be 26 in., and laser scanning of the church building was pursued to quantify the deformation and damage as presented in a following section. Another close-by church (Building G in the map in Figure 6) experienced only nonstructural damage; see Figure 15. The façade windows were smashed and the steel cross and wind-direction arrow permanently deformed after the earthquake; see Figure 15.

Figure 13 Before (left) and after (right) earthquake status of a 100-year-old church (Building F in the map in Figure 6).

Figure 14 Separation gap between the church (Building F in the map in Figure 6) roof and the east wall in a global (left) and zoomed-in (right) views.

Figure 15 Overview of historic church (Building G in the map in Figure 6) non-structural damage: façade smashed windows and deformed top cross.

2.3.2 RESIDENTIAL WOOD BUILDINGS (CRIPPLE WALL)

Many of the residential buildings in the downtown of Napa are more than 100 years old. Although some strengthening and retrofitting has been done by the owners, several failures were observed in the aftermath of the earthquake. One example of a wood building that was red-tagged due to almost complete collapse is presented here. One of the main reasons for the building's collapse is the weak cripple wall. An illustration of a typical mode of failure of a wood frame building due to cripple wall collapse is shown in Figure 16. The extensive damage observed in the old residential building in downtown Napa (Building H in the map in Figure 6) is shown in Figures 17 through 19. Figure 17shows the front side of the building before (Google street view) and after the earthquake. The side sway of the building suggests that the building most likely fell down from the cripple wall in east-to-west direction. Global views of the damaged building are shown in Figure 17. Massive damage can be observed in the additions on the back side of the building as well as the building main frame.

A close-up view of the collapsed cripple wall from the east side of the building is shown at the top left corner of Figure 19. The large deformation at the base of the building caused by the cripple wall led to a large gage and separation between the stairs and the building; see Figure 19. It is clearly noticeable that the elevations of the stairs and the doorstep of the building are different. The global motion of the foundation was east-to-west and down. The residual displacement is most likely is very close to the height of the cripple wall. Figure 19 (lower left corner) also shows that all electrical ducts and plumbing pipes feeding the building were completely damaged due to the extremely large deformations from the earthquake.

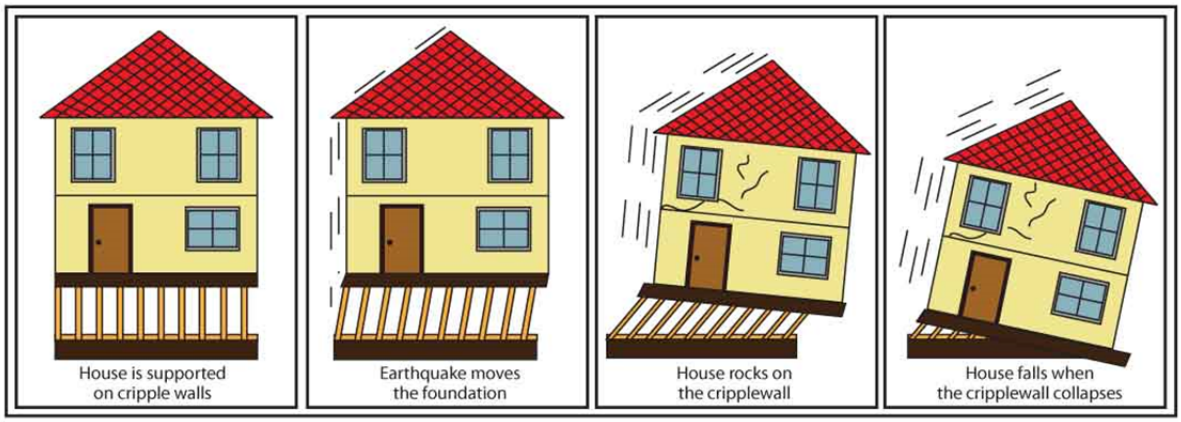

Figure 16 Schematic representation of wood building failure as a result of a cripple wall collapse (Courtesy of Weinstein Construction Corporation).

Figure 17 Before (left) and after (right) earthquake condition of the residential wood frame building with a cripple wall design in downtown Napa (Building H in the map in Figure 6).

Figure 18 Global views of different sides of an old residential wood building (Building H in the map in Figure 6).

Figure 19 Close-up view of the cripple wall collapse at the east side of the building (top left) separation and elevation change in the main building's entrance stairs (top right) and patio fence (bottom right) utility ducts and pipes damage (bottom left).

2.3.3 REINFORCED CONCRETE (RC) STRUCTURES

While most of the damage was observed in UMB and wood buildings, minor cracking was also observed in some RC buildings and bridges. More details about RC bridges inspection after the earthquake are presented in a following section. However, minor cracking in a multi-story RC garage building in downtown Napa is presented here as an example. The multi-story garage is identified as Building I in the map in Figure 6, and it is located across the street from the popular building that experienced the top corner walls and roof damage.

In general, all the RC structures in the areas struck by the earthquake showed no or minor structural damage. In the given multi-story garage example, only minor flexural cracks were observed in the basement floor columns; see Figure 20. Moreover, some diagonal cracks were also observed in a RC shear wall in the basement floor of the same multi-story garage; see Figure 21. Note that the first and second floors of the multi-story garage were inspected and no cracks at all were observed in any of the RC elements.

Figure 20 Flexural cracks in basement floor columns of multi-story RC garage building (Building I in the map in Figure 6).

Figure 21 Minor diagonal cracks in basement floor shear wall of multi-story RC garage building (Building I in the map in Figure 6).

2.3.4 RETROFITTED UMB

As previously mentioned, many of the buildings in the downtown Napa area are very old, and some of them are more than 100 years old. Accordingly, buildings strengthening and retrofitting has been a common practice over the past decade. Most of the retrofitting projects are done on individual basis by private home owners or businesses owners who seek to protect their lives and businesses or avoid downtime after earthquakes. An example of these projects is the restaurant/café building featured in Figure 22. The building is a typical UMB that was recently retrofitted using a steel braced-frame; see Figure 22. What is interesting about this particular retrofitted building is its location in downtown Napa just next to Building C in the map in Figure 6 where the side wall collapsed and damaged the parked car. Unlike most of the buildings in that commercial block, the retrofitted building did not experience any structural or nonstructural damage. An efficient retrofit scheme is then found to be beneficial and properly functioned as intended where it was located only few yards away from the station that recorded the 0.6*g* strong motion (refer to Section 2 above).

Figure 22 Example of a retrofitted UMB using a steel braced-frame that performed well during the earthquake with no signs of any structural or nonstructural damage.

2.3.5 MISCELLANEOUS NONSTRUCTURAL DAMAGE

The most noticeable feature of the 6.0M American Canyon earthquake, which has also been referred to as Napa earthquake, is the massive nonstructural damage that swept the major parts of Napa, Vallejo, and close-by cities struck by the earthquake. The nonstructural damage can be associated with failures or damages that took place in facades or non-load bearing elements, such as chimneys, or non-building components, such as utility ducts. However, a financially devastating form of nonstructural damage is the damage of a building's live parts (for instance, furniture) or a store's inventory, especially expensive wine bottles that have brought worldwide fame to Napa Valley. Estimating all the financial losses of the destroyed merchandise and goods is still in progress. Only few examples of external nonstructural observed damage is shown in this subsection as pictures of internal damage are not available yet.

Figure 23 shows the damage that happened to two chimneys in two different residential buildings in downtown Napa, and identified as Building J and K in the map shown in Figure 6. The cosmetic damage that occurred in the façade of one of the shopping malls in downtown Napa is shown in Figure 24. A different form of nonstructural damage is local failure in wire connections in street power distribution lines, which led to electricity outage for hundreds of buildings. Figure 25 shows a wire end connection failure after the earthquake and the efforts exerted by PG&E officials to fix it to restore electricity before night time in downtown Napa the first night after the earthquake.

Figure 23 Damage of residential buildings chimneys in downtown Napa (Buildings shown are Building J (left) and K (right) identified in map in Figure 6).

Figure 24 Damage in shopping mall façade in downtown Napa.

Figure 25 Efforts to fix wires and connections failures in local street power distribution lines.

2.4 BRIDGES: DAMAGE INSPECTION

Several RC bridges were inspected after the earthquake to check for any damage or residual deformation. Two examples of inspected bridges are presented here. The first is one of the major bridges in the Napa/Vallejo area, which was carefully inspected and laser scanned by the reconnaissance team: the CA-37 Bridge that continues to Sears Point Road to access Mare Island. The location of the bridge is shown in Figure 26. The second example presented is the First Street Bridge over Napa Creek, which is located in the Napa downtown area.

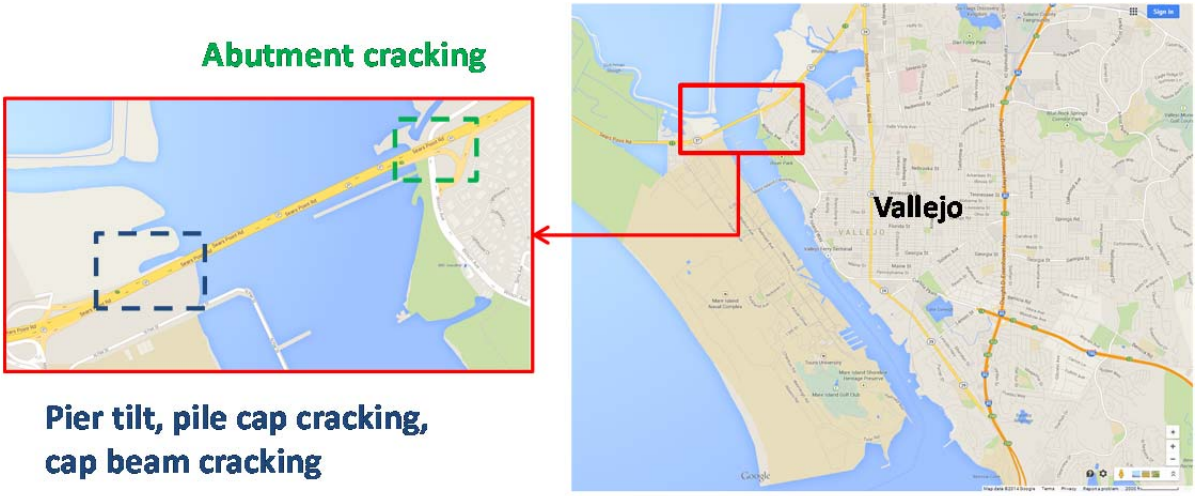

Figure 26 Location of CA-37 Vallejo Bridge (Sears Point Road to Mare Island).

For the CA-37 Bridge, all the observed minor damage was concentrated near the bridge approaches. Several piers are suspected to be have tilted or have residual displacements after the earthquake. Thus, it was decided to undertake a laser scan of the bridge to verify the verticality of the columns and check for any residual deformation or tilt in the piers. An overview of the inspected CA-37 Vallejo Bridge and possible column tilt/residual deformation after earthquake is shown in Figure 27. Cracking was observed in the abutment wall from the Vallejo side and cap beam flange and pile cap of few piers from the Mare Island side. Figure 28 and Figure 29 show the cracking pattern in the cap beam flange and pile cap, respectively. Only the first few piers from the Mare Island side had the minor cap beam and pile cap cracks.

For the First Street Bridge, only minor damage was observed too. Several cracks were observed at various locations in the bridge deck near by the abutment from the Napa downtown side as shown in Figure 30. In addition, relatively large deformations were observed in the expansion joint region after the earthquake. Damage in the filler material used in the expansion joint was observed as shown in Figure 31. The paint marking the traffic lanes at the expansion joint also shows how the joint deformed after the earthquake as shown in Figure 31.

Figure 27 Overview of CA-37 Vallejo bridge (left) and suspected pier tilt close to the bridge approach from the Mare Island side (right).

Figure 28 Cracking of one of the bridge piers' cap beam flange.

Figure 29 Cracking of one of the bridge pier's pile cap.

Figure 30 Cracking at various locations close to abutment of the First Street Bridge over Napa Creek from the Napa downtown side.

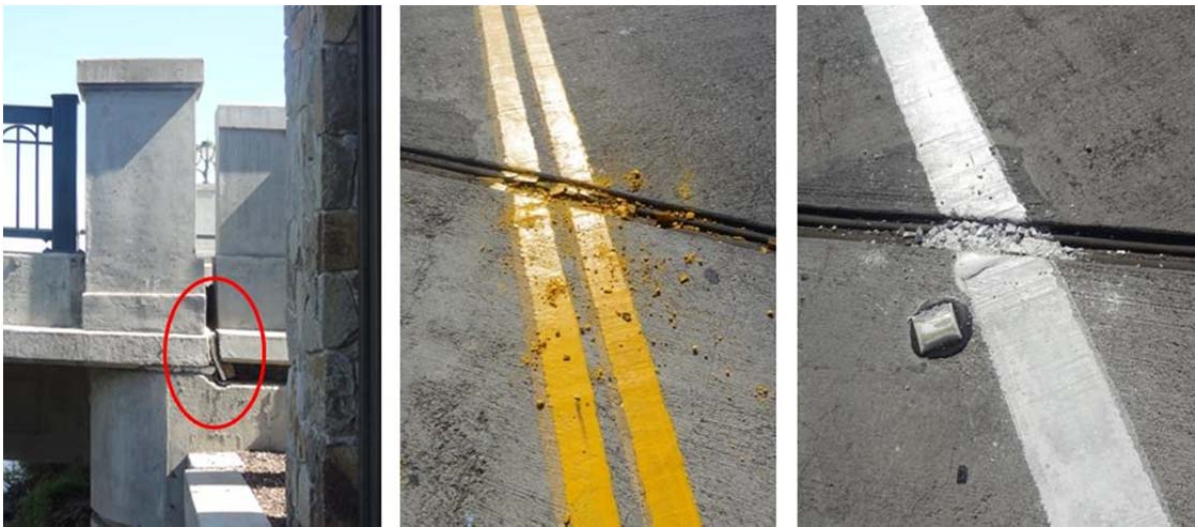

Figure 31 Deformation at First Street Bridge expansion joint led to filler material damage.

2.5 DAMAGE ASSESSMENT USING LASER SCANNING

Several geometric deformations were observed in many buildings and bridges that were inspected after the earthquake. An accurate way of quantifying geometric changes and deformations is the use of a laser scanner. The reconnaissance team used the laser scanner to scan several buildings in the downtown Napa area and a few bridges, which included the CA-37 Vallejo Bridge. This section presents a brief discussion of the undertaken laser scanning for damage assessment. Figure 32 shows one of the laser scanning set-ups used to scan the historical church in downtown Napa that had the east wall separation as previously shown. The figure shows the live view of the building scan as it is being performed. A challenging task during the

laser scanning, especially during scans conducted during the first day after the earthquake, was finding electrical power supply for some of equipment associated with the laser scanner. Because of the power outage, only private TV and news channels equipped with cars had a power source, and they agreed to cooperate with the research team to complete all of the scans conducted on the first day. One of the especially equipped cars that provided the team with power supply is also shown in Figure 32. More details of laser scanning discussion is presented in this section.

Figure 32 Laser scanner setup for historical church scan with live scanning view (bottom right) and power supplied by a TV channel especially equipped car (top right).

2.5.1 UNREINFORCED MASONRY CHURCH

To assess the inclination of the east wall and monitor its condition after the aftershocks, several scans of the church were conducted. On the day of the earthquake the church was scanned from four corners to obtain a complete geometry of the structure. On the following day—about 24 hours later—two more scans of the church were conducted from the east side street. Figure 33 shows the residual deformation of the east wall where color of a point in the point cloud depends on the distance from a vertical plane. The arrows show the locations of visible cracks observed in the wall. Figure 34 shows the location of the vertical slice on the left side and the comparison of the condition of the slices taken right after earthquake and the condition of the same slices 24 hours later. It was concluded that the aftershocks were not strong enough to change the wall's deformation. That said, depending on the magnitude of the aftershocks, future shaking could

cause the wall to fall on the east side street, dramatically changing the situation. Due to the high hazard of passing traffic and pedestrians, the building was fenced out by a tape right after the earthquake and was red tagged on the following day.

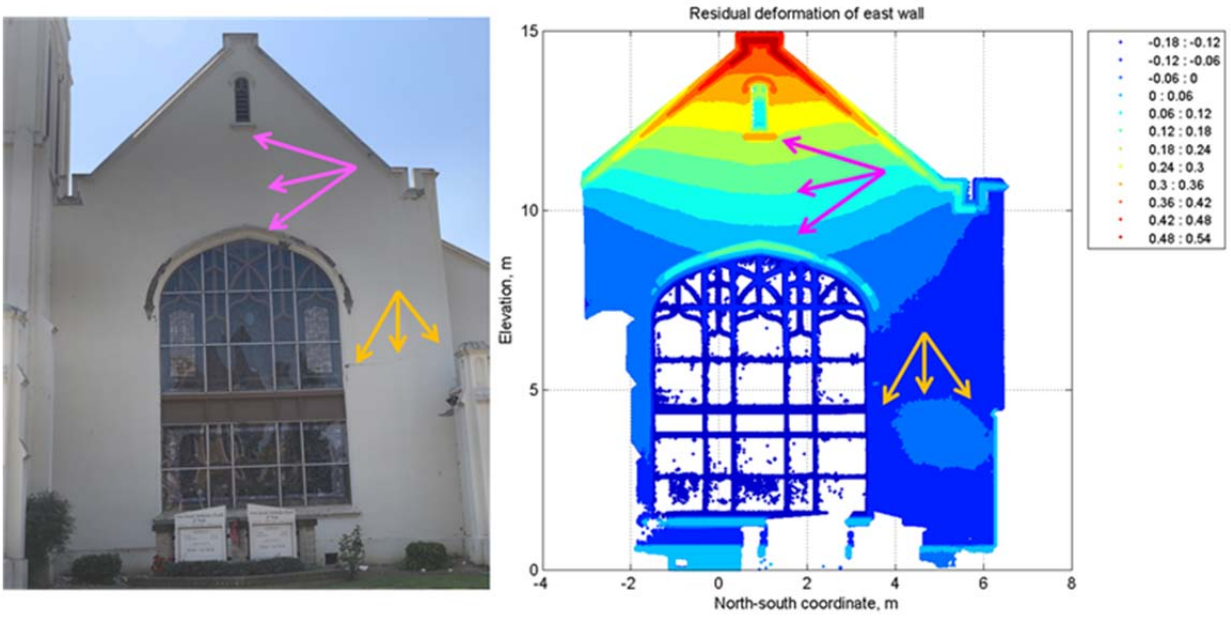

Figure 33 Residual deformation of the east wall.

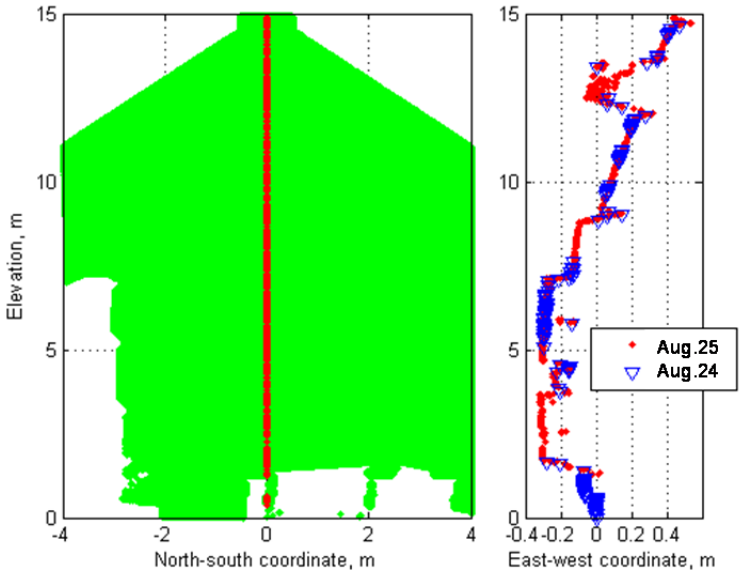

Figure 34 Deformations of the wall did not change during the aftershocks.

2.5.2 RESIDENTIAL WOOD-FRAME BUILDING

To access the residual displacement and the height of the cripple wall, a laser scan of the corner of the building was performed. Several laser scans were recorded from the same location of the laser scanner, which was installed at north-west corner of the building. Figure 35 shows the photo of the scanned region on the left and the point cloud of the corner of the building. A zoomed view of the corner showing some major member of the building's lateral resistance system is presented in Figure 36. The point cloud was best fit to regular geometric shapes to estimate the size and inclination of the stud; see Figure 36. The prism best fit to the point cloud of the stud revealed that it is most likely 2 in. × 6 in., as shown in the object information window displaying the prism's properties in Figure 37. The angle of inclination of the stud (relative to the vertical axis) is estimated to be -0.7503.

Figure 35 After condition of the wood frame building with a cripple wall design.

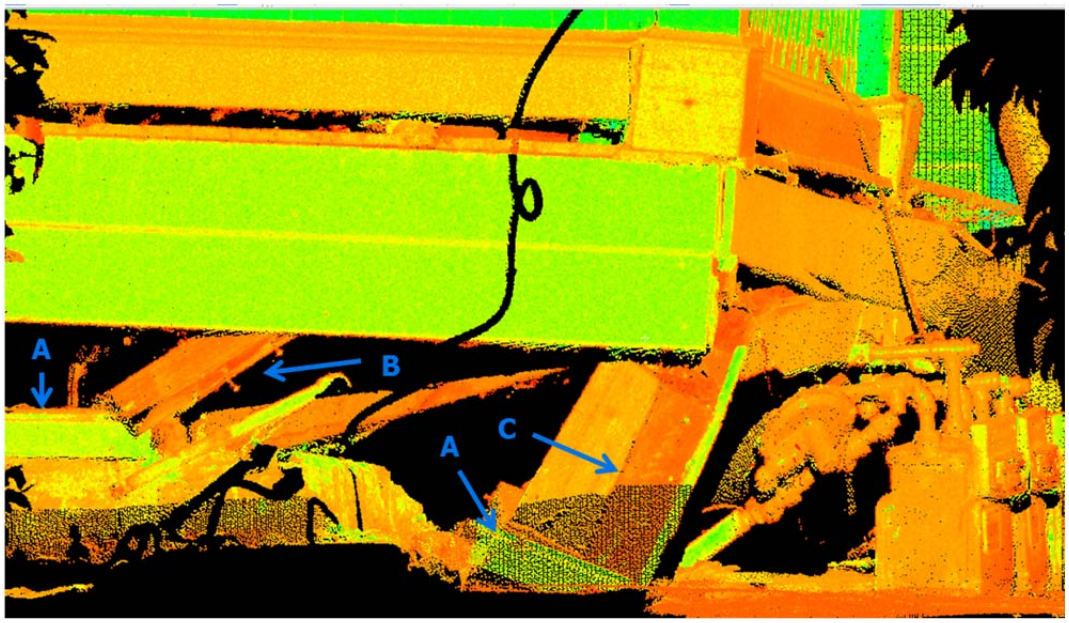

Figure 36 Major structural members of the building: A – sill plate, B- stud, C – corner 4 in. × 4-in.

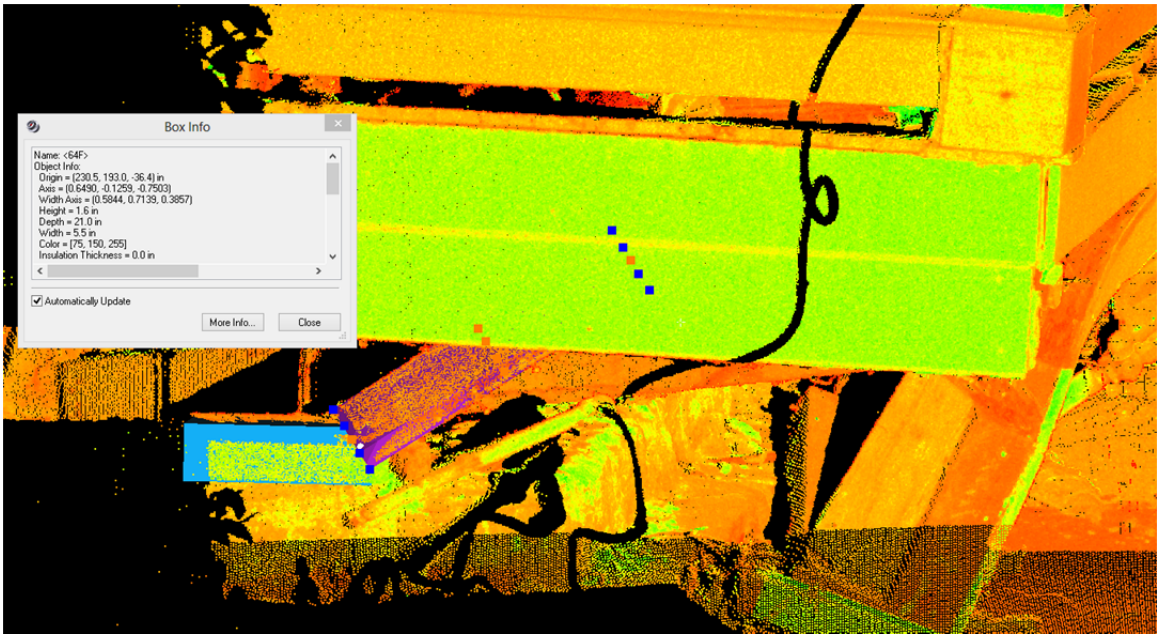

Figure 37 Supporting members of the building: blue – sill plate, pink – stud, most likely 2 in. × 6 in., and 21 in. long based on the point cloud.

2.6 REFERENCES

USGS (2014). U.S. Geological Survey, *http://earthquake.usgs.gov/earthquakes/eventpage/nc72282711#summary*.

3 Field Studies of Seismic Performance of Nonstructural Components in the South Napa Earthquake of August 24, 2014[+]

Shakhzod Takhirov[1], Bob Glasgow[2], Amir Gilani[3], and Khalid Mosalam[4]

3.1 SPECTRAL ACCELERATIONS OF THE SITE WITH RESPECT TO AC156 SPECTRA

A three-component strong motion recorder installed at a station Main Street in downtown Napa was studied for its correlation to AC156 spectra [ICC-ES 2010]. The three-component record was obtained from the CESMD data center [CESMD 2014]. Accelerations for each principal direction are shown in Figure 1.

As it can be observed from these plots, the greatest peak acceleration was recorded in North-South direction. The shaking was dominant in this direction; see Figure 2. The design spectral acceleration, S_a, for city of Napa was taken from the USGS hazard maps [USGS 2014]. The spectral accelerations were computed at 5% critical damping for grade level installations and compared to the AC156 required response spectra used in seismic evaluation of nonstructural components and equipment. As presented in Figure 3, the spectral accelerations in North-South direction are at about the same level as the AC156 spectra. The spectral accelerations in other two directions were lower that the AC156 spectra. Numerous failures of the nonstructural components were observed during the field investigation. The observations are discussed below.

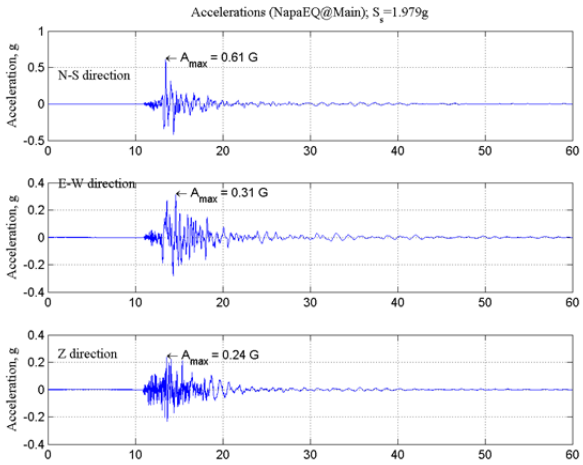

Figure 1 Accelerations recorded by Main Street station.

[+] Any observations, opinions, findings, and conclusions or recommendations expressed in this material are preliminary and are those of the authors, and do not necessarily reflect those of the Pacific Earthquake Engineering Research Center. The information, data and images contained in this report may not be published or presented without permission from the authors.

[1] PhD, PE, Site Operations Manager of nees@berkeley.edu, UC Berkeley.
[2] SE, Principal, Miyamoto International
[3] PhD, SE, Senior Associate, Miyamoto International
[4] Professor, Department of Civil and Environmental Engineering, Principal Investigator of nees@berkeley.edu, UC Berkeley.

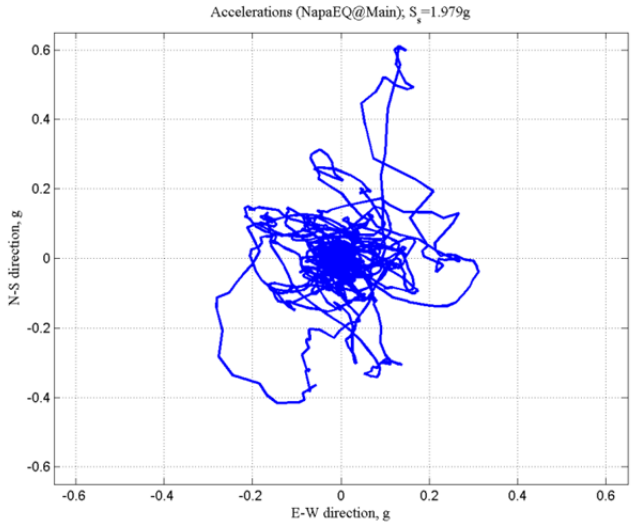

(a) North-South versus East-West accelerations

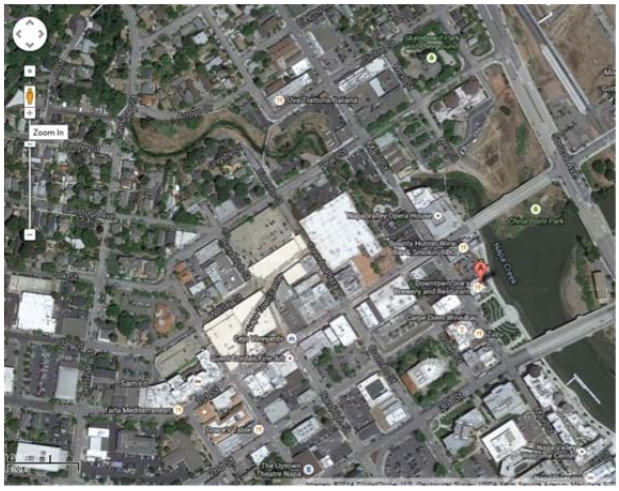

(b) Google map of downtown with a balloon marking location of the station

Figure 2 Accelerations of the shaking north-south direction were much higher than those in east-west direction.

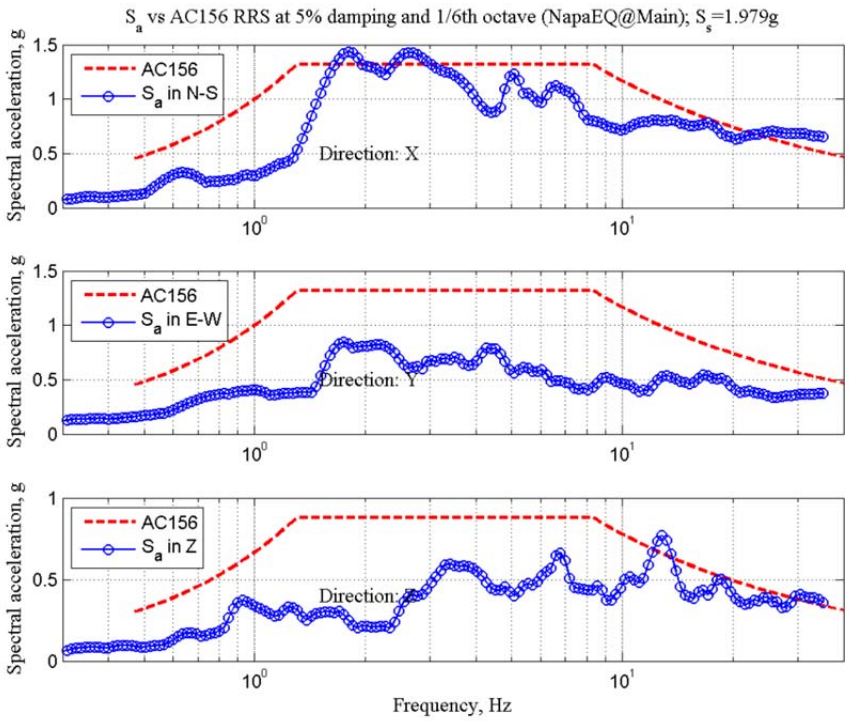

Figure 3 Spectral accelerations in north-south direction were very close to AC156 spectra.

3.2 NONSTRUCTURAL DAMAGE ASSESSMENT

Although a majority of buildings in downtown Napa are more than 100 years old, there are many newer buildings constructed since or older buildings reinforced in the recent years. The report compares the performance of the old installations to those conducted per recent seismic code.

3.2.1 ROOF TILE FAILURES IN A CHURCH BUILDING

The ground shaking in Napa downtown was quite severe as outlined in the previous section that was amplified on the roof level of a church. Figure 4 shows the satellite view and street view of the church before the earthquake (courtesy of Google maps). The ground observation of the site right after the earthquake revealed massive failures of roof tiles; see Figure 5.

(a) Before the earthquake (Google maps) (b) Before the earthquake (Google street view)

Figure 4 Condition of the roof tiles before the earthquake.

(a) Back street view (b) View from the plaza

Figure 5 Failures of ceramic roof tiles due to amplified seismic excitation on the roof.

3.2.2 BRIDGE CONNECTING PARKING LOT WITH A BUILDING RIGHT NEXT TO IT

A small bridge connecting a parking lot to a building right next to it exceeded its travel limit as presented in Figure 6. As the result only minor damage was observed at the bottom flanges of the bridge's deck. This failure could be associated with some pounding effect on the parking structure and the building.

(a) Global view (b) Zoomed view

Figure 6 Small bridge connecting a parking lot and building next to it exceeded its travel limit.

3.2.3 SUSPENDED CEILING SYSTEMS

Old Installations

A suspended ceiling installation dated to early 1990s was investigated in the field studies. The system did not have any splice wires and was most likely floating on all sides. The suspended ceilings were installed in a single-story commercial building, with the major failure concentrated around the perimeter of the building: see Figure 7. Some local damage was also observed; see Figure 8.

(a) No brace wires were installed

(b) Failure concentrated around perimeter on floating side

Figure 7 Old ceiling installation global failures.

(a) Local buckling at tee intersections

(b) Missing tee-bar failure

Figure 8 Local failure of old ceiling tile installations.

Recent Installations

A suspended ceiling installation most likely installed per code with 7/8 in. wall molding was investigated during the field studies. It was installed on the third floor of a three-story building. The building was partially functional one day after the earthquake. The main damage to the offices on the third floor was related to failures of the fire sprinklers, which did not have enough travel clearance in respect to lay-in panels. The majorities of failures were concentrated around the fire sprinklers; see Figure 9. The floor was flooded due to the sprinkler failures and a moisture evacuation procedure was under way during the field studies. Some localized failures at the perimeter were also observed; see Figure 10.

(a) Failure of a panel due to interaction with fire sprinkler

(b) Clearance for the fire sprinkler was exceeded

Figure 9 Recent ceiling installation: local failure.

(a) Localized failures at the perimeter

(b) Localized failures at the perimeter

Figure 10 Recent ceiling installation: global failures.

Metal Lay-in Suspended Ceiling Systems

A recent installation of suspended ceiling system with metal lay-in panels sustained no damage at all on both levels of two-story building; see Figure 11 and Figure 12.

(a) View along the building

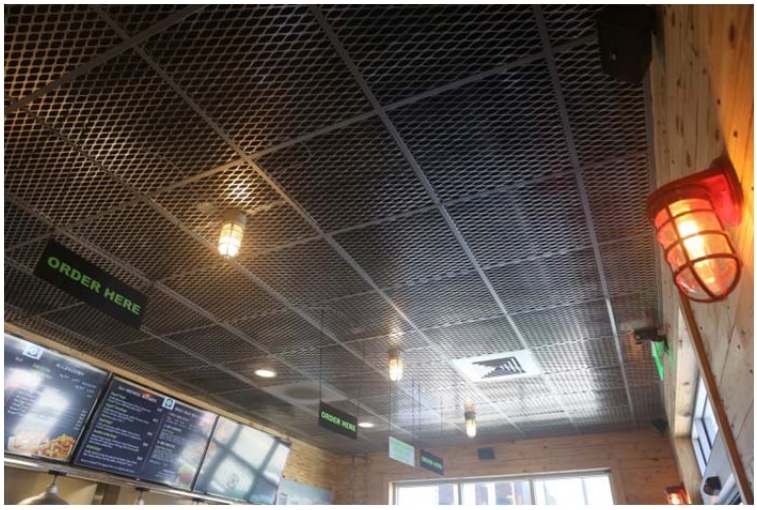

(b) View of order placing area

Figure 11 Recent ceiling installation: metal lay-in panels in a two-story restaurant.

(a) Second floor had smaller ceiling installation

(b) Zoomed in view of the second-story installation

Figure 12 Recent ceiling installation: metal lay-in panels in a two-story restaurant.

Large Panel Installation at a Manufacturing Facility

A manufacturing facility studied by the team consisted of a number of tilt-up buildings was built within last six years. No structural damage was noticed during a survey of the buildings. In one of the buildings a large 4 ft × 4 ft ceiling panel fell down; see Figure 13. No other architectural damage was noticed. However a lot of product tipped over on shelves and pictures fell off walls.

Figure 13 Large 4 ft by 4 ft ceiling panel failed during the earthquake.

3.2.4 INDOOR AND OUTDOOR INSTALLATION OF SHEETROCK AS SUSPENDED PANELS

A failure of outdoor installation of sheetrock panels occurred in a three-story building during the earthquake; see Figure 11. The failures were localized around the columns .These failures of the outdoor panels were accompanied by failures of suspended ceilings inside of the building.

(a) South side: zoomed view

(b) South side: global view

(a) North side: zoomed view

(b) South side: global view

Figure 14 Recent ceiling installation: metal lay-in panels.

3.3 FAILURES IN WINERIES

A failure of a tall tank is presented in Figure 15. The local buckling was observed at the attachment points on the tall tanks (on left side of the global photo). The tanks on the left have not suffered this kind of damage due to smaller size.

(a) Rows of tall (right) and short (left) tanks in a winery

(b) Local buckling at the bottom of a tall tank

Figure 15 Local buckling at the attachment point of the wine tank.

3.4 FAILED LIGHT FIXTURE

A large light fixture installed on a 3.68-m pole fell on the ground during the earthquake as presented in Figure 16. The light pole was installed right next to a large department store. This could have injured shoppers passing by if the earthquake had happened during operational hours.

(a) Light fixture fell from the light pole

(b) Light fixture on the ground

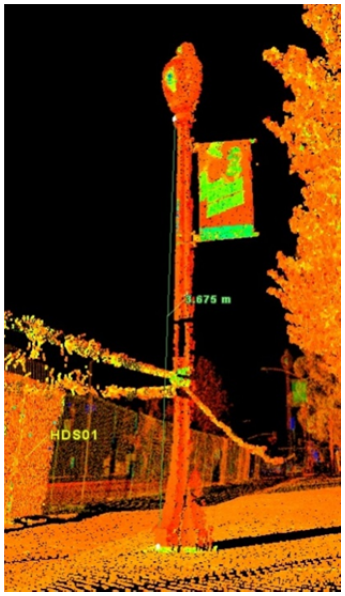

(c) Typical height of light pole measured in a point cloud (3.68 m)

Figure 16 Failure of a light fixture

3.5 ANOMALIES ASSOCIATED WITH LARGE DEFLECTIONS OF FIRE PIPING SYSTEM

3.5.1 FAILURE OF FIRE PIPING SYSTEM IN A DEPARTMENT STORE

A two story department store in downtown was flooded with water after a pipe burst on the roof (shown in a red square) in the photo of the retaining wall in Figure 17. The water eventually broke through the parapet on the roof and shot across the walkway. The water source was close at the time of the field studies (12 hours after the earthquake), and the building was closed for an inspection. Water coming from the roof and upper story caused massive flooding of the first floor of the department store: carpets were soaked and most likely will need to be replaced in the future. Figure 18 shows soaked goods and suspended ceiling tiles as a result of the earthquake and the flooding. Ten days after the earthquake the department store was still closed. If the hole in the parapet has not developed at the time of pipe failure and flooding, a complete collapse of the roof diaphragm could be expected. Flooding resulted in large monetary losses: the piping system needs to be repaired, suspended ceiling to be replaced, goods cannot be sold due the damage, and flooded carpets need to be replaced in addition to other costs.

(a) Water pipe failed on the roof elevation and poured down through a hole in parapet (red square)

(b) Zoomed view of the hole

Figure 17 Water damages in the department store.

Figure 18 Soaked suspended ceiling tiles and goods on the floor.

3.6 LARGE DEFLECTIONS OF FIRE PIPING SYSTEM IN PARKING STRUCTURE

A four-story RC parking structure was studied for large file pipe displacements. Although the parking structure itself did not experience any visible damage, there was clear evidence of large deflections of piping system with some minor damage. The fire system was ideal for the filed studies because all elements of the system were exposed. Scratches on the pipes provided strong evidence of the shaking amplitude and radial deflection. Figure 19 shows parts of the same system branched out along the longitudinal large size pipe. When access hole is moderately oversized, the amplitude of pipe motion is smaller than that for an oversized access hole. The

photos were taken on the third floor of the structure; the fourth floor is an open roof. Failure of a ceiling anchor is presented in Figure 20. Residual deflection of one of the end pipes can be clearly observed from the right photo in the same figure.

(a) Scratches on the pipes show the amplitude of motion within a supporting bracket (larger for a largely oversized access hole)

(b) Scratches on the pipes show the amplitude of motion within a supporting bracket (slightly less for a moderately oversized access hole)

Figure 19 Evidence of large deflections of the piping system.

(a) Failure of the ceiling anchor

(b) Residual deflection of a pipe

Figure 20 Evidence of large deflections of the piping system

3.7 TELECOMMUNICATION EQUIPMENT AND POWER SUPPLY

During the earthquake, a massive concrete wall on top of a telecommunication building top floor gave way. The wall was attached to the upper structure by means of brackets as presented in Figure 21. The wall fell down and cut electric power supply from the building. Since the backup generators had no power to cool down the servers inside of the building, an external power generator and a massive cooling unit were brought to the site to keep the computer servers running while the building is being repaired as shown in Figure 22. The building content was

essential for providing telecommunication services to people, police, and emergency response team.

(a) Nonstructural wall suspended on brackets (orange) failed

(b) Zoomed view of the brackets remaining in place; power conduits were damaged during the wall failure

Figure 21 Failure of nonstructural wall at telecommunication center.

Figure 22 Failure of nonstructural wall at telecommunication center.

3.8 FAILURE OF CHIMNEYS

The chimneys constructed from the bricks and stones represented one of the most vulnerable nonstructural components damaged in the earthquake. Poor seismic performance of chimneys constructed from massive and brittle materials were demonstrated in the previous earthquakes worldwide, including the previous 2004 earthquake in Napa [2004]. The major human casualties in both earthquakes were associated with the chimney failures. This section discusses some typical examples of chimney failures. The chimneys vary in size, location within a building, and elevation above the grade. Depending on a failure mode, the chimney failure can create a variety of hazards, including hazards for building occupants as presented in Figure 23 and/or hazards for people outside of the building as shown in Figure 24.

(a) Chimney leaning away from the street

(b) Complete failure with pieces still on the roof

Figure 23 Chimney failures creating danger for building occupants.

(a) Massive chimney that fell away from the house to the ground

(b) Chimney shattered in pieces on a walkway

Figure 24 Chimney failures creating danger for people outside of buildings

3.9 RESIDENTIAL GAS SUPPLY

In many cases structural damage can lead to excessive displacements, and the response of the building can impact its power and water supply lines. This hazard was studied based on a wood-frame building with a cripple-wall design shown in Figure 25. The left photo presents the damaged state of the building with large residual drifts on the first and the second levels. A photo on the right shows large residual deformation of the cripple wall level. When cripple wall collapsed, the bottom lumber of the building came in a contact with a gas pipe; see Figure 26.

(a) Global view after the earthquake

(b) Corner of the building

Figure 25 Failure of wood frame building with a cripple wall design

(a) Photo of collapsed porch

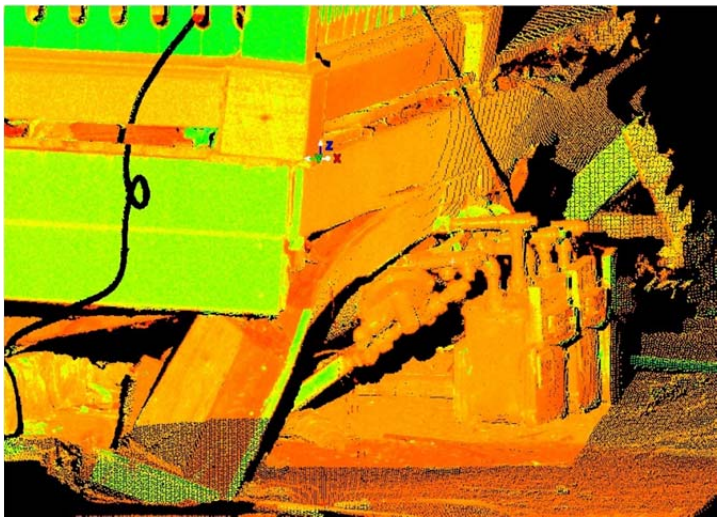

(b) Laser scan of collapsed porch

Figure 26 When cripple wall collapsed the bottom lumber of the building remains in a contact with a gas pipe.

3.10 FAILURE OF GLASS WINDOWS

Failure of glass windows were widespread in downtown Napa. To address security issues of the buildings' occupants, the majority of failures were covered by installing plywood sheets instead of windows. While glass replacement of small window openings in residential buildings are not too costly, the cost of replacing large openings can be quite significant and some supply shortage can be expected. In case of massive glass failure in many large window openings, the building can become un-operational for quite some time. Typical glass failures are presented in Figure 27 and Figure 28.

(a) South side

(b) North side

Figure 27 Typical example of window glass failures in a three-story office building.

(a) All glass windows failed in a small business

(b) The majority of glass windows of the first floor failed

(c) Glass broken on both sides of the two-story building (torsional effect)

(d) Glass broken on both sides of the single-story building (torsional effect)

Figure 28 Typical example of window glass failures in small buildings with soft story effect.

3.11 AUTOMATIC DOOR OPENINGS

During the field studies it was noticed that an automatic door to one of the large department store in downtown Napa was jammed and was not working properly. Since the building did not have any structural damage, the management began repairs to make it as operational as soon as possible. At the time of the visit, the store was undergoing inspection and the door was being replaced as shown in Figure 29.

Figure 29 Damaged door is under urgent repair.

3.12 FAILURE OF BASE ANCHORAGE OF WATER TANK AT LOCAL SCHOOL

The base anchorage of the water tank at the high school near downtown Napa separated from the tank wall, as shown in Figure 30. As the result, the tank experienced large amplitude shaking during the earthquake, resulting in breaks of the rigid water pipes; see Figure 31. As a result of these deflections, a rain leader pipe from roof failed (left photo). Obviously, this pipe connection needed to be flexible to accommodate the relative displacement between the wall and the tank. Movement of cistern during earthquake caused elbowing of the pipe, which caused it to break; see Figure 31 (right photo).

Figure 30 Base anchorage separated from the tank wall.

(a) Rain leader pipe roof failed

(b) Elbow of the pipe on right failed

Figure 31 Failure of water tank.

3.13 CRACKING OF GYPSUM WALL PARTITIONS IN HIGH-SCHOOL BUILDING

Deformation of the building's frame caused cracking and tearing of gypsum wall panels and their joints. The damage was observed at wood frame building built on school property within last 10 years. Widespread tearing marks were observed in the gypsum board on walls (see Figure 32), mostly at horizontal joints; see Figure 33. This kind of architectural damage is expected after a moderate to strong event.

Figure 32 Tear in gypsum board on walls.

Figure 33 Wide spread tearing marks in gypsum board on walls mostly at horizontal joints.

3.14 REFERENCES

CESMD (2014). Data for latest earthquakes, Center for Engineering Strong Motion Data, *http://strongmotioncenter.org*/.

ICC-ES (2010). *Acceptance Criteria for Seismic Qualification by Shake-Table Testing of Nonstructural Components and Systems, AC156*, International Code Council Evaluation Service Inc. ICC-ES.

USGS (2014). Seismic Design Maps and Tools, United States Geological Survey, *http://earthquake.usgs.gov/hazards/designmaps*/.

4 Overview of URM Buildings Tagged in Napa 24 August 2014 M_w 6.0 South Napa Earthquake[+]

Matthew J. Schoettler, Andreas Schellenberg, Clément Barthes, and Jenna Wong

A survey of several unreinforced masonry (URM) buildings was conducted in Napa on the day following the earthquake (25 August 2014). These were located in the downtown area and sustained varying degrees of damage from mortar cracking, to pounding, and all the way to façade collapse. In the area of interest, ground shaking was very strong with moderate damage potential according to the USGS [2014]. The downtown area likely experienced similar levels of ground shaking on the order of 40% to 50%g PGA [USGS 2014]. However, local site effects may have been present as the only strong-motion sensor in downtown Napa recorded 0.65*g* PGA [USGS 2014].

Seven URM buildings were visited during the field investigation. All received unsafe (red) tags during their initial inspection. Most of these buildings were two stories high, but one was three-stories and another one story. Façade collapse and diagonal cracking were observed at two locations; see Figures 1 and 2. A stone parapet was damaged and several stones fell to the ground; see Figure 3, at the historic Goodman Library that houses the Napa County Historical Society. Mortar cracking was visible particularly above the second floor windows in the 113-year-old stone-masonry building. The building at 1245 Main St. (Figure 1) and the Goodman Library sustained minor cracking as was reported after the September 3, 2000, Yountville/Napa Earthquake [Miranda and Aslani 2000], but the remaining URM buildings were reported as undamaged.

Figure 1 URM building at 1245 Main Street.

[+] Any observations, opinions, findings, and conclusions or recommendations expressed in this material are preliminary and are those of the authors, and do not necessarily reflect those of the Pacific Earthquake Engineering Research Center. The information, data and images contained in this report may not be published or presented without permission from the authors.

Figure 2 URM building at 810 Brown Street.

Figure 3 URM building at 1219 1st Street.

The façade of a vacant building at 1212 1st St. looked undamaged, see Figure 4, but the second-floor diaphragm was cracked. Windows on the first floor shattered, but debris was cleaned and building secured by the day following the earthquake.

The second floor of 822 Brown Street was damaged, see Figure 5, due to pounding with the adjacent building. Wall-to-roof diaphragm anchorage failure was also observed on the North face of the second floor. The fifth and sixth anchorages from the front of the building protruded from the wall about 8 in. and 3 in., respectively. In two locations, one above and one below the roof diaphragm anchorages, bricks were dislodged from the façade. A portion of the parapet (17 bricks) of the same wall shifted about a half inch.

Figure 4 URM building at 1212 1st Street.

The three-story building at 1040 Main St. was retrofitted in the 1980s with steel braced frames; see Figure 6. Exterior cracks were visible especially noticeable at brace foundation connections. The building was initially red tagged due to parapet safety concerns, but once mitigated the building received a yellow tag and was occupied within 30 hours of the earthquake. Damage was concentrated on the first floor, with localized buckling of several braces and gusset plates.

The one story building at 1210 1st St. had no visible structural damage, see Figure 7. It was red-tagged due to safety concerns at an adjacent building.

A list of 40 URM buildings in the City of Napa was provided by Fred Turner [2014] of the California Seismic Safety Commission. It included the buildings' retrofit statuses stemming from the City of Napa Ordinance O2006-1, which updated chapter 15 of the Napa Municipal Code. The ordinance required review and rehabilitation of URM buildings to "improve their safety in the event of an earthquake" [City of Napa 2006]. The proactive action was incentivized with financial reimbursements made possible through the Napa Community Redevelopment Agency, and in March of 2006 the ordinance passed [City of Napa 2006]. Of the 40 URM buildings on the list, half were designated as retrofitted. This designation, however, may not be accurate since the retrofit status appears last updated in 2006, and the ordinance is expected to have impacted the remaining 20 un-retrofitted buildings.

The URM buildings' retrofit statuses are provided in Tables 1 through 3, according to post-earthquake inspection tags. Four additional URM buildings, which had reinforced walls, are not included in this synopsis, but two were green tagged and two were yellow tagged. Figure 10 shows the building locations, their inspection tag color, and retrofit status overlaid on the expected ground shaking intensity. Ground shaking with a 0.65g PGA was recorded on the 900 block of Main St. [USGS 2014] with 38 of the buildings within 0.5 mile from that station. However, local site effects may influence this station, and with no other instruments in the vicinity this figure shows the USGS estimate of 40% to 50%*g* PGA. There is no apparent correlation with geographic location and tagging in this figure.

Figure 5 URM building at 822 Brown Street

Figure 6 URM building at 1040 Main Street.

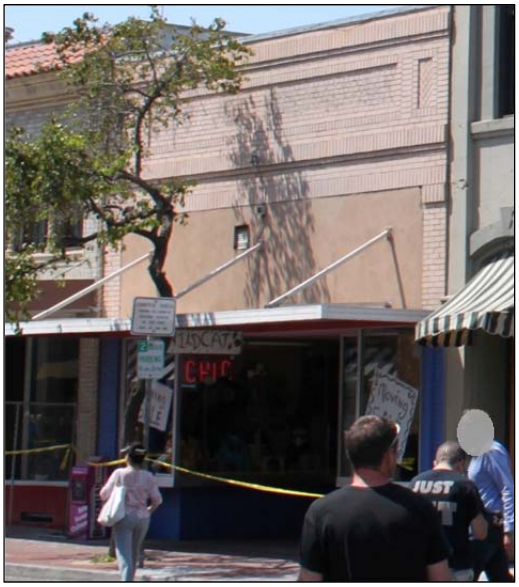

Figure 7 URM building at 1210 1st Street.

A summary of the initial building screenings is illustrated in Figure 11. This shows an equal number of retrofitted and un-retrofitted URM buildings received red tags. Additionally, more un-retrofitted URM buildings received green tags than those retrofitted. This may be partially explained by an inaccurate account of completed retrofits thus skewing the number of un-retrofitted green-tagged buildings. However, the performance of these buildings raise an opportunity to investigate retrofit scenarios in terms of performance. Three of the buildings posed a significant risk to life-safety due to falling debris. Two were previously retrofitted, and one is listed as un-retrofitted. Fortunately there were no pedestrian victims due to the hour of the early morning event.

In total, fourteen of the 40 buildings were deemed unsafe. Two of these red tags were initiated by dangerous parapets, but were subsequently downgraded to a cautionary (yellow) tag after remediating the threat. Four red-tagged buildings were cited because of adjacent unsafe buildings, not necessarily because of safety with the structure itself. However, it is not known what tag the building will receive once the safety threat from the adjacent building is mitigated. In the week following the earthquake, eight URM buildings remained unsafe due to problems with the building itself. To account for these updates, a revised summary of tags is illustrated in Figure 12. This isolates the buildings with red-tags induced by an adjacent building, and shows that the same number of red-tags was given to retrofitted buildings as un-retrofitted. Structures deemed unsafe due to problems with adjacent buildings have interesting ramifications and poses a problem to performance-based seismic design. Ensuring seismic performance levels in an urban environment requires interdependency considerations.

Two brick buildings that exhibited severe damage and posed a risk to life-safety but were omitted from the list of 40 URM buildings discussed were the Napa U.S. Post Office and 1001 2nd St.; both buildings were red-tagged. The post office had severe diagonal cracking, see Figure 8. Large windows along the front of the building broke, as many had previously in 2000 [Miranda and Aslani 2000]. A partial collapse occurred at the second building, see Figure 9. While specific structural details of these buildings are not known, the list of URM buildings may

lack comprehensiveness. A complete list should be compiled with records on file with the City of Napa to more accurately assess the performance of URM buildings.

Figure 8 U.S. Post Office at 1321 2nd Street.

Figure 9 Partial collapse at 1001 2nd Street.

Table 1 URM buildings with unsafe (red) tags [Turner 2014; City of Napa 2014].

No.	Location	Retrofit status	Note
1	975 1st St.	Complete	
2	1141 1st St.	Complete	
3	1040 Main St.	Complete	Red tagged due to parapet then downgraded to yellow; see Figure 6.
4	1917 3rd St.	Complete	Red tagged due to parapet then downgraded to yellow.
5	1219 1st St.	Retrofit design in progress in 2000.	See Figure 3.
6	826/830 Brown St.	Retrofit design in progress in 2000.	Adjacent to unsafe building.
7	1245 Main St.	Retrofit permit issued in 2000.	See Figure 1.
8	810 Brown St.	Un-retrofitted as of 2006.	See Figure 2.
9	822 Brown St.	Un-retrofitted as of 2006.	See Figure 5.
10	1015 Coombs St.	Un-retrofitted as of 2006.	Adjacent building red tagged.
11	1210 1st St.	Un-retrofitted as of 2006.	Damage at neighbor causing threat to safety at this address. See Figure 7.
12	1212 1st St.	Un-retrofitted as of 2006.	See Figure 4.
13	1005 Coombs St.	Unknown; presumed un-retrofitted.	
14	1424 2nd St.	Unknown; presumed un-retrofitted.	Adjacent building failing.

Table 2 URM buildings with cautionary (yellow) tags [Turner 2014; City of Napa 2014].

No.	Location	Retrofit status	Note
1	900 Brown St.	Complete	
2	1026 1st St.	Complete	
3	500 Main St.	Complete	
4	942 Main St.	Complete	
5	1122 Main St.	Complete	
6	1139 1st St.	Retrofit design in progress in 2006.	Yellow tag downgraded to green.
7	1227 1st St.	Unknown; presumed un-retrofitted.	
8	807 Main St.	Un-retrofitted as of 2006.	
9	813 Main St.	Un-retrofitted as of 2006.	
10	815 Main St.	Un-retrofitted as of 2006.	

Table 3 URM buildings with slight or no damage (green) tags [Turner 2014; City of Napa 2014].

No.	Location	Retrofit status	Note
1	1720 Brown St.	Complete	
2	809 Coombs St.	Complete	
3	1005 1st St.	Complete	
4	903 Main St.	Complete	
5	920 3rd St.	Retrofit design in progress in 2000.	
6	1018 Main St.	Retrofit design in progress in 2000.	
7	902 Main St.	Retrofit design in progress in 2006.	
8	926 Coombs St.	Un-retrofitted as of 2006.	
9	1025 Coombs St.	Un-retrofitted as of 2006.	
10	829 Main St.	Un-retrofitted as of 2006.	
11	1325 5th St.	Unknown; presumed un-retrofitted.	
12	1130 1st St.	Unknown; presumed un-retrofitted.	
13	1015 1st St.	Unknown; presumed un-retrofitted.	
14	1202 Main St.	Unknown; presumed un-retrofitted.	
15	1600 Main St.	Unknown; presumed un-retrofitted.	
16	376 Soscol Ave.	Unknown; presumed un-retrofitted.	Not shown in Figure 10.

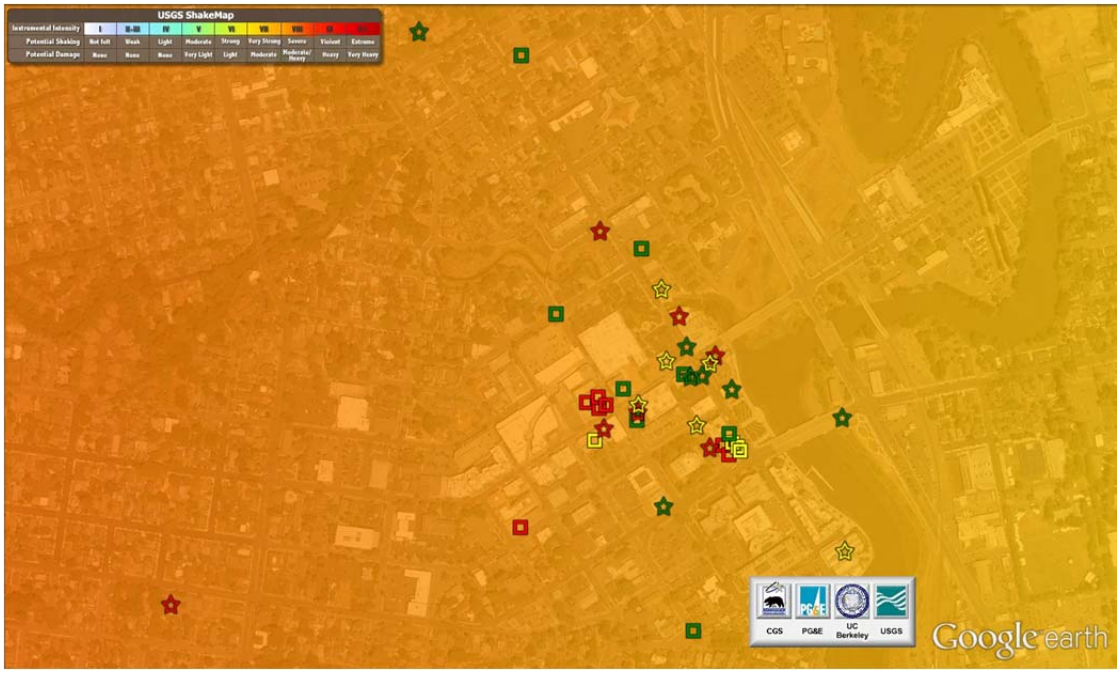

Figure 10 URM locations with initial tag type in the City of Napa overlaid on USGS ShakeMap: 24 Aug 2014 S. Napa M_w 6.0 Earthquake [Turner 2014; City of Napa 2014; USGS 2014].

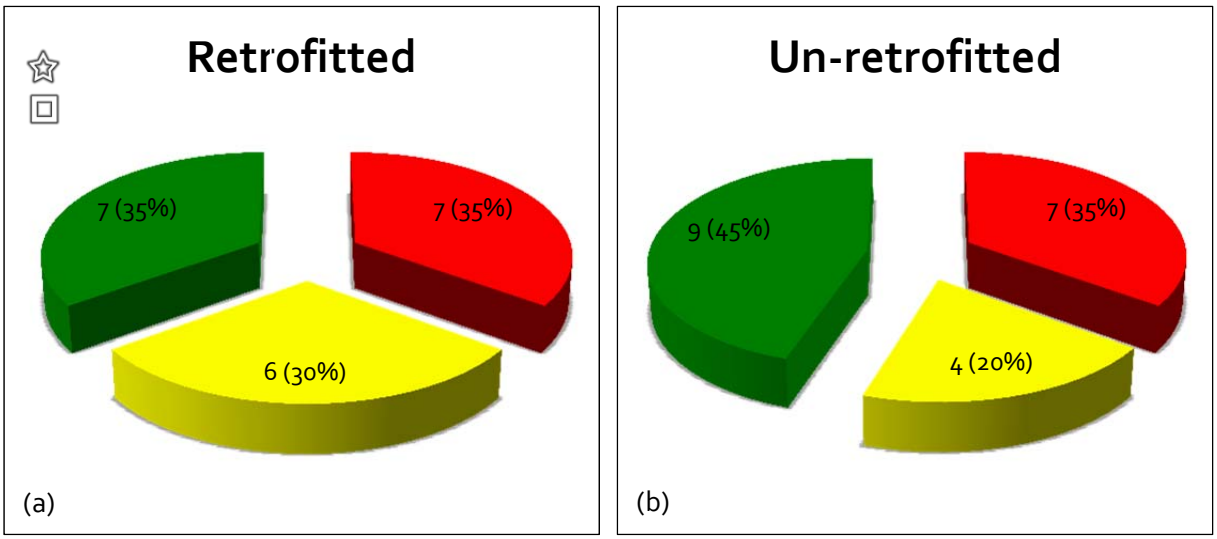

Figure 11 Initial tag types for (a) retrofitted and (b) un-retrofitted URM buildings in the City of Napa: 24 Aug 2014 S. Napa M_w 6.0 Earthquake [Turner 2014; City of Napa 2014].

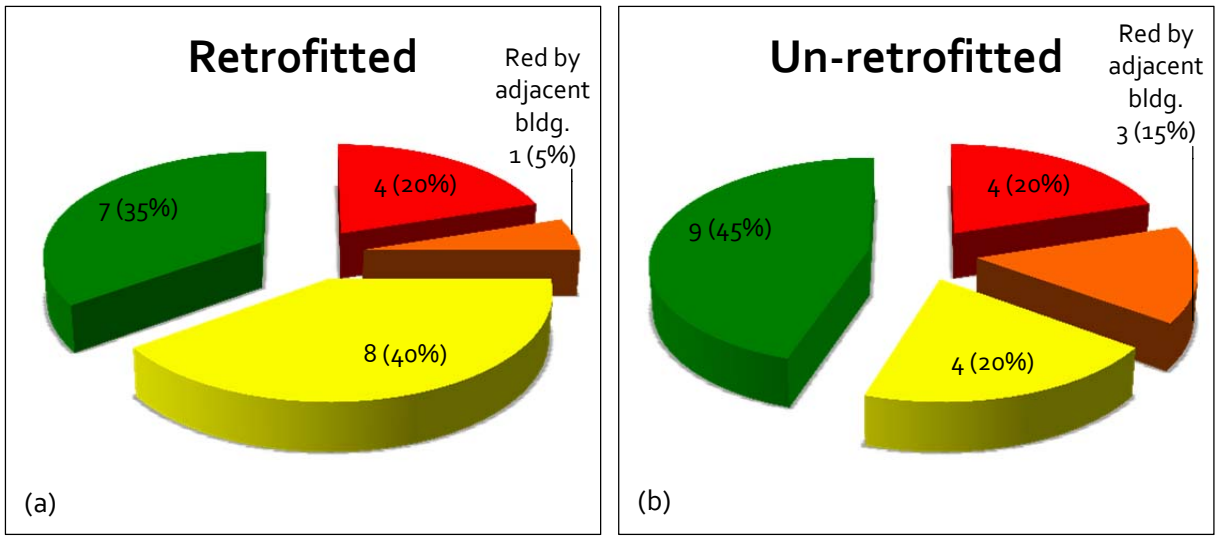

Figure 12 Revised tag types for (a) retrofitted and (b) un-retrofitted URM buildings in the City of Napa: 24 Aug 2014 S. Napa M_w 6.0 Earthquake [Turner 2014; City of Napa 2014].

4.1 REFERENCES

Turner, F. (2014). Personal communication.

City of Napa (2006). Municipal Code.

City of Napa (2014). Earthquake Information Map. Accessed September 4th, 2014. <*http://cityofnapa.maps.arcgis.com/apps/Viewer/index.html?appid=82a341fa5c5b4f4bb32381b82541e7fc*>.

Miranda, E. and Aslani, H. (2000). Brief Report on the September 3, 2000 Yountville/Napa, California Earthquake. <*http://peer.berkeley.edu/publications/yountville-napa_sep-2000.html*>.

USGS (2014). M6.0 – 6km NW of American Canyon, California 2014-08-24 10:20:44 UTC. <*http://earthquake.usgs.gov/earthquakes/eventpage/nc72282711#shakemap*>.

5 Preliminary Observations of Building Structures in Downtown Napa, California[+]

Barb Simpson, Shanshan Wang, and Jiun-Wei Lai

5.1 OBSERVATION DATE: 25 AUGUST 2014

625 Randolph Street (Corner of 5th & Randolph)

Building Description	First United Methodist Church
Structural Damage	Separation of exterior wall; see Figure 1 and Figure 2
Nonstructural Damage	N.A.

Figure 1

Figure 2

[+] Any observations, opinions, findings, and conclusions or recommendations expressed in this material are preliminary and are those of the authors, and do not necessarily reflect those of the Pacific Earthquake Engineering Research Center. The information, data and images contained in this report may not be published or presented without permission from the authors.

810 Randolph Street

Structural Damage	No structural damage
Nonstructural Damage	Buckled awning bracing; see Figure

Figure 3

1220 3rd Street

Structural Damage	No structural damage
Nonstructural Damage	Cracks in exterior drywall; see Figure 4

Figure 4

810-822 Brown Street

Building Description	Masonry (URM) and Wood Construction
Structural Damage	Exterior masonry collapse on South-West face; see Figure 5
	Separation of exterior masonry cladding on North face
	Damage (cracks in masonry) at roof of 816 Brown Street; see Figure 6
	Only limited damage to cafe (possibly retrofitted)

Figure 5

Figure 6

828 Brown Street

Building Description	Masonry (URM) and possibly retrofitted with steel moment frames
Structural Damage	No obvious structural damage seeing from outside but the building was red tagged; see Figure 7

Figure 7

820 Randolph Street; 13512 2nd Street

Building Description	U.S. Post Office
Structural Damage	Red-tagged; see Figure 8 and Figure 9. Substantial cracking of exterior masonry walls
Nonstructural Damage	Broken glass on north-west face.

Figure 8

Figure 9

825 Randolph Street

Building Description	Napa County Court House: Wood and masonry (URM) construction
Structural Damage	Collapse at roof; see Figure 10 and 11

Figure 10

Figure 11

944 Main Street

Building Description	Retrofit by Degenkolb Engineers (Source: *http://www.earthquakeretrofit.org*)
Structural Damage	Crack between South-East wall from structural system; see Figure 12
Nonstructural Damage	Broken storefront windows; see Figure 13

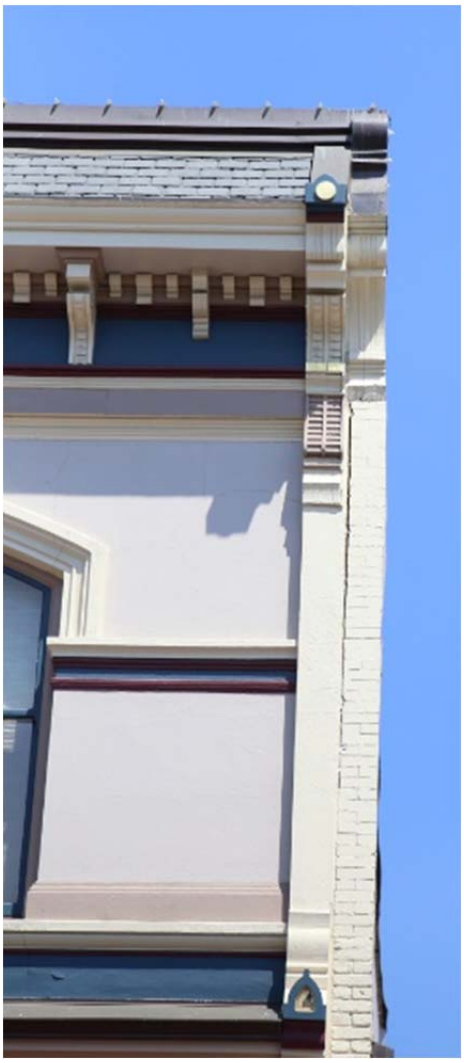

Figure 12

Figure 13

1122 Main Street:

Building Description	Steel Retrofit (Source: from an engineer (?) who was tagging the building)
Structural Damage	Masonry parapet damage, most likely due to insubstantial lateral support; see Figures 14, 15, and 16
Repair	Began on 26 August 2014

Figure 14

Figure 15

Figure 16

1201 Main Street

Building Description	Napa Firefighters Museum: Vintage wood construction
Structural Damage	Exterior wall dropped out; insulation exposed; see Figure 17
Nonstructural Damage	Grocery fallen off, twisting light and ceiling cracks; see Figure 18

Figure 17

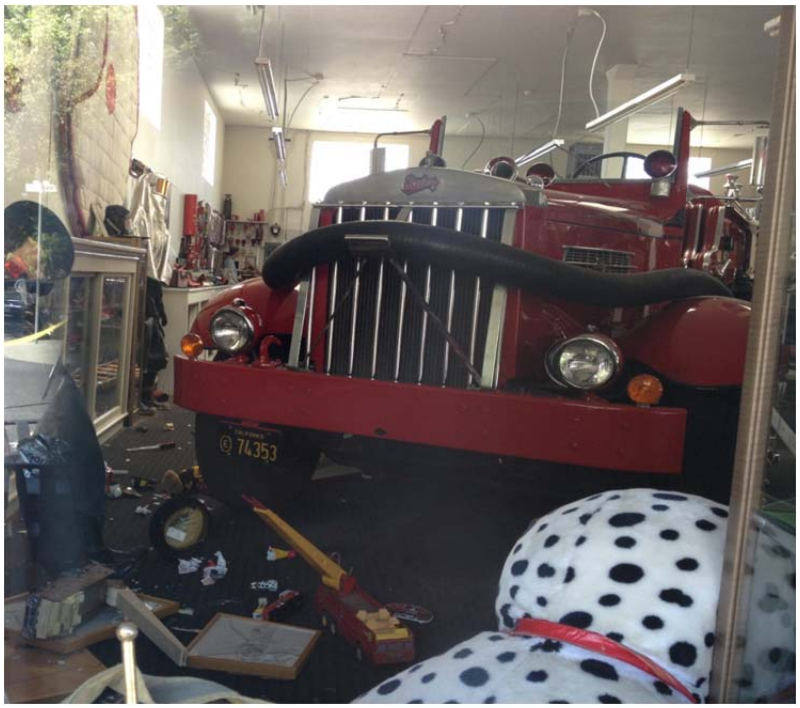

Figure 18

1140 Main Street

Building Description	Masonry structure
Structural Damage	Exterior wall cracking and falling; see Figure 19

Figure 19

1241 4th Street

Building Description	Wood residential structure
Nonstructural Damage	Chimney damage; see Figure 20

Figure 20

1219 1st Street

Building Description	Goodman Library: FEMA subsidized retrofit (source: *http://www.earthquakeretrofit.org*); exterior masonry
Structural Damage	Significant damage to roof parapet; see Figure 21

Figure 21

1333 3rd Street

Building Description	1st Presbyterian Church: Wood construction
Structural Damage	Roof damage, possible pounding; see Figure 22
Nonstructural Damage	Broken glass windows

Figure 22

1001 2nd Street

Building Description	Unreinforced masonry (URM)
Structural Damage	Significant damage at 3rd story; see Figure 23

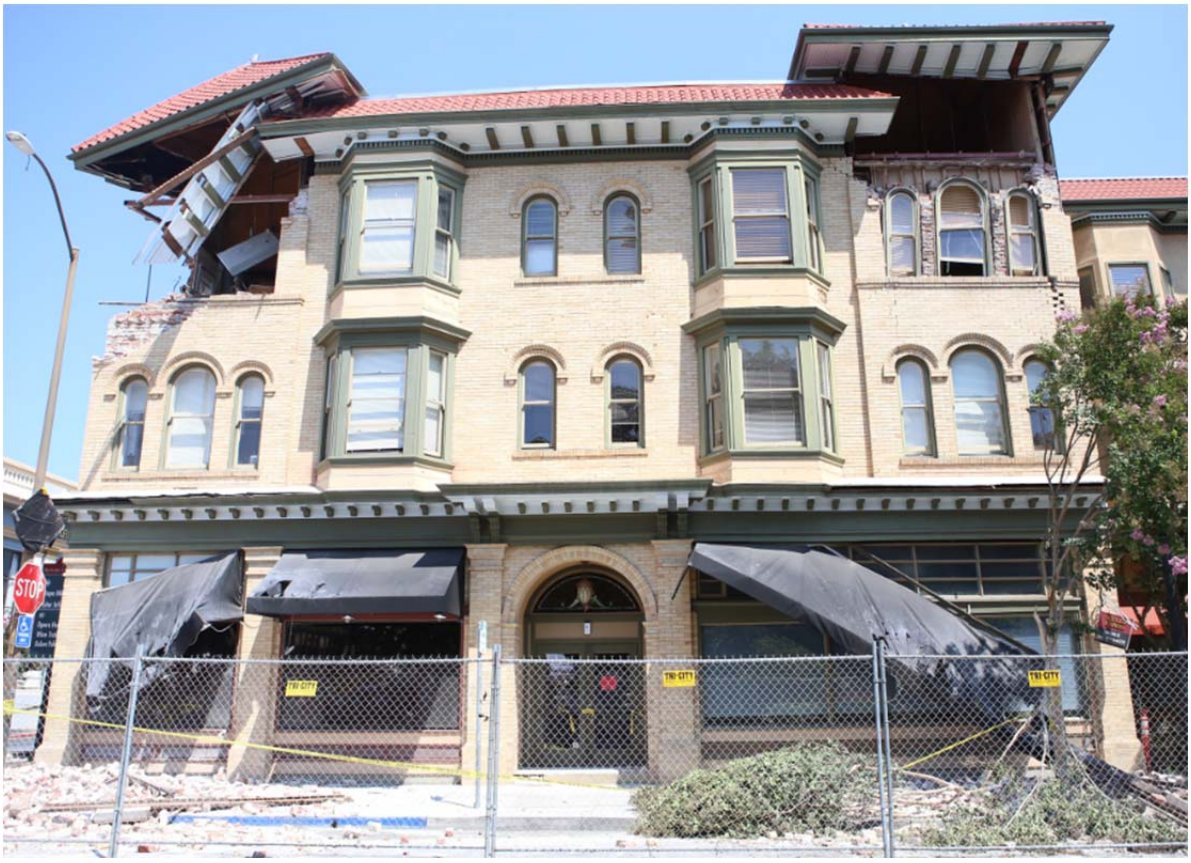

Figure 23

1245 Main Street

Building Description	Vintner's Collective: Vintage masonry and wood construction
Structural Damage	Substantial damage/collapse of exterior masonry; see Figure 24

Figure 24

Napa Valley College, 2277 Napa-Vallejo Highway

Building Description	Life Sciences Building	
	New Construction	Two-story ordinary concentrically braced frame (OCBF)
		Square hollow structural section (HSS) braces; see Figure 25
		Weak axis column bending; see Figure 26
Structural Damage	None	
Nonstructural Damage	Minor; displaced piping (see Figure 27) and concrete spalling (see Figure 28) at east-south corner of building.	

Figure 25

Figure 26

Figure 27

Figure 28

Napa Valley College, 2277 Napa-Vallejo Highway

Building Description	McCarthy Library & Media Center	
	New Construction	Two-story special concentrically braced frame (SCBF)
		Round hollow structural section (HSS) braces; see Figure 29
		Stiffened gusset plates (see Figure 30) and net section reinforcing plates are provided to the round HSS brace ends
Structural Damage	None	
Nonstructural Damage	Minor; books were thrown from shelves (see Figure 31), twisted lighting (see Figure 32), dropped ceiling panel (see Figure 33), and dropped fire sprinkler covers (see Figure 34)	

Figure 29

Figure 30

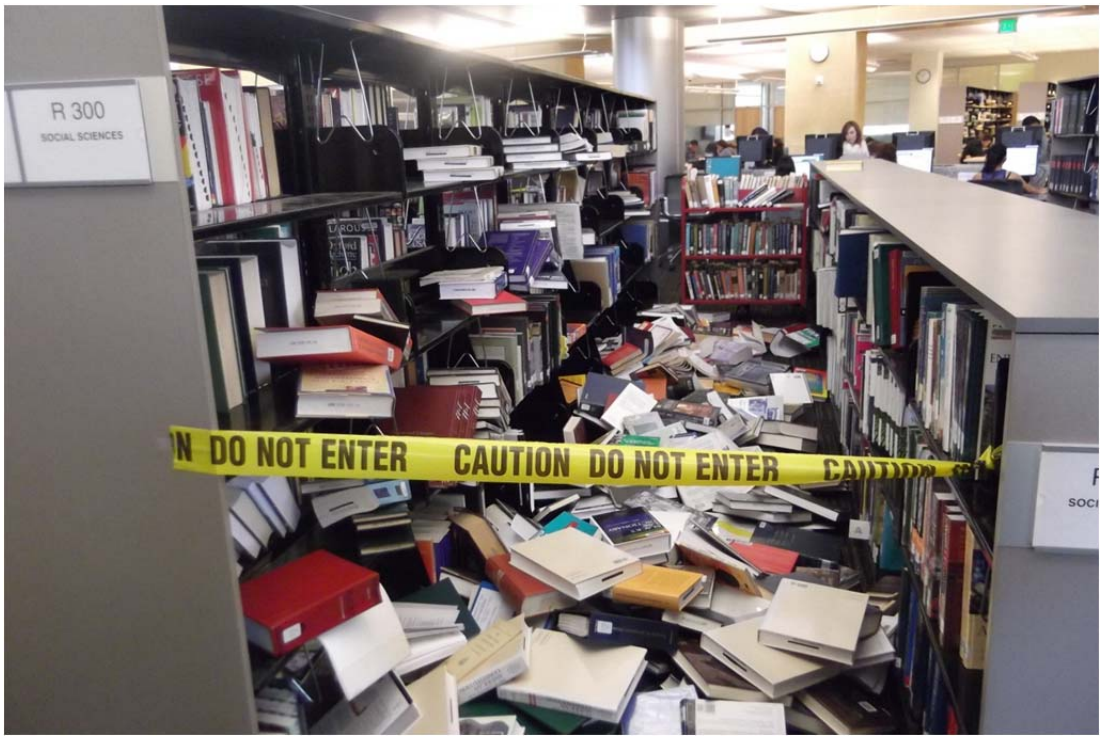

Figure 31

Figure 32

Figure 33

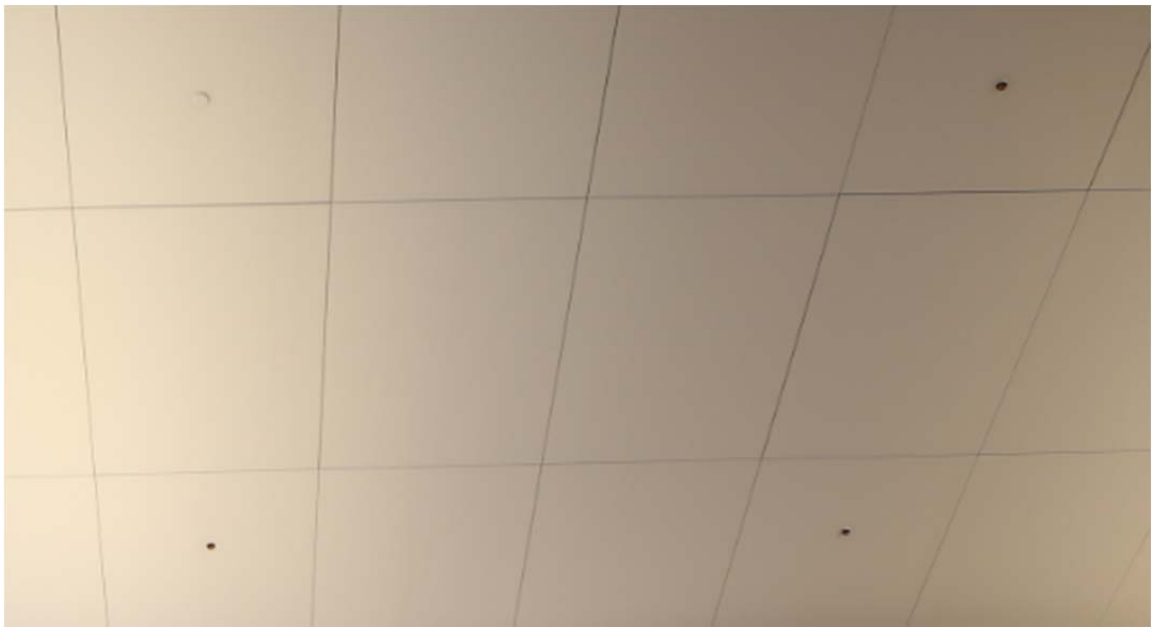

Figure 34

5.2 OBSERVATION DATE: 26 AUGUST 2014

1040 Main Street

Building Description	Steel concentrically braced Frame retrofit (with in-plane buckling connection detail)
	Square HSS braces in "Chevron" configuration (perimeter of the building); see Figure 35
	Extremely long slot at net section region; see Figure 36
	Kept steel cage from original vintage building
	Steel cage made up of truss system of double angles; see Figure 37
Structural Damage	Out-of-plane buckling interior double angle braces running in south-east to north-west direction; see Figures 38 and 39
	Slight cracking at base plate of interior columns; see Figures 40 and 41
	Buckling of gusset plate; see Figures 42 and 43
	Separation and pulling out of square HSS retrofit from original structure; see Figures 44, 45, and 46. Anchor bolts seem to be too small at some connecting points.
	Visible drop of back balcony (see Figure 47); crack runs from interior of building to outer balcony (see Figure 48).
Nonstructural Damage; see Figure 49	Cracking in exterior façade at 1st story;
	Broken windows at 1st story
	Cracking in dry walls; see Figure 50

Figure 35

Figure 36

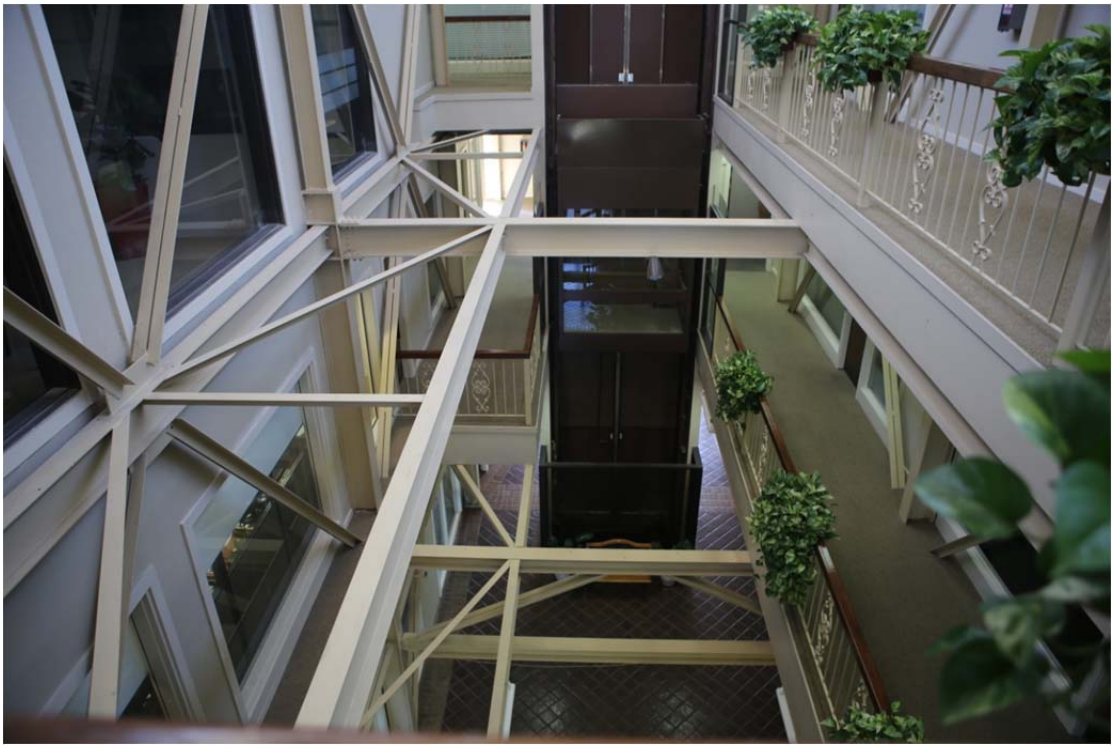

Figure 37

Figure 38

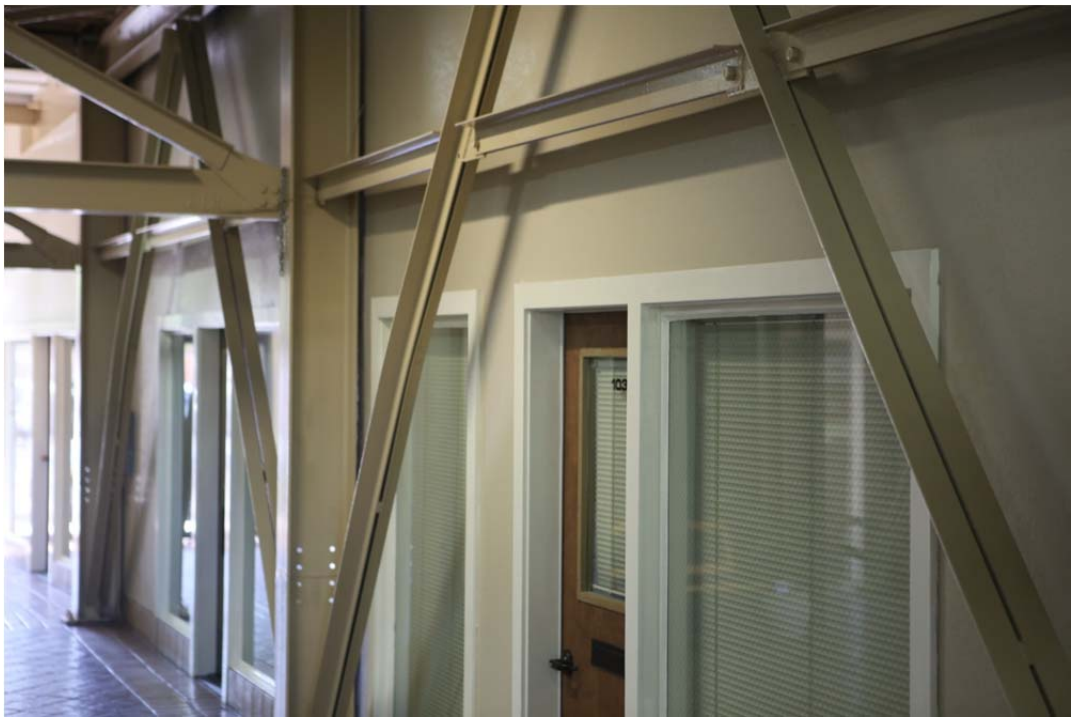

Figure 39

Figure 40

Figure 41

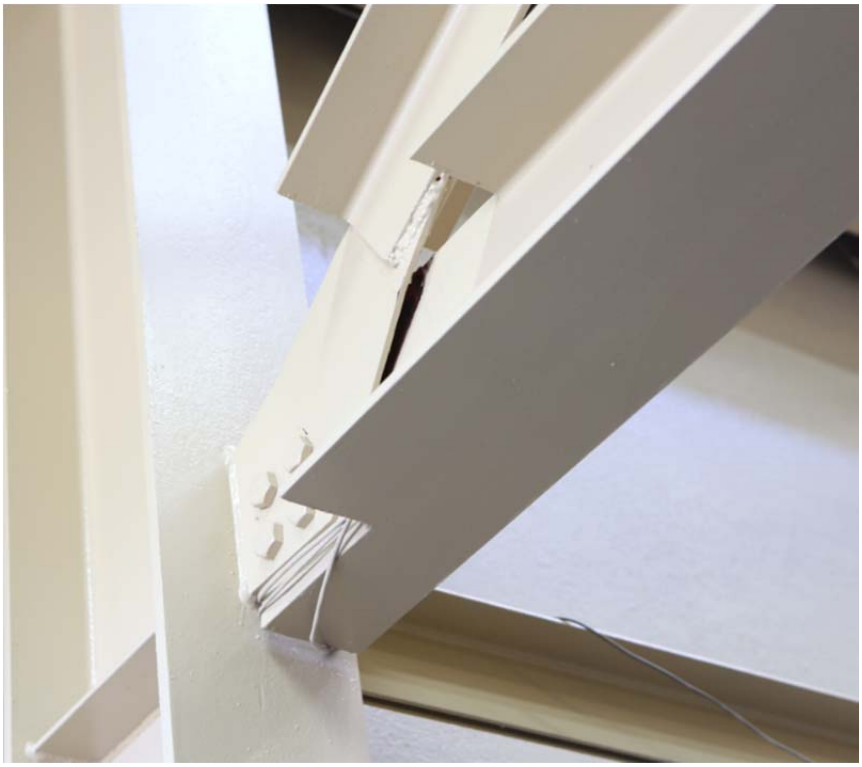

Figure 42

Figure 43

Figure 44

Figure 45

Figure 46

Figure 47

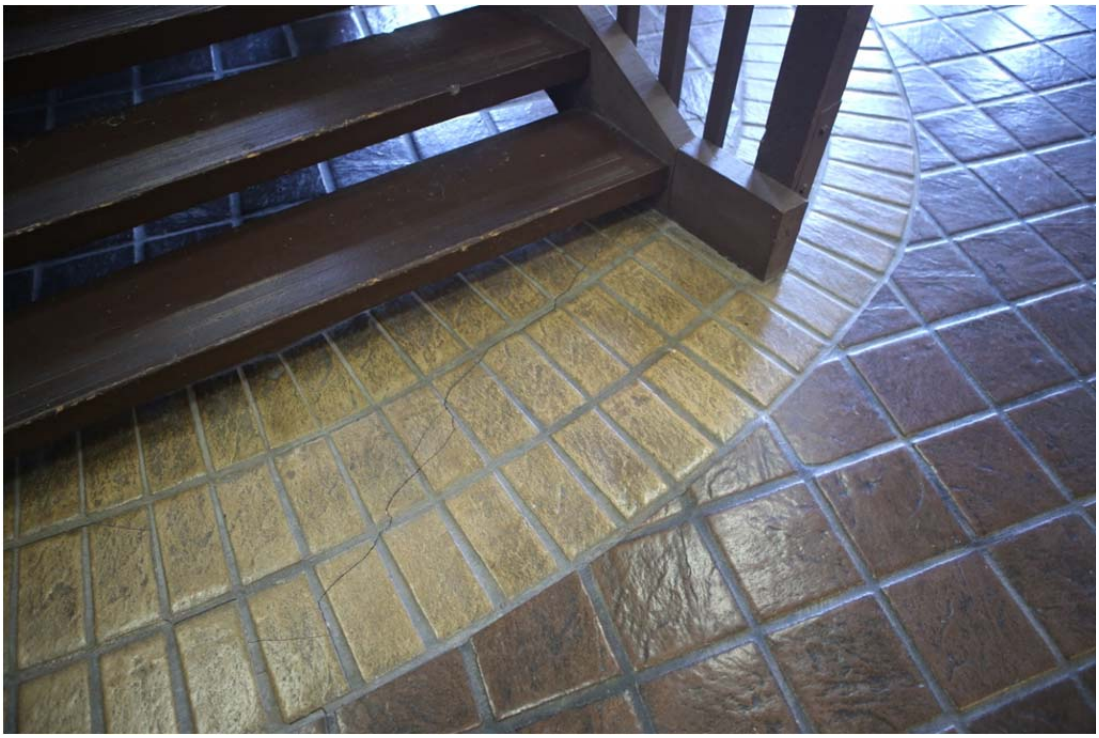

Figure 48

Figure 49

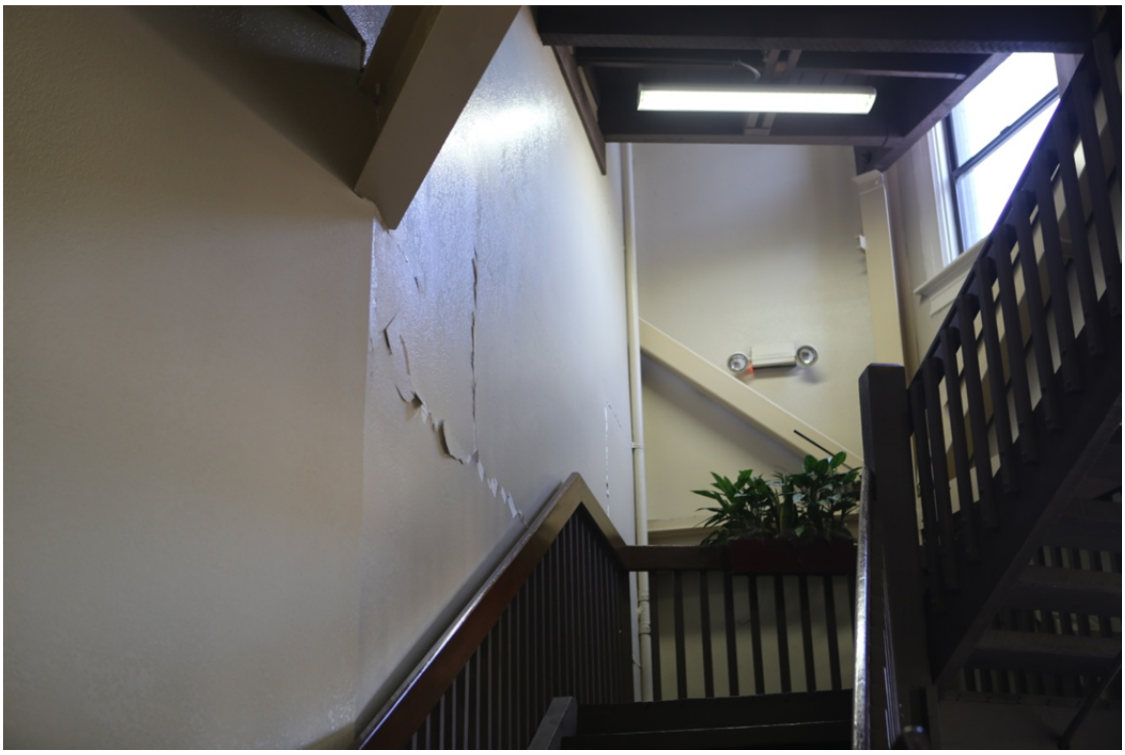

Figure 50

975 Sereno Drive, Vallejo, CA – Kaiser Vallejo Medical Center

Building Description

Buckling-Restrained Brace Frame (BRBF) Construction;

- Core Brace BRB
- BRBs with all bolted connection; see Figure 51

Structural Damage

No visible damage to BRB reinforced structure (the main building)

Buckling of tension-only braces at roof of concrete parking structure holding roof solar paneling (see Figures 52 and 53). Wood temporary supports were provided as shown in the figures.

- All tension only-braces buckling along single outside column line; no visible buckling of other braces at other column lines; see Figure 54.
- Tearing out of base at base of column and bracing; see Figures 55 and 56. Grout crushing and yield of tension rods are also shown in the pictures.

Figure 51

Figure 52

Figure 53

Figure 54

Figure 55

Figure 56

1000 Trancas Street

Building Description	New construction
	StarSeismic BRB; see Figure 57
Structural Damage	We were not able to go inside; told there was no structural damage; see Figure 58

Figure 57

Figure 58

3421 Villa Lane

Building Description	Steel concentrically braced frame system
Structural Damage	No visible structural damage.

4th street

Building Description	Residential wood construction.
Structural Damage	Soft story at 1st floor; Collapse of 1st story; see Figures 59 and 60

Figure 59

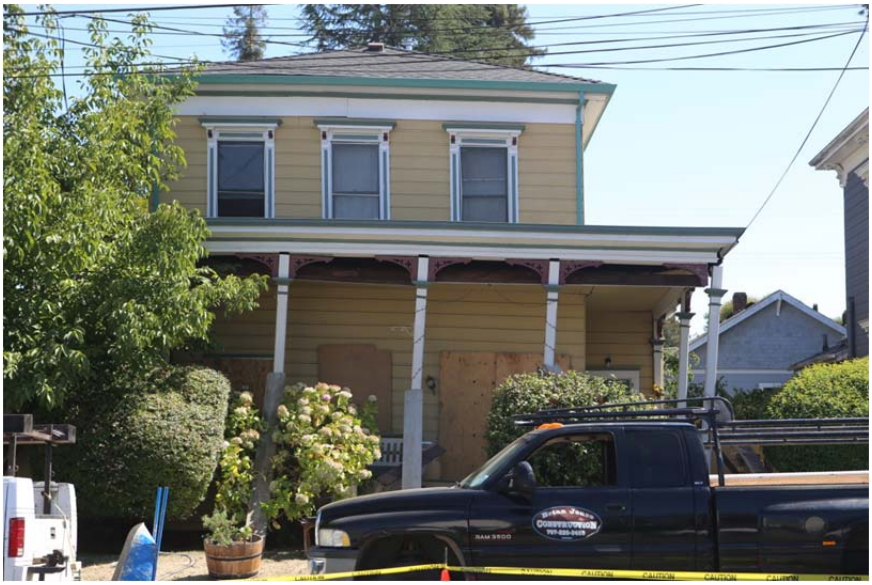

Figure 60

6 Drone-Based Aerial and Ground-Based LiDAR Image Survey conducted by University of California, San Diego[+]

Christine Wittich[1], Tara Hutchinson[1], Eric Lo[2], Dominique Meyer[2], and Falko Kuester[2]

6.1 OVERVIEW

On Sunday, August 24, 2014, the American Canyon (South Napa) Earthquake occurred at 3:20am local time with moment magnitude M_W of 6.1 at a depth of 11 km. The epicenter of the earthquake was located in American Canyon, California, in Napa County, 8 km SSW of Napa, and 81 km WSW of Sacramento. The fault was delineated largely in a North-South orientation. The effected region has a large array of seismic recording stations with a station in downtown Napa observing a peak horizontal ground acceleration of 0.61g at an epicentral distance of 9.1 km. The regional map of peak ground acceleration and peak ground velocity are included in Figure 1.

Two teams from UC San Diego surveyed the area following the earthquake (led by Professors Hutchinson, Kuester, and research students Wittich, Meyer, and Lo). On Friday, August 29 and Saturday, August 30, aerial photography and drone surveys were conducted on eleven various sites throughout Napa County. Sites from this survey are mapped in Figure 2. On Tuesday, September 2, a second team from UC San Diego surveyed the area with the intended focus of documenting the response of unattached statues and other objects. This survey included photographic documentation as well as laser scans of two overturned statues. Sites included in this survey are mapped in Figure 3. This report summarizes the observations and data collected from each site of the two surveys organized by site.

[+] Any observations, opinions, findings, and conclusions or recommendations expressed in this material are preliminary and are those of the authors, and do not necessarily reflect those of the Pacific Earthquake Engineering Research Center. The information, data and images contained in this report may not be published or presented without permission from the authors.

[1] Department of Structural Engineering, University of California, San Diego
[2] Center of Interdisciplinary Science for Art, Architecture and Archaeology (CISA3), Qualcomm Institute (QI), University of California, San Diego

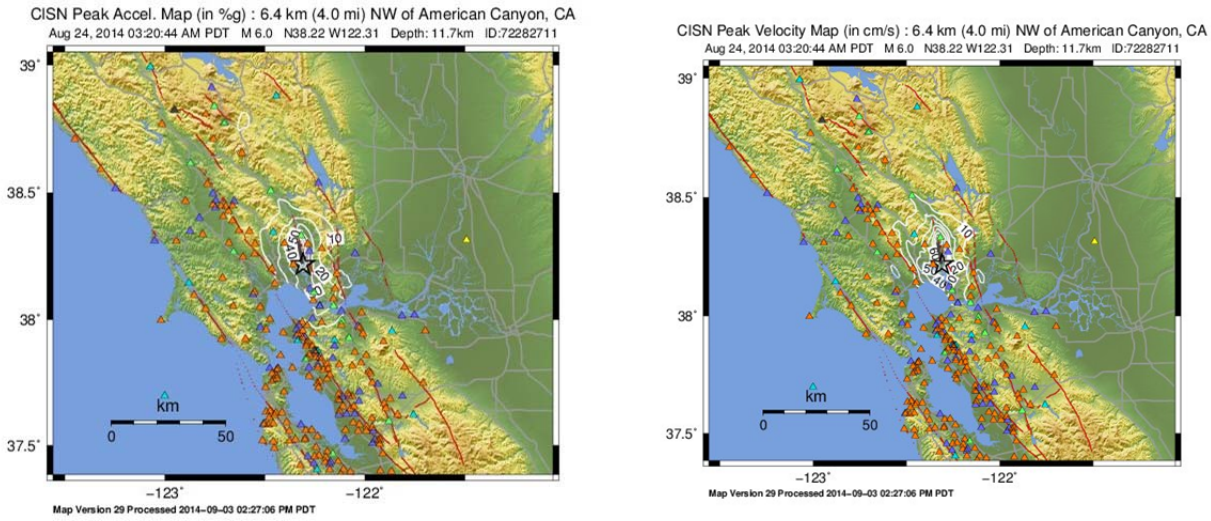

(a) (b)

Figure 1 (a) Peak ground acceleration contour map for the South Napa earthquake from CISN; and (b) Peak ground velocity contour map for the American Canyon Earthquake from CISN (*http://earthquake.usgs.gov/earthquakes/eventpage/nc72282711#shakemap_pga*).

(a)

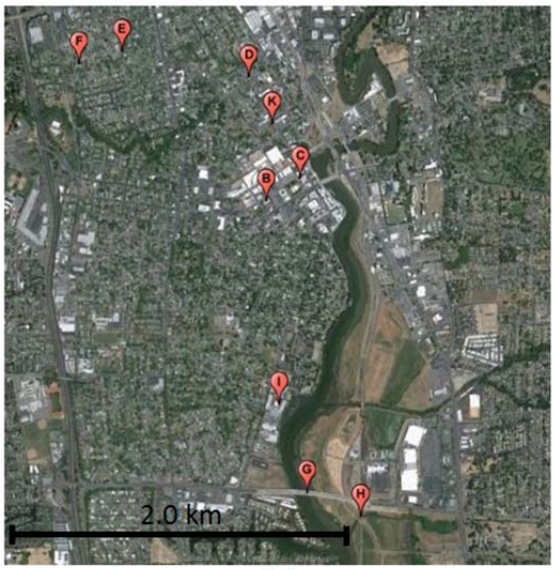

(b)

ID	Location Name
A	Trefethen Vineyards
B	United States Post Office
C	Alexandria Square
D	Mixed Use Building
E	Residential Block
F	Residential House
G	121 Bridge
H	Railroad Bridge
I	Water Tower
J	SR37
K	Vinter's Collective

Figure 2 (a) Map of sites surveyed on August 29-30 (ID: A-K) overlaid with epicenter, delineated fault from USGS as well as nearest recording stations. (b) Close-up map of surveyed sites in downtown Napa.

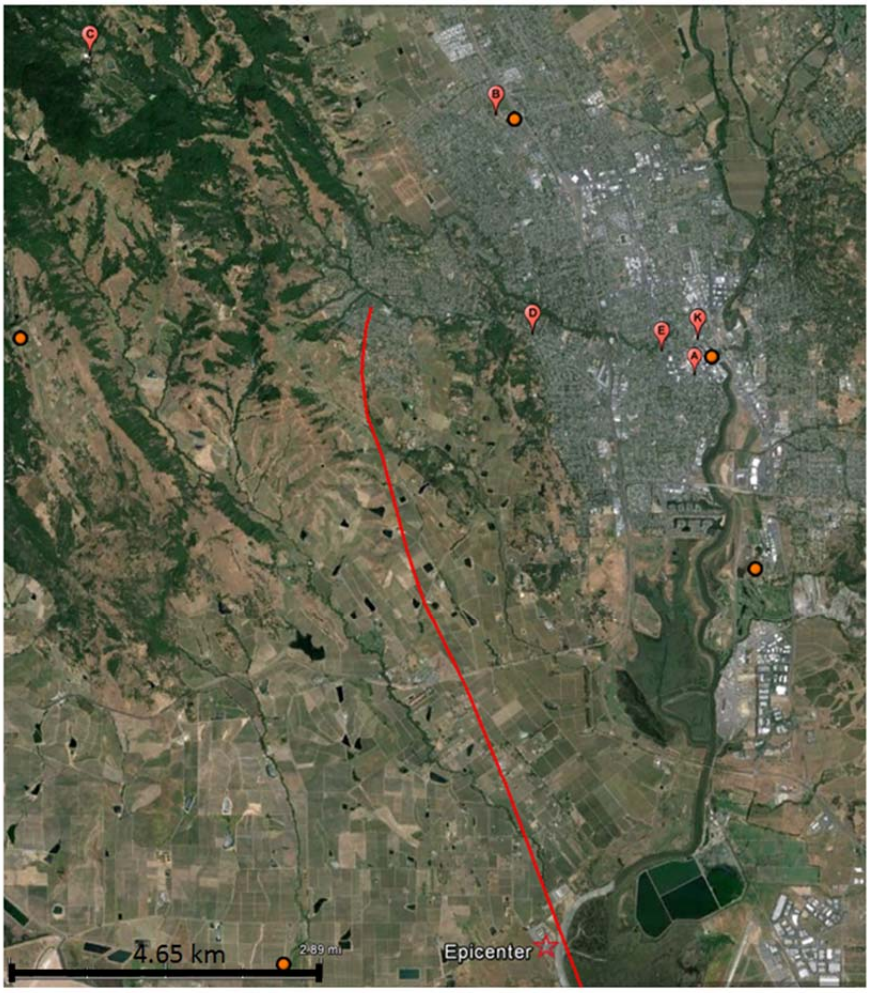

ID	Location Name
A	Ceja Vineyards
B	Justin-Siena High School
C	The Hess Collection
D	Charter Oaks Apartment Complex
E	Downtown Napa - Residential

Figure 3 Map of sites surveyed September 2, (ID: A-E) overlaid with epicenter and delineated fault from USGS as well as the recording stations closest to the surveyed sites. Zoom views of each site are included in each section.

6.2 AUGUST 29-30, 2014, DRONE AND GROUND-BASED LiDAR SURVEYS

6.2.1 TREFETHEN FAMILY VINEYARD - WINERY (N38.360348, W122.332279)

The Trefethen Family Vineyard (Figure 4) is located 8 km North of Napa and spans 0.16 km^2. Its Eschol building was constructed in 1886 and served as a tasting room for visitors of the winery. During the earthquake, the wooden structure was heavily damaged and weakened to an unknown extent. Access to the structure has been limited and interior surveys delayed due to the risk of collapse. Based on visual inspection from the outside, it appears that multiple, 5000-gallon tanks, partially filled with water have partially toppled, pushing against the west-side of the building, further threatening its structural integrity. Contractors are currently working towards securing the building, by bracing its west-facing side, after observing steady daily drift of about 2.5 cm of a marker placed at the roofline, following the days after the earthquake.

Imaging Approach: The aim for this site was to obtain a high-resolution 3D model of the damaged structure, as well as the surrounding surface topology, including signs of possible ground failure. Multiple drone missions were flown with two specific objectives: (1) to acquire a high-quality image record for the heavily damaged Eschol building; and (2) to capture a detailed record of the surrounding terrain. Manual, semi-automated and fully-automated mapping missions were explored in the process, to study the impact of different flight patterns, altitude ranges, and image-acquisition rates as a function of time, complexity, and image quality. Another critical parameter being studied is the quality of the 3D models that can be extracted from the collected image data in the context of overall achievable quality/accuracy as a function of the image input set selection and allocated computational time budget. Collected image data as well as a preliminary 3D model are shown in Figure 5.

Two manual and semi-automated flights, spanning an altitude band between 3–120 m were executed to image all sides as well as the roof of the Eschol building. For this the drone demonstrated its unique ability to access areas otherwise difficult, impossible or simply too dangerous to explore. The drone was able to bypass vegetation, storage tanks, machinery, and construction equipment that otherwise would have limited the field of view, while also operating in areas deemed too dangerous to access, due to a possible collapse of the structure. A central imaging objective was to capture the overall geometry of the damaged building, and assess damage to its façade. To capture the required image data the drone's camera was oriented horizontally to providing the highest possible detail.

To augment the building data with the terrain surrounding it, two fully automated mapping missions were flown, with the camera pointing downward at an angle of 60° from the horizontal. The two flights were comprised of flight patterns perpendicular to each other to optimize vertical stitching. Over 400 aerial images were collected and subsequently used to compute the model shown in Figure 5d.

To further complement aerial data, an additional image set was acquired with a Canon 5D and 7D from the ground, for multiple viewing angles around the building (where accessible). This data was acquired to explore how terrestrial and airborne imaging campaigns may be combined to enhance the overall quality (resolution, accuracy, and detail) of the reconstructed building

model. In addition a LiDAR scanner was used to capture three scans, intended for both ground-truthing of the computed 3D model, as well as enhancing it by combining the two data records.

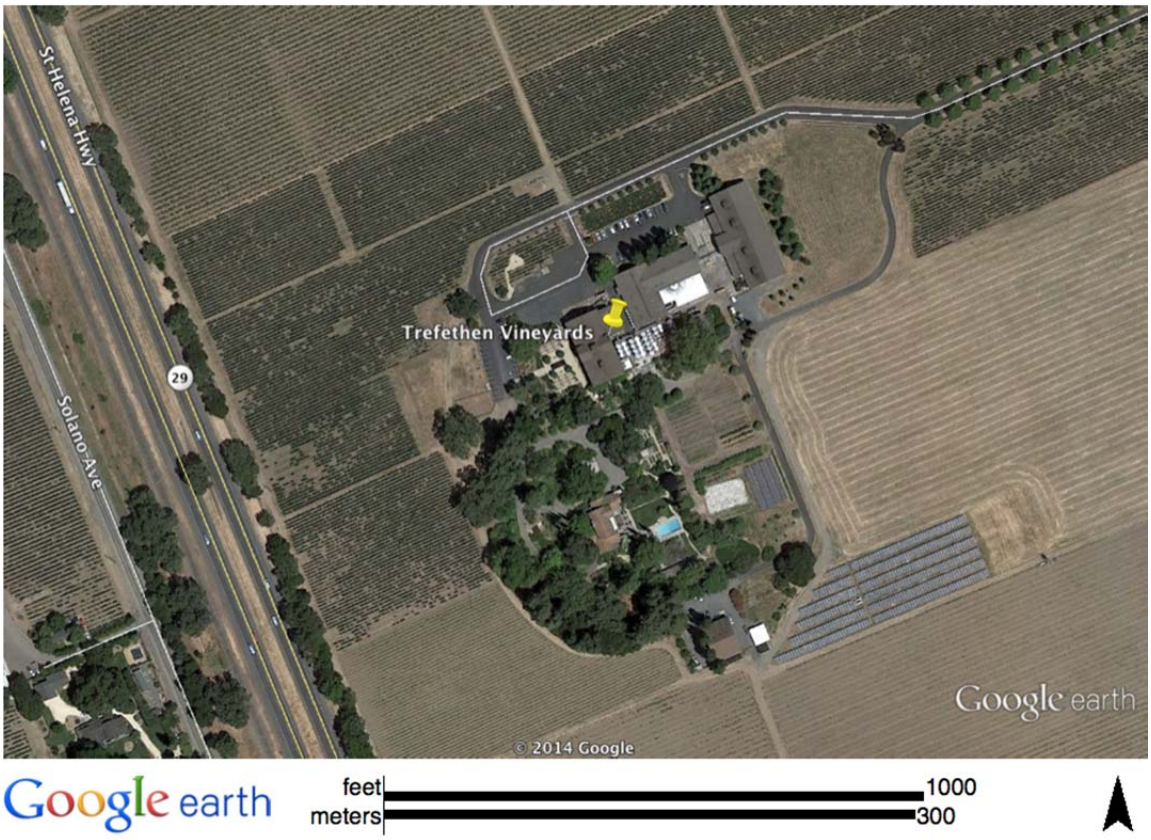

Figure 4 Satellite view of the Trefethen Family Vineyard. The damaged building is marked with the pin.

(a) (b)

(c) (d)

Figure 5 (a) Ground view of damaged structure supported by bulldozers; (b) aerial view of damaged structure; (c) aerial view of damaged structure; and (d) reconstructed model capturing building displacement and façade damage.

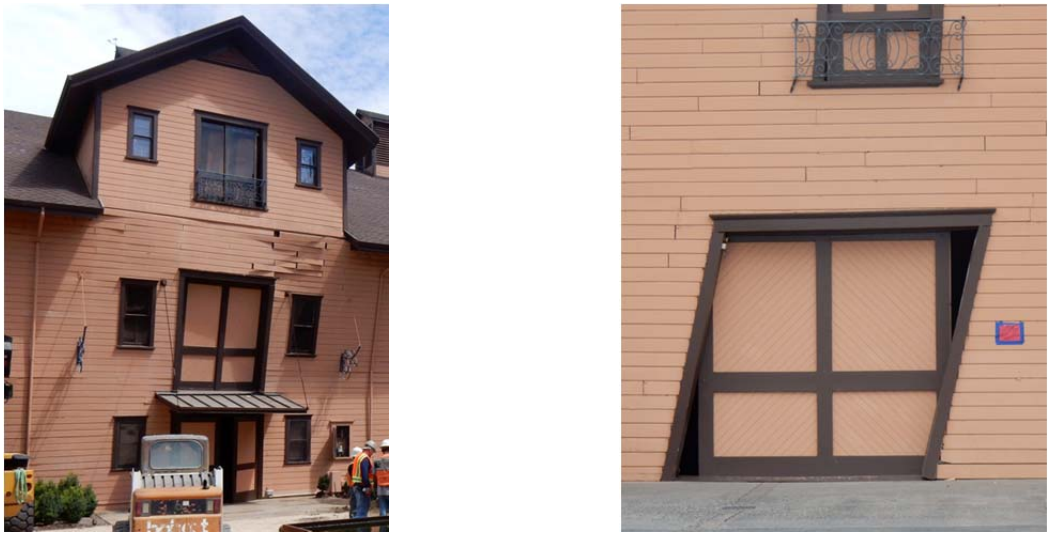

(a) (b)

Figure 6 (a) Damage to west façade and (b) close-up of main entrance on north side.

6.2.2 POST OFFICE (N38.296987, W122.287584)

The U.S. Post Office, located on 2nd St. in the center of Napa, also known as the Franklin post office, dates back to 1933. A satellite view of the site is shown in Figure 7. The building's façade was the primary imaging target, with the objective of determining how well cracks in the masonry as well as the massive damage to its large glass panes can be established through remote imaging. Image capture focused on ground level data for all accessible sides of the structure using a Canon 5D that was used for subsequent SfM reconstruction (Figure 8).

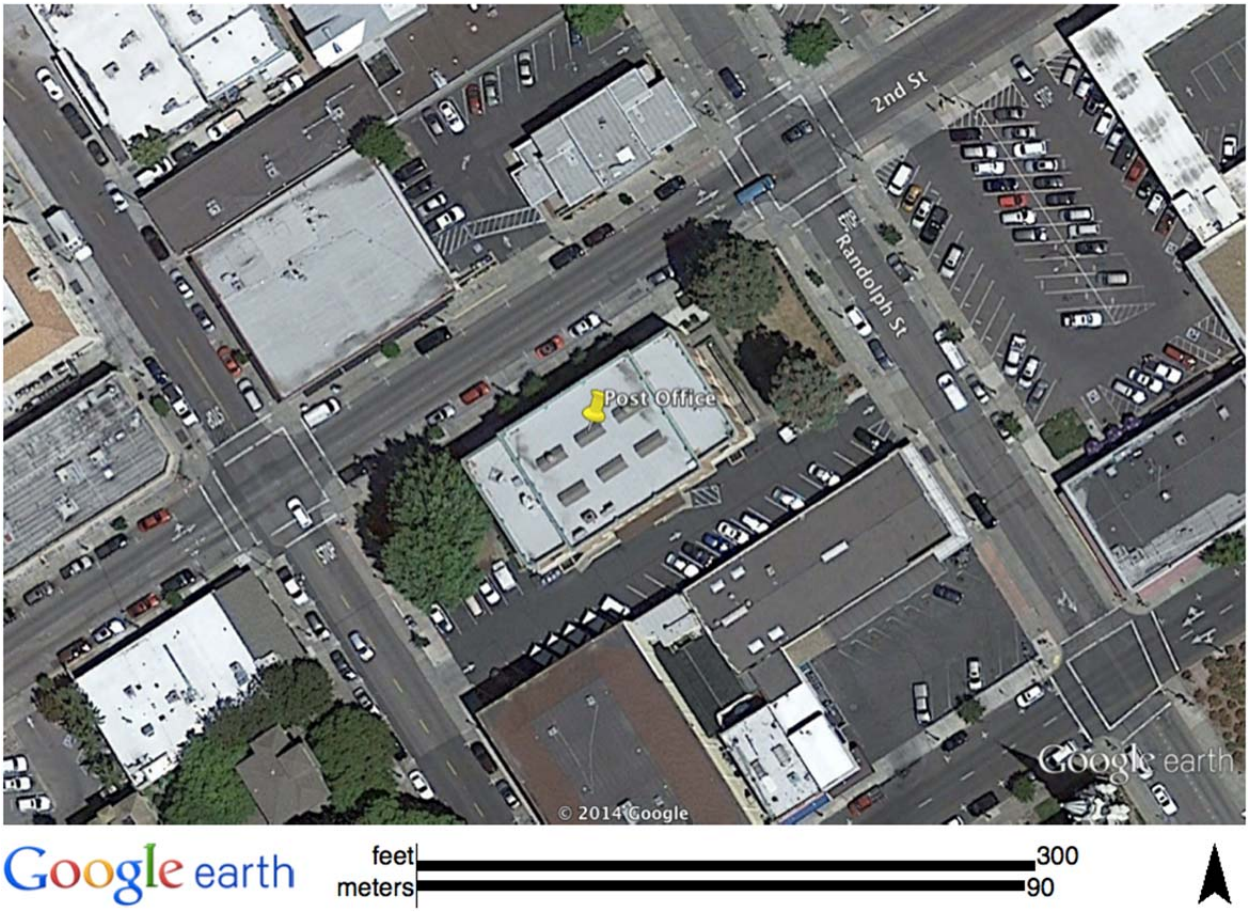

Figure 7 Satellite view of post office.

(a) (b)

Figure 8 (a) Ground view of post office; and (b) reconstructed model capturing façade and window damage.

6.2.3 ALEXANDRIA SQUARE AT 2ND AND BROWN (N38.298206, W122.285309)

This office building at the corner of 2nd and Brown Streets, suffered from localized wall and roof collapses, as well as significant cracks in its façade, among others. The western corner of the building experienced a top floor collapse, resulting in debris on the ground and an unsupported roof section (Figure 9-10).

Imaging approach: Significant damage to the building was observed on the upper floor and at the roof level, at the corner of 2nd and Brown. Extensive fences and cleanup support infrastructure put in place to secure the site, greatly limited access and visibility. The drone in this case provided access as well as data acquisition opportunities from perspectives otherwise inaccessible from the ground. Due to the low altitude required for this image acquisition run, manual and semi-automated flight modes were explored to take a series of images focusing on the corner of the building. LiDAR data was again acquired for ground-truthing purposes. Do to access constraints on proximity of nearby buildings ground-based image collection was limited.

Figure 9 Satellite view of Alexandria Square. The building with the most damage is marked with the pin.

(a)

(b)

(c)

(d)

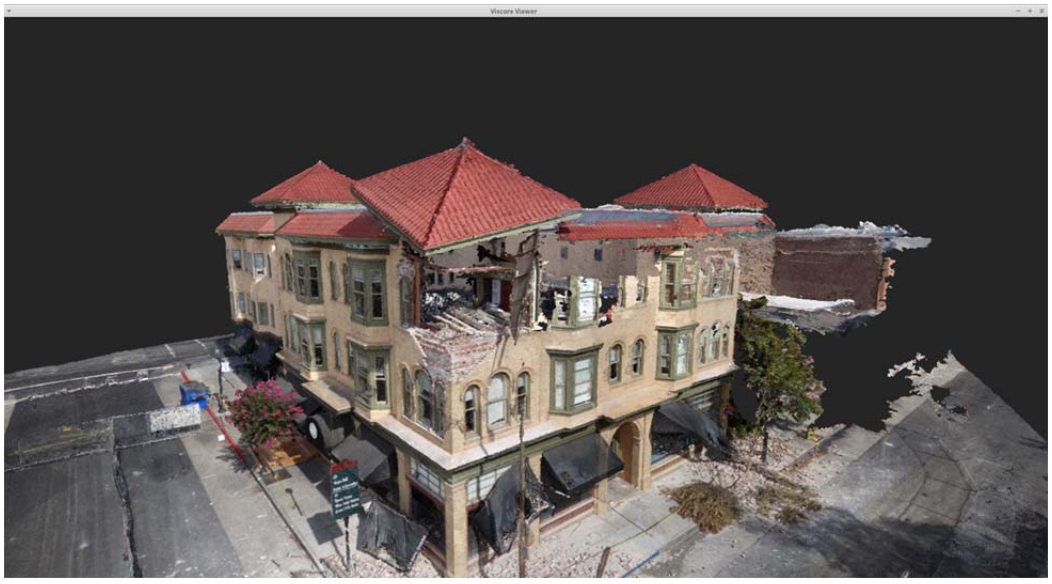

(e)

Figure 10 (a) Ground view; (b) close up aerial view; (c) top down aerial view; (d) reconstructed model of building; and (e) reconstructed model of damaged building corner.

6.2.4 VINTNER'S COLLECTIVE (N38.301113, W122.287289)

Vintner's Collective, a small two-story building located at the corner of Main and Clinton Streets, served as wine tasting and selling facility. The building was constructed in 1875 and was built using stone/cement blocks. During the earthquake, large portions of the façade collapsed onto the sidewalk facing Main Street (Figures 11 and 12).

Imaging Approach: Image capture focused on ground level data, using a full circular sweep around the building, using a Canon 5D, followed by SfM reconstruction.

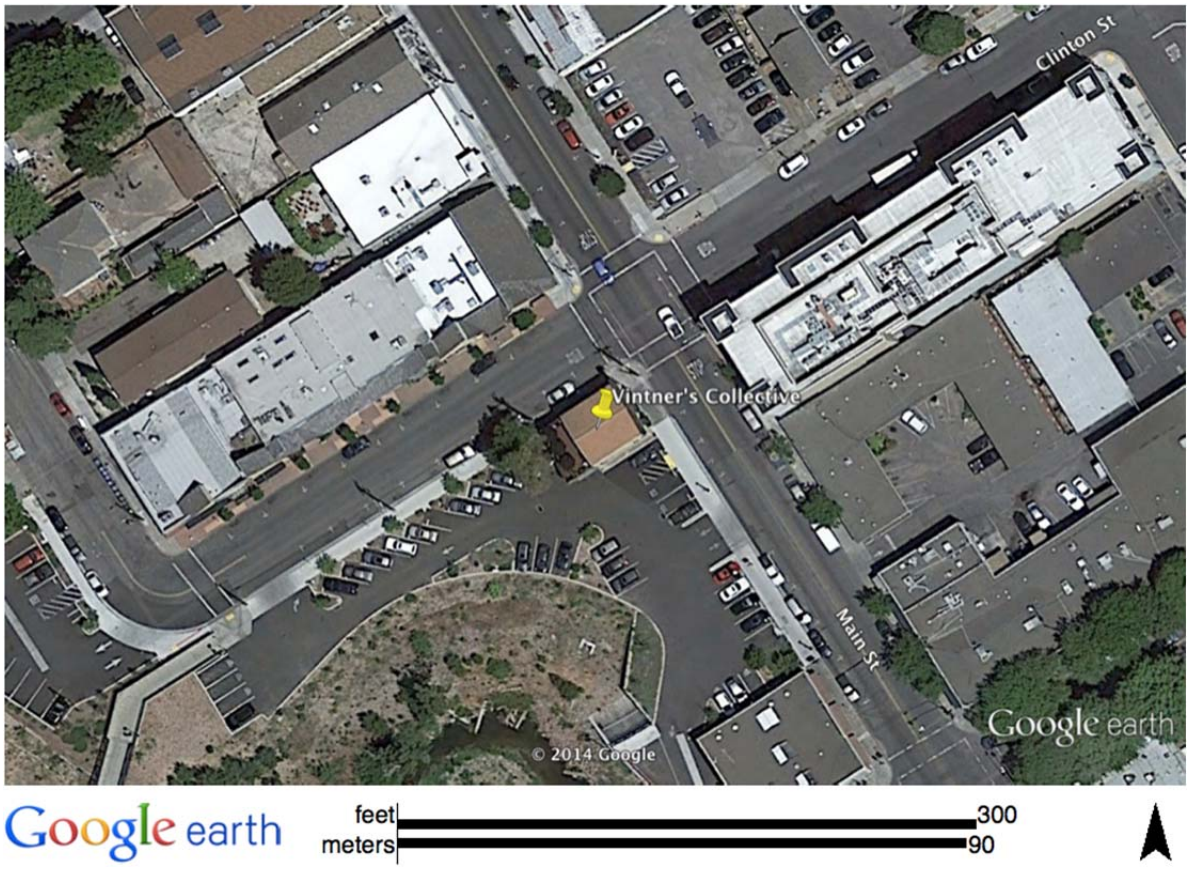

Figure 11 Satellite view of Vintner's Collective.

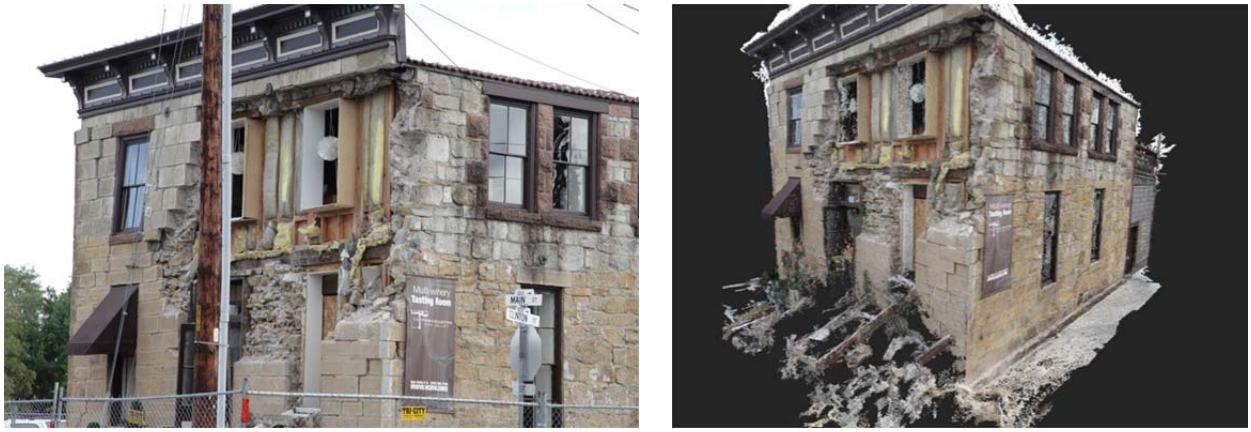

(a) (b)

Figure 12 (a) Ground view and (b) reconstructed model showing façade damage and debris field.

6.3 MIXED-USE BUILDING: RETAILS, APARTMENTS (N38.303587, W122.288886)

This test-case is a mixed-use building located on Main St, with extensive damage to its façade. The building itself was already in the process of being repaired, exposing the different building materials and reinforcement strategies that had been used over the years (Figures 13 and 14).

Imaging approach: Imaging focuses on the building itself, using a circular flight path at multiple altitude bands with the camera aimed at the building center. The pilot walked around the building, accompanying the copter as the pictures were taken and maintaining line of sight at all time. Additional images were taken with the Canon 5D and 7D, with particular focus on the heavily damaged and previously reinforced façade facing Vallejo Street.

Figure 13 Satellite view of the mixed-use building.

(a)

(b)

(c)

(d)

(d)

Figure 14 (a-b) Ground-level view; (c) detail view of damage masonry façade; (d) aerial view; and (e) reconstructed model.

6.3.1 RESIDENTIAL BLOCK (N38.305757, W122.297779)

This survey explored airborne acquisition of entire residential blocks in a neighborhood where multiple buildings suffered foundation failures, cracks appeared along roads, sidewalks and driveways and water mains ruptured. Most of the dwellings were single story, wood frame structures with elevated foundation (Figures 15 and 16).

Imaging approach: The objective was to create, a high-resolution, orthorectified image mosaic of the residential city block, to explore the rapid creation of baseline records and damage detection strategies. An orthogonal survey pattern was flown with the camera oriented 60° downward from the horizontal axis.

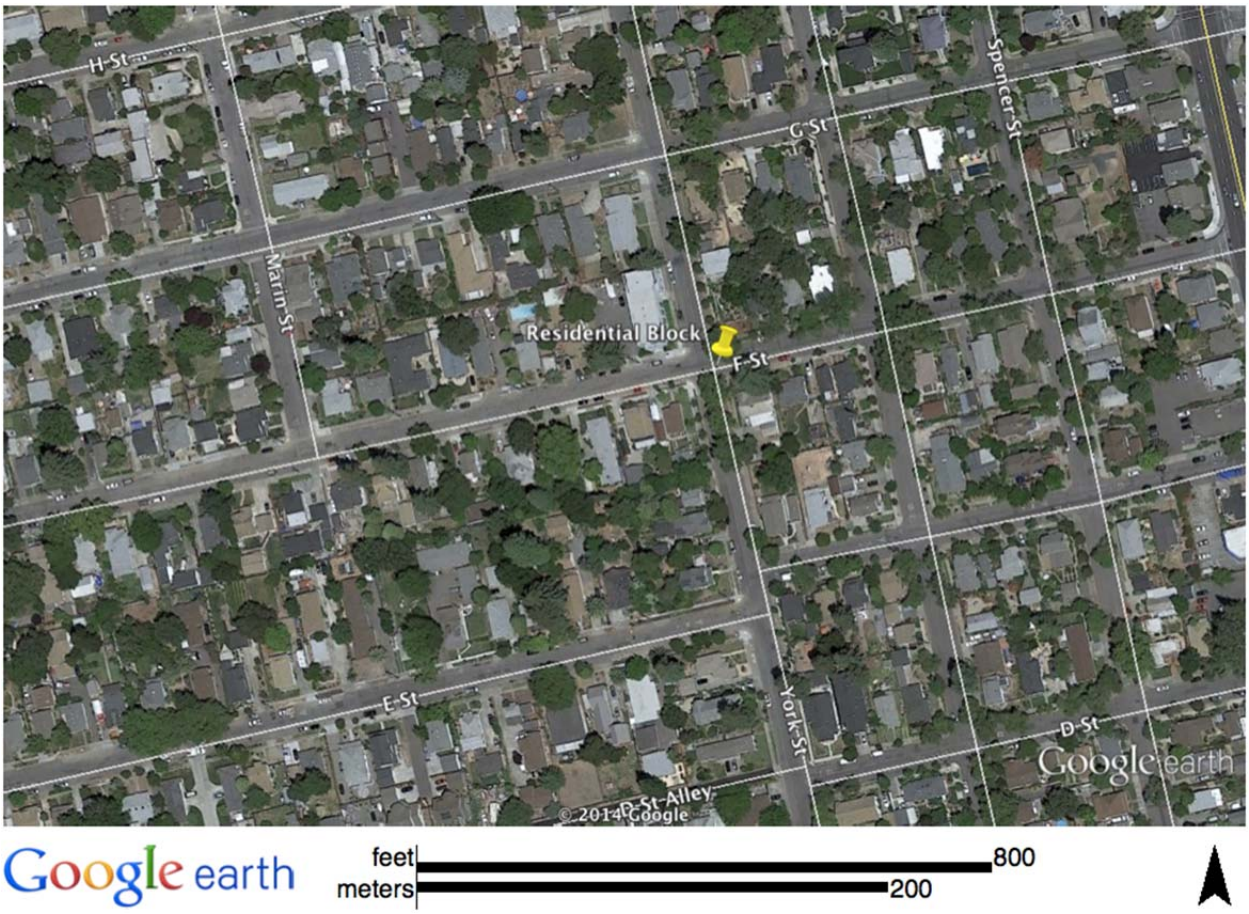

Figure 15 Satellite view of surveyed block.

Figure 16 Reconstructed model of surveyed residential city block, capturing structural and non-structural damage to buildings and roadways.

6.3.2 RESIDENTIAL HOUSE (N38.304305, W122.300419)

A single story, wood-frame dwelling with complete elevated foundation failure was surveyed, to explore rapid assessment of red-tagged buildings inaccessible through traditional means. This dwelling slid off of its foundation and approximately 1.2 m onto the adjacent property (Figures 17 and 18).

Imaging Approach: Manual and semi-automated survey techniques were tested, using different altitude bands and a circular flight path around the dwelling. Additional, road-side images were taken with a Canon 5D to compliment the aerial imagery.

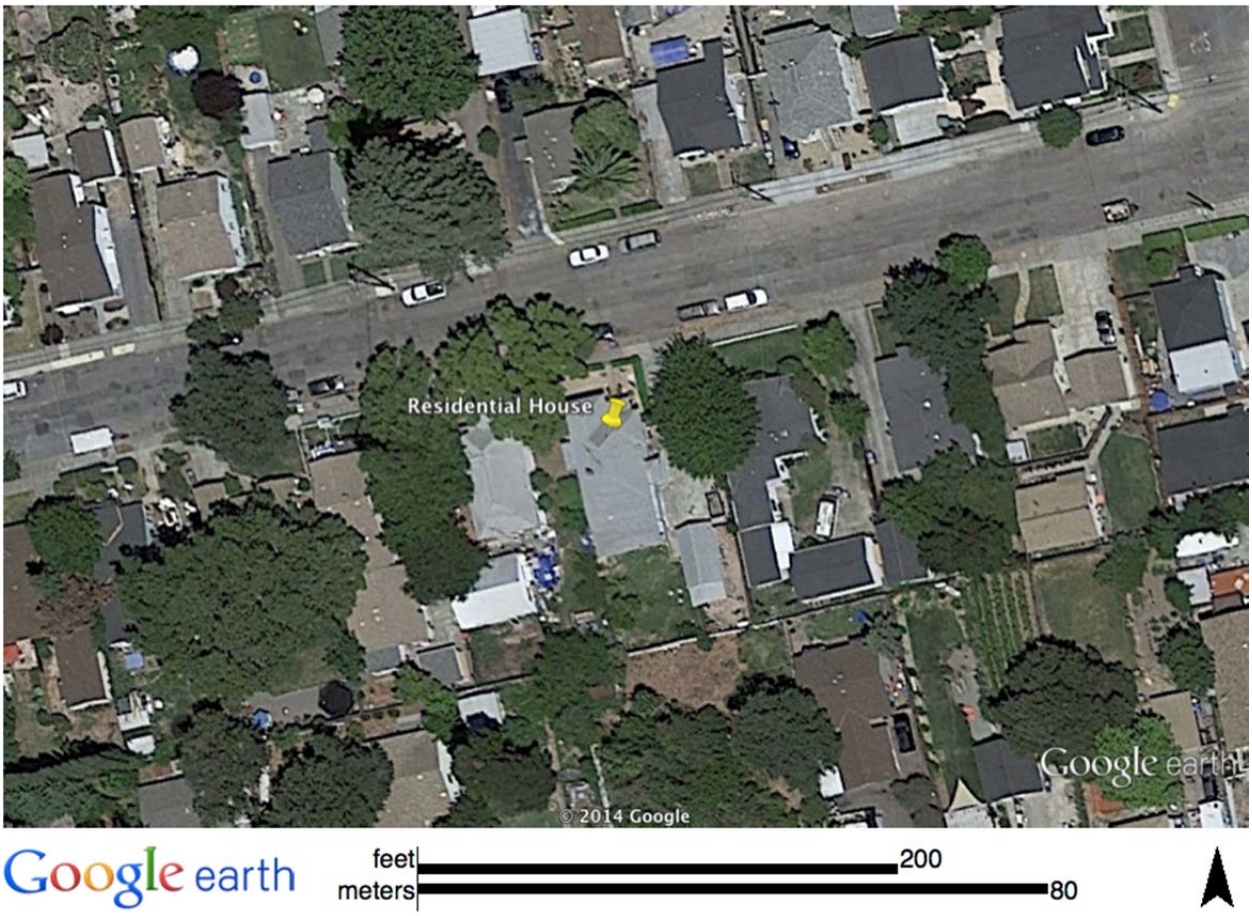

Figure 17 Satellite view of red-tagged house.

(a)

(b)

(c)

(d)

(e)

Figure 18 (a) Ground view; (b) aerial view of the back; (c) aerial view of the front; (d) reconstructed model of the front; and (e) reconstructed model of the back.

6.3.3 WEST IMOLA AVENUE (121) BRIDGE (N38.281577, W122.284612)

The 121 Bridge is located at the south-east corner of Napa town center, crossing a small river, and was used to explore post-earthquake bridge survey strategies. Points of interest included the superstructure, expansion joints and bridge columns (Figures 19 and 21).

Imaging Approach: A semi-automated and fully automated survey strategy was tested, using a GPS and altitude guided mode, allowing the drone to fly parallel to the bridge, maintaining constant altitude and distance while capturing imagery at regular intervals. Two flights were completed; one from the north and one from the south, each consisting of one flight, with each pass conducted at two different altitudes. To explore rapid health assessment strategies for bridge columns multiple close-up imaging runs were conducted using flight paths with horizontal and vertical sweeps respectively.

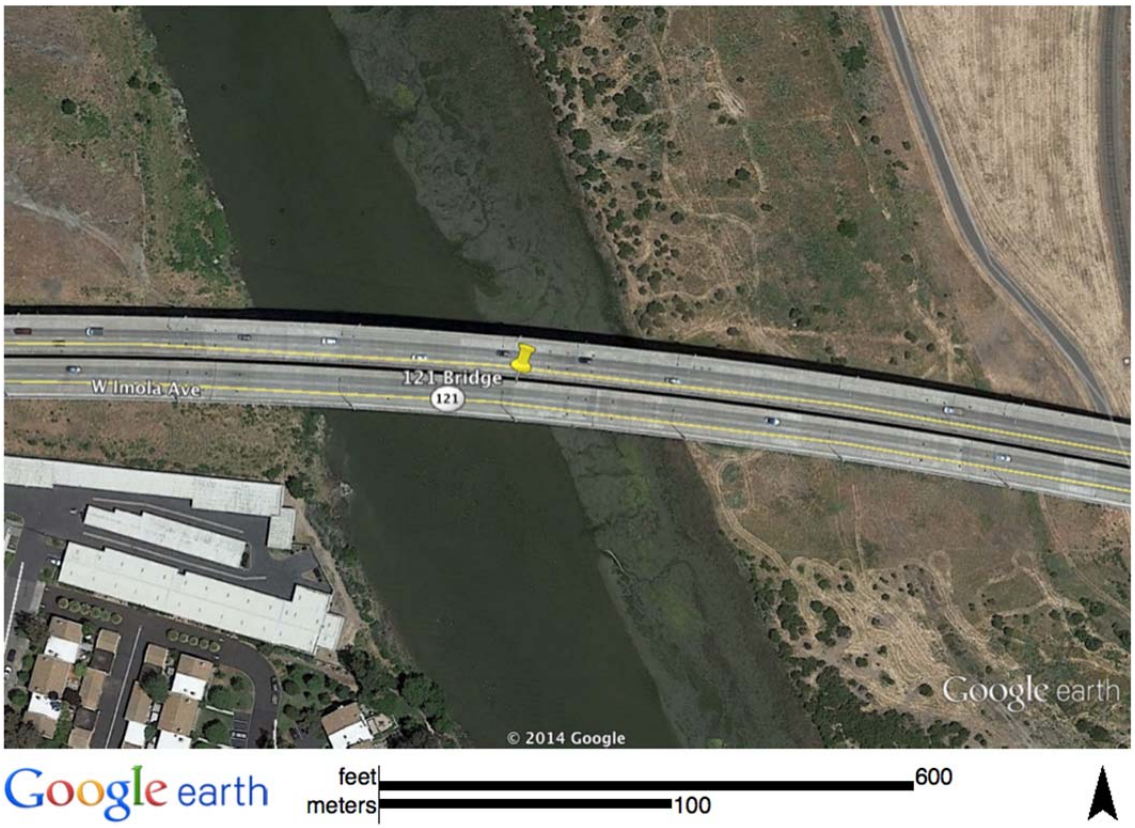

Figure 19 Satellite view of the 121 Bridge.

(a)

(b)

(c)

(d)

(e)

Figure 20 (a) Ground view; (b) aerial view from low altitude; (c) aerial view from high altitude; (d) complete reconstructed model of bridge; and (e) close up of reconstructed model.

(a)

(b)

(c)

(d)

Figure 21 (a) Ground view; (b) reconstructed model; (c) aerial view; and (d) aerial close up.

6.3.4 RAILROAD BRIDGE (N38.280319, W122.280973)

Drone Launch Point: San Francisco Bay Trail, Napa, CA, 38.280110, -122.281042

A railroad bridge crossing a small river (adjacent to the 121 bridge) was selected as a case study for structures and structural members with limited access. Terrain and vegetation as well as the river and adjacent structures limited conventional access from beneath the bridge (Figures 22 and 23).

Imaging Approach: For this survey, the drone was operated manually to explore different altitude bands, from 0.3 m above the river (i.e., below the bridge for detail views of its piers) to 60 m above the bridge providing a birds-eye view of the target environment.

Figure 22 Satellite view of railroad bridge.

(a) (b)

(c) (d)

Figure 23 (a) Ground view; (b) aerial close up view; (c) aerial view of bridge; and (d) reconstructed model.

6.3.5 WATER & CELL TOWER (N38.286242, W122.286568)

This site was selected to explore drone-based imaging for the assessment of water and communications towers (Figures 24 and 25).

Imaging Approach: To optimize flight time and sensor coverage, an automated circular flight path was selected around the water tower. The flight path was automated setting a different imaging radius for each of the two passes. The passes were conducted at different altitudes while always keeping the camera pointed at the water tank at the top of the structure. The automated flight was followed by a manually-controlled flight, to compare the effectiveness of manual data collection against that of automated data collection.

Figure 24 Satellite view of water tower.

(a)

(b)

(c)

(d)

Figure 25 (a) Ground view; (b) aerial close up view; (c) aerial perspective view; and (d) reconstructed model of water tower.

6.3.6 NAPA RIVER BRIDGE (SR-37) (N38.121684, W122.276811)

Drone Launch Point: River Park, Vallejo, CA 94590, 38.121691, -122.276010

The multi-lane Napa River Bridge (SR-37) was imaged to explore drone utility for the rapid assessment of lifelines with limited access. In this particular case the bridge spanned open water, creating unique challenges for swift, post disaster health assessment (Figures 26-27).

Imaging Approach: This bridge poses unique challenges to multi-rotor drone acquisition with a span greater than 975 m pushing the available flight-time to the limit. For this proof-of-concept, approximately half of the bridge was imaged using automated-flight mode, with particular focus on the expansion joints and the piers.

Figure 26 Satellite view of SR-37.

(a)

(b)

(c)

(d)

Figure 27 (a) Ground view; (b) aerial perspective view; (c) aerial close up view; and (d) reconstructed model.

6.4 DRONE MAPPING PLATFORM

Different multi-rotor drone types have emerged as flexible deployment platforms for a broad range of sensor payloads. A hexa-copter designed by UCSD researchers (Kuester et al.) was equipped with a 20MP Sony QX100 camera mounted on a brushless gimbal for camera stabilization and used for data capture (Figure 28). This custom-build hexa-copter adopts an open-hardware and open-source approach. A central component is an open-source autopilot system, which uses onboard sensors to determine drone position and orientation, supporting mixed-mode operation that can be seamlessly switched from manual, user-guided to automated fight.

Figure 28 Hexacopter imaging setup (Kuester et al., UCSD).

6.5 DATA PROCESSING

Once an image set with proper coverage of the target site has been acquired, it is passed to the structure-from-motion (SfM) reconstruction pipeline. Following identification of corresponding features between image pairs, a 3D point cloud is extracted that forms the basis of a flexible and realistic 3D model. This model can then be intuitively visualized, explored and analyzed. Due to the computational complexity of the reconstruction process, mobile devices were used to upload the images from the drone to a remote server for accelerated model computation.

6.6 DATA VISUALIZATION

A custom point-based visualization and analysis framework was used to visualization data directly on-site while UCSD's Wide Angle Virtual Environment (WAVE) is currently being used for intuitive, interactive and fully immersive data exploration. The WAVE allows researchers to literally step into the acquired 3D models, explore them from arbitrary vantage points, and extract geometric information (Figure 29).

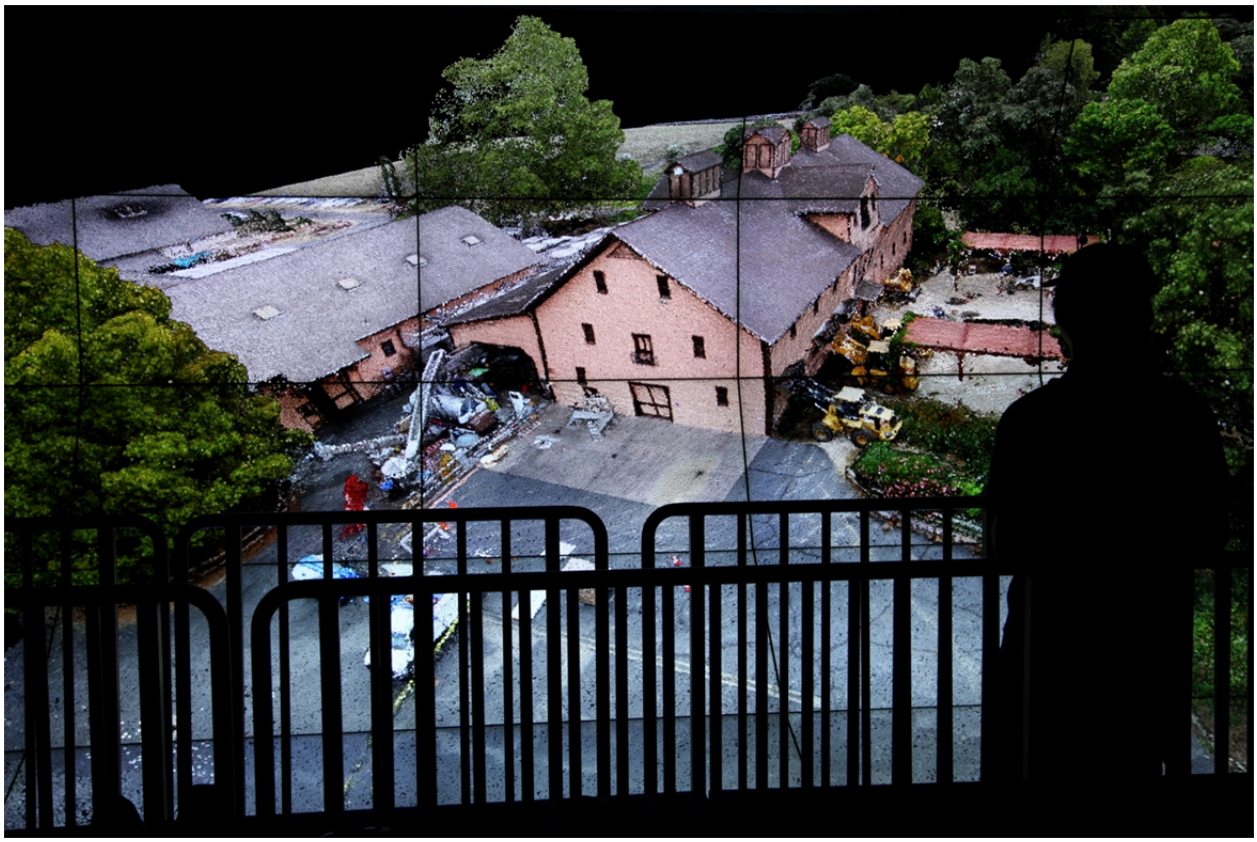

Figure 29 Viewing the Trefethen model on the Wide Angle Virtual Environment (WAVE).

6.7 SEPTEMBER 2, 2014, GROUND-BASED VISUAL & LIDAR SURVEYS

6.7.1 CEJA VINEYARDS (N38.298344, W122.287810)

Ceja Vineyards is a small, commercial lounge and wine store in downtown Napa, California. The winery is located in a single-story timber-framed structure which houses four commercial establishments, two lounges and two clothing stores (see Figures 30 and 31). The timber-framed structure has a stucco façade for the end-unit that houses the winery. The structure was inspected by the city and green-tagged; however, the businesses were not open at the time of survey. While no structural damage was observed, cosmetic stucco façade damage occurred at the winery (see Figure 32a). The winery is located 0.25 km from the nearest station, USGS-NCSN Station N016, which observed a peak horizontal ground acceleration of 0.61*g*.

The winery was not open for business at the time of survey; however, site cleaning had concluded and overturning of a large statue was noted by the owner, Amelia Moran Ceja. Photographs of the overturned statue were provided by the owner and were taken the morning following the earthquake, Sunday August 24. The large fiberglass-reinforced concrete statue overturned inside the winery in the northeast direction (see Figure 32b-c). The statue was resting unrestrained on a pedestal of similar material facing northeast. The statue weighs approximately 615 kg and is 1.75 m tall; whereas, the pedestal weighs approximately 590 kg and is 0.46 m tall. Geometric and mass properties were aided in calculation by laser scanning (see Figure 33). The interface between the statue and pedestal was concrete-concrete; and, the interface between the pedestal and the tile floor was concrete-flagstone. Both interfaces can be considered high-friction.

Slight damage was observed on the statue likely due to the impact with the tile floor. Significant cracks developed in the neck and a portion of the head was broken in the immediate vicinity of the impact (see Figure 32). No other areas of damage were observed on the statue or on the adjacent walls. There was approximately 0.2 m of clearance between the at-rest statue and the wall. This clearance and lack of damage indicate that the overturning may have been the only impact event. Given the large ground accelerations and velocities in the downtown area as well as the high aspect ratio (approximately 4), overturning without impact is a plausible mode. No translation or rotation of the pedestal was observed.

Figure 30 Google earth view of Ceja Winery in downtown Napa with 'X' denoting the location of the large overturned statue.

(a) (b) (c)

Figure 31 Exterior of Ceja Vineyards.

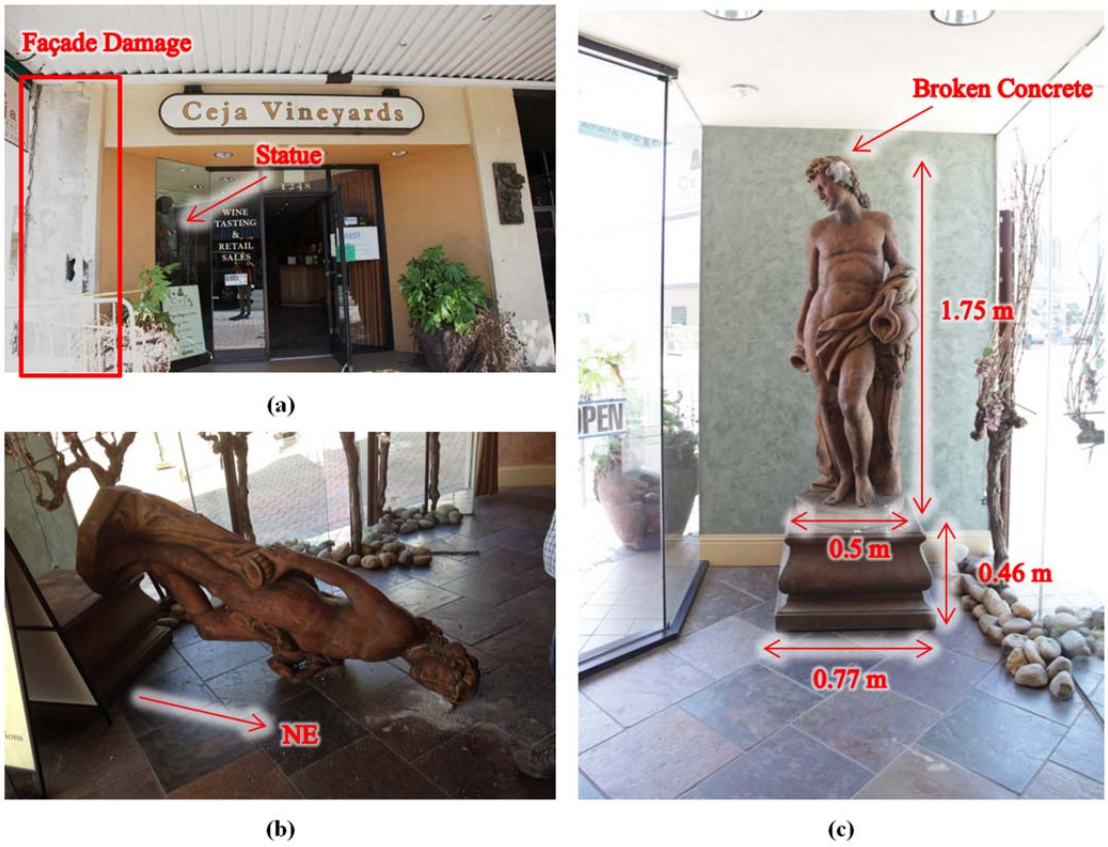

Figure 32 (a) Storefront of Ceja Winery with stucco damage noted and statue location marked; (b) overturned statue following earthquake (photo courtesy of winery owner Amelia Moran Ceja); and (c) erect statue on pedestal.

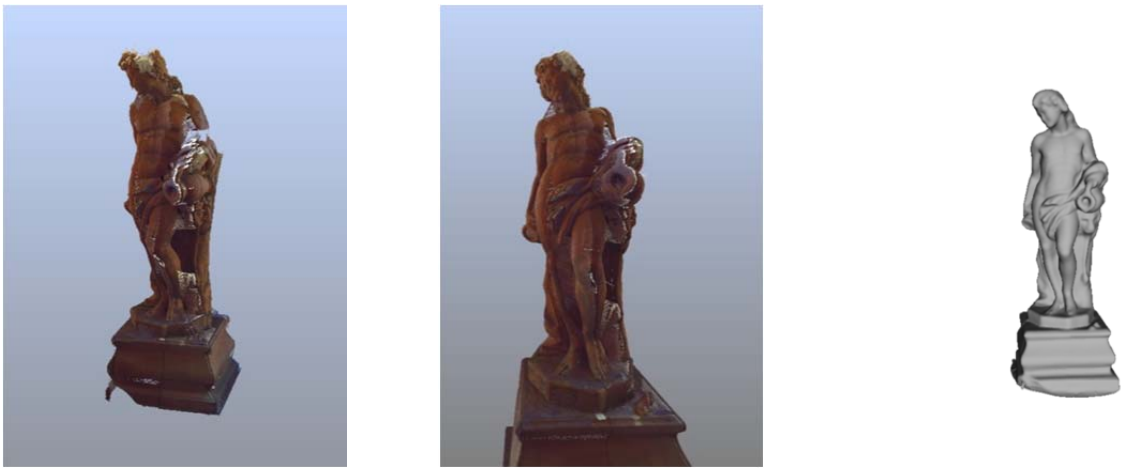

Figure 33 (a, b) Snapshots of point clouds from laser scan data of the Ceja Winery statue; and (c) snapshot of digital reconstruction of statue as a triangulated mesh for geometric and mass calculations.

6.7.2 JUSTIN-SIENA HIGH SCHOOL (N38.331248, W122.321717)

The Justin-Siena High School consists of over ten individual structures interconnected by breezeways and courtyards. The majority of the campus buildings are single-story, timber-framed structures built in 1966. An overview map of the campus layout is included in Figure 34. No structural damage was observed and the school was safe for occupancy immediately following the earthquake and was open to students at the time of the survey. Significant clean-up of building contents such as overturned bookcases, kitchen contents, and laboratory items was necessary in the days following the earthquake, according to the school president Mr. Robert Jordan. The Justin-Siena High School is located approximately 12 km north of the epicenter of the earthquake and approximately 0.2 km from the USGS recording station at the Napa Fire Station. This station observed a peak horizontal ground acceleration of 0.43*g*.

For the scope of the survey, the chapel building, interior courtyard, and campus grounds were surveyed for overturned statues and other contents. Each surveyed object is mapped in Figure 34 along with the overturning direction of the statue/content (if applicable). Each of the six surveyed statues or objects is presented in Figure 35 in which approximate dimensions are provided as well as a figure of the overturned object (if available or applicable). The building structure and/or ground conditions for each object are described in the pertinent sub-sections. Photos before the earthquake were provided by the high school. Although many of the statues/objects had been returned to original locations, photographs post-earthquake were also provided by the high school (taken: Monday August 25). All other photographs were taken on September 2.

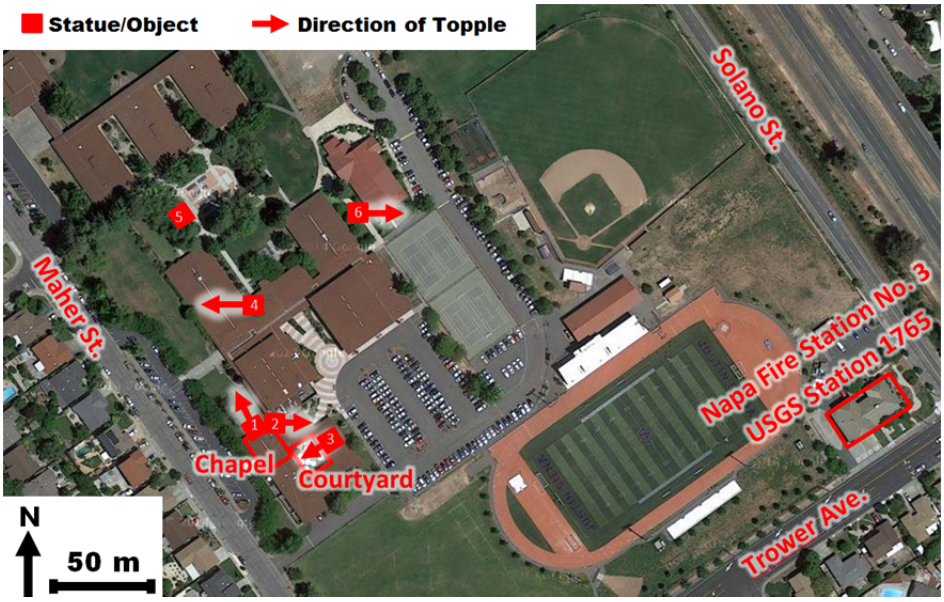

Figure 34 Map of Justin-Siena High School including locations and orientations of statues (or other tall, slender object) and the corresponding direction of topple/overturning. The nearby USGS station is included at Napa Fire Station No. 3.

Figure 35 Images of overturned (if available) and original placement of surveyed statues/objects. Approximate dimensions are provided. Some images provided by Justin-Siena High School.

Chapel

The chapel is located off the Main Office building of the high school, as denoted in Figure 34. The chapel's structure dates back to the original 1966 construction and is a single-story, timber-framed structure attached to the Main Office on its southeast end. The exterior of the building is shown in Figure 36. The religious contents, namely the marble altar and marble tabernacle, were also constructed and placed in 1966. Both objects consisted of a hollow rectangular marble frame and marble top (see Figure 35a and 35b). The top of the altar was significantly wider than that of the base creating a top-heavy structure. Similarly, the tabernacle was constructed of a heavy, metal piece atop the tall marble base. Both the altar and the tabernacle were resting unrestrained on a carpeted surface and can be considered symmetric in elevation. Following the earthquake, the altar was found overturned in the northwest direction. This overturning direction corresponds to the slender (or critical) side of the rectangular structure. The marble tabletop impacted the adjacent wall causing superficial damage to the wall and breaking the tabletop off the base (see Figure 35a). The tabernacle was found overturned in the east direction, resting against the adjacent window. The tabernacle is symmetric in both horizontal directions indicating the overturning direction was indicative of the earthquake and the object's orientation (facing south and east), rather than geometry. Only superficial scratches were incurred to the tabernacle, while the impacted window suffered minor damage (see Figure 36c).

(a) (b) (c)

Figure 36 Exterior of Justin-Siena High School: (a) chapel facing northeast; (b) main office facing northeast; and, (c) altar of chapel facing southwest. (a, b: Google Earth Street View; c: Justin Siena High School).

Courtyard

The courtyard is an outdoors area enclosed on four sides by the main office and adjacent buildings. The central portion of the courtyard consists of a small concrete pad and stone inset; while, the perimeter of the courtyard was a garden of mulch and soft soil. Two primary objects occupied this area, namely a concrete Marian statue and a large fountain (see Figure 37a). The fountain, while unrestrained in the center of the courtyard, was originally held together by the interior water pipe and consisted of multiple rigid blocks. The original and collapsed fountains are shown in Figure 37. The Marian statue consists of a likeness of Our Lady of Guadalupe with a smaller hexagonal base and is wider in the central portion of the statue (at the sun rays). The geometric details and shape of the statue are concentrated in the front (originally facing southeast) with a flat, undetailed backside. The statue was placed unrestrained on an unrestrained concrete pedestal in the garden perimeter (soil interface). While no evidence of pedestal

movement was observed, the statue overturned in the southeast direction. Furthermore, the statue was found rotated 180° about the vertical and located a distance from the pedestal. This indicates that the statue did not simply overturn, but rather responded in a complex three-dimensional mode.

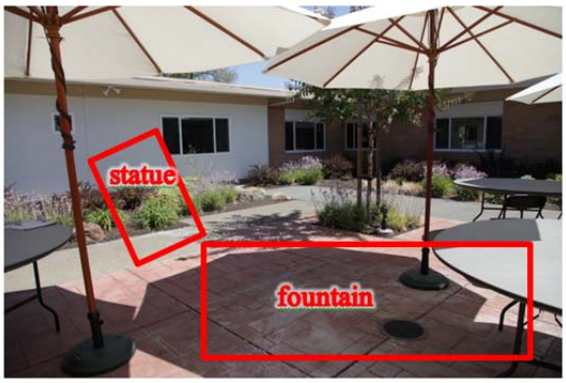

(a)

(b)

(c)

Figure 37 (a) Overview of courtyard from the southwest corner post-earthquake with original locations of statue and fountain marked; (b) Fountain of the interior courtyard before; and (c) after the earthquake. (b ,c: photos courtesy of Justin-Siena High School).

Campus Grounds

The high school included three additional surveyed statues throughout the campus grounds, as indicated by objects #4-6 in Figures 34 and 35. Each of these three statues had unique boundary conditions, geometric configurations, and restraint mechanisms. The first statue is a small, hollow, copy of the Pieta by Michelangelo (Figure 35f). This lightweight statue was resting unrestrained on a bed of soft mulch and overturned backwards. The overturning was indicated by the school president during the walk-through; although, no photographic documentation is available. The overturning direction correlates to the highly eccentric center of mass of the statue. The second statue is a large statue of St. John Baptist de La Salle and two students (Figure 35e). The statue is originally a hollow cast structure; however, it was recently filled with cement and bolted to the sidewalk in an anti-theft measure. The statue, although quite tall and slender, performed well and no evidence of cracking or translation was observed.

The final surveyed statue was a statue of Mary (Figure 35d), located on the campus grounds adjacent to the Gasser Center Building. This statue is approximately 1.5 m tall with an aspect ratio of approximately 4 and weighing approximately 295 kg. The statue is fiber-reinforced concrete with a rectangular base and complex geometry and mass eccentricities. The statue was resting on a hollow, concrete, rectangular pedestal which was resting unrestrained on a bed of mulch. Similar to the Marian statue in the courtyard, this statue was found rotated 180°about the vertical and a distance away from the pedestal. This is in contrast to the statue found overturned in the Ceja Winery, which remained partially on the pedestal. The response of this statue of Mary was a complex three-dimensional interaction, yet overturned in a direction correlating to an edge of the pedestal. This statue, pedestal and ground system was laser scanned for further analysis (see Figure 38). The response of the two Marian statues on campus in comparison with that of the Pieta replica and the chapel objects emphasizes the complex response of stiff multi-body systems.

(a) (b) (c)

Figure 38 (a, b) Snapshots of resultant point cloud from laser scan data as well as (c) a snapshot of the triangulated mesh used for calculation of geometric and mass properties.

6.7.3 THE HESS COLLECTION (N38.338517,W122.389079)

The Hess Collection is a vineyard, winery, and art museum combined on a single estate. In contrast to the other surveyed sites, the Hess Collection is located at nearly 200 m elevation on Mount Veeder. The nearest recording of the earthquake is approximately 4.3 km away at similar elevation which observed a peak horizontal ground acceleration of 0.34*g*. The Hess Collection is located at approximately 13.5 km from the epicenter of the earthquake.

The structure of the Hess Collection is a combination of historical and modern construction. The original stone-mortar structure is indicated in sections A and B of the site map in Figure 39. Section A was retrofitted and serves as a modern art gallery. Section B is a single-story barrel chai consisting of the original stone-mortar walls on the interior which are approximately 6 m in height. Section C is an entirely modern, two-story structure with new foundation poured in 1989 adjacent to the existing structure. Exterior views of the structure are included in Figure 40. In

addition, an entirely modern constructed warehouse is adjacent to the main winery buildings, but is not connected. Significant details on the retrofit and additional construction was not made available.

The structures were inspected following the earthquake and were cleared for public access with the exception of Section B which observed out-of-plane motion of the original unreinforced stone walls. In addition to this structural damage, there was significant nonstructural damage at the site including overturning and translation of art objects in the gallery (Section A), collapsed barrel stacks and pallets in the warehouse (see Figure 41), and buckled wine tanks in the storage areas (Section C). Furthermore, failure of two full wine tanks resulted in flooding of the courtyard as seen in Figure 40c. During the site survey, cracking in the concrete floor along the length of the tank storage facilities (Section C) was observed as seen in Figure 42. The cracks may be related to inconsistencies of the foundation along the edge of Sections B and C. Damage to wine tanks in Section C and art objects in Section A are summarized in the following two sub-sections. Images of the art objects, warehouse, and courtyard immediately following the earthquake on Sunday, August 24, were provided by The Hess Collection. All other images were taken on September 2.

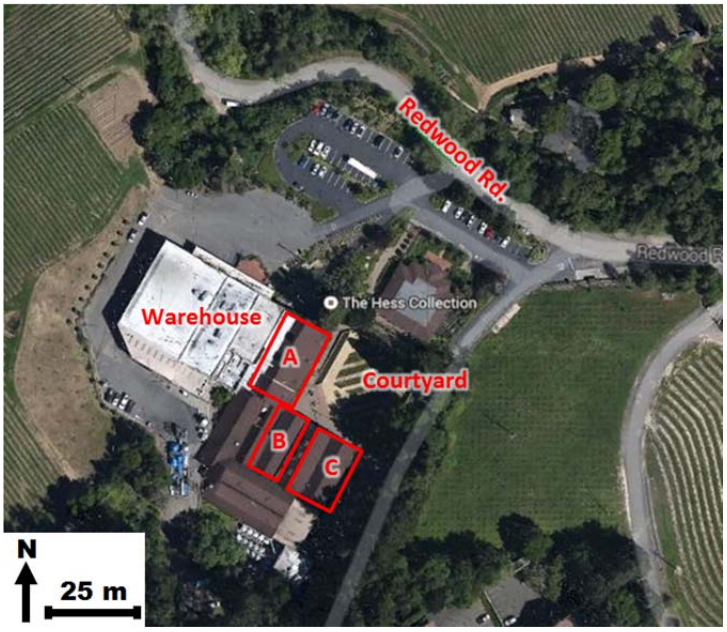

Figure 39 Google Earth view of The Hess Collection with 1989 warehouse and courtyard denoted, as well as, three primary section of the structure: (a) art gallery/museum renovated from original winery structure in 1989; (b) original 1903 distillery structure with 1989 roof; and (c) 1989 addition to the structure for expansion of wine fermentation tanks.

(a) (b) (c)

Figure 40 Exterior of The Hess Collection: (a) the art gallery, section A facing northwest; (b) the barrel chai and fermentation tank storage facilities, sections B and C; and (c), the flooded courtyard after failure of two 10,000 gallon wine-filled fermentation tanks.

Figure 41 Panoramic view of the contents damage of the modern warehouse. Wine barrels and cases of wine bottles were stacked very high for storage and subsequently collapsed and fell during the earthquake.

Figure 42 Cracking of concrete floor along the length of structure C, the 1989 addition for wine tank storage.

Wine Tanks

The winery houses over seventy individual 10,000 gallon wine fermentation tanks, largely in the modern addition on the SE portion of the estate. The tanks are thin-walled steel cylinders which appeared to be unanchored to the concrete podium on which they are placed, as seen in Figure 43. The tanks have an approximate diameter of 2.75 m and an approximate height of 6.1 m. At the time of the earthquake, not all tanks were liquid-filled. In total, ten tanks must be replaced due to buckling failure. Eight of these buckled tanks were empty. Two of these tanks were filled with wine during the earthquake and lost the entire contents through the base failure which subsequently flowed into the courtyard (see Figure 43c). In addition to the buckling failures, many of the tanks appeared to translate/slide against the podium resulting in overhang of up to 0.3 m (see Figure 43c).

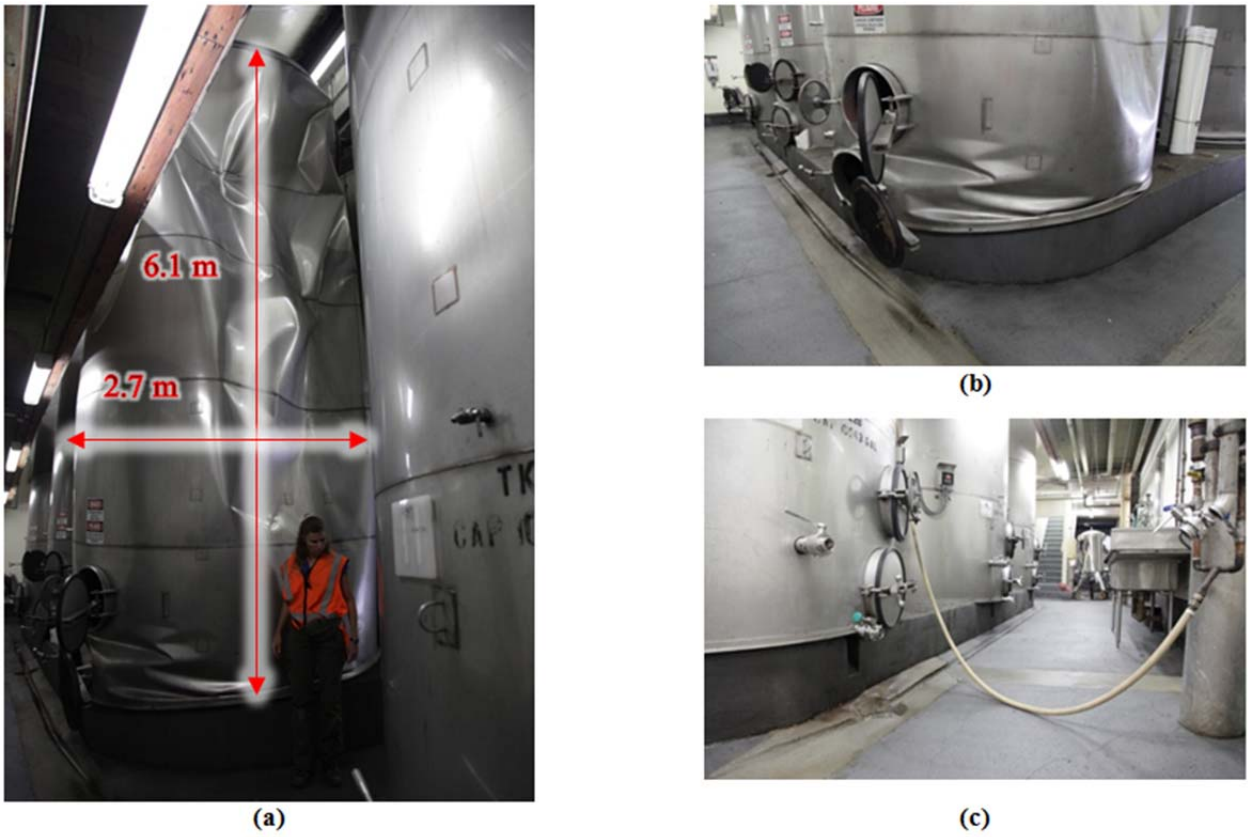

Figure 43 Condition of 10,000 gallon wine tanks following the earthquake: (a) empty buckled tank; (b) buckling of the base of a tank; and (c) significant translation of tanks in the NNW direction.

Art Collection

A significant portion of the winery is dedicated to a substantial modern art gallery. The gallery is a three-story, retrofitted stone-mortar structure. While no structural damage was observed in the gallery, many art objects translated or rotated from original locations (see Figure 44). In comparison to other surveyed sites, there were fewer instances of overturning and little documentation for these cases. One exception is an exhibit of lightweight (approximately 1 kg.) full-scale, human-form, hollow statues, as seen in Figure 44a, on the second floor of the gallery. The statues translated, rotated, and interacted with each other resulting in some overturned statues and others significant twisting and shifted.

Two large, heavy, highly asymmetric statues were observed to translate and rotate without overturning. These statues are seen in Figure 44b and 44c, where the first is a cast metal structure on the ground-floor and the second is a wooden structure on the second-floor. Both statues are resting unrestrained on painted wooden pedestals. The metal sculpture appears to have rotated which correlates with the eccentric center of mass and asymmetric footprint. The wooden statue has a predominantly wide-rectangular footprint causing the statue to be quite tall in the transverse direction, and quite squat in the longitudinal. This statue appears to have translated along its squatter dimension. Given the aspect ratios and asymmetric translations, the response of these statues may have been a combination of rocking, sliding, and twisting. A final example is a tall statue in the courtyard (Figure 44d) where many unrestrained statues were present but few experienced any noticeable movement. This tall statue is a similar cast metal sculpture resting on a brick pathway (high friction interface). The statue appears to have twisted which is likely the result of a rocking mode on one of its corners due to the anticipated high friction and tall aspect ratio. However, no overturning of this eccentric structure occurred.

Figure 44 Movement of art objects within the museum with estimated dimensions: (a) overturning and rotation of lightweight, human-form statues on the second-floor; (b) rotation/translation of a large, asymmetric hollow metal sculpture on the ground-floor; (c) rotation/translation of a large, asymmetric wooden sculpture on the second-floor; and (d) rotation/translation of a large, hollow metal sculpture in the courtyard.

6.7.4 CHARTER OAKS APARTMENT COMPLEX (N38.301742,W122.31593)

The fourth surveyed site was the Charter Oaks Apartment Complex. The complex consisted of a number of two-story, timber-framed, multi-family homes and timber-framed carports. The structures are further described in the following sections. The complex was inspected by the City of Napa on the afternoon of Sunday, August 24. The apartment structures were green-tagged and occupancy was not interrupted. However, multiple carports collapsed and all carports experienced some degree of damage. The carports were red-tagged by the city and no entry is permitted. In addition, an electrical transformer was red-tagged as unsafe for use. Figure 45 contains the site map and orientation of the discussed carports and transformer. The complex is located approximately 7.5 km from the epicenter of the earthquake and approximately 2.5 km from the nearest recording station located in downtown Napa which observed a peak horizontal ground acceleration of 0.61*g*. Despite the epicentral distance in comparison to other sites, this site is the closest of all surveyed locations to the delineated fault line (see Figure 3).

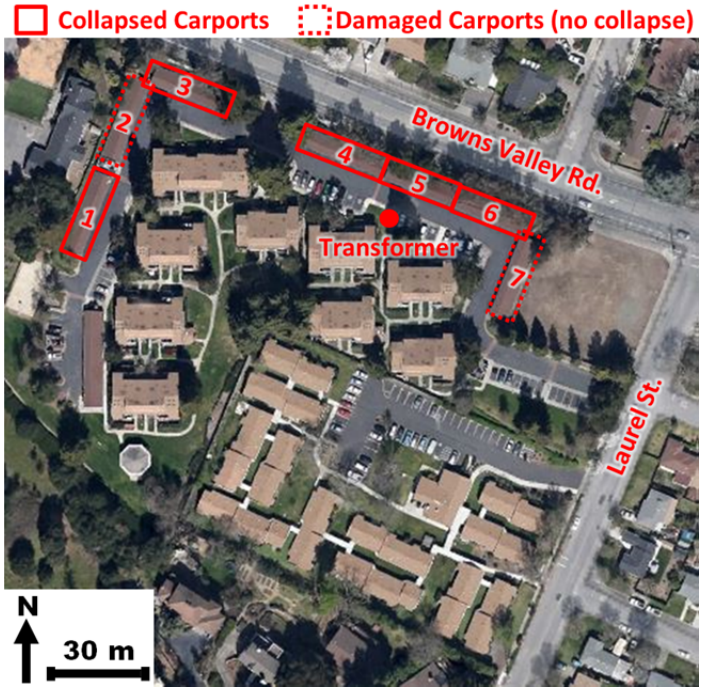

Figure 45 Google earth view of Charter Oaks Apartment Complex site indicating the locations of the collapsed carports and the surveyed transformer.

Transformer

A transformer located on the northeast side of the complex appeared to have translated during the earthquake (see Figure 45). The transformer was hollow, steel and cubic with approximate dimensions of 1 m in length, width, and height. The internal composition of the transformer was not able to be inspected. Prior to this survey, the electrical transformer had been red-tagged and labeled unsafe by the City of Napa on Sunday, August 24. The translation of the transformer was not uniform and a degree of twisting was observed, as seen in Figure 46. Although the anchorage was not able to be inspected, it is likely that the transformer was resting unrestrained on the concrete pad. The transformer translated approximately 0.05 m on the northeast corner. Given the approximate squat aspect ratio of 1, it is likely that the transformer responded in a sliding-

twisting mode. The mass distribution within the transformer was not able to be investigated to understand the twisted position. Although a recording is not available very close to this site, it can be inferred from the response of this transformer that significant peak ground accelerations were experienced to overcome a relatively high level of friction between the steel and concrete.

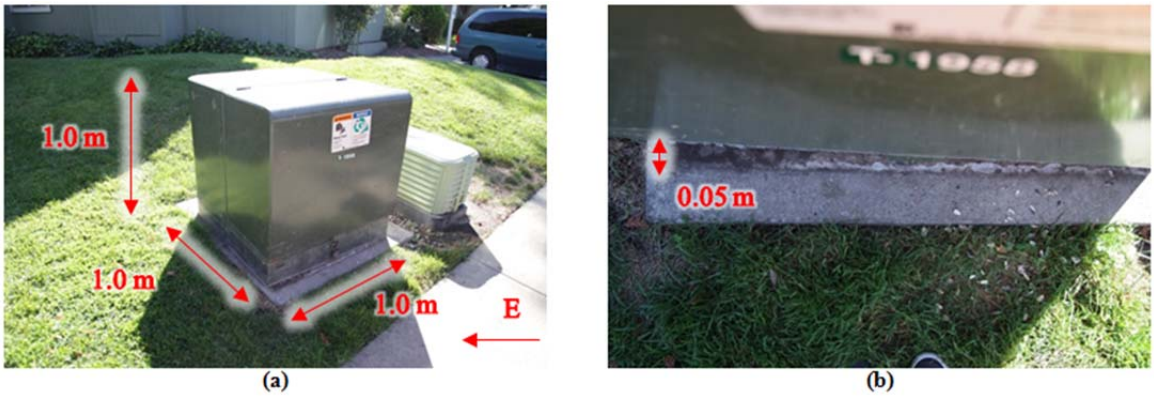

Figure 46 Rotated electrical transformer (a) facing west, and (b) northeast side facing down.

Carports

Seven carports were surveyed at the Charter Oaks Apartment Complex, as mapped in Figure 45. The carports were single-story, timber-framed structures with five bays as shown in Figure 47a. Each bay is dimensioned to accommodate two parked vehicles. The carport had a trussed roof system and is supported by timber columns (approximately 20 cm × 20 cm). The interior columns were embedded in concrete posts and surrounded by pavement; whereas, the exterior columns were typically wrapped in aluminum and embedded in soil. The rear of a typical carport was enclosed with a longitudinal timber wall, as shown with the roof system in Figure 47b. Two additional transverse walls typically enclosed the shorter sides of the carport creating a carport enclosed on three sides. An exception to this is Carport #1 (see Figure 45), which did not have enclosed transverse walls. Following the earthquake, five out of seven carports collapsed while two remained standing with noticeable signs of damage. The carport nearest the entrance was red-tagged by the City of Napa on Sunday, August 24 – within 24 hours of the earthquake. The remaining carports did not have red-tags but were cordoned off. Four of the five collapsed carports were oriented with the longitudinal wall in the northwest-southeast direction. The collapse of Carports #3 and #4 is shown in Figure 48 with the perpendicular carports standing. The exception was the collapse of Carport #1 which is likely related to the missing transverse walls.

Carports #3-6 collapsed due to interior column shearing, as shown in Figure 49 using Carport #4 as an example. Interior columns sheared at the base embedment in the concrete post. The southernmost exterior column failed similarly at the base; however, the northernmost column was embedded in soil likely with a larger embedment depth (at the curb elevation). This northernmost column did not pull out completely and did not shear at the base. An asymmetric collapse was observed with complete detachment of the roof from the longitudinal and transverse wall at the southern end. Each of these four carports (#3–6) in the northwest-southeast orientation collapsed toward the southwest.

In contrast, the perpendicular carports (#2 and #7) did not collapse yet withstood damage at the connections. Carport #7 is shown in Figure 50a with the longitudinal wall in the southwest direction. A yielded connection of a rear-interior column with the roof is shown in Figure 50b. The connection yielded a permanent displacement of the roof to the southeast. This behavior indicates that the longitudinal wall acted as a shear wall during the earthquake even though it was likely not intended to be load bearing. This correlates to the collapse of the perpendicular carports with much shorter transverse walls.

The response of Carports #2-7 indicates a very strong Northwest-Southeast component of the earthquake. However, Carport #1 collapsed despite the longitudinal wall in the southeast direction. Images of the collapse are included in Figure 51. This carport is different from the remaining carports by the lack of transverse walls. In addition, the collapse of this carport was opposite that of Carports #3–6 in that it collapsed toward the longitudinal wall. In this carport, the longitudinal wall collapsed (see Figure 51b) and the interior columns sheared (see Figure 51b and c). However, the exterior columns which were embedded in soil at curb elevation completed pulled out of the embedment (see Figure 51d).

(a) (b)

Figure 47 (a) Carports facing northwest before earthquake (Google Maps); and (b) Non-collapsed carport showing the roofing and wall system.

(a) (b)

Figure 48 Views of carports post-earthquake showing collapsed and non-collapsed carports facing; (a) Southeast and (b) Northwest.

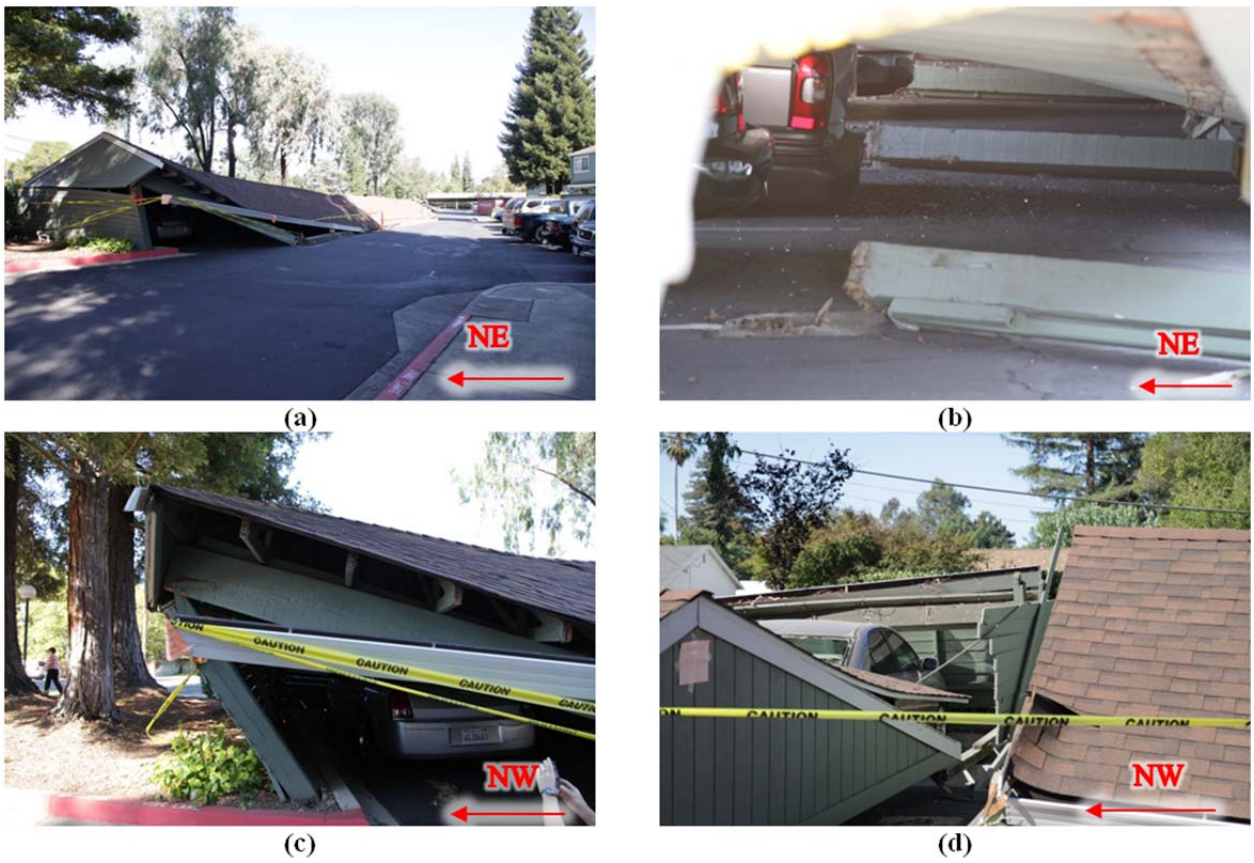

Figure 49 Collapse details for Carport #4: (a) overall collapse along length of carport; (b) view of interior column; (c) west end of carport with partial pullout of column; and (d) east end of carport with complete detachment of roof from the longitudinal and transverse walls.

Figure 50 Details for Carport #7: (a) view looking southwest along longitudinal wall; and, (b) yielded connection of a rear-interior column and roof system showing permanent displacement to the southwest.

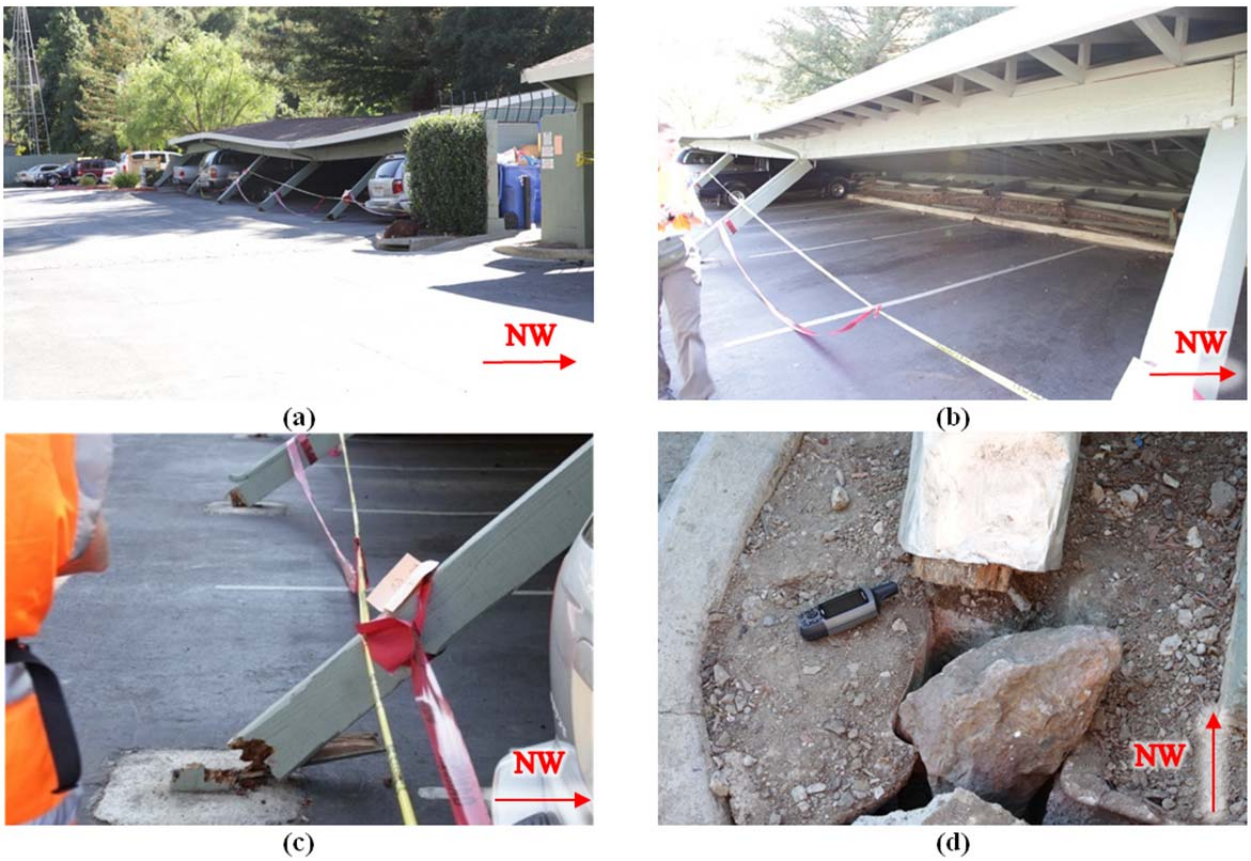

Figure 51 Collapse details for Carport #1: (a) overall collapse along length of carport; (b) view of collapse of longitudinal wall; (c) sheared interior columns; and (d) wrapped timber column pull-out on north end.

6.7.5 DOWNTOWN NAPA: RESIDENTIAL (N38.299505,W122.293388)

Three residences were surveyed on Jefferson Street in downtown Napa. An aerial view of the residences is included in Figure 52. The three structures are on two adjacent lots with two structures located on the same lot. The first lot is 1251 Jefferson Street, which consists of a larger, historical residence (denoted as Residence R1) on the portion of the lot closest to the street and a second, smaller residence (denoted as R2) in the rear of the lot. The second lot is 1261 Jefferson Street, which consists of a single, larger residence (denoted as R3). These residences were occupied during the earthquake and continued to be occupied post-earthquake. However, the City of Napa inspected and red-tagged the residences on Thursday, August 28. The survey was conducted with assistance from the resident caretaker.

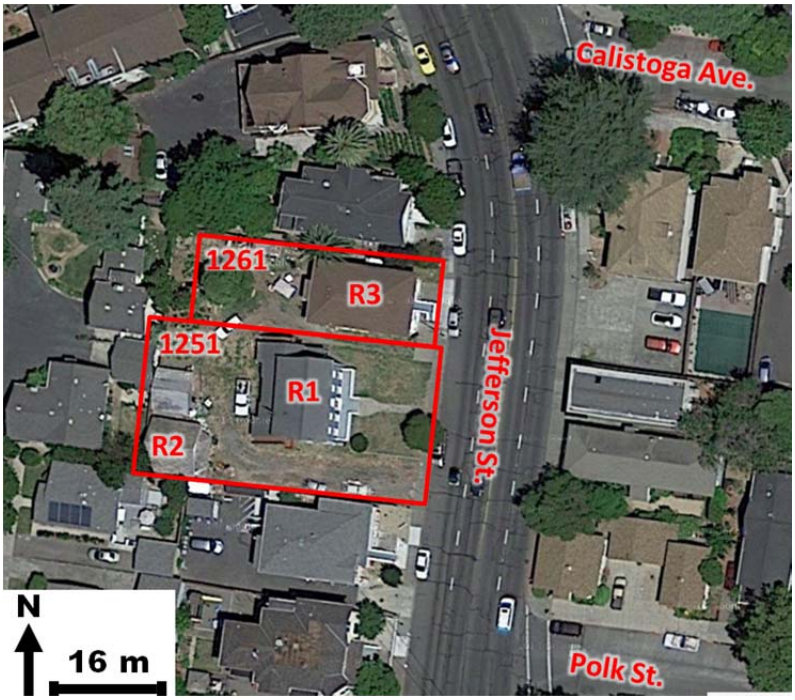

Figure 52 Google Earth view of the surveyed downtown Napa residential properties.

Residence R1, as seen in Figure 53, is a timber-framed structure originally constructed in the 1860s with a rectangular footprint and a pitched roof. The structure was supported on a cripple wall, estimated to be approximately 0.3-0.6 m above the foundation. Additions to the residence in the 1900s included the single-story room on the north side (Figure 53a) as well as the single-story rear expansion and second-story rear dormer (Figure 53b). Two exterior single-story staircases were incorporated on the north and south sides of the house, as seen in Figure 53b and c. The residence experienced cripple wall failure during the earthquake and significant shifting of the superstructure atop the foundation was observed on the order of 0.5 m to the east-southeast. This shifting can be seen in Figure 54a near the front porch of the residence. The angle of the front porch also indicates the vertical shift of the superstructure (collapse of cripple wall). This image also highlights the presence of the gas lines at this location of large displacement. This horizontal shifting left the front of the structure unsupported on the foundation and cracking at the roof ridge was observed (Figure 54b). In addition to the structural damages, the exterior staircases were significantly damaged. In Figure 54c, a support is missing from the landing causing twisting of the staircase. In addition, the staircase moved horizontally with the structure creating a gap with the concrete stair base (Figure 54c and d).

Residence R2 is a modern, slab-on-grade, single-story, timber-framed structure, which is significantly smaller than the adjacent residences (less than 50 m^2). The structure is likely a renovated cottage or detached garage. Although no photographic documentation is included or available, shifting of the superstructure over the foundation to the east-southeast was observed. However, the structural damage to this residence and horizontal displacement was significantly less than the adjacent residences.

Figure 53 Red-tagged residence at 1251 Jefferson Street: (a) view from Jefferson St; (b) view of dislocated stairs from backyard facing east-southeast; and (c) view of stair damage from backyard facing east-northeast.

Figure 54 Details of damage at red-tagged residence at 1251 Jefferson Street: (a) collapsed cripple wall and relative displacement between foundation and super-structure of approximately 0.3-0.6 m; (b) crack at roof ridge due to translation of superstructure off of the foundation; (c) displacement of wooden staircase and concrete foundation stairs; and (d) vertical and horizontal displacement of superstructure observed at the rear doorway and staircase.

Residence R3, located at 1261 Jefferson Street, is a two-story, wood-frame, multi-family residence with the primary residence on the second floor. Figure 55 presents views of the residence from the street which has a first-story, garage on the north half of the structure extending to the rear of the residence. A separated residential unit occupies the south half of the structure (Figure 55b). The sub-floor of the top-story was cross braced, as viewed from exterior windows of the unfinished first-floor garage. The structure was red-tagged citing failure of the northeast column support, the subsequent tilt of the structure, and the potential for collapse. This structure developed a soft-story type mechanism during the earthquake, as evidenced near the garage door (see Figure 56). The northeast column support failed – as seen in the top, right corner of the garage in Figure 56 resulting in a jammed garage door which emphasizes the tilt of the structure. Furthermore, significant cracks were observed in the vicinity of the gas pipes located on the south side of the exterior staircase (Figure 56c).

Figure 55 Views of red-tagged residence from Jefferson St. facing: (a) southwest and (b) northwest. (Google Earth Street View).

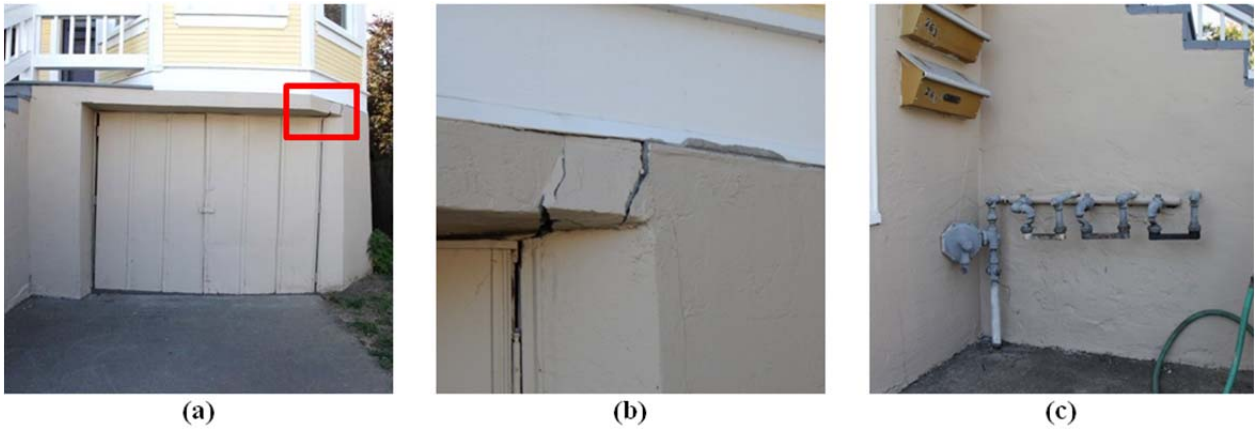

Figure 56 Details of damage at red-tagged residence at 1261 Jefferson Street: (a) soft-story development seen at garage door with outline of support failure; (b) close-up of top-right corner of garage door and corner support failure; and (c) horizontal cracks along gas line.

6.8 ACKNOWLEDGMENTS

Data regarding earthquake location, fault, and recordings were obtained from the USGS, CISN, and CESMD. We thank the many residential and commercial building and other structure owners for allowing access to their sites following this important event. Additional information regarding the Ceja Winery and the Justin Siena High School were provided by winery owner Amelia Moran Ceja and school president Robert Jordan. Appreciation is particularly extended to all individuals for their time and communication. Laser scanning, camera equipment, and drones were provided by the Center for Interdisciplinary Art, Architecture, and Archaeology at UC San Diego. Funding for these two field investigations were provided by PEER and the NSF and are greatly appreciated.

7 Fire Following Earthquake[+]

Charles Scawthorn

A survey of fire sites was conducted on the day following the earthquake (i.e., 25 August), and data obtained from an interview with senior officers of Napa City Fire Department (NFD). A complete list of incidents the NFD responded to was not available at the time of the interview. Fires attributable to the main shock are summarized in Table 1 and shown in Figures 1 and 2.

Table 4 Fires attributed to the 24 August main shock (from handwritten notes).

No.	Time of Report (approx.)	Location	Description (see below)
1	0330	Orchard Ave	Napa Valley Mobile Home Park (NVMHP) – actually two ignitions – see narrative
2	0400	Laurel St. (no. street number)	2 story, 2 unit residence, roof collapse, started fire
3	0500	162 Robin at Solano	Dbl wide home
4	0630	1990 Trower	Smoke inside structure
5	0730	770 Lincoln x Soscol	Electrical fire in substructure of a mobile home
6	1200	4072 Rohlffs Way x Fair	Kitchen fire in single story multi-unit senior housing complex

7.1 LIST OF FIRES

7.1.1 ORCHARD AVENUE FIRE

This was the largest fire in the earthquake. First dispatch was of T1 to a report of gas odor but en route, T1 observed a fire in the Napa Valley Mobile Home Park (NVMHP) off of Hwy 29 at Orchard Road and diverted to this incident. T1 encountered a broken water main spewing water at the entrance to the NVMHP on Orchard Road and proceeded to enter the NVMHP. T1 then encountered a single structure fire at 313 Mark Way. The structure was 50% involved; they also observed a second fire at 317 Patty Way, which was 100% involved and impinging on neighboring buildings; see Figure 2. Wind conditions were calm.

Approximately 20 minutes into the incident (i.e., about 0400) Water Tenders 15 and 25 arrived from Napa County Fire Department. NFD E6 had also arrived and took water from one of the WT 15 and suppressed the Mark Way fire. T1 and WT 25 similarly suppressed the Patty Way fire; See Figures 3 and 4. Overhauling continued until about 10am.

[+] Any observations, opinions, findings, and conclusions or recommendations expressed in this material are preliminary and are those of the authors, and do not necessarily reflect those of the Pacific Earthquake Engineering Research Center. The information, data and images contained in this report may not be published or presented without permission from the authors.

7.1.2 1990 TROWER AVENUE

This was a report of smoke inside a structure. Scawthorn visited this site, which is a restaurant. Employees reported some equipment had fallen onto other equipment in the kitchen, causing a call to the fire department. No significant damage occurred.

7.1.3 ROHLFFS WAY

This was a report of smoke in a kitchen area of a senior citizen's residence.

7.1.4 MUTUAL AID

As reported above, Napa County FD responded quickly with water tenders. By noon, two OES strike teams had arrived in Napa.

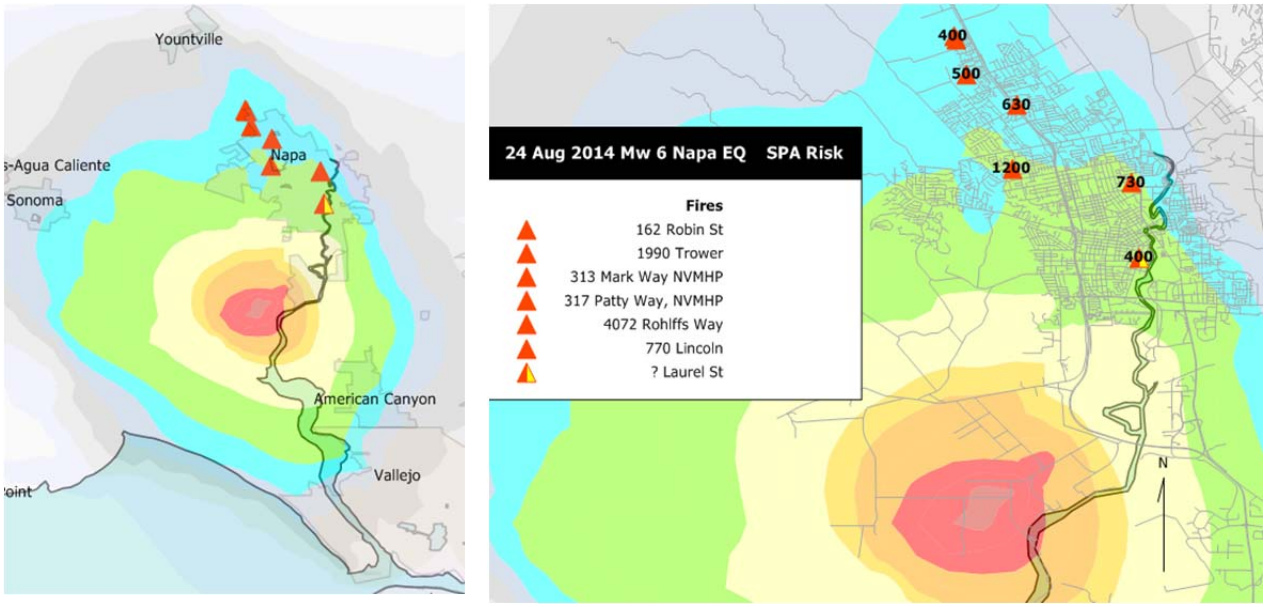

Figure 1 Fires and approx. times overlaid on PGA, 24 Aug 2014 S. Napa M_w 6.0 earthquake (half shaded triangle indicates street number unknown).

(a) (b)

Figure 2 (a) NVMHP Park and locations of fires, 24 Aug 2014 S. Napa M_w 6.0 earthquake; and (b) 317 Patty Way fireground, showing locations of photos 31, 33, 38 in Figs. 3 and 4 (damaged buildings outlined in red).

Figure 3 Fireground at 317 Patty Way, NVMHP Park, 24 Aug 2014 S. Napa M_w 6.0 earthquake.

Figure 4 Damage to exposure structures, 317 Patty Way, NVMHP Park, 24 Aug 2014 S. Napa M_w 6.0 earthquake: (a) structure to east of fireground; and (b) structure to south of fireground.